Technical and Economic Feasibility of a Regenerative Braking System with On-board Energy Storage for Freight Trains

by

Andreas Pyper

Dissertation presented in partial fulfilment of the requirements for the degree of Master of Engineering (Mechanical) in the Faculty of Engineering, Built Environment and Information Technology at the University of Pretoria.

April 2018

Summary

This dissertation presents the technical and economic feasibility of a novel regenerative braking system (RBS) for the freight rail industry. A concept for a distributed RBS, integrated into the bogies of freight rail wagons, is proposed in a patent by Transnet SOC Ltd. The system allows for numerous RBSs to be installed on a single freight train, in a distributed manner, which collectively functions together to perform regenerative braking on the train with the goal of reducing the energy consumption of the train. The proposed system would, if implemented successfully, alleviate challenges and limitations with current RBS on diesel-powered freight trains. The patent also proposes that the RBS utilise mechanical energy storage by means of a high-speed flywheel which is connected to the train axles by a continuously variable transmission (CVT).

The proposed RBS is conceptualised in this study by first establishing the requirements of the system from in-service train data, followed by the development of the subsystems to deliver workable concepts that would meet the requirements identified. A multi-domain, physical system simulation model is subsequently developed to establish the energy savings performance of each of the system concepts for typical freight train routes. The simulation results show that energy savings of between 10% and 24% can be realised by the feasible system concepts, depending on the configuration of the RBS concept and the duty-cycle of the specific train route. This proves the technical feasibility of the proposed system.

Next, the proposed system and the candidate concepts are evaluated in economic terms. A cost-benefit analysis (CBA) is performed in which the cost and benefits over the life cycle of the RBS were combined into a single distribution and analysed. The decision criteria calculated in the CBA provide unanimous results as to which of the candidate concepts are economically feasible. It is shown that four of the candidate concepts, all utilising the same transmission topology incorporating a CVT with different flywheel configurations, are economically feasible. The RBS concepts show good return on investment and provide an internal rate of return (IRR) of 17% and a benefit-cost ratio (BCR) of 2.13. These results therefore indicate that the proposed distributed RBS for freight trains is economically feasible and would deliver favourable financial returns if pursued.

Table of Contents

Symbols

P	Power
E	Energy
E_k	Kinetic Energy
I	Mass-moment of Inertia
S_{max}	Ultimate Tensile Strength
U_{max}	Maximum Energy Density
P_M	Motoring Power
P_B	Braking Power
$f_{B,RBS}$	Percentage braking energy captured by RBS
E_M	Motoring Energy
R	Radius
E_F	Flywheel energy
E_{usable}	Usable energy
K	Flywheel shape factor
V_f	Flywheel volume
P_{loss}	Power loss
T_{circ}	Flywheel circumference resistive torque
T_{side}	Flywheel side resistive torque
C_{circ}	Flywheel circumference torque coefficient
C_{side}	Flywheel side torque coefficient
w_f	Flywheel width
Re	Reynolds number
t	Airgap distance
R_{air}	Gas constant for air
T_{air}	Air temperature
R_{bi}	Bearing bore radius
d_{shaft}	Shaft diameter
R_T	Overall transmission gear ratio
R_{FG}	Fixed-gears ratio
$R_{CVT,spread}$	CVT ratio spread
R_{REQ}	Required gear ratio
T_f	Flywheel torque
T_v	Vehicle torque
P_{TM}	Traction motor power
N	Locomotive notch
DC_N	Duty cycle for notch
B_t	Benefits of period
C_t	Costs of period

Greek Symbols

ω	Rotational velocity
ρ	Density
η_{PC}	Power converter efficiency
ω_{max}	Maximum Rotational velocity
ω_{min}	Minimum rotational velocity
ξ	Flywheel outer to inner diameter ratio
η_u	Usable energy fraction

σ_a	Allowable material stress
v_{air}	Air viscosity
μ_b	Bearing coefficient of friction
η_{drive}	Electrical drive efficiency
η_{RBS}	Energy saving from regenerative braking
η_{TM}	Traction motor efficiency
η_{FD}	Final drive efficiency
η_N	Notch specific fuel efficiency

Abbreviations

KERS	Kinetic Energy Recovery System
RBS	Regenerative Braking System
ESS	Energy Storage System
OEM	Original Equipment Manufacturer
GE	General Electric
FESS	Flywheel Energy Storage System
CVT	Continuously Variable Transmission
DoD	Depth of Discharge
SS	Self-sufficiency
PHP	Power-hybridisation potential
EPP	Energy-hybridisation potential
IRR	Internal Rate of Return
EROI	Energy Return on Investment
NPV	Net Present Value
CBA	Cost Benefit Analysis
BCR	Benefit Cost Ratio
ESS_{SOC}	Energy Storage System, State of Charge

1. Introduction

1.1. Background

It is becoming a worldwide trend and necessity for countries to reduce their dependence on power generated from conventional fossil fuels. An increase in global energy demand, environmental constraints such as the effects of greenhouse gasses (GHG) and the depletion and rising cost of conventional fuels are all drivers of this global trend. The increase experienced in global energy demand is largely due to the industrialization and expansion of emerging economies as well as increases in global passenger vehicles and freight transport. Concern over the effect of greenhouse gasses is evident from the Paris Agreement in which 195 countries pledged to address and curb greenhouse gas (GHG) emissions over environmental concerns (European Commission, 2015; United Nations Climate Change, 2016). South Africa, a global top 20 carbon emissions emitter, has pledged to reduce GHG emissions by 34% by 2020 and 42% by 2025 at the 2009 Copenhagen climate negotiations (National Treasury, Republic of South Africa, 2010).

The solution to gaining independence from conventional fossil fuels and reducing GHG emissions is twofold: firstly, finding alternative energy sources and secondly reducing energy demand. Several alternatives to conventional fossil fuels exist and contribute to the global energy mix. The most prominent alternative energy source is nuclear energy and provides around 4% of the world's energy. Renewable energy sources have become increasingly popular in recent times as the technologies required to harvest this energy have through extensive research and development become more efficient and affordable. Although renewable energy sources do not contribute significantly to the global energy mix currently, it is believed that they will contribute significantly within the next 20 years. In South Africa, the Department of Energy believes that by 2030 renewable energy power plants will have a generating capacity at least 20 000 MW (South African Government, 2015).

Despite technological advancements and an increase in up-take, the energy density of renewable energy sources is still lower than those of fossil fuels and as a result has a lower generating capacity potential. It is therefore crucial that, to become less dependent on fossil fuels and reduce GHG emissions, the global energy demand be curbed. As a result, finding ways to reduce the energy demands of energy intensive industries has become a popular field of study in the engineering environment. This study explores a means of reducing the energy intensity of one these industries: the transport sector and more specifically the rail transport sector.

The transport sector is one of the largest energy consumers in the world, making up at least 18% of the world's energy consumption (Barrero, et al., 2010; International Union of Railways, 2013; US Energy Information Administration, 2015). The sector consists of four primary freight and human transportation modes namely road, rail, maritime and air. Of these, rail is considered the most efficient and offers the highest transportation capacity (Rodrigue, et al., 2013; Barrero, et al., 2010; Oak Ridge National Laboratory, 2015). This is largely a result of the low rolling resistance due to the stiff steel-on-steel contact between the wheel and rail as well as the low aerodynamic drag due to the convoy formation of trains (Hillmansen & Roberts, 2007). The rolling resistance on railway tracks is roughly 3-4N/kN compared to 10-25N/kN for road transportation (Gräbe, 2008).

Globally 50% of railway lines are electrified and about 70% of rail traction energy is provided from electricity grids (International Union of Railways, 2013). In the passenger sector, more than 75% of traction energy is from electricity compared to 60% for the freight sector. The railways in the USA and Europe account for more than 50% of the world's railway lines. Interestingly, the traction energy-mix on these continents is vastly different. The annual traction energy consumption of railways in Europe is around 122 million MWh (28% diesel and 72% electricity). Of this energy, approximately 75% is consumed by passenger trains and the remaining 25% by freight trains (International Union of Railways, 2013). American railways consume about 100 million MWh of energy (93% diesel and 7% electricity) of which more than 95% is used for freight transportation (International Union of Railways, 2013).

In the South African context, the rail sector consists predominantly of low speed commuter and freight transportation, with the medium speed (160km/h) Gautrain system being the exception. Transnet State Owned Company (SOC) is the company who owns and operates the South African freight railways, pipelines and ports. Transnet is one of the largest industrial energy consumers in South Africa, whose primary energy sources are electricity (57%) and diesel (38%). Transnet's rail traction energy consumption amounts to more than 3.5 million MWh of electrical energy and 2 million MWh of energy from fuel (about 250 million litres of fuel) annually. Although less diesel energy is used than electrical energy by Transnet, the cost of diesel energy is significantly more than that of electrical energy (roughly R3.50/kWh for diesel vs. R1.00/kWh for electricity), which means that diesel energy makes up 65% of Transnet's total traction energy cost.

A recent study conducted by Transnet predicts that their energy consumption will increase by 300% over the next 30 years, resulting in an almost nine-fold increase in energy cost to R53 billion (Transnet SOC Ltd, 2015). This shows that the potential savings in energy cost and CO_2 emissions that could result from a relatively small percentage reduction in energy consumption of the South African railways alone are immense.

Although railway transport is reputed as an environmentally friendly mode of transport, the sector is coming under pressure to curb its energy demand and improve environmental performance (Hillmansen & Roberts, 2007). It is therefore important that innovative technologies that show promise of reducing the energy consumption of railways are explored by railway companies to ensure the sustainability of rail transport. It is also important that ways of improving the energy efficiency of the railway sector are pursued to retain its competitive advantage over other modes of transport.

One of the most promising means of reducing the energy consumption of railway vehicles is the implementation of regenerative braking systems (RBS), also referred to as Kinetic Energy Recovery Systems (KERS). It is well understood that the energy generated during traditional braking operations of vehicles is dissipated in the form of heat and noise and that it would be beneficial to rather capture this energy for reuse. Regenerative braking is a type of braking that enables this by capturing the braking energy of a vehicle and redelivering it when it can be used again. The railway sector is particularly well suited to regenerative braking systems as trains are highly utilized and have a well-defined duty cycle when compared to the automotive industry (Hillmansen & Roberts, 2007). The potential for energy savings by these systems have been investigated extensively in the literature and have shown that these systems show great potential and are worth pursuing (González-Gil, et al., 2013; Barrero, et al., 2010; Hillmansen & Roberts, 2007; Spiryagin, et al., 2015).

Although many different RBS concepts and designs exist, relatively few have made it past the prototype phase to the point where it is adopted for operation by rail companies. This is due to challenges with the storage and utilization of the regenerated energy, limitations in terms of the train types to which these systems are suited as well as the economic feasibility of these systems.

This study investigates the feasibility of a distributed RBS proposed in a patent held by Transnet SOC which intends to alleviate some of the shortcomings and limitations of existing RBSs. The distributed RBS system may provide a solution to railway operators to implement a regenerative braking system on both electrified and non-electrified lines and could also be suited to both passenger and freight trains. By conceptualising the proposed invention as well as a simulating the system to establish its performance, the study aims to prove the technical and economic feasibility of the proposed invention.

1.2. Rationale for Considering On-Board Regenerative Braking Systems with Flywheel Energy Storage in the Rail Industry

The aim of this section is to provide an understanding of regenerative braking systems in the rail industry and to investigate findings made in literature regarding these systems. Firstly, the basic functionality of these systems will be discussed and a distinction is made between two broad types of RBSs, namely Wayside- and On-board RBSs. The requirements and limitations of on-board RBSs are investigated to determine the potential benefit that the proposed distributed flywheel based RBS might have.

1.2.1. Overview of Regenerative Braking Systems in the Rail Industry

A regenerative braking system (RBS) consists out of three main subsystems: an Energy storage system (ESS) that stores the captured braking energy, a power converter enabling the transfer of energy to and from the ESS as well as a controller to manage the power converter (González-Gil, et al., 2013; Foiadelli, et al., 2006). These systems typically work in tandem with the existing propulsion system of a vehicle and as a result a conventionally powered vehicle becomes hybrid powered which significantly reduces the energy consumption of the prime mover. RBS technologies have been matured and successfully commercialized by original equipment manufacturers (OEMs) in the automotive industry including Toyota, Volvo and Ferrari to name a few. Besides passenger cars, RBSs are also utilized by transit busses and off-highway construction and excavation vehicles (Torotrak Group, 2016). RBSs have been explored by railway companies and OEMs of rolling stock, but these systems have failed to gain traction in the rail industry.

Trains (passenger and freight) are made up of a set of powered and non-powered rail vehicles, referred to as a train-consist. Powered vehicles can either be locomotives or motor coaches such as Diesel multiple units (DMUs) or Electrical multiple units (EMUs) that have the ability to pull several non-powered vehicles whilst transporting passengers. Non-powered vehicles are trailers that either carry passengers (coaches) or freight (freight wagons). Passenger train-consists typically have a ratio of motor coaches (DMUs or EMUs) to coaches of 50-100%, whereas for freight trains the ratio of locomotives to non-powered wagons is much lower at 2-10%. Freight trains are typically made up of one or more consists of locomotives and a multitude of freight wagons. The most common configuration of a freight train is called head-end power in which the locomotive consist is located at

the front of the train and pulls the trailing freight wagons. Distributed power is an alternative configuration where in addition to the locomotive consist at the front of the train, a locomotive consist is placed in amongst the trailing wagons to alleviate excessively high in-train coupler forces.

Regardless of the energy source of modern trains, traction is applied to the wheels by means of electrical motors that are mechanically connected to the wheel axles of the vehicle, commonly referred to as traction motors. The traction motors can in turn act as generators and convert kinetic energy into electrical energy to perform braking, called dynamic braking (González-Gil, et al., 2013). Dynamic braking is used to perform most of the braking on modern trains and holds several advantages above friction type brakes (González-Gil, et al., 2013). Friction braking systems require power consuming auxiliary equipment such as compressors or vacuum pumps for operation and also suffer from wear and tear. The electricity generated by trains during instances of dynamic braking is traditionally dissipated by converting the electrical energy to the thermal domain through a bank of resistors on board the train, which is referred to as rheostatic braking (González-Gil, et al., 2013). In some cases, a small percentage (<5%) of the generated electricity is used to power the auxiliary systems (fans, compressors, vacuum pumps etc.) of the driven rail vehicle.

As the demand for regenerative braking systems became apparent, coupled with advancements in power electronic- and energy storage technologies, recycling the electricity generated during dynamic braking became a commercially- and technologically viable possibility (González-Gil, et al., 2013; Painter & Barkan, 2006). RBSs can be categorized into two broad types based on the storage mechanism of the regenerated, namely Wayside- and On-Board energy storage (ESSs).

Wayside ESSs are systems in which the recovered energy during braking is not stored on the rolling stock but at a remote location. These systems are implemented on railways that are electrified by an overhead catenary- or third rail electrification system, as the electrification system provides a means to transport the energy away from the train. The electrification system provides power to rolling stock which is used to drive the electrical traction motors connected to the rolling stock's wheel axles, and in turn can serve as a transmission system to transport/transfer the electricity generated during dynamic braking to the desired location. The energy can then either be used to (a) power other nearby or passing rolling stock, (b) returned to the electricity distribution network permitting that the network is receptive and the necessary infrastructure is in place or (c) stored in a stationary ESS to be reused when the energy is needed at a later stage.

Wayside RBSs are particularly attractive in cases where minimal modifications need to be made to existing infrastructure as would be the case for scenarios (a) and (b) explained above. Scenario (a) mainly occurs in high traffic networks such as urban rail networks. Scenario (b) requires the distribution network to be receptive which is the case for DC networks and AC networks in some cases (van der Meulen & Moller, 2014). Scenario (c) requires the installation of energy storage infrastructure at sections of the rail network where significant braking effort (and motoring effort in the opposite direction) is required. There are a variety of energy storage technologies that can be implemented for both wayside and on-board ESSs. These technologies will be briefly reviewed in the subsequent paragraphs. The efficiency of RBSs with a Wayside-ESS can be relatively low due to line losses in the transmission system (González-Gil, et al., 2013). The receptiveness of the distribution network can also limit the amount of energy that can be regenerated by the system, in some cases less than 50% of the capacity available for regeneration can be pushed back into the network (van der Meulen &

Moller, 2014). Although there are challenges to overcome to implement Wayside RBSs, the fact that almost no modification to existing infrastructure is required has made these systems attractive to railway operators and should become common practice for electrified railways in the future (Hillmansen & Roberts, 2007; van der Meulen & Moller, 2014).

The second type of RBS utilises an ESS located on-board the rail vehicle which accumulates the regeneration energy during braking and releases the energy when it is required again to provide motoring effort, thereby reducing the energy consumption of the train. These systems require no modification to- or interaction with external infrastructure as is the case for wayside RBS. On-board ESSs exhibits higher efficiencies than their wayside counterparts as line losses associated with the transferring of energy over distances are avoided (González-Gil, et al., 2013). The result is a more modular system that is easier to integrate into a rail network as they can function on both electrified rail lines as well as non-electrified lines where diesel traction is used. The on-board ESS does however occupy a large space on the vehicle and can increase the weight of the rolling stock significantly. On-board RBSs in the rail industry are similar to the systems used in the automotive industry, but difficulties experienced in the automotive industry such as long stand-by periods and varying duty cycles are not common in the rail environment (Hillmansen & Roberts, 2007). Although on-board RBSs show great potential for energy savings and enable regenerative braking on diesel- locomotives and motor coaches, engineers have struggled to make these systems technically and financially feasible. The following section will consider the requirements and limitations of these systems in more detail.

In terms of the potential performance of RBSs in the rail industry, various studies have been conducted to determine the magnitude of energy savings that can be achieved with these systems. The predicted energy savings from these studies range from 10% to 36% based on train type, route topography and duty cycle (Barrero, et al., 2010; Hillmansen & Roberts, 2007; Rupp, et al., 2016; Spiryagin, et al., 2015).

1.2.2. Focus on On-Board Regenerative Braking Systems

According to a study conducted by Pike Research, a market research and consulting firm for global clean technology markets, sales of hybrid locomotives (locomotives with on-board RBSs) will reach almost 500 units in the ten years leading up to 2020 (Navigant Research, 2011). Despite the evident market for locomotives with on-board RBS, technological constraints have halted the development of these locomotives for certain train types. DMUs for passenger trains with on-board RBSs have been successfully developed such as the JR East New Energy train fitted with lithium-ion batteries, and the DDFlytrain developed jointly by Ricardo, Artemis Intelligent Power and Bombardier Transportation in which Ricardo's Torqstor flywheel ESS (FESS) was fitted to a Bombardier DMU (Fujii, et al., 2014; Ricardo PLC, 2015). Switcher or Shunter locomotives, smaller locomotives that operate in train yards to assemble freight trains, equipped with on-board RBSs have also been developed successfully such as the Railpower Green Goat which incorporates a small diesel engine to charge a battery pack that in turn is used to provide the tractive power for the locomotive (Rail Industry Resource Center, 2002).

The train type which has proved the most difficult for the implementation of on-board RBSs is freight trains hauled by diesel-electric locomotives. The General Electric (GE) Evolution Hybrid, a switcher locomotive capable of hauling freight over long distances as well, is an example of an attempt at such a locomotive. The locomotive was unveiled by GE in 2007 and at the time planned on rolling out the first production locomotive in 2010, no application results have been found however (Railway Gazette,

2007). The power rating of the RBS installed to the locomotive was around 1500kW, less than 50% of the 3200kW rating of the prime mover and other traction equipment. This would mean that during full braking, the RBS would be able to capture less than 50% of the available braking energy. GE estimated a reduction in fuel consumption of 10% for hybrid locomotive, which is significantly less than the potential energy savings of up to 35% as mentioned previously. To identify the limiting factors and constraints that have prevented the application of on-board RBSs to freight trains hauled by diesel traction, the requirements posed by this train type will be investigated in more detail.

As existing RBS technologies for railway rolling stock exploit the electricity generated during dynamic braking, the location of the on-board ESSs are usually confined to the powered vehicles of trains which implies spatial and weight constraints to the on-board ESSs. Both the size and mass of an ESS are dependent on the energy capacity and the charge and discharge rate (power rating) required. A first order approximation of these factors will be done to investigate the feasibility of implementing on-board RBSs to different types of trains, namely passenger- and freight trains. In the literature, Van der Meulen and Möller (2014) performed a similar study and used a simplified method of determining the required energy storage capacity and charge rates and only considered heavy haul electrified trains with distributed traction. Barrero et al. performed simulations to determine the requirements of a supercapacitor ESS for a metro line, therefore not investigating the requirements of an ESS for freight trains and only considered a single ESS technology. Hillmansen and Roberts performed an analysis to determine the requirements of an ESS but made no attempt to match the requirements with ESS technologies and only considered passenger trains in their analysis (2007).

A rule-of-thumb approach can be used to determine the energy capacity and charge/discharge rate required from the ESS. The first rule of thumb is that the ESS charge and discharge rating (power rating) should be approximately equivalent to the peak breaking power requirement of the vehicle (Hayes, et al., 1998). Secondly, the ESS energy capacity should roughly be equivalent to the kinetic energy of the vehicle at cruising speed, which is the same as the amount of energy required to accelerate the vehicle to cruising speed from standstill if losses are neglected (Hayes, et al., 1998). A more detailed expression for the required energy capacity is presented by Barrero et al. (2010) for the sizing of an on-board energy storage system which includes the effects of potential energy due to elevation of the train, energy losses due to rolling resistance and aerodynamic drag as well as the efficiency of transferring energy to the storage system. However, due to the very low rolling resistance and aerodynamic drag experienced by trains as well as the general lack of undulations in railway lines, the rule-of-thumb proposed by Hayes et al. to predict the required storage capacity is deemed to be adequate for a first order approximation. The approximations for both the power rating and the energy capacity is also verified by González-Gil et al. who state that a general criterion for an ESS is that it must be able to absorb the braking energy during a sudden braking application (full braking power) to bring the vehicle to a standstill (2013).

Passenger trains typically have a ratio of powered- to non-powered coaches of 50-100%. Therefore, regardless of the length of train, each powered coach is in effect required to accelerate and decelerate itself as well as either one or two non-powered coaches. The passenger train considered is the South African 5M2A trainset which usually operates at a powered to non-powered ratio of 100%. The motor coach has a power output of 925kW (motoring and braking), has a tare weight of 60 tonnes and can carry 166 passengers, whilst a trailer coach has a tare weight of 30 tonnes and can carry 201

passengers. The mass of passengers is taken as 80 kg per person in accordance to the British Standard 13103 (2009).

The ratio of powered to non-powered rail vehicles in freight trains is much lower than for passenger trains at 2-10%, which in effect means that a locomotive has to accelerate and decelerate itself as well as 10-50 non-powered wagons when required. A diesel-electric locomotive, such as Transnet's Class 43 General Electric Locomotives, has a power output of 2500kW and weighs around 120 tonnes, whilst general freight wagons have a laden weight of 80 tonnes.

Based on the first rule of thumb explained above, the required charge and discharge rate of on-board ESS for both passenger and freight is equal to the rated power output of the powered vehicle. The required energy storage capacity is equal to the kinetic energy at cruising speed of the powered vehicle as well as the non-powered vehicles which it effectively must haul. This approach was implemented and the results are shown in Table 1-1.

Table 1-1: Inputs and Result of the First order ESS Requirements Approximation

	Freight Train	Passenger Train
Prime mover	Diesel-Electric Locomotive (2500 kW, 120 tonnes)	South African Class 5M2A EMU (925kW, 73 tonnes)
Non-powered vehicles	Freight Wagon (80 tonnes)	Trailer Coach (46 tonnes)
Powered to non-powered vehicle ratio	6%	75%
Operating speed	80km/h	100 km/h
Effective mass hauled per powered vehicle	1453 tonnes	179 tonnes
ESS required storage capacity	358.85 MJ	69.32 MJ
ESS required charge rate	2500 kW	925 kW
Number of annual charge cycles*	77 500	77 500
*Based on 85% utilization of rolling stock (310 days per year) at 250 charge-discharge cycles daily		

To match the ESS requirements established in Table 1-1 to an energy storage technology, a review of energy storage technologies that show promise for regenerative braking applications will be done to determine their characteristics. Only energy storage technologies that have reached an adequate technological maturity are considered. According to the research of Akli et al. energy storage technologies that satisfy these criteria are chemical batteries, supercapacitors and flywheels (2007).

Electrochemical batteries (referred to as batteries from here on) is a well-established energy storage mechanism that stores energy in chemical form by means of reversible electrochemical reactions (González-Gil, et al., 2013). Depending on the electrode materials and electrolyte solution types, batteries can exhibit a wide range of characteristics. Common battery types are Lead-Acid, Nickel-based and Lithium-based. Of these, based on their energy- and power densities as well their useful life (number of charge-discharge cycles they can perform), Lithium-based batteries are the most suited for ESSs in hybrid vehicles and regenerative braking systems. Lithium based batteries have been

successfully commercialised as an ESS in hybrid road vehicles such as the Toyota Prius as well as electrically driven vehicles such as the Tesla Model S and the BMW i8 and i3. Although batteries offer a high energy density their power density is relatively low, especially during charging. Batteries also suffer from a relatively short useful life in terms of number of charge-discharge cycles, especially when the depth of discharge is high.

Supercapacitors, an energy storage technology that has been commercially matured in recent times, are high capacity electrochemical capacitors that store energy in an electrostatic field. Due to the mechanism of energy storage, supercapacitors have very low internal losses and are therefore very efficient (González-Gil, et al., 2013). These storage devices can handle high charge and discharge rates and have a lifetime of up to a million charge-discharge cycles making them a promising option for energy storage in the rail environment (González-Gil, et al., 2013). These storage devices have a relatively low energy density however and suffer from relatively high self-discharge rates (González-Gil, et al., 2013).

Flywheels are mechanical energy storage devices that store kinetic energy in a rotating mass. The amount of energy stored in a rotating mass is proportional to the mass moment of inertia of the rotor as well as the rotational velocity squared. This means that high energy density in flywheel ESSs can be achieved at high rotational velocities. Flywheels exhibit high power densities as there is no real limit to how quickly the rotational velocity of the flywheel can be increased or decreased and can be designed to withstand an almost infinite number of charge-discharge cycles, unaffected by depth of discharge. These ESSs typically suffer from high self-discharge rates due to friction and drag losses but advanced bearing technologies and operating the flywheel in an evacuated chamber can greatly reduce these losses. Either an electric motor or mechanical transmission can be used to control the flow of energy to and from a flywheel, with the latter exhibiting extremely high efficiencies. Flywheels have been implemented as an ESS in hybrid road vehicles including busses as well as off-highway excavation vehicles (Torotrak Group, 2016).

To compare and select the most appropriate energy storage technology, it must be established what the most important performance characteristics are for the specific application. The primary objective of the on-board RBS that we are investigating is energy savings, which implies that the amount of energy captured and returned to the vehicle must be maximised. To maximise the amount of energy captured it is important that the energy storage system has an adequate power rating to capture (charge) and deliver (discharge) energy at the required rate during braking and motoring operations as well as provide a large enough energy capacity to most of the available braking energy. As weight and volume constraints play a big role in on-board energy storage, the density of the above two parameters (power and energy capacity) are of critical importance. In the research by Van der Meulen and Moller as well as Gonzalez et al. these two factors were also found to be essential and decisive (2013, 2014). Further important factors that influence energy savings are the efficiency of the energy storage technology as well as the self-discharge rate. These factors dictate what portion of the available braking energy is returned to the train and therefore regarded as important factors when evaluating energy storage technologies.

The durability of an ESS is another important parameter to take into consideration as it plays a big role in the lifecycle cost of the RBS. On-board ESSs on passenger trains could see between 50 000 and 300 000 load cycles per year, illustrating how important the durability of the ESS is (González-Gil, et al.,

2013). If the ESS requires replacing periodically throughout the life of the RBS, the costs involved with doing so will drive down the financial savings produced by the RBS. Finally, the capital cost of the energy storage technology needs to be considered as well. The capital cost in conjunction with the durability will determine the total cost of the ESS for a certain service life.

Table 1-2: Summary of the Characteristics of ESS Technologies

	Lithium-Ion Batteries	Lithium-polymer Batteries	Super-capacitors	Flywheels
Energy Density (kWh/m^3)	100-500	100-200	2–30	4–80
Energy Density (Wh/kg)	100- 200	100-200	2.5–15	4 –50
Power Density (W/kg)	100 - 500	100 -1000	500 - 5000	1000 - 5000
Charge-Discharge Efficiency	77.5 – 95	70 – 95	90 - 95	92.5 - 96
Self-discharge Rate (daily % of capacity)	0.1 - 0.3	0.15	20 - 40	100 - 500
Durability (number of cycles)[1]	1000-10 000	1200-1500	50 000-10^6	200 000-10^6
Capital Cost (R/kWh)[2]	7500–37 500	13 500–19 500	4500–30 000	15 000-75 000

[1]Number of cycles at 100% depth of discharge. [2]Based on an exchange rate of R15/1$. Sources: (González-Gil, et al., 2013, p. 4), (Vazquez, et al., 2010, p. 3882), (van der Meulen & Moller, 2014, p. 691).

A summary of the characteristics of the above mentioned ESS technologies is provided in Table 1-2. By matching the requirements outlined in Table 1-1 to the ESS characteristics of Table 1-2, the expected mass and volume of the ESS for each technology type can be determined. In cases where the characteristics in Table 1-2 were specified as a range, the mean value was used to determine the ESS parameters. For each ESS type, the mass and volume can be calculated by using either the power- or energy density with the corresponding power or energy requirement. To determine which one of the densities and corresponding requirement is the limiting factor, the mass of the ESS was calculated using both power- and energy density ($m_{ESS\text{-}power}$ and $m_{ESS\text{-}energy}$) as shown in equations (1-1) and (1-2) from density principles. The density yielding the highest ESS mass is the limiting factor. The energy requirement ($E_{required}$) refers to the required energy storage capacity given in Table 1-1 and the power requirement ($P_{required}$) refers to the required charge rate in the same table. The energy- and power density (ρ_{energy} and ρ_{power}) is taken from Table 1-2. If the energy density is found to be the limiting factor, the ESS volume is calculated using equation (1-2), using the volumetric energy density found in Table 1-2. If the power density is found to be the limiting factor, it would imply that the energy capacity of the ESS would have to be larger than the required capacity as the ESS will be sized based on power requirement. As the volume of the ESS is related to the energy capacity, the resulting capacity must be calculated and from this the volume can be determined with equation (1-3). The results are shown in Table 1-3.

$$m_{ESS-power}(kg) = \frac{E_{required}\ (Wh)}{\rho_{energy}\left(\frac{Wh}{kg}\right)} \qquad \textit{(1-1)}$$

$$m_{ESS-energy}(kg) = \frac{P_{required}\ (kW)}{\rho_{power}\left(\frac{kW}{kg}\right)} \qquad \textit{(1-2)}$$

$$V_{ESS}(m^3) = \frac{E_{required}\ (kWh)}{\rho_{power}\left(\frac{kWh}{m^3}\right)} \quad \textit{(1-3)}$$

Table 1-3: Characteristics of Various On-Board ESS Technologies

	Freight Train On-Board ESS Size		Passenger Train On-Board ESS Size		Limiting Factor
	Mass (kg)	Volume (m^3)	Mass (kg)	Volume (m^3)	
Lithium-Ion Battery	8333	4.17	3083	1.54	Power Density
Lithium-Polymer Battery	4545	4.55	1681	1.68	Power Density
Supercapacitors	11391	6.23	2200	1.20	Energy Density
Flywheels	3691	2.37	713	0.46	Energy Density
Average	**6990**	**4.33**	**1919.7**	**1.22**	-

With the required ESS energy capacity and charge rate for passenger trains being significantly lower than that of freight trains, the mass and volume requirements of the ESS for passenger trains are also significantly lower. For passenger trains, the average required volume and mass of an ESS is 1.22m^3 and 1919.7kg respectively. An ESS of this size could be accommodated in a motor coach without increasing the mass of the vehicle significantly (less than 3%) and without losing significant passenger capacity. In the case of flywheels being used as the energy storage medium, the volume requirement is a mere 0.46 m^3 and added mass in the region of 1% of the vehicle`s mass. This is not the case for freight trains however. Although the additional mass of 7 tons would not pose a problem, as mass is often added to locomotives to increase their maximum tractive effort, integrating an ESS with a volume of 4.33 m^3 (mean required volume) into a diesel-electric locomotive would be challenging as these locomotives have very limited vacant space available. Furthermore, the space and mass requirements identified may require further packaging and integration components, as well as the power converter component of the RBS, which would increase the mass and volume requirements further. This shows the difficulty with on-board energy storage for freight trains. Due to the low powered- to non-powered vehicle ratio, the kinetic energy of numerous vehicles have to be stored at a single location on-board the locomotive.

We can also evaluate the other important performance criteria of an on-board ESSs, efficiency and lifecycle cost, based on the information provided in Table 1-2. To evaluate the efficiency of the energy storage technologies the energy return on investment (EROI) measure is used. The EROI is defined as the ratio of the usable energy output over the energy input. The EROI is calculated as a function of time by combining the charge-discharge efficiency and the self-discharge rate of the energy storage technologies from first principles as shown in equation (1-4). The daily self-discharge rate (*SD*) as a percentage of energy capacity is found in Table 1-2. The losses due to self-discharge increase with the time fraction (τ) which represents time as a fraction of a 24-hour day. The EROI is influenced by the square of the (dis)charge efficiency (η_c) as the energy flow is subjected to this efficiency twice, once upon entry into the ESS and again as it exits the ESS. The results of this analysis are illustrated in Figure 1-1 and is also tabulated in Table A-1.

$$EROI(\%) = (1 - SD \cdot \tau) \cdot \eta_c^2 \qquad \textbf{(1-4)}$$

Flywheels exhibit the best EROI for storage times up to eight minutes after which supercapacitors have the best EROI. As 250 charge-discharge cycles are expected daily, the average cycle will take less than six minutes. Consequently, the efficiency over long time periods is not expected to be of critical importance for this specific application.

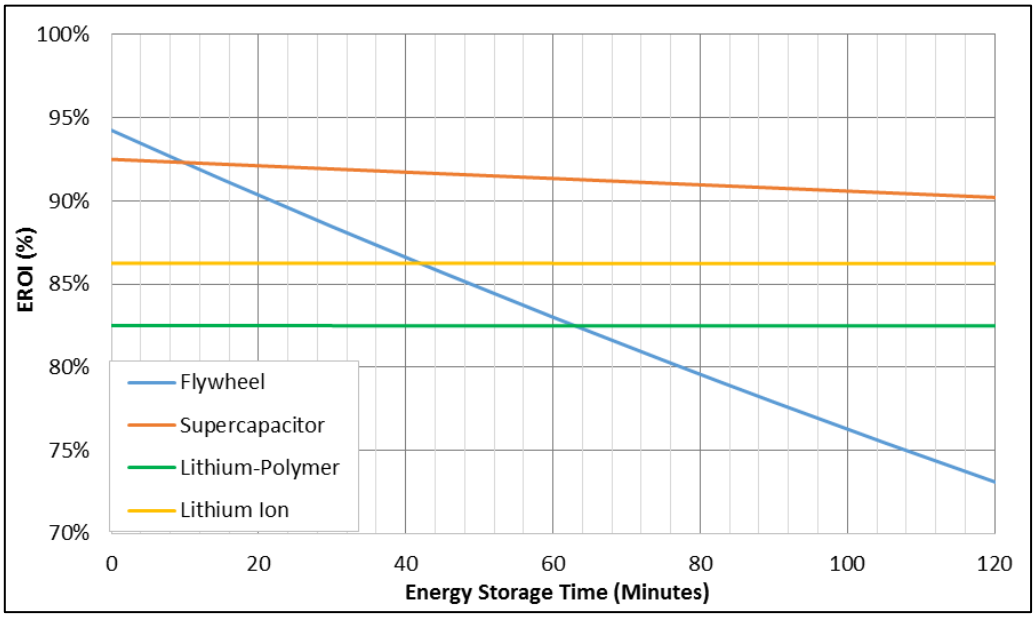

Figure 1-1: Return Efficiency of Various Energy Storage Technologies

As mentioned previously, the durability of the energy storage technologies and the initial capital cost can be used to calculate an indicative lifecycle cost for each technology. To do this, the capital cost per unit of energy capacity is divided by the durability of the ESS to calculate the cost per kWh cycle. These results are shown in Figure 1-2 and tabulated results can also be found in Table A-2. It was previously mentioned that for the ESS technologies with power density as their limiting factor for the sizing of the ESS, the energy capacity would be larger than required to meet the power requirement. As a result of this, the durability of the ESS will be extended as only a portion of the energy capacity would be utilised during operation. This is accounted for by multiplying the durability of the ESS as shown in Table 1-2 by the factor with which the ESS is oversized. Although this is a simplistic approach to modifying the durability, it will provide some insight into the life cycle cost of these technologies. From Table 1-3, this is the case for Lithium-Ion and Lithium-Polymer batteries and the factor by which these systems were oversized as well as their modified durability is shown in Appendix A.

The results highlight the longevity problems of certain energy storage technologies. Although lithium-ion and lithium-polymer batteries have lower initial capital costs than flywheels and supercapacitors, their low durability means that their cost per cycle is higher than that of flywheels and supercapacitors. This is especially the case for Lithium-polymer batteries as shown in Figure 1-2. It is obvious that with the significantly lower lifecycle cost of flywheels and supercapacitors, utilizing these energy storage technologies would be financially advantageous for on-board RBSs. It is also worth noting that by comparing the modified durability of the battery technologies to the annual number of charge cycles in Table 1-1, it reveals that lithium-polymer batteries would require replacing several

times throughout a year, and once a year for lithium-ion batteries, which would make these systems very maintenance intensive.

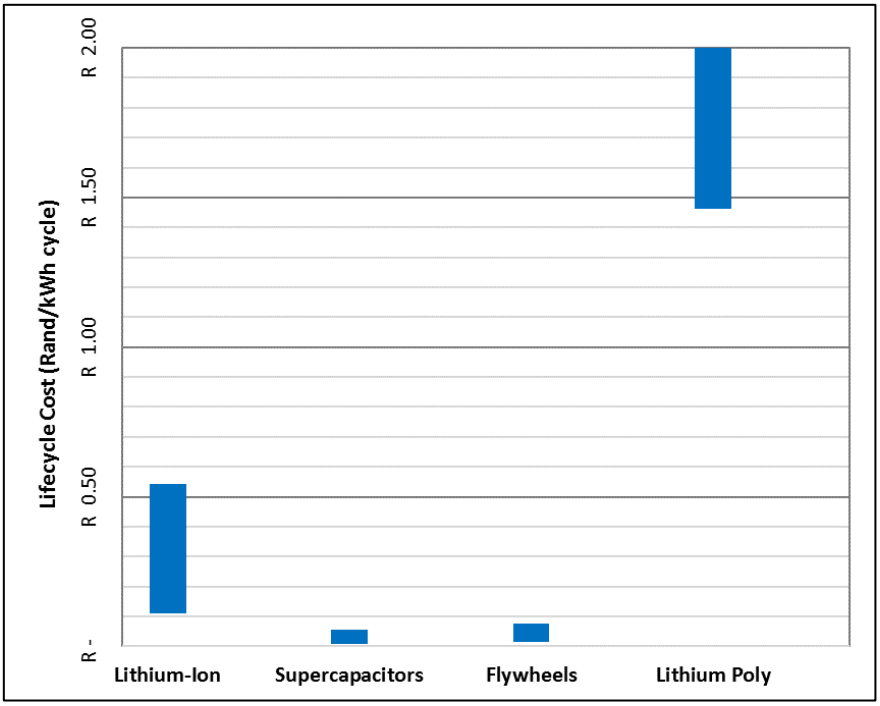

Figure 1-2: Energy Storage Lifecycle Cost

It is clear from the evidence provided above that based on densities, efficiency and lifecycle cost flywheels and supercapacitors appear to be superior to the two battery types for on-board energy storage. In terms of efficiency and lifecycle cost, flywheels and supercapacitors perform almost equally well, but as flywheel ESSs require significantly less space and mass than supercapacitors the technology promises to be the most suited for on-board RBSs in the rail industry.

1.3. Problem Statement and Project Objectives

The applicability of the two types of RBSs to different train types in the rail industry is summarised in Table 1-4. Wayside RBSs can be applied to electrified trains as the electrification system also serves as the transmission system to transport regenerated energy away from the train. This implies that for diesel trains an on-board ESS is required to perform regenerative braking. The analysis in section 1.2.2 showed that an on-board RBS can be applied to passenger trains that utilize diesel traction fairly easily. The analysis also revealed that implementing an ESS onto a freight locomotive that meets the energy capacity and power requirements is problematic due to space limitations on these locomotives. This conclusion was also reached in the work of Van der Meulen and Moller when they deemed on-board energy storage for heavy haul locomotives as ‘impractical’ (2014). The result is, as shown in Table 1-4, that currently no effective and optimal solution exists to perform regenerative braking on freight trains hauled by diesel traction. The implication of this is that 40% of the freight sector by energy consumption (section 1.1) has no feasible regenerative braking solution. This shortcoming is further magnified by the high cost of diesel energy compared to electrical energy as mentioned in section 1.1, with diesel making up 69% of traction energy cost globally.

Table 1-4: Applicability of Regenerative Braking Systems to Different Train Types

		Transport Type	
		Passenger Trains	**Freight Trains**
Traction Energy Source	**Diesel**	On-board RBS	No feasible solution
	Electricity	On-board RBS Wayside RBS	Wayside RBS

It was previously mentioned that the proposed distributed RBS would be suited to both electrified and non-electrified railways as well as both passenger and freight train types. The proposed system could therefore fulfil the needs of RBS for all train and traction types. If the distributed RBS proves to fulfil the needs of a RBS for freight trains hauled by diesel traction, it would tap into an untouched market for regenerative braking. For a RBS to be implemented by a commercial entity, it needs to be shown that these systems can deliver sufficient energy savings that would result in financial returns that justify the capital- and running cost of the system.

This study therefore focuses on the implementation of a distributed RBS on freight trains driven by diesel traction as this would be the most beneficial application of the proposed system. It was established in the previous section that a flywheel ESS proves to be the most suited to an on-board RBS and therefore the study will focus on using this energy storage technology for the proposed system.

The core aim of this study is to determine the technical and financial feasibility of a distributed RBS in the rail industry. The following research objectives were set in order to fulfil the core aim of the study:

1. Conduct a literature review in order to evaluate the current state of energy recovery systems using flywheels as the energy storage medium. The requirements for applying RBSs to freight trains are also investigated.

2. Quantify potential for energy savings with regenerative braking systems by analysing in-service train trip data.

3. Establish a concept design of the system through further developed of the proposed system, taking into account requirements and limitations of the rail vehicles, which will be used to determine the characteristics of the system.

4. Evaluate the performance of the system by simulation, which includes identifying a suited simulation method, modelling of the system and critical evaluation of the simulation results.

5. Develop a financial model and perform a cost-benefit analysis (CBA) of the system with the aim of providing concrete evidence for the economic feasibility of the proposed RBS.

With the successful completion of the research objectives stated above, this study contributes to the field by establishing the feasibility of regenerative braking on diesel-powered freight trains with on-

board energy storage in a distributed manner for the first time. The holistic methodology that is developed to reach the research objectives of this study is a further contribution made by this study.

1.4. Research Methodology

The following research methodology is followed in this study to meet the objectives set out above:

Chapter 2 presents the literature review conducted. An overview of the current applications and shortcomings of flywheel based regenerative braking systems is provided. Methods of integrating these systems into freight trains are discussed and the considerations that need to be accounted for in the integration process are established. The review goes on to discuss possible methodologies for simulating and quantifying the potential energy savings of the regenerative braking system.

Chapter 3 covers the development of a conceptual design of each subsystem of the distributed RBS and the integration of these subsystems, along with the accompanying analyses. Once the conceptual design is established, the system is characterised and serves as a baseline for the simulations to follow.

Chapter 4 details the simulation method used for evaluating the performance of the proposed RBS. The modelling process and procedures are outlined and is followed by a discussion and critical evaluation of the results.

Chapter 5 presents the financial model of the distributed RBS to evaluate the economic viability of the proposed system. The methods of analysis are discussed in detail as well as a discussion on the results.

Chapter 6 discusses the findings of the project and draws conclusions on the technical and financial feasibility of the distributed RBS. Conclusion are drawn from the findings of the study and provided in this section as well as suggestions for further work.

2. Literature Survey

2.1. Regenerative Braking Systems with Flywheel Energy Storage

Flywheels have long been an attractive prospect for energy storage in transport applications due to their almost infinite service life with very little maintenance required as well as their insensitivity to charge and discharge rates. Flywheels ESSs (FESS) traditionally suffered from low energy density, high self-discharge rate and presented safety risks however, which made them unsuited to most applications at the time. Most of the problems associated with FESSs (high self-discharge, low energy density and safety) have been overcome, or at least vastly improved, over the past two decades. The incorporation of high tech materials has increased the energy density, advancements in bearing technologies and operation in a vacuum environment have decreased self-discharge rates and through extensive testing and better containment their safety has been improved. The result of this is that flywheels are now used in various industries for energy storage purposes, and is a prime candidate for energy storage in the transport section as shown in section 1.2.2. A review of the current state of flywheel ESS applications will follow focusing on transport applications.

Important characteristics that will be considered when reviewing flywheel ESS applications include information regarding the flywheel- rotor, bearing system and enclosure. The transmission type and configuration as well as the system energy capacity, power rating and size will be reviewed where the information is available. RBSs can be configured either as series- or parallel- hybrid systems. In the parallel configuration, both the primary- (prime mover) and secondary- (FESS) energy sources can deliver power to the wheels of the vehicle (Druten, 2001; Berkel, et al., 2014). In the series mode, only the flywheel ESS is connected to the wheels and therefore all wheel power is delivered through the secondary energy source (Berkel, et al., 2014). The ESS is energised by the primary energy source as well as through regenerative braking in certain applications.

2.1.1. Automotive Industry

Within the transport sector, the automotive industry was the first in which flywheel RBSs were commercialised. The application of FESS to automotive vehicles has also been the subject of extensive research in the literature over the past two decades. Some of the main focus areas of previous research includes optimization of the system topology and flywheel size (Berkel, et al., 2014; Druten, 2001; Thoolen, 1993; Kok, 1999; Read, et al., 2015) as well as control methodologies (Vroemen, 2001). These papers, amongst others will be reviewed in detail in the following sections.

Flybrid Automotive, acquired by Torotrak Group in, commercialised a flywheel RBS in 2009 for racing cars (Formula 1 and Le Mans), passenger vehicles (Volvo Car Company), commuter busses (WrightBus) and off-highway (construction) vehicles (Torotrak Group, 2016). The Flybrid system utilises a composite flywheel mounted on a steel rim that can spin up to 60 000 rpm on its roller bearings. Various flywheel sizes have been used in the system depending on the application, ranging from 195 mm to 240 mm in diameter and 5.2kg to 8.5kg in mass. The flywheel is housed in a vacuum enclosure to reduce drag losses. The system utilises a mechanical power converter in which the flywheel shaft is connected to a transmission consisting of a toroidal CVT and clutches, which in turn is connected to the vehicle's primary transmission in a parallel configuration (Berkel, et al., 2014). The system can store 590 kJ of energy and weighs only 25kg. GKN Hybrid Systems, formerly Williams Hybrid Power,

developed a RBS that utilises a composite flywheel with magnetic bearings that spins up to 45 000 rpm in a vacuum enclosure (GKN Land Systems, 2015; Williams Grand Prix Engineering Limited, 2014). The RBS uses an electric motor integrated into the flywheel as its power converter which converts electrical energy to mechanical energy and vice versa as required. The GKN flywheel RBS has been utilised in racing cars (Formula 1 and Le Mans), road cars (Porsche) as well as commuter busses (London buses).

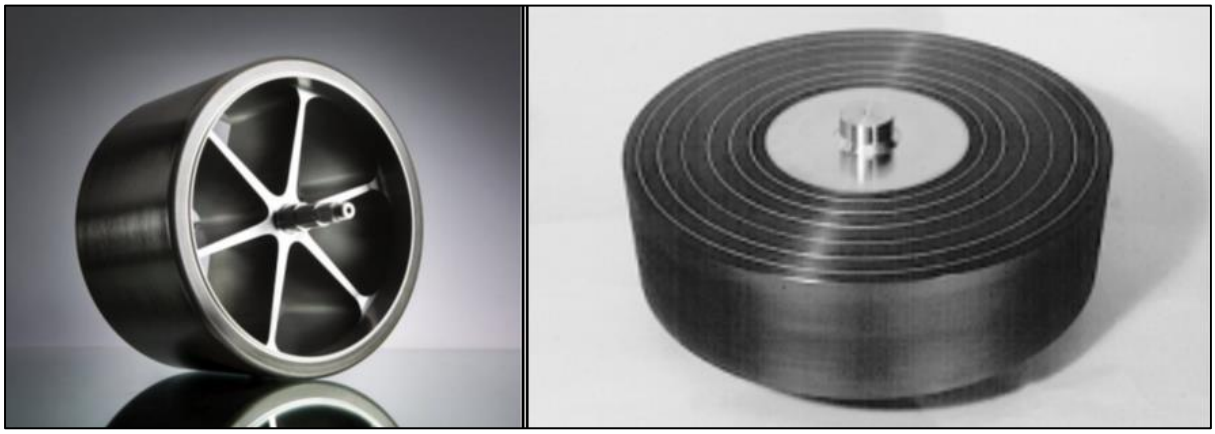

Figure 2-1: Left - Flybrid Automotive (Torotrak Group) Carbon Fibre Composite Flywheel. Right - University of Texas 440mm Diameter Composite Flywheel (Hayes, et al., 1998)

A FESS was developed by the Centre for Mechatronics at the University of Texas for application in a transit bus with the aim of reducing the size of the prime mover by performing regenerative braking. As shown in Figure 2-1, the flywheel is made up of cylindrical concentric composite rings and can store 2kWh of energy at a rotational speed of 40 000 rpm (Hayes, et al., 1998). The FESS utilises non-contacting magnetic bearings to minimize rotor heating and a permanent magnet motor-generator as a power converter.

2.1.2. Rail Industry

The Centre for Mechatronics was also involved in the development of an Advanced Locomotive Propulsion System (ALPS), a parallel hybrid RBS for a diesel locomotive for high speed passenger trains (Herbst, et al.). A 2MW, 360 MJ (100 kWh) FESS was used as the ESS. The flywheel (including casing) has a length and diameter of 1.9m and 1.6m respectively and weighs 8.6 tonnes. The flywheel is constructed of 14 concentric filament wound rings assembled with interference fits and has an operating speed range of 7 500 and 15 000 rpm. Rotational losses are minimised by a magnetic bearing system and a vacuum inside the enclosure of $1x10^{-3}$ torr (0.133 Pa).

In a study done by Spiryagin et al. an innovative RBS for diesel-electric freight trains is investigated (2015). The authors propose that one of the three locomotives hauling the train is converted to a FESS. The diesel engine, its cooling system, main generator and fuel tank are removed from the locomotive and replaced by a battery of 20 flywheels each with a power rating of 100 kW and storage capacity of 25kWh, resulting in an overall system rating of 2 MW and 500 kWh storage capacity with an overall weight of 52 tonnes. The flywheels operate at rotational velocities between 8000 and 16000 rpm. A simulation was performed to investigate the effectiveness of the proposed system. It was found that although the system would affect fuel savings in the region of 15% for the route analysed, the concept had flaws that need to be overcome to ensure reliable train operation. As the prime mover capability

of the train is reduced by the proposed system, it is a possibility that the train could stall on some of the inclines during the trip if the FESS was not sufficiently charged to deliver the required power, which would be unacceptable to any rail network operator. The design aspects of a FESS in the rail environment, considering the dynamic loads that the flywheels would experience and also exert on the train, were not addressed in this study and requires further work (Spiryagin, et al., 2015). The financial feasibility of the proposed system was also not addressed at all in the study.

In 1979, the Federal Railroad Association (FRA) investigated the use of a FESS to enable regenerative braking on freight trains in the US (Painter & Barkan, 2006; Cook, et al., 1979). It was proposed that an additional rail vehicle with a FESS operate in conjunction with a switcher (shunting) while operating in train yards. The electricity generated during dynamic braking by the traction motors of the locomotive is transferred to the energy storage vehicle through jumper cables for storage until the locomotive requires power for motoring, at which time the energy is transferred back to the locomotive. The flywheel was made up of a multitude of alloy steel laminated discs and could store 4.5 kWh at its maximum rotational speed of 11 000 rpm. The FESS which made use of roller bearings operated in a partial vacuum inside the containment shield. The flywheel suffered from a self-discharge rate of 7.2kW when fully charged and roughly half of that at 70% charge, which is very high compared to modern flywheel systems. The investigation concluded that implementing the system was technically feasible but did not make financial sense (Cook, et al., 1979; Painter & Barkan, 2006). Several factors contributed to the findings in the FRA investigation. Firstly, implementing the system to shunting locomotives was the only operational scenario considered and it was determined that the potential for energy savings are minimal during these activities. This contrasts with long distance train operation where it has been shown that there is significant potential for energy savings. Secondly, due to the limitations in FESSs at the time, the inefficiencies of the power converting system, low energy density and high self-discharge rates diminished the potential energy savings.

A prototype series hybrid light passenger rail vehicle was developed by Siemens Transportation Systems in conjunction with the Centre for Concepts in Mechatronics (CCM) amongst others. (Ultra Low Emission Vehicle - Transport using Advanced Propulsion, 2005). The ULEV-TAP 2 roof mounted propulsion system utilizes a flywheel based RBS in conjunction with a diesel prime mover. A composite flywheel on roller bearings (with shock proof rolling elements) with a maximum speed of 22 000 rpm operating in a vacuum/safety containment can store 4 kWh of energy with a nominal power rating of 250 kW. The power converter used for this system is a permanent magnet motor-generator. As a testimony to the recent improvements made in FESSs, the ULEV-TAP 2 model that was completed in 2005 achieved a volume reduction of 75% and a weight reduction of 50% when compared to the ULEV-TAP 1 in a period of just 4 years.

More recently, Ricardo Engineering, Artemis Intelligent Power and Bombardier collaborated on a project named DDflyTrain in which they equipped a DMU with a FESS developed over seven years by Ricardo called the TorqStor. The Torqstor has a 21kg filament wound composite rotor with a diameter of 280 mm that spins at up to 45 000 rpm and can store 1.25 KWh of energy. Ricardo developed an innovative magnetic coupling to the flywheel which makes it possible for the flywheel enclosure to be hermetically sealed during production with a permanent vacuum in which the flywheel can operate. The digital displacement pump technology of Artemis Intelligent Power is used as the power converter for the RBS. The consortium predicted that these systems could be introduced to the Bombardier fleet as early as 2017.

2.2. The Distributed Flywheel Based Regenerative Braking System Concept

In chapter 1, it was stated that the primary objective of this study is to establish the feasibility of a distributed regenerative braking system for freight trains proposed in a patent titled 'Regenerative Railway Braking System' filed by Transnet SOC. In this section, the proposed concept is discussed in further detail

In the patent application, a novel regenerative braking system for freight trains is proposed (Transnet, 2016). The patent proposes that regenerative braking systems (ESS and power converter) are installed in the bogies and mechanically connected to the wheel axles of the non-powered vehicles (wagons) in freight trains. Figure 2-2 illustrates the proposed location of the RBSs on freight wagons by means of a red design envelope. There is no traction equipment installed in the bogies of wagons, in contrast to locomotive bogies, which means that there is fair amount of space available to install a RBS in these bogies. Figure 2-3 shows a typical non-powered wagon bogie, the available space for integrating a RBS is shown as a yellow design envelope and it is observed that two RBSs can be installed in each bogie. The design envelope has a volume of 0.44m^3. The equipment would be mounted to the wagon axles and bogie, similar to that of the traction equipment in locomotive and motor coach bogies. Although the change in axle load and dynamics as a result of the RBS is not considered explicitly, the assumption is made that due to this being standard practice for locomotive and motor coach bogies the axle loads and dynamics can be addressed using existing methodologies. As multiple energy recovery units can be installed in each wagon, a single train may be equipped with up to a couple of hundred of these systems distributed throughout the train. The large number of units installed on a train means that each individual ESS will be small compared to conventional RBSs in the rail industry.

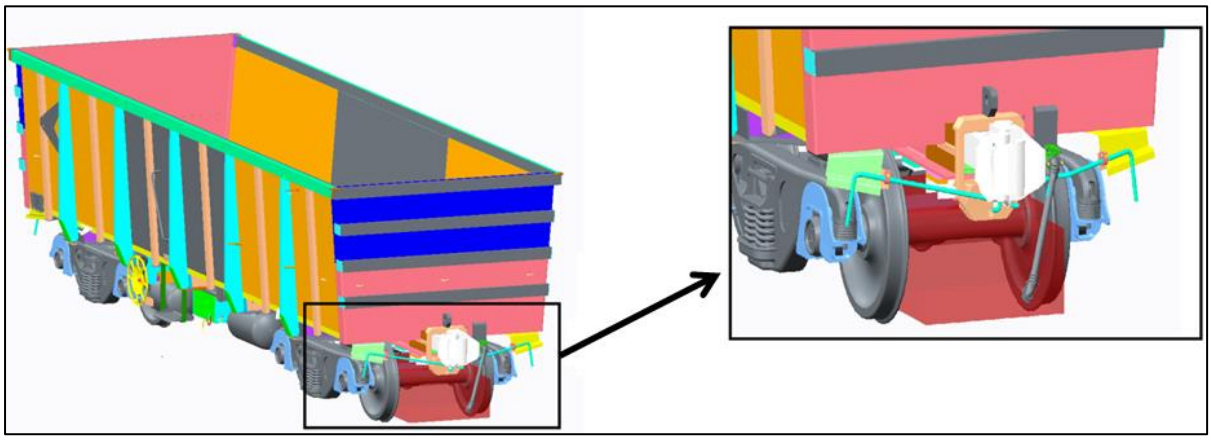

Figure 2-2: Proposed Location of Regenerative Braking Systems on Freight Wagons

The research conducted in section 1.2.2 and 2.1.2 revealed that existing RBSs in the rail industry are located at or close to the prime mover of trains as they usually exploit the electricity generated by the traction motors of trains during dynamic braking resulting in a central ESS. It was also shown in section 1.2.2 that this approach is problematic for freight trains due to the large amount of energy that needs to be stored at a single location. The proposed distributed RBS is distinctly different from existing RBSs in the rail industry in that it is not located at the prime movers of a train, the result of which is a decentralized ESS and regenerative braking is performed throughout the length of the train, as illustrated in Figure 2-4.

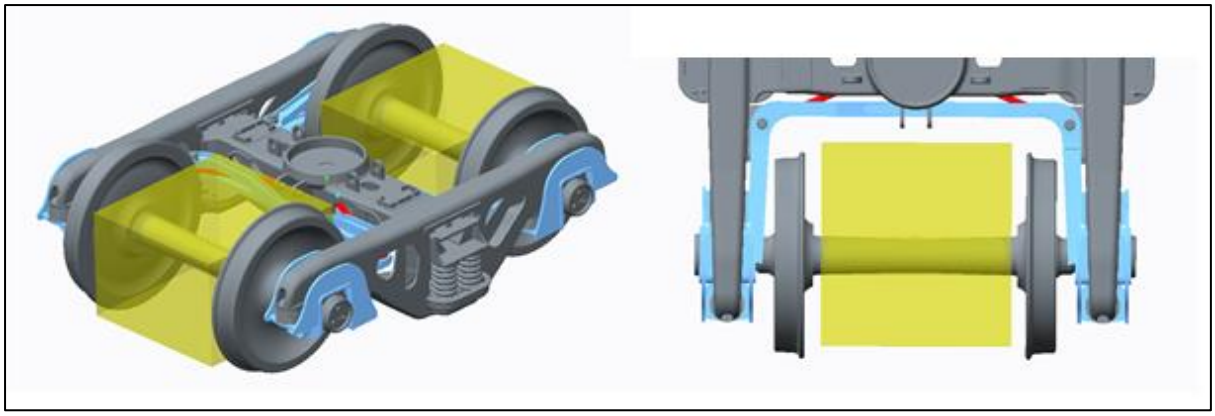

Figure 2-3: Available Space for a Regenerative Braking Unit in a typical Wagon Bogie

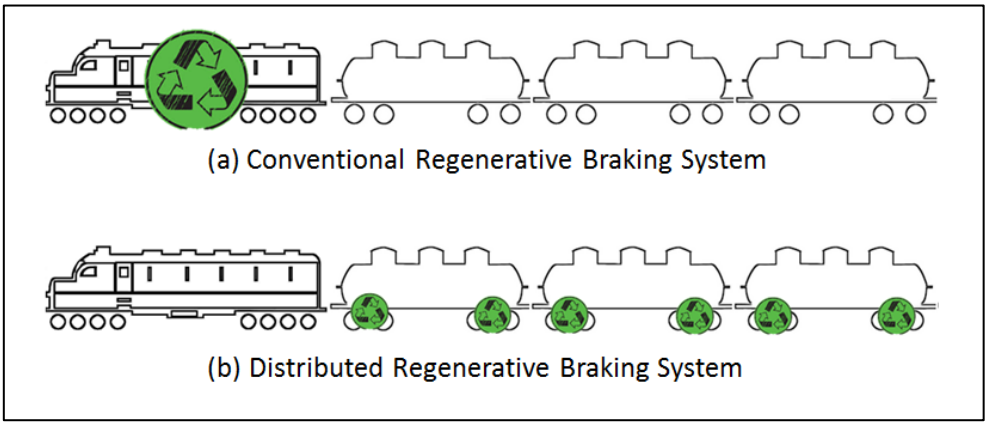

Figure 2-4: Distributed Regenerative Braking System Illustration

The system is also unique in that it does not capture the energy generated during braking through the traction equipment of the prime mover. Installing regenerative braking units in the bogies of wagons enables these vehicles to capture braking energy by applying braking traction, store the energy and deliver the energy back to the train by providing tractive effort on the wagon. As a result of this, the regenerated energy is never transmitted to the locomotives on the train as tractive effort is distributed throughout the length of freight trains which was not possible before. Therefore, by the definition established in 2.1, a train with the proposed distributed RBS will be a parallel hybrid train as both the primary energy source (locomotives) and secondary energy source (distributed RBS) are connected to the train wheels and can provide tractive effort.

Although the patent is not confined to a specific embodiment of a RBS, the patent envisions that the RBS be flywheel based with a mechanical power converter. This would mean that the regenerated energy is never converted from the mechanical domain throughout the energy recycling process, thereby avoiding the losses associated with the conversion of energy between domains. It has also been shown in section 1.2.2 that flywheels possess the best characteristics for energy storage in transport applications when compared to other energy storage technologies.

Section 1.3 explained that existing RBS technologies are not suited to freight trains hauled by diesel-electric locomotives and that no feasible way of recovering brake energy could be found for these train types. The distributed RBS covered in this section shows potential to overcome the limitations

that existing RBS technologies have and present a feasible way to perform regenerative braking on freight trains hauled by diesel-electric locomotives.

2.3. Simulation Methods

Simulation is a key tool that will be used to reach the research objectives of this study. Simulation models are used to both generate the requirements for and validate a flywheel based RBS for application in freight trains. For this study, a simulation method will be required to simulate two interacting systems; the train system and the RBS. In this section, a short review of simulation methods used in applications similar to this study will be conducted followed by a discussion on the methods to identify the most appropriate simulation approach for our study.

A simulation method used in two studies for flywheel RBSs in the automotive industry was found in the literature. In the work of Berkel et al., a method for optimising RBSs with FESSs through simulation for motor vehicles is described (2014). The power flows of individual components were modelled and combined for various RBS topologies and simulated. Simulations of certified driving cycles in combination with a costing model was used to determine the optimum system topology and ESS size that results in the best payback period. In research by Kok, a vehicle with a FESS hybrid propulsion system is optimised by means of simulation (1999). A computer simulation model based on the energy flows in the hybrid propulsion system was created. The energy flows and the functionality of the driveline was captured by a set of non-linear differential equations. The mission of the simulation was defined by a vehicle speed profile from which the required torque from the propulsion system is determined throughout the simulation. In the study, the simulation model was used to optimise both the energy management system as well as the components of the driveline. Kok also explains that to accurately evaluate energy consumption for a trip, the energy balance of the system must be the same at the start and the end of the trip. It is therefore important that the SOC of the ESS at the start and finish of the trip be considered when calculating the energy consumption for the trip.

Simulation methods found for applications in the rail industry predominantly involved simulating the train and the RBS separately. In the work of Hillmansen and Roberts, a simulator was developed to determine the duty cycle (power curve) for passenger trains that operate on non-electrified railway lines (Hillmansen & Roberts, 2007). The simulator utilized a kinematic model of the rail vehicles that was solved for a specific train route representative of typical passenger train operations. The power curve was then used as an input to a simulation of a generic series hybrid propulsion system to determine the potential energy savings through regenerative braking and load-levelling. No specific energy storage device was optimised in this study and it was suggested that this should be considered in detail in future work.

A similar simulation method is explained in the work of Sun et al. in which differential equations were derived that represent the longitudinal train dynamics of a freight train, named the Centre of Railway Engineering Longitudinal Train Simulation (CRE-LTS) (2013). The simulator receives information regarding the train setup and operating environment and runs through a specified route for which it provides various output parameters, amongst others the locomotive tractive effort. The locomotive tractive effort in combination with the train speed is used to calculate the power requirement (mission power curve) for the specific route. The power curve is then subjected to analysis to evaluate the potential for hybridisation. A similar approach is taken in the work of Wu et al. but with a different

longitudinal train dynamics simulator, Train Dynamics and Energy Analyser/Simulator (TDEAS) developed by the State Key Laboratory of Traction Power in China (Wu, et al., 2014). Another example of this simulation method is found in a study on the sizing and energy management strategy of a RBS for a locomotive by means of simulation (Jaafar, et al., 2009). A system modelling approach was used to model the power flow through each component of the hybrid propulsion system. By combining these power flow models of the components, the system could be simulated as a whole. The mission for the simulation was defined by the power curve and performed for two different energy management strategies. The energy management strategies were evaluated based on their ability to meet the power requirement as well as their utilization of the ESS capacity. Generic software for train energy simulation is also available such as the Association of American Railroads (AAR) Train Energy Model as was used by Painter and Barkan in their studies on the feasibility of regenerative braking on freight locomotives (2006). The software simply allows the user to determine the power requirement and energy consumption of a train for a certain train route.

Only one case was found in the literature where an integrated simulation of both the train and the RBS is used. Spiryagin et al. made use of a system modelling approach to model the energy flows of a hybrid propulsion system for freight trains using Simulink (2015). The train speed profile for a certain route served as the simulation mission and a longitudinal train dynamics model is used to determine the required tractive effort from the propulsion system at each time step. When compared to actual performance of locomotives on train routes, simulation programs have been found to give results that correlate well.

From the information provided above, it be can be deducted that to simulate the train system, a longitudinal train dynamics simulation is required to determine the power and energy requirements for a train on a specified route and duty cycle. A simulation model of the hybrid propulsion system must represent the functionality and energy characteristics of each component in the RBS and receives the train power requirement as an input. The hybrid propulsion system also requires a control strategy and the method of simulation must be able to capture the control strategy.

In the above-mentioned studies involving simulations of train systems and RBSs, two studies utilised a system modelling approach to model the hybrid propulsion system (Jaafar, et al., 2013; Spiryagin, et al., 2015). A study on the optimisation of FESSs was found that also utilized system modelling to perform simulations (Read, et al., 2015). The authors state that dynamic system modelling is highly suited to power-train simulation, and would therefore be an appropriate simulation method for our investigation. Various software packages exist with which system modelling of physical components can be implemented. These software packages allow the user to model complex physical systems consisting of components spanning across multiple domains such as mechanical, electrical, hydraulic, pneumatic, and control (Modelica, 2016; Mathworks, 2016; Siemens, 2017). Some of the software packages available include Modelica (non-proprietary), Simscape by Mathworks and LMS Amesim by Siemens.

2.4. Analysing Freight Train Trips

In this section, methods for analysing the freight train routes that will serve as the mission profile for our simulations are investigated. Two representative general freight train trips in South Africa will be investigated for this study for which in-service data was available for this study. General freight is

characterised by axle loads that generally do not exceed 20 ton per axle as opposed to heavy haul lines where axle loads can exceed 30 tons per axle. The reason for selecting general freight trains for this study is that these trains are usually hauled diesel electric locomotives which is the focus area of this study. Heavy haul lines are greatly utilised and therefore justifies electrification infrastructure in most cases. The first trip to be investigated runs from Phalaborwa to Richards Bay in South Africa and the second trip is from Transnet's inland container depot in Johannesburg to Durban Harbour. Further details on the two trips are shown in Table 2-1.

Table 2-1: Train Trip Information

	Trip 1	**Trip 2**
Route	Phalaborwa to Richards Bay	Johannesburg to Durban
Distance	720.3 km	644.2 km
Time	14.21 hours	15.3 hours
Train Setup	5 Locomotives 80 Wagons	4 Locomotives 50 Wagons

To predict the potential savings through regenerative braking on these freight trains hauled by diesel-electric locomotives, the mission power curve, which represents the power required from the locomotive consist (motoring and braking) to haul the train throughout the trip, is required. In the previous section it was mentioned that the power curve can be determined with a longitudinal train dynamics simulator for a specific route and specified speed profile. Alternatively, operational data from in service trains can be used to calculate the power delivered by locomotives throughout train trips. The operational data is gathered from in service trains by means of a test coach. A test coach is an instrumented, non-powered rail vehicle that travels with in-service trains with the purpose of gathering data from each locomotive in the train to determine whether the locomotives are functioning as they should. The data recorded by test coaches include speed, locomotive coupler force, elevation, tractive effort, traction motor currents and voltages, brake pipe pressure and 'notch' selected by driver for braking or motoring.

From the measured data fields, the power curve (mission power) for the trip needs to be calculated. The first method that can be used to calculate the power versus time is by using the voltage and current readings of the traction motors to calculate the locomotive consist power (P_{VI}) using equation (2-1) where n_{TM} is the number of traction motors, $V_n(t)$ is the traction motor voltage, $I_n(t)$ is the traction motor current and TS, traction signal, is either -1 or 1 when the locomotives are braking or motoring respectively.

$$P_{VI}(t) = \sum_{0}^{n_{TM}} V_n(t) \cdot I_n(t) \cdot TS \qquad \textit{(2-1)}$$

The second method involves using the coupler force of the last locomotive as well as the train speed to calculate the power curve (P_{FC}) using equation (2-2) where F_C is the coupler force and v is the train velocity.

$$P_{FC}(t) = F_C(t) \cdot v(t) \qquad \textit{(2-2)}$$

Lastly, the notch data for the trip can be used to calculate the power curve (P_N) by using equation (2-3) where P_{Loco} is the locomotive power rating, N_{locos} are the number of locomotives in the consist, n(t) is the selected notch and n_{max} is the highest notch (full power).

$$P_N(t) = \frac{n(t)}{n_{max}} \cdot P_{Loco} \cdot N_{Locos} \qquad \textit{(2-3)}$$

To compare the three methods mentioned above, the mission power was calculated from measured data for a train travelling between Phalaborwa and Hoedspruit in the Limpopo province of South Africa. The trip is 50km long and takes the 80-wagon train hauled by three Transnet Class 39 locomotives just over two hours to complete. The results obtained from equations (2-1) to (2-3) are shown in Figure 2-5. The figure shows that although the power calculated from the coupler force and the traction motor voltages and currents match fairly well, the power from the coupler force is lower during motoring. This can be attributed to the fact that the power calculated from the traction motor voltage and current does not account for the efficiencies of the traction motors and final drives. During braking, the power calculated from the coupler force exceeds the power calculated from the voltages and currents on several occasions, this might be scenarios where the train driver applied the locomotive friction brakes to supplement the dynamic braking effort and thereby increasing the braking force without an increase in the traction motor voltages and currents. The power calculated from the locomotive notch matches that of the other two methods reasonably well during motoring, the same cannot be said during braking.

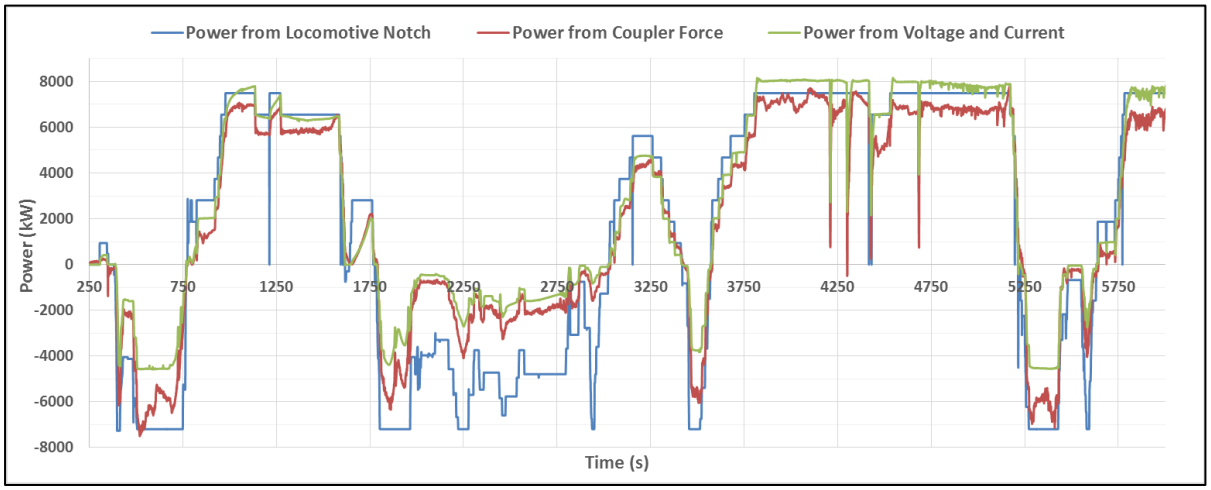

Figure 2-5: Mission Power Calculation Method Comparison

To further evaluate the different calculation methods further, the energy consumption for the two-hour trip can be calculated from the mission power curve using equation (2-4). This allows us to investigate the cumulative effect of the variations between the power curves. The results are shown in Table 2-2, the braking and motoring energy consumption were calculated separately by using a simple if statement to check whether the power at each time step is smaller or greater than zero.

$$E = \int_0^t P(t)\, dt \qquad \textit{(2-4)}$$

The observations made from Figure 2-5 are verified by the data in Table 2-2. We see that the energy consumption for the three different methods agree reasonably well, and that the energy consumption calculated from the coupler force gives the lowest results as it incorporates the efficiencies of the locomotive traction equipment and therefore is a measure of the actual energy applied to haul the freight. The braking energy calculated from the coupler force represents the braking effort of both the traction motors as well as any potential braking from the locomotive friction brakes and is therefore larger than the energy calculated from the traction motor voltages and currents. It can be concluded that the power calculated from the coupler force most accurately represents the power required to haul the train as it incorporates the efficiencies of the locomotive traction equipment as well as the braking effort of the locomotive friction brakes. It should be noted however that the coupler force of the last locomotive in the consist is not always recorded during testing and in these cases the power will be calculated from the traction motor voltages and currents. The results obtained from this method are reasonably accurate and provides conservative results in that it does not overestimate the available braking energy which would result in unrealistic potential energy savings.

Table 2-2: Mission Power Calculation Method Comparison Results

Parameter	Calculated from Coupler Force	Calculated from Voltage and Currents	Calculated from Locomotive Notch	Average
Motoring Energy Consumption (kWh)	8277.4	9364.3	9738.4	9126.7
Braking Energy Consumption (kWh)	-1733.1	-1212.1	-3021.1	-1988.8

With the mission power curve of a trip known, the energy characteristics of the trip can be calculated to determine the potential energy savings for the trip. As shown in equation (2-4), by integrating the power curve with respect to time the energy consumption and braking energy for each time step in the trip can be obtained. The energy capacity of each motoring and braking instance can also be determined and used to establish the required ESS capacity.

To determine the potential for energy savings by a hybrid propulsion system for a specific route, it is also necessary to know what the primary mechanism of energy saving will be. Two means of saving energy in vehicles with hybrid propulsion systems exist namely regenerative braking and load-levelling. The regenerative braking mechanism of energy saving has been discussed extensively in chapter 1. The load levelling mechanism of energy saving aims to optimise the duty cycle of the prime mover by ensuring that it operates at its most efficient power output throughout the trip. This is done by selecting a prime mover that at its most efficient duty cycle delivers the average power requirement of the vehicle, and relies on the ESS to deliver the additional power when the requirement exceeds the average power. The ESS in turns receives the excess power at times when the power requirement is lower than the average power. Although both mechanisms of energy savings can be performed by most hybrid propulsion systems, different sizing techniques are used to optimise the ESS for the either regenerative braking or load-levelling. According to Berkel et al. (2014) the energy storage capacity is the key parameter to influence energy savings for mechanical hybrid systems and therefore it is critical that the correct approach to determining this capacity is used.

From the mission power curve of a route, several measures can be calculated which indicate the potential for energy savings on the route. For hybrid systems which provide both load-levelling and regenerative braking as its primary mission, the power hybridization potential factor (PHP = 1 – $P_{average}/P_{max}$) and energy hybridisation potential factor (EHP = 1 - $E_{average}/E_{max}$) provides insight into the potential benefit of the hybrid system for a specific mission profile (Sun, et al., 2013). In the case of hybrid systems that have regenerative braking operations as its primary mission, the mission self-sufficiency factor (SS (%) = $E_{braking}/E_{motoring}$) is a measure of the potential benefit of the system for the specific mission profile (van der Meulen & Moller, 2014; Sun, et al., 2013).

In terms of ESS sizing, a method for sizing the ESS of a series hybrid load-levelling system is found in the research of Akli et al. (2007). The mission power of the ESS is integrated with time to determine the relative level of energy the ESS throughout the mission. The difference between the maximum and minimum values on the relative energy curve yields the required energy capacity (Akli, et al., 2007; Sun, et al., 2013). The required power rating of the ESS is determined by the peak of the absolute of the mission power curve. A similar method is described in the research of Jafaar et al. (2013) but a saturated integral with an upper limit of zero was used so that only the discharge cycles were considered when sizing the ESS. This was done to ensure that the ESS, in a series hybrid configuration, is able to meet the energy requirements of the largest discharge cycle without oversizing the ESS for long charge phases.

For hybrid propulsion systems that primarily perform regenerative braking, a method commonly used in the literature to determine ESS capacity is to calculate the kinetic energy of the vehicle at its operating speed, as this will be the maximum energy that can be recovered during a braking event if potential energy is not considered (Barrero, et al., 2010; Hayes, et al., 1998; Chymera, et al., 2008). Another method for determining the required capacity of the ESS is to use the mission power curve to determine the energy capacity of each braking cycling. In a study on subway systems, the energy storage capacity was made equal to the energy capacity of the largest braking cycle using this method (Foiadelli, et al., 2006). In the research of Van der Meulen and Moller, a severe braking scenario was identified and the required ESS capacity was set equal to the braking energy capacity of the scenario (2014).

The distributed RBS considered in this study has the regenerative braking as its primary energy storage mechanism. Load-levelling systems require that the ESS be charged at times when the power requirement is below the average power which the prime mover will output throughout the trip. Due to the distributed nature of the system of interest, this would require motoring effort applied to the locomotive wheels while the distributed RBSs apply braking effort to provide the desired power. This method of transferring energy is expected to be inefficient and not yield adequate energy savings. It should also be noted that the proposed system would be installed to existing trains, which means that the prime mover size is adequate to meet the maximum power requirement. Applying load-levelling would result in the diesel engines of the prime movers to operate at lower loads and knowing that diesel engines exhibit poor efficiencies at lower loads, this is undesirable. It is rather desired that the diesel engine operates at higher loads for which it is optimised but for smaller time periods, which is what the regenerative braking system will aim to do.

As the parameters of each braking and motoring cycle in a trip can be calculated from the power curve as explained above, the percentage of the total braking energy that a RBS can capture can be

determined for a given ESS capacity. This method can be used to evaluate the utilization of an ESS for a range of capacities to aid in optimizing the capacity.

2.5. Designing Flywheel Based Regenerative Braking Systems

In this section, the important design considerations of RBSs that utilize flywheel energy storage systems (FESS) in mobile applications will be established based on findings in the literature. The kinetic energy stored in a flywheel is governed by Equation (2-5). The equation implies that the amount of energy stored in a flywheel can be increased by either increasing the mass moment of inertia, *I*, or by increasing the rotational velocity of the flywheel, ω. A high energy density is required for an ESS for mobile applications as has been explained in previous sections. To achieve this FESSs need to operate at high speeds, as the stored energy increases quadratically with rotational speed without requiring an increase in mass. Although an optimal flywheel geometry can also increase the energy density of the flywheel, the increase is not as significant as increasing the flywheel speed. It is therefore not uncommon for FESSs to operate at speeds of 40 000 – 100 000 rpm which can result in outer surface speeds as high as 1000 m/s (Hayes, et al., 1998; Ashely, 1996). We can therefore at this stage narrow our investigation down to only consider high-speed flywheels, as this is what is required for mobile applications.

$$E_k = \frac{1}{2} I \omega^2 \qquad \textbf{(2-5)}$$

Flywheels operating at high speeds require a different design approach to low speed flywheels, as high speeds pose serious challenges in terms of structural and thermal considerations as well as power losses in the ESS (U.S Department of Energy, 2003; Hayes, et al., 1998). The structural design of high-speed flywheels has been the subject of extensive research, with the main goal being to optimise the flywheel geometry to allow for higher rotational speeds and therefore increased energy storage density. This topic is addressed in the work of Herbst et al. which is focused on the design, manufacturing and testing of a 10MJ flywheel (1998). Design techniques are discussed that increase the energy density of the flywheel and mitigate the high stresses generated during high speed operation are discussed. Once such method involves constructing a flywheel out of concentric cylindrical rings that are press-fitted together (Hayes, et al., 1998; Krack, et al., 2011). This results in a radial preload that keeps the rings in contact with each other during rotation. The radial preload from press-fitting opposes the radial load created from the rotational forces, therefore resulting in a reduced stress state in the flywheel. Methods have been developed to use this preload between the concentric rings of a flywheel as a safety mechanism to avoid destructive failure of the flywheel. The preloads can be specified so that the radial stress between two rings goes into tension before the stress in the outer ring reaches the ultimate strength of the material (Hayes, et al., 1998). The flywheel designs are typically evaluated using finite element models. A comprehensive study on the optimisation of high speed flywheel rotor geometry is also found in the work of Krack et al. (2011). The authors confirm that for mobile applications, the flywheel design must be optimised for energy density. Design techniques that can be used to address the structural requirements of high speed flywheels, as well as the material selection to achieve as high as possible energy density are discussed in detail. In the work of Druten as well as Okou, more studies on the optimisation of the flywheel rotor

are found (2010; 2001). In the study performed by Okou, cost was the parameter for which the ESS was optimised.

Part of the structural optimisation of flywheels involves selecting the appropriate material, or combination of materials, for the construction of the flywheel. A closed form solution for the maximum energy density per unit-mass for a flywheel based on certain material properties is presented in the work of Spiryagin et al. (2015) and shown in Equation (2-6). The expression is based on the hoop stress that develops in a rotating thin walled cylinder. In the expression, S_{max} represents the ultimate tensile strength of the material (Pa), ρ is the material density (kg/m^3) and U_{max} is the maximum theoretical energy density (J/kg). The equation shows that materials with high tensile strengths relative to density will result in high energy density flywheels. For this reason, engineers have reverted to materials such as carbon fire composites as a solution which is now commonly used in high speed flywheels (Hayes, et al., 1998). Another benefit of composite flywheels is that they do not experience catastrophic failures as is the case when steels fractures in a brittle manner, but rather experiences delamination of the composite upon failure (Spiryagin, et al., 2015). The safety aspects of metal flywheels versus composite flywheels are also addressed in the work of Okou (2010) and Pichot et al. (1997). Pichot et al. state that one benefit of metallic flywheels is that the failure mechanisms of these flywheels are well understood based on a long history of operating experience, this is not the case for composite flywheels.

$$U_{max} = S_{max}/2\rho \qquad \textbf{(2-6)}$$

The second design aspect of high speed flywheels that was identified is the thermal design of the FESS, which is directly related to the power losses of the flywheel as the energy is converted to heat energy. It is well understood that the two main modes of power loss are drag losses and bearing losses as is discussed extensively in the literature (González-Gil, et al., 2013). The losses due to the drag forces develop as a result of the high surface speeds at the outer diameter of the flywheel which results in a torque on the flywheel opposing the rotation of the flywheel resulting in unacceptable energy losses and a high self-discharge rate for the ESS. The kinetic energy that is taken out of the flywheel is converted to thermal energy and is enough to cause overheating in the FESS to the point where the material properties of the flywheel are affected. This becomes especially problematic when the flywheel is constructed out of composite materials as their resin systems can be sensitive to temperature. Characterisation of the drag losses on the flywheel is a well understood subject and is covered in the work of Kok (1999). To remedy the above-mentioned problems, high speed flywheels operate in an enclosure with an evacuated environment (partial vacuum) (Hayes, et al., 1998; Murphy, et al., 1997). This vacuum is in the order of 0.1 Pa (Murphy, et al., 1997). Kok performed an optimisation study on a FESS of which the goal was to minimise the energy losses in the RBS with the use of models that define the energy characteristics of each component in the RBS (1999).

Despite the obvious requirement of being able to spin at very high speeds, selecting a bearing solution for high speed flywheels requires careful consideration. As the flywheel operates in a partial vacuum, heat transfer from the flywheel is for all practical purposes only by radiation. This means that the heat generated in the bearings due to losses, which is in turn conducted to the flywheel, must be kept to a minimum to avoid the flywheel heating up to unwanted high temperatures (Hayes, et al., 1998). As a result of this, as well as the desire to keep the self-discharge rate of the flywheel to a minimum,

extremely efficient bearings need to be used in a flywheel energy storage system. Other requirements of the bearing system include adequate stiffness to constrain the flywheel and ensure dynamic stability, long lifespan and sufficient loading capacity (Murphy, et al., 1997).

Two feasible bearing technologies are considered to be suited to flywheel batteries in the literature. The first is high speed roller bearings, similar to traditional roller bearings, with ceramic rolling elements and therefore also called hybrid roller bearings. These bearings are relatively cheap, are widely available and can usually be provided as an off-the-shelf solution. These bearings are however limiting in that they have a limiting speed, have significant losses at high speeds and suffer from wear which limits their lifetime. The second bearing technology suited to flywheel batteries is magnetic bearings. These bearings are non-contacting bearings and support the flywheel rotor with magnetic force so that the flywheel levitates around the bearing. As there is no contact between the flywheel and the shaft around which it rotates, there are almost no contact losses or wear involved. These bearing systems usually consist of a combination of passive and active bearings, the latter being adjusted by a control system based on the displacement of the flywheel. Conventional roller bearings are usually found in magnetic bearing systems as well to serve as backup to the magnetic bearings and in some cases to absorb the axial forces on the flywheel. Magnetic bearings are often not considered to be feasible for mobile applications due to their high cost, complexity and low force density (resulting in a heavier bearing system) which are all unfavourable characteristics (Thoolen, 1993).

In addition to performing the function of providing the vacuum environment for high speed flywheels to operate in, the enclosure must ensure that the FESS is safe during failure (Thoolen, 1993). As the risk of catastrophic failure of flywheels can never be completely eliminated, the containment system of the flywheel must be able to resist the impact of flywheel fragments in the case of flywheel failure (Pichot, et al., 1997). Designing a containment system for flywheels that is light and cheap enough is another technological challenge that must be addressed for flywheel RBSs (Ashely, 1996). The containment must be able to resist the impact of flywheel fragments if the flywheel was to fail. An overview of the various failure scenarios of composite flywheels is provided in the work of Pichot et al. (1997). As mentioned previously, a lack of operating history means that the failure of composite flywheels is not as well understood as that of metallic flywheels. To better understand the failure modes of flywheels which will enable the design of adequate containments, engineers conduct over speed (to failure) tests in heavily reinforced testing facilities (Ashely, 1996; Hayes, et al., 1998; Pichot, et al., 1997; Ricardo PLC, 2015).

Rotor dynamics is another design consideration of flywheels addressed in literature. An in-depth analysis of the dynamics of the flywheel is required to help ensure that critical speeds are avoided in the flywheel operational range, to minimise vibrations and dynamic loads and prevent instability of the flywheel (Thoolen, 1993). The dynamic characteristics of high speed flywheels result in two possible operating modes to avoid excessive vibration in the flywheel namely sub-critical and super-critical operation (Druten, 2001). In sub-critical operation, the flywheel operates at speeds below the first critical speed (natural frequency) of the flywheel. In super-critical operation, the flywheel operates at speeds that fall within two critical speeds of the flywheel. The approach to the design of the stiffness elements constraining the flywheel is different for these two modes of operation in an effort to manipulate the critical speeds of the flywheel to suit the specific mode of operation. Finite element analyses are commonly used for this analysis and can easily handle the complexity involved with regards to the mass, stiffness and damping elements that influence the dynamics. To perform

the dynamic analysis, both the dynamic flywheel model and the imposed loads on the flywheel should be characterised. An elaboration on the characterisation of the imposed loads on the flywheel is found in the work of Murphy et al. (1997).

The design considerations mentioned in the paragraphs are all primarily focussed on the energy storage component of the RBS. Upon investigation of these requirements it can be argued that there would be no significant variation in the requirements and methods used in the design of a FESS for application on automotive- or rail vehicles as both applications are for on-board energy storage in mobile applications.

A FESS requires a power converter that can synchronise the speed of the flywheel to the rotating speed to which power is being delivered to or received from. Adding or removing energy from the flywheel results in an increase or decrease in the flywheel speed respectively through the application of torque to the flywheel. The power converter is required to facilitate this continuous change in speed as well as induce and transmit the required torque. To do this in a controllable manner, a transmission with a continuously variable gear ratio fulfils the role of the power converter in the RBS (Druten, 2001; Read, et al., 2015). Components that can realise this are continuously variable transmissions (CVTs) of the electrical, hydraulic or mechanical type as well as torque converters, couplings and planetary gears. Alternatively, transmissions with a fixed gear ratio with sliding contact in a brake or clutch component can be used for this application as described in the work of Berkel et al. (2014) and Read et al. (2015).

Various mechanical CVTs of different types (push belt (V-belt) and pulley, toroidal etc.) are available commercially with efficiencies that are similar to those of standard stepped transmissions (Druten, 2001; Torotrak Group, 2016; Ultimate Transmissions, 2011). Planetary gears can be configured as fixed gear ratio transmissions or in an epicyclic configuration in which case it can provide a continuously variable gear ratio. Couplings can either be in the form of a fluid coupling or a mechanical clutch. These mechanisms are limited to a gear ratio of 1:1 but the torque being transmitted can be varied in these mechanisms. In mechanical clutches, the clutch pressure can be varied to manipulate the torque transmitted and in fluid couplings the same can be achieved by varying the oil level (Druten, 2001).

Electrical CVTs typically consist of an electrical motor-generator pair in a back to back configuration. The first motor is connected to the flywheel, acting as a motor when the flywheel speeds up and a generator as the flywheel speed decreases. The second motor is connected to the load which is the vehicle powertrain in the case of a RBS. The second motor will function opposite to the first motor; when the first motor is acting as a generator, the second motor will function as a motor converting the generated electricity to mechanical torque and vice versa. The use of power electronics allows the speed of the motors to be controlled independently (Druten, 2001). Methods have been developed to integrate the first motor and the flywheel into a single component which has benefits and drawbacks, and is used regularly for stationary FESSs as well as in the on-board FESS of GKN Land Systems (Hayes, et al., 1998; GKN Land Systems, 2016). Electrical CVTs have traditionally been bulky and inefficient and therefore not suited to transport applications (Druten, 2001). In recent times however, improved power electronics using IGBTs, incorporation of rear earth magnets and sophisticated methods of control have increased the efficiency and power density of these CVTs (Druten, 2001).

The efficiency of the power converter significantly affects the energy savings that an RBS can deliver and is therefore one of the critical requirements of a FESS transmission. In general, mechanical CVTs have superior efficiencies when compared to electrical CVTs (Berkel, et al., 2014). Another benefit of mechanical transmissions is that they are cheaper than their equivalent electrical counterparts (Berkel, et al., 2014). Based on the findings in the literature, mechanical transmissions promise to provide the best solution for the distributed RBS for freight trains and are the only transmissions that will be considered in the rest of the study.

The mechanical power converter of a FESS does not only consist out of a CVT transmission. The CVT is used in conjunction with a range of clutches, gear sets and/or torque summing devices that are required for the RBS to operate efficiently. It is therefore possible to vary the constituents as well as the configuration of a mechanical power converter for a FESS. Berkel et al. state that the topology of the transmission is one of the key parameters of a mechanical hybrid propulsion system and it can therefore be said that it will influence the feasibility of hybrid system significantly (2014). Several studies were found in the literature relating to this subject. In the work of Berkel et al., the topology of a hybrid propulsion system for an automotive vehicle is optimised for energy savings and cost. Druten focussed on the design of a transmission for a FESS used in an automotive vehicle to recycle the kinetic energy of the rotating engine and driveline components (Druten, 2001). Another study was found on the optimisation of a transmission for a RBS for an automotive vehicle, focussing on the impact that the flywheel size and the depth-of-discharge has on the transmission efficiency.

2.6. Financial Feasibility

Systems that aim to reduce energy consumption and improve energy efficiency, whether in the transport sector or any other, usually require a significant capital investment. The investor providing the capital will in turn demand a sufficient benefit or return from his investment. These systems must therefore be evaluated in economic terms to determine whether the resulting benefits justify the investments (Du Plessis, 2011).

There are three types of analysis that can be used to evaluate the financial feasibility of a project or system namely Cost-benefit Analysis (CBA), Economic Impact Assessment (EIA) and a Cost-effectiveness Analysis (CEA) (Beukes, 2013). CBA is used to evaluate the feasibility of a project by establishing the equivalent monetary value of benefits and costs based on decision making criteria. An EIA is broader in scope than a CBA and considers all conceivable economic variables that may affect the project. A CEA is used to establish the most cost-effective means of reaching a specified effect or outcome and is usually performed when it has already been decided that a certain project will be undertaken.

According to the Integrated Management Information Series by the Department of Environmental Affairs and Tourism (DEAT) there are two types of CBAs, these are financial- and social CBAs. Social CBAs are usually performed by government entities or public decision makers and accounts for factors such as the social merit of project or policies, unpriced project impacts as well as distorted and missing prices. These analyses consider the costs and benefits to a society as a whole to establish whether the project would benefit the society. A financial CBA is used in cases where the costs and benefits are in monetary form and evaluates the cost and benefits to an individual stakeholder. This type of CBA is used in both the public- and private sectors to justify equipment and technology investments, measure

life cycle costs as well as quantify hidden costs of a project. From these definitions, a financial CBA is the analysis most suited for the purpose of this study as the aim is to investigate the feasibility of investing in a regenerative braking system by a fleet owner or rail operator.

The outcome of a CBA presents the lifetime cost and benefit of a project as a single number which can be compared to a decision rule to determine whether the project is justified. The Integrated Management Information Series by the Department of Environmental Affairs and Tourism (DEAT) of South Africa provides a framework to perform CBAs from both industry and academic perspectives (DEAT, 2004). The framework prescribes the following steps for a CBA:

Step 1: Identify and define the project (system)

Step 2: Identify the consequences of the project (system)

Step 3: Determine the type of CBA and decision criteria

Step 4: Identify incidences of costs and benefits in income distributional terms

Step 5: Adjust costs and benefits using weight based on the existing and desired distributions (if appropriate)

Step 6: Discount the flows of cost and benefits and use the appropriate decision tool.

Step 7: Conduct a sensitivity analysis.

A similar process is defined by Beukes (2013) with an additional step for identifying which of the project consequences (or impacts) are economically relevant. Step 5 above is not included in the framework of Beukes and it is also mentioned in the DEAT framework that this step is not always considered to be in line with CBA best practice.

There are numerous decision rules that can be applied to a CBA to serve as a benchmark or target to indicate whether the project is feasible. Net Present Value (NPV) is calculated by discounting the net benefits (benefits – costs) using a discount rate over the life cycle of the project and total these discounted values to give a single value for the project as shown in equation (2-7). The benefits (B_t) and costs (C_t) for a certain time period (usually per annum) is discounted by the discount rate (i) which is compounded by the time into the project (t). The first requirement of the NPV criteria is that a project can only be acceptable if the NPV is positive (DEAT, 2004; Beukes, 2013). The NPV can also be used to compare two projects in which case the preferred project would exhibit the highest NPV. The shortcoming of using the NPV as decision rule is that it does indicate how efficient the input resources are used. If a larger project has the same NPV as a similar smaller project, this decision rule would not reflect that the smaller project is more efficient user of input capital and therefore this measure will favour larger projects. The NPV metric is synonymous to the Life Cycle Savings (LCS) which is also calculated as the present value of the savings (benefits – costs) over the lifetime of the system of interest (Du Plessis, 2011).

$$NPV = \sum_{t=0}^{n} \frac{\mathrm{B_t}}{(1+i)^t} - \sum_{t=0}^{n} \frac{\mathrm{C_t}}{(1+i)^t} \qquad \textit{(2-7)}$$

The Internal Rate of Return (IRR) of a project is the interest (or discount) rate which results in a NPV equal to zero and indicates the percentage return on the capital investment into the project as show in equation (2-8). A project is only justified financially if its IRR is higher than the discount rate, which could be equal to the interest rate at which the money could be invested or the borrowing cost for raising the project capital. The Benefit-Cost Ratio (BCR) of a project, is the ratio of the present value of the project benefits (PVB) to the present value of the project costs (PVC) as shown in equation (2-9) and a project is justified when the ratio is larger than one (DEAT, 2004; Beukes, 2013). The benefit of the Benefit-Cost Ratio over the NPV is that it gives an indication of the efficiency of capital use but does not regard project size.

$$\sum_{t=0}^{n} \frac{\mathrm{B_t} - C_t}{(1 + i_{IRR})^t} = 0 \qquad \textit{(2-8)}$$

$$BCR = \frac{\sum_{t=0}^{n} \frac{\mathrm{B_t}}{(1+i)^t}}{\sum_{t=0}^{n} \frac{\mathrm{C_t}}{(1+i)^t}} \qquad \textit{(2-9)}$$

Return on Investment (ROI) is a decision rule commonly used in the private sector which is calculated by dividing the project profit by the total cost. The ROI provides a simple method to represent the project benefit as a single value but does not account for the time-value of money. Payback Period, also commonly used in the private sector, is the time taken for the project benefits to overtake the initial capital investment and on-going costs of the project. The payback period can be calculated with either the nominal (actual) net benefits or the real (discounted) net benefits. The shortcomings of this decision rule are that it does not account for the time value of money if nominal benefits are used in the calculation and it does not give a view of the benefits generated after the payback period is reached (Beukes, 2013; DEAT, 2004).

Levelized Cost of Energy (LCOE) is a metric commonly used in the energy sector, especially when comparing electricity generation projects as in the work of Du Plessis (2011). The LCOE is the cost of for the duration of a project that would result in the same value as the project costs. The LCOE can either be calculated in real terms, not taking into consideration inflation effects, or in nominal terms which accounts for inflation. The LCOE can be used to compare the cost of the energy saved by a RBS to the current energy cost for railway transport to determine the benefit of the RBS. It can also be used to compare various RBS concepts in which case the RBS with the lowest LCOE would be best concept.

Although there is a possibility of obtaining conflicting results from the various decision rules, the NPV, IRR and BCR usually provide consistent results as these focus on the present value of project costs and benefits (Beukes, 2013). The payback period should be used as a complementary criterion due to the shortcomings mentioned.

The most difficult part of a CBA is the accurate calculation of costs and benefits over the project life cycle (DEAT, 2004). The complexity arises in identifying the complete set of resulting costs and benefits and differentiating between costs and benefits that should be included or excluded for the analysis.

Costs that need to be included for the CBA include initial investment cost (initial capital expenditure), operating cost, maintenance cost, opportunity cost as well as decommissioning or disposal costs. The opportunity costs represent the next best used of a scarce resource used in the project. An example of this could be the weight added to a rail vehicle with the addition of a RBS that could otherwise be used for additional payload which would generate income. When identifying and evaluating the costs of a project it is important to identify 'sunk' cost, these are costs that would take effect regardless of whether the project is pursued or not. These costs should not be included in a CBA (DEAT, 2004). The costs of new and immature technologies may reduce with time due to economies of scale and learning by doing (Du Plessis, 2011). This occurrence can be accounted for in CBA by incorporating a Learning Rate for developing technologies, which is a factor by which the cost of the technology (in real terms) reduces versus time. Costing throughout the project life-cycle is usually done in real terms (i.e. accounting for inflation), which means the cost of a certain product or service will only increase or decrease in time if the price increases or decreases relative to inflation (DEAT, 2004).

Further uncertainty arises with the selection of the discount rate for the calculation of NPV, IRR and BCR. The discount rate selected for CBAs is a much-debated topic and has a significant impact on the outcomes of the analysis (Beukes, 2013). The discount rate also varies for the type of CBA performed (financial- or economic CBA). In the study performed by Beukes, the discount rate for a financial CBA is taken as the difference of the prime lending rate and the inflation rate i.e. the real (above inflation) cost of borrowing money. The DEAT guideline states that the appropriate discount rate for the private sector is the market rate of interest. As the DEAT guideline makes no reference to inflation, it can be assumed that this interest rate is the nominal interest rate not accounting for the time value of money. As most large corporations, including rail operators and fleet owners, are expected to have a loan book of some sort, it would be fair to assume that available capital would be used to settle debt rather than invest in interest bearing mechanisms. For this reason, the discount rate equal to the prime lending rate used by Beukes (as opposed to market interest rate suggested by the DEAT) would be the more appropriate discount rate as it provides a better reflection of the opportunity cost of capital. Furthermore, in both the work of Beukes and the DEAT guideline, it is mentioned that the cost and benefits are accounted for in real terms (not taking the effect of inflation into account) and for this reason it would be appropriate to use a real lending rate (prime lending rate minus the inflation rate) as the discount rate.

The uncertainty that arises with the estimation of costs and benefits as well as the discount rate raises the need for a sensitivity analysis to investigate the effect of variations in estimate values. According to Beukes there are three types of sensitivity studies that can be performed in a CBA namely a gross sensitivity analysis, stress testing and Monte Carlo simulation (2013). The details of these analyses are beyond the scope of this study, for this study a gross sensitivity analysis will be performed which involves varying a single variable at a time and recording the effect on the CBA outputs.

3. Distributed Regenerative Braking System Design

At this stage, we have identified the need for a RBS for freight trains and that the main goal of this study is to investigate the feasibility of a distributed system to fulfil this need. We have also established that flywheel ESSs exhibit promising characteristics for RBS applications and determined the state of the art of RBSs with flywheel energy storage in both the automotive and rail industry. In this chapter, we attempt to bring together this technology with the distributed regenerative braking systems for freight trains described in section 2.2.

The goal of this chapter is to establish one or more feasible conceptual designs for the system based on similar implementations found in other transportation sectors, taking into account the design considerations identified in chapter 2. It is important that the selected concept meets the functionality requirements while performing efficiently enough to affect energy savings that justify the system financially. Certain new design requirements will be imposed on the RBS that are specific to the rail environment that need to be considered when selecting the appropriate technology.

The distributed RBS is analysed at four different system levels in this chapter. The highest level, the train system as a whole, does not require any design decisions to be made due to the constraint that the train- setup and performance should not be changed in any way as this may affect train operation adversely. Nevertheless, the train system will be analysed in section 3.1 by implementing a generic RBS to determine the requirements of the RBS which will feed into the analyses of the lower system levels. At the second system level, the system boundary is reduced to encompass an individual freight wagon fitted with the distributed regenerative braking units. At this level, the only design decision that will be made is the number of RBSs installed on a wagon. This decision will affect the requirements of the regenerative braking units e.g. when more units are installed on a wagon the energy storage requirement for each unit decreases. At the third level, the system boundary is reduced so that only the individual RBSs are encompassed and at this level the topology of the major components is decided. The fourth and lowest system level that will be considered in this study is that of each of the major components of the system.

A combination of the top-down and bottom-up design approaches will be used for the concept design of the RBS. The top down approach is used at the top level, as the analysis at this level provides the requirements that serves as input to the lower levels. This approach cannot be used at the following levels as the design decisions at the lowest level and performance of the major components may affect the choice of RBS topology as well as the number of RBSs installed per wagon. Therefore, information will flow both upward and downward between the second to fourth system levels in this design process.

3.1. Establishing the energy characteristics of freight train braking- and motoring-cycles

3.1.1. Analysing freight train data

In section 2.4 we established that from in-service train data sets, the power requirement of the train for the duration of the trip can be determined. This power curve can in turn be separated into braking and motoring instances. In this section, these braking and motoring instances will be analysed to determine the requirements of a RBS for these freight trains.

A MATLAB program was created to analyse the previously mentioned train data sets. The power curve of the train for the specific train is calculated from the train data as explained in section 2.4. The program receives the power curve of the trip as an input which it uses to calculate the energy characteristics of the trip. The program first calculates the roots of the power curve which are used to identify the braking and motoring instances. The program then goes on to integrate the power curve between each consecutive pair of roots and to calculate the energy capacity of each instance using equation (2-4 and stores it in a single vector before separating the braking and motoring cycles into separate vectors. At this stage, a minimum energy capacity threshold is incorporated to discard any braking or motoring cycle that does not meet the capacity threshold as these cycles are regarded as noise that will lead to misleading results during analysis of the data. After this, some post processing is done to determine the parameters shown in Table 3-1. The MATLAB program is shown in Appendix B. The results shown in Table 3-1 can be used to make first order estimations of the ESS requirements for the RBS on the two freight trains being analysed. We have already established in the previous chapter that the system of interest uses regenerative braking as its energy saving mechanism rather than load levelling. It is important that this operational objective of the system is defined before the power and energy capacity requirement of the ESS can be determined, as the mission will dictate the sizing methodology used (Akli, et al., 2007).

Considering the data of Table 3-1, the self-sufficiency measure (as defined in section 2.4) can be calculated to determine the maximum potential energy saving through regenerative braking for the two train trips. The self-sufficiency for Trip 1 and Trip 2 is calculated as 41.4% and 78.5% respectively. This indicates that for these two typical freight train trips the potential exists to save significant amounts of energy. The results of this analysis highlight the significant potential for energy savings on freight trains even though these trains do not stop frequently and stay as close as possible to their operating speeds throughout a trip.

The self-sufficiency measure calculated above is indicative of the amount of energy that can be saved without considering the energy capacity limit of the ESS which means that 100% of the available braking energy could be captured. This measure is purely a characteristic of the train operational data. Next, we consider the amount of braking energy that can be captured by the proposed distributed RBS, with a finite energy storage capacity. To define the ESS capacity range in which the optimal capacity is expected to be found, the lower bound is set equal to the average braking cycle capacity. The upper bound of the ESS capacity is calculated by calculating the maximum ESS capacity for each RBS installed in the non-powered wagons and multiplying it by the number of these RBSs in the train. The energy storage capacity installed in each wagon bogie can be calculated by using the volume of the design envelope specified in section 2.2 and the volumetric energy density provided in Table 1-2.

If we assume that for mobile applications the energy density will tend towards the lower end of the range provided in Table 1-2 and use an energy density of 20 kWh/m^3 in combination with the design envelope volume of 0.44m^3 of which we assume 50% can be used for the ESS, the maximum energy storage capacity per RBS is 4.4 kWh. As the number of wagons in each train as well as the maximum number of RBSs per wagon is known, the total energy storage capacity for each train can be calculated. The train setup for Trip 1 has a maximum of 320 RBSs (80 wagons, 4 RBSs per wagon) and a total maximum storage capacity of 1408 kWh while the train for Trip 2 has a maximum of 200 RBSs (50 wagons, 4 RBSs per wagon) which results in a maximum storage capacity of 880 kWh.

Table 3-1: Trip Energy Characteristics

Mode	Parameter	Unit	Trip 1	Trip 2
Braking	Total Energy	kWh	15 886	11 827
	Number of Cycles		250	150
	Average Cycle Capacity	kWh	64	79
	Maximum Cycle Capacity	kWh	1 261	1 393
	Average Cycle Time	s	164	80
	Average Power	kW	947	834
	Maximum Power	kW	5 946	5 404
	Maximum Tractive Effort	kN	418	805
Motoring	Total Energy	kWh	38 334	15 062
	Number of Cycles		266	274
	Average Cycle Capacity	kWh	144	55
	Maximum Cycle Capacity	kWh	4 856	1 086
	Average Cycle Time	s	113	111
	Average Power	kW	1 224	637
	Maximum Power	kW	8 295	6 050
	Maximum Tractive Effort	kN	1495	578

The analysis does not consider any of the inefficiencies associated with the ESS or power converter and assumes that the ESS is completely discharged between each braking cycle. The calculation was performed for the above-mentioned range of ESS capacities and the results are shown in Figure 3-1. The results are also shown in Figure 3-2 with the percentage of the available braking energy captured plotted versus the energy storage capacity per wagon. From these results, we can narrow down the capacity range that would provide good utilization of the ESS, as well as capture a desirable amount of the braking energy.

Considering Figure 3-1, a high marginal gain for the *percentage braking energy captured* is observed for both trips at the lower end of the *energy storage capacity* range. The marginal gain tapers down towards the higher end of the energy capacity range once it moves beyond the point of diminished returns. In Figure 3-2, it is observed that this point of diminished returns coincides well for both trips when the energy capacity is viewed on a per wagon basis, in the region of 4-8kWh of energy storage capacity per wagon. A more detailed analysis will be presented in the following section to establish the requirements of the ESS and power converter for the RBS.

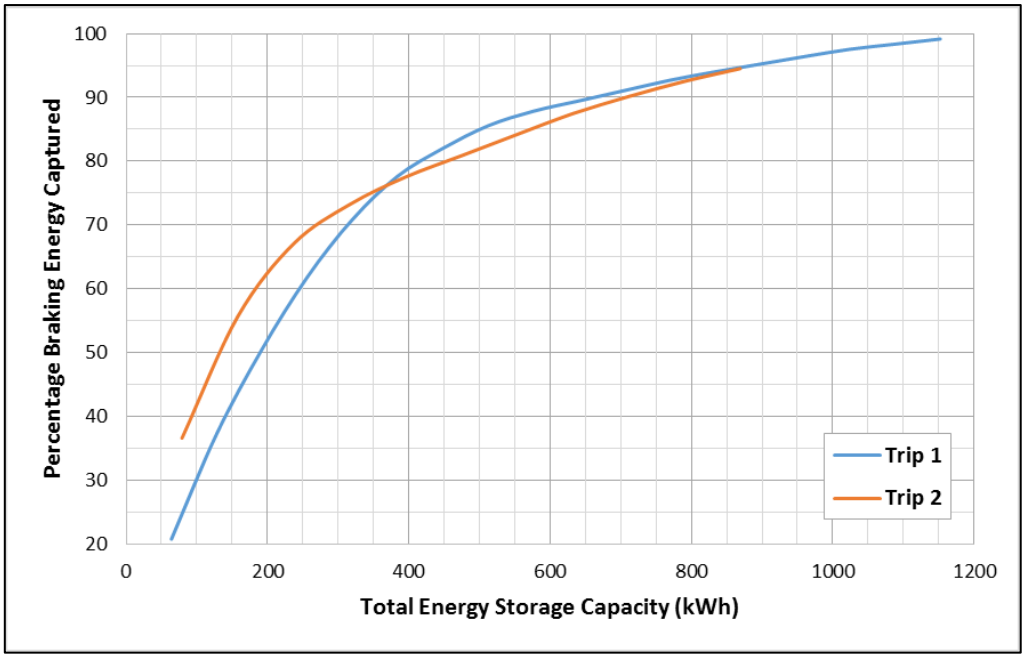

Figure 3-1: Braking Energy Captured versus Total Energy Storage Capacity

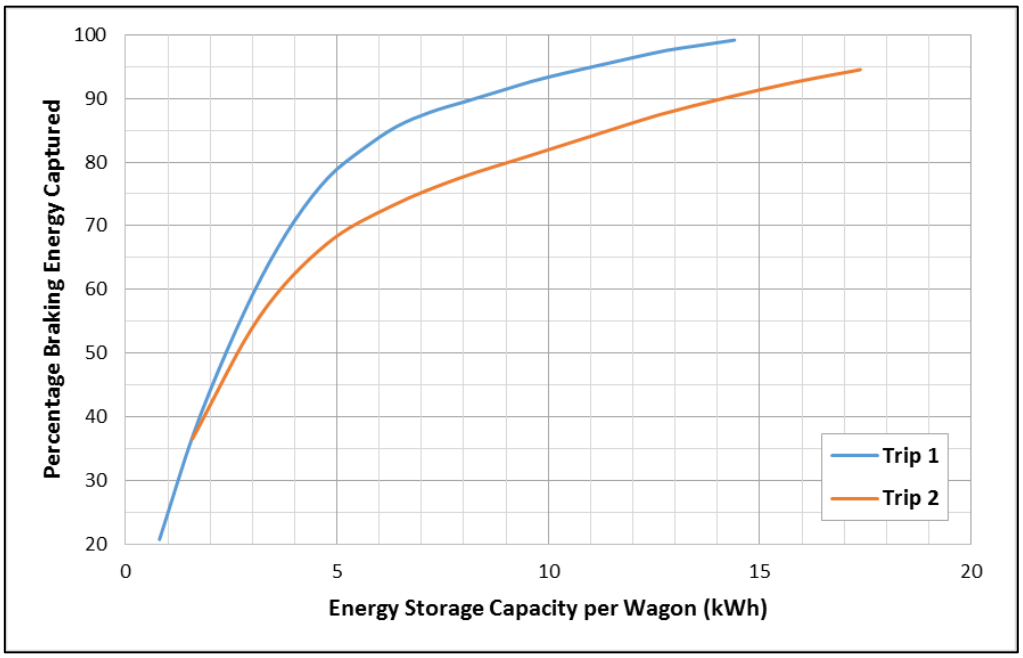

Figure 3-2: Braking Energy Captured versus Energy Storage Capacity per Wagon

3.1.2. Numerical Simulation

With the route characteristics known and the potential for energy savings on a typical freight route established, a simulation will be performed to determine how much energy can be saved by an actual flywheel RBS when the inefficiencies and limitations of the system components are incorporated in the analysis. The simulation will be based on a generic RBS topology in a parallel configuration with the prime mover according to the definition given in section 1.2.1 and 2.1 and is illustrated in Figure 3-3 with the arrows representing the flow of power.

In the figure, the block titled prime mover represents the locomotives in the train set, the primary energy source can be in the form of diesel fuel or electricity for electrified railway lines. The purple arrows represent the power flow from the energy source to the prime mover, P_{PES}, and subsequently to the unpowered wagons, P_{M_PM}. Due to inefficiencies in the locomotives, some energy is discarded to the environment and is represented by the yellow arrow P_{L_PM}. The red arrows P_{B_PM} and P_{B_RBS} represent the power flow from the wagons to the locomotives and RBS respectively during braking. For a conventional train setup without a RBS, the complete braking requirement of the train during operation must be met by the locomotive braking P_{B_PM}. All the braking power of the locomotives is discarded to the environment as illustrated in Figure 3-3. The power converter of the RBS receives the braking power of the RBS, P_{P_RBS}, and in turn charges the flywheel ESS with this power, P_{C_ESS}. When power is requested, power is discharged from the flywheel ESS, P_{DC_ESS}, to the power converter which transfers the power to the unpowered wagons, P_{M_RBS}, as illustrated by the green arrows in the figure. For the train setup illustrated in Figure 3-3, the power requirement of the train is met by the combination of locomotive power, P_{M_PM}, and power from the RBS, P_{M_RBS}, whereas a conventional train is motored solely by the locomotives. When power is transferred to and from the flywheel ESS through the power converter, power is lost and discarded into the environment due to inefficiencies in the power converter, illustrated by the yellow arrow P_{L_PC}. The flywheel ESS discards power to the environment while charged due to self-discharge losses and is illustrated by the yellow arrow P_{L_ESS}. The two yellow arrows represent the two primary energy dissipation mechanisms in a RBS, the power losses due to inefficiencies in the power converter (P_{L_PC}) and self-discharge of the ESS (P_{L_ESS}).

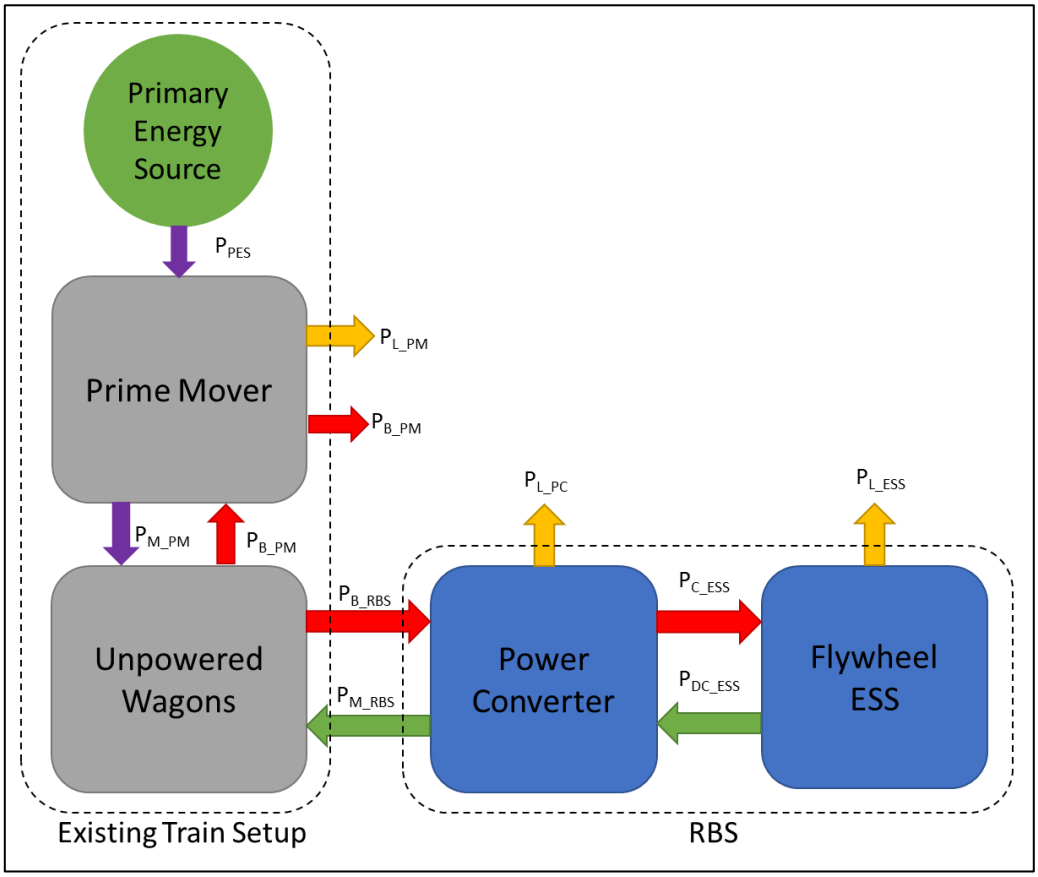

Figure 3-3: Generic RBS Power flow

A distributed RBS for freight trains consists of a multitude of RBSs in a single train. At this stage it is necessary to define the assumptions made regarding the operation of the distributed RBS as a whole. The first assumption we make is that each non-powered wagon in the train has the same net coupler force (difference between front- and back coupler force) if the wagons are of equal mass and on the same gradient. This is due to the fact that there is negligible relative motion between the wagons which means that they will always experience the same acceleration and therefore net force based on Newton's second law of motion. Based on this and recalling equation (2-2) from section 2.4, we can deduct that all non-powered wagons in a train will have an identical power requirement throughout the train trip. The mission power curve for the train can thus be divided by the number of wagons in the train to determine the mission power curve for each wagon and also for each of the RBS in the wagon. We can therefore take either one of the following approaches when performing this simulation, the first approach involves subdividing the mission power curve to each RBS and simulate only a single RBS in the train. The second approach that can be taken is to lump the multitude of RBSs in the train together and determine the characteristics of the distributed RBS as a whole and use it in conjunction with the power curve for the entire train. In section 3.1 it was observed that the point of diminished returns for energy capacity coincides if the energy capacity was viewed on a per wagon basis, rather than for the energy storage capacity of the entire train. This is to be expected as the energy capacity requirement for regenerative braking is related to the mass of the total train which varies from train to train as the number of wagons in the train varies. It is therefore decided to use the first approach and subdivide the mission power curve to each wagon. Thus the RBS will be optimised for a typical freight wagon and the complete distributed RBS will scale with the number of wagons in the train, rather than the RBS being optimised for a particular train setup.

A MATLAB program was created to perform the simulation of the hybrid propulsion system illustrated in Figure 3-3 for the two train trips analysed in the previous section. The MATLAB program uses Equations (3-1) to (3-5) which represent the flow of power illustrated in Figure 3-3 to perform the analysis. The program evaluates the power requirement of the train for each time step in the trip data. It determines whether the train is currently in motoring or braking. If the train is in motoring, the algorithm checks if there is enough energy in the ESS to deliver the power ($P_{M\_Required}$) and if so, the power (or a portion of the power) is delivered by the RBS (P_{M_RBS}) and the ESS is discharged by P_{DC_ESS} calculated from Equation (3-5) with n_{PC} representing the power converter efficiency. The power that cannot be provided by RBS is provided by the prime mover (P_{M_PM}). If the train is found to be in braking, the algorithm checks the ESS state of charge (ESS_{SOC}). If the ESS is not fully charged, the braking is performed by the RBS (P_{B_RBS}) and the ESS is charged with P_{C_ESS} calculated from Equation (3-4). The effect of self-discharge of the ESS is incorporated by using equation (3-1) in which the ESS state of charge (ESS_{SOC}) is calculated. The self-discharge power (P_{L_ESS}) is calculated by assuming that the ESS charge level discharges linearly from full charge to zero in the specified time. The method described above ensures that power delivered by the RBS (P_{M_RBS} and P_{B_RBS}) is preferred to the power of the prime mover (P_{M_PM} and P_{B_PM}), thereby utilizing as much as possible of the potential for regenerative braking.

$$ESS_{SOC}(t) = ESS_{SOC}(0) + \int_0^t P_{C\_ESS}dt - \int_0^t P_{DC\_ESS}dt - \int_0^t P_{L\_ESS}dt \qquad \textbf{(3-1)}$$

$$P_{M\_REQUIRED} = P_{M\_PM} + P_{M\_RBS} \quad \textit{(3-2)}$$

$$P_{B\_REQUIRED} = P_{B\_PM} + P_{B\_RBS} \quad \textit{(3-3)}$$

$$P_{C_{ESS}}(t) = P_{B_{RBS}}(t) \cdot n_{PC} \quad \textit{(3-4)}$$

$$P_{M_{RBS}}(t) = P_{DC_{ESS}}(t) \cdot n_{PC} \quad \textit{(3-5)}$$

The program requires two input fields from the train data to perform the simulation; these are the time steps as well as the power curve of the locomotive consist. A set of parameters describing the train setup and RBS is also required. These include the ESS capacity (per wagon), ESS self-discharge rate (time) and the transmission (power converter) efficiency for each RBS installed in the wagons. The number of wagons in the train must also be provided so that the power curve for the whole train can be subdivided to each wagon. A range of ESS capacities will be evaluated in the simulation as determined in section 3.1. These parameters are all shown in Table 3-2.

Table 3-2: RBS Parameters

Parameter	Trip 1	Trip 2
Number of Wagons	80	50
Number of RBS per Wagon	2 – 4	2 – 4
Energy Capacity per Wagon (kWh)[1]	4 – 8 kWh	4 – 8 kWh
ESS Self-Discharge Time (min)[2]	288	
Power Converter Efficiency[3]	92.5 %	

[1]Determined from the analysis performed in section
[2]From Table 1-2: ESS Self-Discharge Time = 24 hours / Daily Self-Discharge (500%)
[3]From Table 1-2: Use mean value of range

Once the program has completed the simulation, post processing is done to calculate key parameters such as the percentage of the available braking energy captured by the RBS (equation (3-6)), motoring energy delivered by the RBS which equates to the absolute energy saving by the RBS (equation (3-7)) and the resulting energy saving as a percentage (equation (3-8)) as well as the EROI (equation (3-9)) of the RBS.

$$f_{B_{RBS}}(\%) = \frac{\int_0^t P_{B\_RBS} dt}{\int_0^t P_{B\_REQUIRED} dt} \quad \textit{(3-6)}$$

$$E_{M\_RBS} = \int_0^t P_{M\_RBS} dt \quad \textit{(3-7)}$$

$$Energy\ Saving\ (\%) = \frac{\int_0^t P_{M\_RBS} dt}{\int_0^t P_{M\_REQUIRED} dt} \quad \textit{(3-8)}$$

$$EROI(\%) = \frac{\int_0^t P_{M_{RBS}} dt}{\int_0^t P_{B\_RBS} dt} \quad \textit{(3-9)}$$

The tabulated results of the simulation can be found in Appendix B. Figure 3-4 shows the percentage of the braking energy captured by the RBS for the range of energy storage capacities. The first observation that can be made is that when the results in Figure 3-4 are compared to the results from the analysis in section 3.1, the percentage braking energy captured is significantly less than was observed in section 3.1 for corresponding ESS capacities per wagon. This is due to the fact that the analysis of 3.1 assumed that the ESS was completely discharged before each braking cycle. In reality, the ESS may carry some residual energy from a previous braking instance at the start of a new braking instance which means that a smaller fraction of the new braking cycle's energy can be stored.

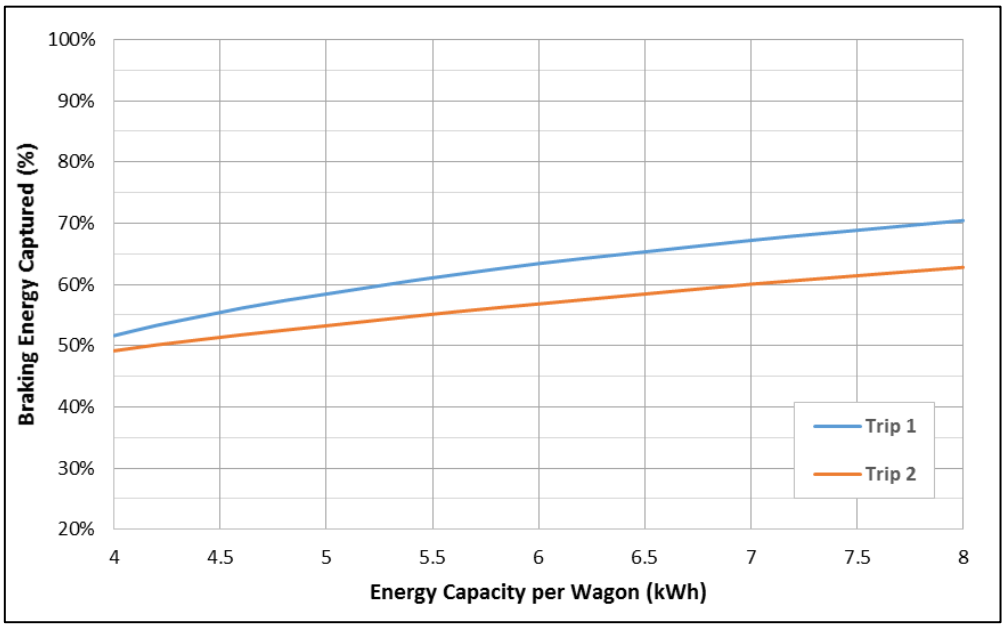

Figure 3-4: Percentage Braking Energy Captured for Trip 1 and 2

Figure 3-5 shows the percentage energy saved by the RBS for the range of ESS capacities for both train trips. Although we observe significant energy savings for both cases, the energy savings are significantly lower than the self-sufficiency measure calculated in section 3.1.1, 41.4% and 78.5% for Trip 1 and Trip 2 respectively. This variation is due to the finite ESS capacity, ESS self-discharge and power converter efficiency that is not taken into account by the self-sufficiency measure.

As different train routes have different energy characteristics, the potential for energy saving varies significantly from route to route as shown by the self-sufficiency measure for the two trips analysed in this study. Furthermore, the energy intensity of the routes can vary significantly as is shown in Table 3-1 by the total motoring energy required for each trip. The motoring energy required per wagon is 479- and 301-kWh for Trip 1 and Trip 2 respectively and therefore the absolute energy savings for Trip 1 is higher than for Trip 2 although the percentage energy saved is lower for trip 1. Therefore, the percentage energy saving as shown in Figure 3-5 can be misleading when evaluating the performance of a RBS as well as the benefit of the system. To get a better indicator of the overall performance of the RBS, a new measure termed the *normalised energy saving* is introduced. The *normalised energy saving* is calculated by dividing the energy savings result (equation (3-8)) with the self-sufficiency value of the specific route. The measure will therefore indicate how much of the maximum potential energy saving has been affected by the RBS. The normalised energy savings results are shown in Figure 3-6

and we observe that although the energy savings as a percentage for trip 1 is lower than for trip 2, a larger percentage of potential energy savings is realised for this trip when compared to trip 2.

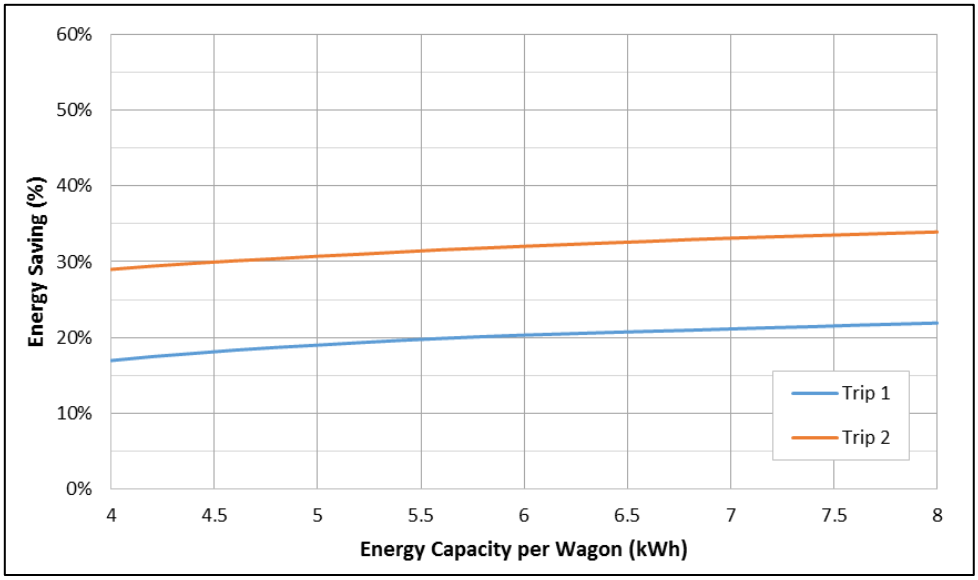

Figure 3-5: Percentage Energy Saved per Wagon for Trip 1 and 2

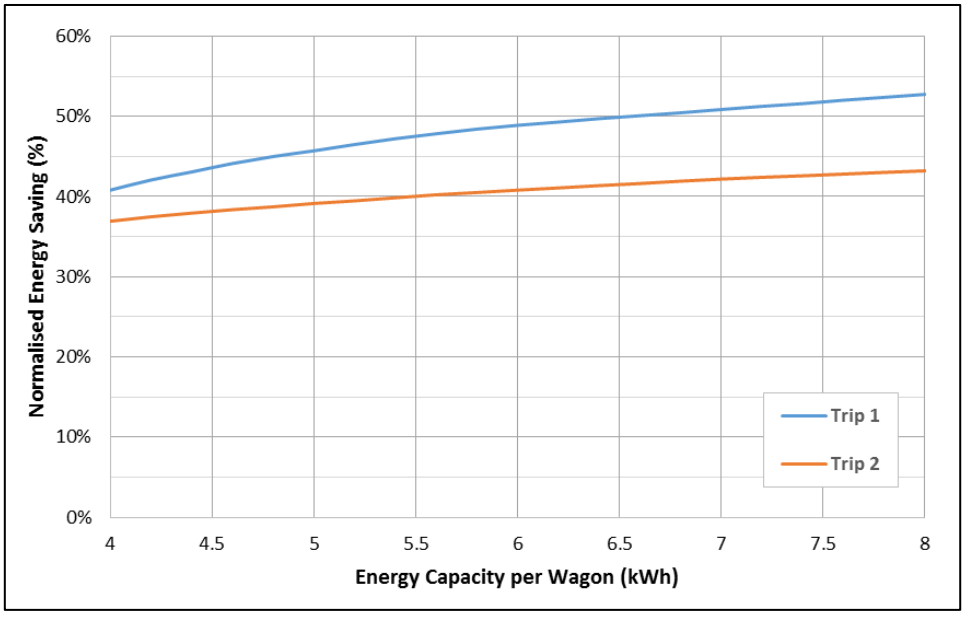

Figure 3-6: Normalised Energy Saving per Wagon for Trip 1 and 2

The last parameter provided by the post processing function is the energy returned on energy invested (EROI) which is used to evaluate how efficiently the RBS can deliver the energy it has absorbed back to the train. The EROI results are shown in Figure 3-7. It is observed that the EROI reduces as the energy capacity per wagon is increased. This decrease is due to higher self-discharge from the flywheel as the utilization of the flywheel decreases.

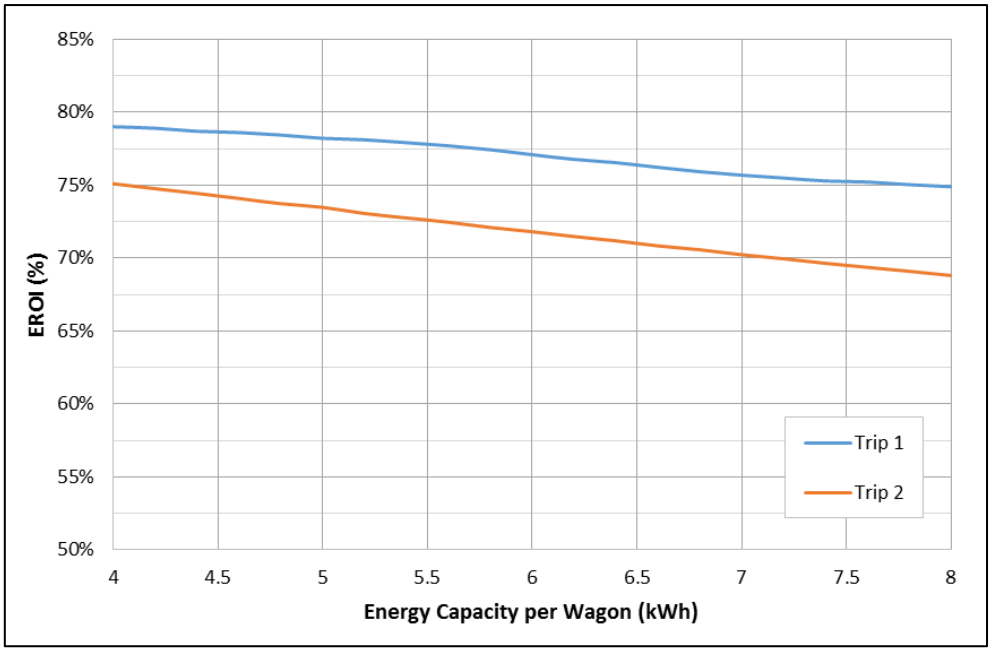

Figure 3-7: Return efficiency of regenerative braking system for various energy storage capacities

3.2. System Topology

At this stage of the study, the transition is made from analysing a non-physical RBS represented by expected characteristics and performance parameters, to analysing the physical system and the components which make up the RBS. In this section, we analyse the second and third system levels as described in the introduction of this chapter. At these levels the system topology, synonymous to system architecture, is decided. As mentioned previously, the system topology is affected by the analyses of the fourth system level, the major component level, and information from the analysis of the fourth level will inform the design decisions made at this level. The system topology is also affected by the energy management- and control strategy of the system.

3.2.1. Topology at Wagon Level

In section 2.2, a method for integrating regenerative braking systems into non-powered rail wagons was presented according to a PCT application titled 'Regenerative Railway Braking System'. The method involves utilizing the available space in the bogies of these wagons. In Figure 2-2 and Figure 2-3 it is shown that two RBSs can be installed in each wagon bogie and therefore up to four systems can be installed on each wagon. It may however not be required, or make financial sense, to install four systems on each bogie and therefore the effect of installing fewer than four units must be investigated as well.

To determine the power-, tractive effort- and energy storage requirement for each RBS, these requirements for each wagon must be divided depending on the number of systems in the wagon. In the analysis performed on the train data in section 3.1.1, the maximum power and maximum tractive effort requirement of the train during motoring and braking was calculated for each of the two train trips. These values can be used to calculate the power requirement for each wagon by dividing the values specified in Table 3-1 through the number of wagons in the train as specified in Table 3-2. The results are shown in Table 3-3. We see that the worst case maximum power experienced per wagon

is during motoring on Trip 2, 121 kW, and the highest tractive effort experienced is during motoring on Trip 1, 18.69 kN. From this, the power- and tractive effort requirement of the RBSs is calculated and results are shown in Figure 3-8. Similarly, from the energy storage capacity requirement per wagon established in section 3.1.2, the required capacity for each RBS was calculated and shown in Figure 3-9.

Table 3-3: Power Requirement per Wagon

	Mode	Maximum Power (kW)	Maximum Tractive Effort (kN)
Trip 1	Motoring	103.7	18.69
	Braking	74.3	10.06
Trip 2	Motoring	121.0	11.56
	Braking	108.1	8.36

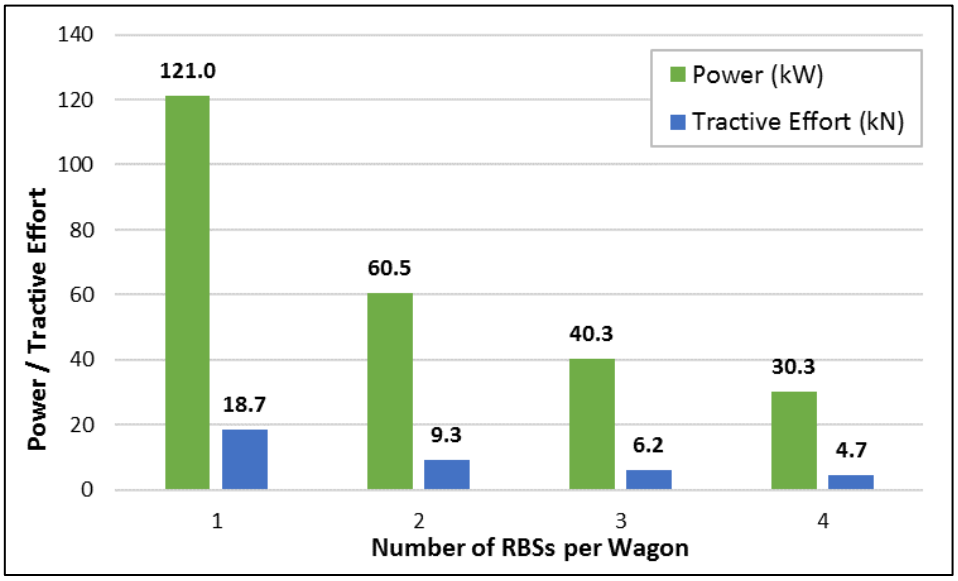

Figure 3-8: Power- and Tractive Effort requirement per Regenerative Braking System with change in number of systems per wagon

3.2.2. RBS Level

In this section, the architecture of the RBS units that will be installed on the freight wagon bogies is investigated and the most suited architectures selected. In chapter 2 it was explained that flywheel based RBSs have been adopted to some extent in the automotive industry while in the rail industry these systems have not been adopted beyond the experimental and proof of concept stages. It is for this reason that that we will consider automotive applications of the technology to identify system topologies that have been proven to work and is suited to our application. Further motivation for considering automotive solutions is that, with the large number of RBSs in the train, the size of each RBS in terms of required power and storage capacity resembles that of automotive applications.

Due to the separation of the prime mover and RBS, the distributed RBS concept will inherently be a parallel hybrid system as both the prime mover and the secondary power source (the RBS) will be connected via final drives to the axles. Therefore, series-hybrid topologies will not be considered a

feasible solution. Also, we will focus only on hybrid topologies specifically suited to regenerative braking as the energy saving mechanism and therefore systems such as the system developed by Kok in which the ESS is energised by the prime mover will not be considered either (Kok, 1999).

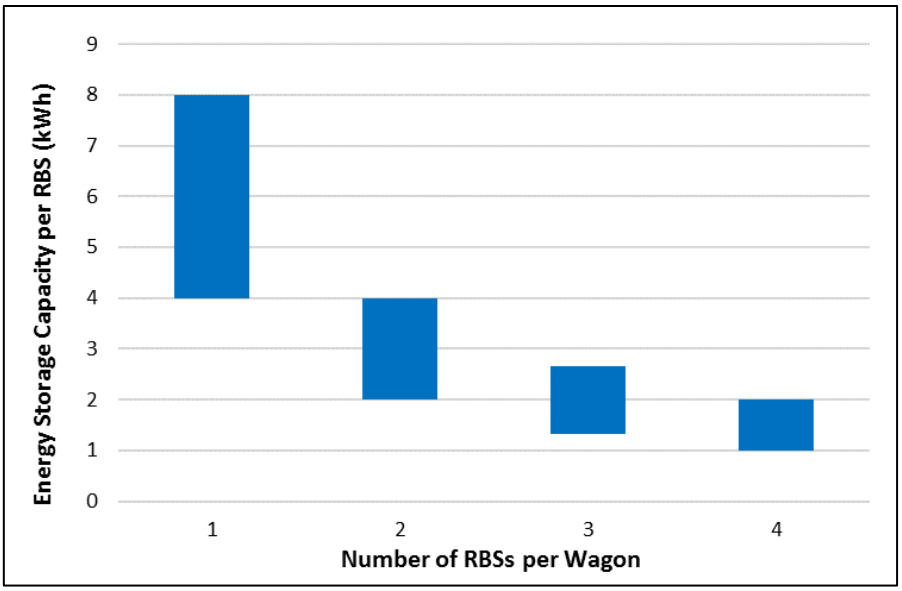

Figure 3-9: Energy Storage Capacity Requirement of Regenerative Braking Systems with change in number of Systems per Wagon

Berkel et al. (2014) evaluated mechanical hybrid powertrain topologies based on fuel saving potential (i.e. transmission efficiency), cost and control complexity. The topologies were classified based on certain characteristics and the best in class were chosen for further investigation. In their work, it was found that the parallel topologies proved to be more efficient and less costly than series type hybrid topologies and narrowed their study down to the four most promising topologies. The common components between the topologies are the flywheel ESS, final drive and at least one transmission component with a varying gear ratio and a clutch. Two types of clutches are found in the topologies, *drive clutches* which can transmit high power while slipping and *mode clutches* that are present only to select the operating mode of the powertrain. The main differentiating factors between the topologies are whether the flywheel was connected before the primary transmission (primary energy source side of the primary transmission) which means only one transmission is required or whether the flywheel is connected to a smaller secondary transmission which is then connected to the output of the primary transmission (vehicle side of the primary transmission).

Adapting the hybrid transmissions evaluated by Berkel et al. for the application of this study, the engine (primary energy source) and primary transmission (if not used for flywheel driving) are omitted as the primary energy source is not located at the RBS in the distributed RBS application (2014). Also, as the RBS will only have a single driving mode (not a combination of energy sources), the mode clutches in the topologies are omitted as well. With this adaptation, three of the four promising topologies became identical and therefore two candidate topologies remained as shown in Figure 3-10. The original topologies are shown in Appendix B.

As explained in section 2.5, the function of the transmission components is to synchronise the speed of the flywheel to the speed of the wheel axle as well as facilitate the continuous change in speed of the flywheel to transmit the required torque. Topology A relies on two clutches to deliver the

demanded torque to the vehicle by varying the contact force between the clutch plates while there is a difference in the velocity between the input and output shafts. This type of system was also the subject of investigation in the work of Read et al. (2015). A set of fixed gears is present to compensate for the high flywheel rotational velocities compared to the vehicle axles. A clutch, acting as a slipping component, has low efficiencies but can be implemented at a low cost which is why they are considered as a competitive option. Although there is a clutch on either side of the fixed gears in this topology, only one of these clutches are required for the functionality of the RBS. The second clutch is present for improved heat distribution of the energy losses (Berkel, et al., 2014). Topology B utilises a controllable CVT to transmit the required torque to the wheel axle and flywheel. The CVT can transmit torque at much higher efficiencies than slipping components, but comes at an added cost. A clutch is still required in this topology to change the mode of operation of the RBS when changing between the open and closed position. As for Topology A, a set of fixed gears are required to compensate for the high flywheel rotational velocity in relation to that of the wheel axle.

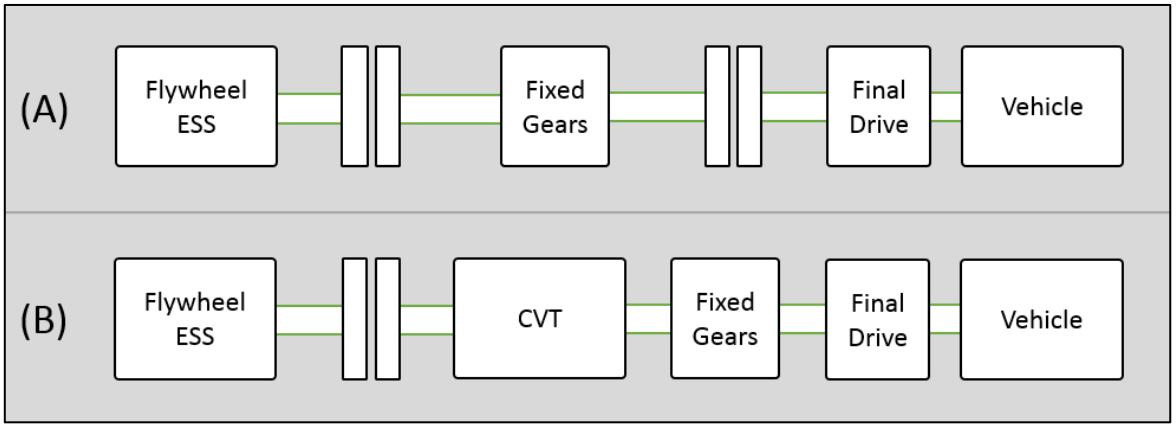

Figure 3-10: Adapted Hybrid Topologies

The two topologies identified in this section will serve as candidate topologies for the evaluation of the RBS and are evaluated based on the energy savings achieved with the topology as well as their cost after which the most feasible solution will be selected. The three-dimensional design of the RBS topology is beyond the scope of this study, it is however necessary to establish the overall dimensional constraints of the subcomponents for further analysis. If we consider the available design space shown in Figure 2-3 and assume that the RBS drivetrain components are installed co-axially to the wheel axle of the wagon bogies similar to existing methods for installing traction motors in locomotive- and motor coach bogies, the maximum diameter of any of the drivetrain components should not exceed 420mm and the overall length of the drivetrain, including the flywheel, cannot exceed 800m.

3.3. Flywheel Energy Storage System

It has already been demonstrated that the total energy storage capacity is one of the critical factors that determine the energy savings of a RBS. The energy storage and power (charge/discharge) requirements of the flywheel energy storage system (FESS) has been defined through the analyses conducted in section 3.1.2 and 3.2.1 with the resulting requirements shown in Figure 3-8 and Figure 3-9. Due to the high power-density of FESSs, it is assumed that the energy capacity is the limiting factor in the ESS sizing and that if this requirement is met the power requirements will inherently be met as

well. The goal of this section is to identify appropriate FESS technologies and parameters to meet the required energy capacities defined in previous sections.

The optimal FESS problem is the subject of extensive research and consensus is yet to be reached on the ideal design process (Janse van Rensburg & Groenwold, 2011). With the energy storage capacity set, there are various objectives that the flywheel can be optimised for including weight energy density, volumetric energy density, self-discharge (coast down) losses and cost. Weight energy density is a critical requirement for automotive industry and strict weight limitations are imposed on RBS when implemented on vehicles. Due to the much higher tare- and gross vehicle masses found in the freight rail industry compared to the automotive industry, the weight of the RBS will contribute significantly less towards the overall vehicle mass when compared to road vehicles. Although the effect of the added mass should not be neglected, the FESS will not be optimised for this parameter and no explicit limit is placed on the overall weight. With the available volume known for the ESS, the volumetric energy density will not be maximised, and is only required to be sufficient to adhere to the available design volume. The self-discharge losses will have a significant impact on the energy saving, and ultimate feasibility, of the RBS. Therefore, it is required that these losses be kept to a minimum. Similarly, the cost of the FESS will also impact the ultimate feasibility of the system.

The flywheel ESS setup that will be analysed in this section is schematically illustrated in Figure 3-11. For this study, we will analyse a disc shaped flywheel as was done in the work of Druten as well as Hayes et al. (2001; 1998). Although it is possible to achieve higher mass energy density characteristics with other geometries such as ring shaped- and constant stress disc flywheels, we are primarily concerned with volumetric energy density and will consider only disc shaped flywheels. Equations (3-1) to (3-3) are used to calculate the energy content of such a rotating flywheel with the ratio of inner radius to outer radius (ξ) being zero for a disc shaped flywheel. Disc shaped flywheels can be manufactured as a single component when made from metallic materials but for composite materials the flywheel is typically constructed from a metallic hub and a composite tyre that assembled to the hub, as shown in Figure 2-1. The analysis in this section will not take the effect of the metallic hub into consideration however and will assume a flywheel constructed from a single material, as the hub as a negligible effect on the energy characteristics of the flywheel. The air-gap between the flywheel and the flywheel housing can adversely affect the aerodynamic drag on the flywheel if not sufficiently large. To avoid this the ratio of the air-gap to the flywheel radius must be at least 0,022 for the circumferential air-gap and 0.3 for the side air gap (Kok, 1999).

In section 2.5 it was explained that either magnetic- or roller bearings can be used for flywheel energy storage. Although magnetic bearings provide the benefit of reduced wear and drag losses as well as higher flywheel speeds, they are not considered suited to mobile applications due to their higher complexity, weight and cost when compared to conventional roller bearings. Modern day hybrid, high-precision roller bearings offer competitively low friction and allow for rotational speed exceeding 50 000 rpm (SKF, 2017; NSK, 2017). Beside the thermal and mechanical limiting speeds of roller bearings, the flywheel speed is also limited by the natural frequency of the flywheel and bearings setup. This limiting speed, also known as the critical speed of the flywheel, is a function of the bearing stiffness and flywheel mass. Due to this critical speed, energy storage flywheels can either operate sub-critically, which is below the first critical speed or super-critically which is between critical speeds of the flywheel (Druten, 2001). For this study, it will be assumed that the critical speed of the flywheel arrangement is not a limiting factor in the flywheel analysis as an appropriate bearing solution can be

selected to mitigate the adverse effects of operating a flywheel through its natural frequency. The application of flywheels in transport applications, significant dynamic loading (shock and vibration) will be generated which significantly affects bearing loading. The study of these effects is beyond the scope on this study and the assumption is made that these problems can be addressed based on existing applications of the technology discussed in section 2.1. This would however require consideration in the development of the proposed system. Based on the above and the dimensional constraints imposed in section 3.2.2, the dimensions of the flywheel system are given in Table 3-4.

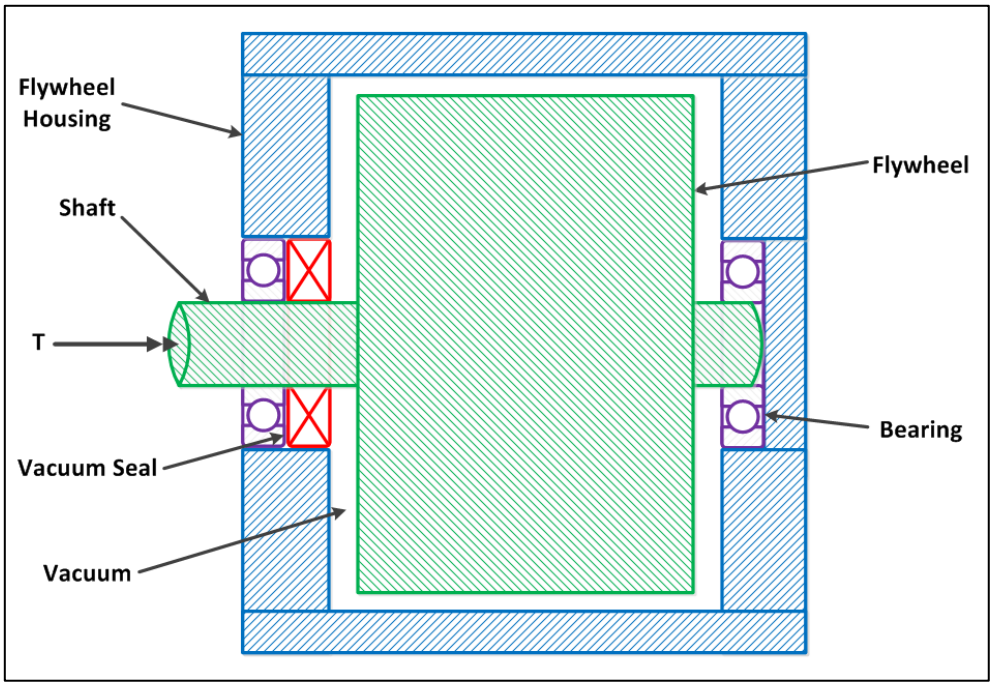

Figure 3-11: Schematic representation of flywheel setup

Table 3-4: Flywheel Geometric Limits

Parameter	Value
Flywheel housing outer diameter (mm)	420
Flywheel housing inner diameter (mm)	400
Circumferential air-gap (mm)	10
Side air-gap (mm)	10
Maximum flywheel diameter (mm)	380
Maximum flywheel length (mm)	300
Flywheel shaft diameter (mm)	30

The operational philosophy of FESSs involves placing a lower limit on the rotational speed of the flywheel (ω_{min}), as the lower end of the speed range contains a relatively small portion of the stored energy and by doing so the ratio spread (ω_{max}/ ω_{min}) of the flywheel is reduced significantly and torque values are kept to a reasonable level (Spiryagin, et al., 2015). The implication of this is that there is a difference between the absolute and usable energy content of a FESS which must be accounted for. The minimum operating speed of the flywheel is usually a function of the transmission capabilities, however 50% of the maximum flywheel speed (ω_{max}) is a value typically used and will be used for the analysis in this section (Spiryagin, et al., 2015; Rupp, et al., 2016). From equation (3-3) it can be shown that at 50% of the maximum flywheel speed, the flywheel contains 25% of its maximum energy

capacity, which implies that 75% of the flywheel energy capacity is usable. From this, equation (3-4) is derived showing how the absolute (maximum) energy capacity of the flywheel ESS (E_{max}) is related to the usable energy (E_{usable}) with n_u representing the portion of the flywheel energy capacity that is usable.

$$I_F = \frac{1}{2} m R_o^2 (1 + \xi^2) \quad \textit{(3-1)}$$

$$\xi = R_i / R_o \quad \textit{(3-2)}$$

$$E_f = \frac{1}{2} I_F {\omega_F}^2 \quad \textit{(3-3)}$$

$$E_{usable} = E_{max} . n_u \quad \textit{(3-4)}$$

The maximum energy that can be stored in a flywheel (and therefore maximum flywheel rotational velocity) is limited by the stress generated in the flywheel material due to the centrifugal force that comes with high speed rotation. An expression for the maximum energy due to stress limitations ($E_{max(stress)}$) is shown in equation (3-5) in which K is a geometrical shape factor of the flywheel, σ_a is the allowable material stress and V_f is the flywheel volume (Druten, 2001). The geometrical shape factor is calculated using equation (3-6). For a disc shaped flywheel (ξ=0), the shape factor is 0,303. A similar expression for maximum flywheel energy capacity is found in the work of Spiryagin et al. but a thin ring flywheel shape was assumed (ξ=1) which results in a shape factor of 0.5.

$$E_{\max(stress)} = K \sigma_a V_f \quad \textit{(3-5)}$$

$$K = \frac{1+\xi^2}{3.3+0.7\xi^2} \quad \textit{(3-6)}$$

With the above equations and the geometrical constraints for the flywheel in Table 3-4 we can calculate the characteristics of the flywheel for candidate materials and the results are shown in Table 3-5. The calculations were performed in Octave and are shown in Appendix B. The range of maximum energy storage capacities obtainable with the candidate materials ranges from 0.63 kWh for an E-Glass composite up to 3.69 kWh for the carbon composite. The usable energy capacity range becomes 0.47 to 2.77 kWh. When comparing the energy capacities that can be achieved to the required energy storage capacities for the system configurations shown in Figure 3-9, we observe that certain configurations are not achievable. In the configuration where only one RBS is installed per wagon, the bottom end of the required energy capacity range is 4 kWh which is more than the highest usable energy capacity that can be achieved by a single flywheel (2.77kWh). We can therefore conclude that installing only a single RBS per wagon would not meet the minimum energy storage requirement. It is also observed that the usable energy storage capacity obtained with the E-glass and S-glass composites does not meet the minimum requirement for any of the system configurations in Figure 3-9 and will therefore not be considered further.

Before an attempt is made to select flywheel- materials and geometries to match the energy storage requirements of Figure 3-9, the flywheel discharge losses must be calculated to ensure that the best flywheels are selected. The major power losses associated with a flywheel (P_{loss}) are drag losses (P_{drag}),

bearing friction losses ($P_{bearing}$) and losses associated with the vacuum system (P_{vacuum}) which includes the vacuum pump (P_{pump}) and vacuum seal (P_{seal}) as shown in equation (3-7).

$$P_{loss} = P_{drag} + 2P_{bearing} + P_{vacuum(pump+seal)} \quad \textit{(3-7)}$$

Table 3-5: Flywheel characteristics for candidate materials

Parameter	Tool Steel [1]	E-Glass - Epoxy[2]	S-Glass - Epoxy[3]	Carbon – Epoxy[4]	Aramid-Epoxy[5]
Density (kg/m^3)	7850	1850	1850	1580	1400
Tensile Strength (MPa)	1000	1103	>1103	2578	1379
Allowable Stress (MPa)[6]	550	220	350	1600	700
$E_{max(stress)}$ (kWh)	1.58	0.63	1.00	3.69	2.00
E_{usable} (kWh)	1.18	0.47	0.75	2.77	1.50
Flywheel Mass (kg)	267.1	62.9	62.9	53.8	47.6
Flywheel Speed at E_{max} (rpm)	14 647	19 082	24 068	49 979	39 127

[1]BS 970 PD – Condition U Alloy Steel [2]E-Glass - Epoxy with fibre volume fraction of 0.45 [3]S-Glass - Epoxy with fibre volume fraction of 0.45 [4]Carbon - Epoxy (IM7/88551-7) with fibre volume fraction of 0.6 [5]Aramid - Epoxy (Kevlar 49) with fibre volume fraction of 0.6 [6] For 10^6 load cycles. Sources: (Druten, 2001; Gibson, 2012; Smith, 1990; British Standards Institution, 2005)

The calculation of drag losses on flywheels is explained in the work of Druten and Kok both of which are based on the work of Genta (2001; 1999; 1985). The drag power loss is calculated from the resistive torque experience on the circumference (T_{circ}) and sides (T_{side}) of the flywheel as shown in equation (3-8). The resistive torque experienced is dependent on a torque coefficient (C_{circ} and C_{side}), the air density in the vacuum housing (ρ_{air}), flywheel geometry (radius (R_f) and width (w_f)) as well as the rotational velocity of the flywheel in radians per second (ω_f) as shown in equation (3-9) and (3-10).

$$P_{drag} = (T_{circ} + 2.T_{side}).\omega_f \quad \textit{(3-8)}$$

$$T_{circ} = \frac{\pi}{2} C_{circ}.\rho_{air}.w_f.{R_f}^4.{\omega_f}^2 \quad \textit{(3-9)}$$

$$T_{side} = \frac{1}{2} C_{side}.\rho_{air}.R^5.{\omega_f}^2 \quad \textit{(3-10)}$$

The torque coefficients are dependent on the dominant flow regime in the flywheel housing and can be established by calculating the Reynolds number (Re_{circ} and Re_{side}) which is dependent on the rotational speed of the flywheel, flywheel radius, kinematic viscosity of air in the flywheel housing (ν_{air}) as well as the airgap between the flywheel and the flywheel housing (t). The equations used to determine the flow regime in the flywheel housing and calculate the torque coefficients (C_{circ} and C_{side}) are shown in Appendix B. The air density (ρ_{air}) inside the flywheel housing is calculated from the ideal gas equation (Cengel & Cimbala, 2010). R_{air} is the gas constant for air which is equal to 0.287, the air temperature (T_{air}) is taken as 60 degrees Celcius or 333 Kelvin. Air pressures (P_{air}) of 1 to 10 mbar are commonly achieved in flywheel housings to reduce drag losses, for this study a value of 1 mbar will be used to ensure minimal power losses.

$$Re_{circ} = \frac{\omega_f R_f^2 t}{\nu_{air}} \quad \textit{(3-11)}$$

$$Re_{circ} = \frac{\omega_f R_f^2}{\nu_{air}} \quad \textit{(3-12)}$$

$$\rho_{air} = \frac{P_{air}}{R_{air} T_{air}} \quad \textit{(3-13)}$$

The kinematic viscosity of air, used in equation (3-11) and (3-12), is calculated from the dynamic air viscosity (μ_{air}) as shown in equation (3-15) which in turn is calculated using equation (3-14) with the constants *a* and *b* equal to 1.458x10^{-6} and 110.4 respectively.

$$\mu_{air} = \frac{a T_{air}^{0.5}}{1 + b/T_{air}} \quad \textit{(3-14)}$$

$$\nu_{air} = \frac{\mu_{air}}{\rho_{air}} \quad \textit{(3-15)}$$

The bearing power losses ($P_{bearing}$) is estimated by using equation (3-16) in which $T_{bearing}$ is the frictional moment of the bearing. The frictional moment is calculated with equation (3-17) and is dependent on the bearing coefficient of friction (μ_b) which is 0.0015 for deep groove roller bearings, the bearing load (L_b) and the bearing bore radius (R_{bi}).

$$P_{bearing} = T_{bearing} . \omega_f \quad \textit{(3-16)}$$

$$T_{bearing} = \mu_b L_b R_{bi} \quad \textit{(3-17)}$$

The power losses associated with the vacuum system of the flywheel housing can be calculated with equations (3-18) and (3-19) (Druten, 2001). The vacuum pump power is dependent on the vacuum pressure, constants A and B with values of 6000 Pa.W and 75 W respectively as well as the efficiency of the vacuum pump electrical drive (n_{drive}) which is assumed to be 80%. The power loss from the friction torque at the vacuum seal is dependent on the flywheel shaft diameter (d_{shaft}) and flywheel speed.

$$P_{vacuum,pump} = (\frac{A}{P_{air}} + B)/n_{drive} \quad \textit{(3-18)}$$

$$P_{vacuum,seal} = 1.7\, d_{shaft} . \omega_f \quad \textit{(3-19)}$$

The power loss calculations were performed in Octave. The script containing the calculations can be found in Appendix B and the results are shown in Table 3-6. To better understand the power loss in each flywheel and to compare the self-discharge characteristics of different flywheels, the half-life time rating of the various flywheels is calculated. The half-life time rating refers to the time it takes for a flywheel to discharge to a 50% state of charge. Since the total power loss in flywheels is usually dominated by drag losses and that both the drag power losses and energy state of the flywheel is related to the square of the flywheel speed, the total power loss of the flywheel scales with the charge state of the flywheel (i.e. at 50% charge the total power loss is 50% of the maximum power loss). A similar observation is made in the work of Berkel et al. (2014). Based on this, the absolute state of charge (energy content) of the flywheel can be calculated for a time series using equation (3-20). The

analysis must account for the portion of the flywheel energy that is not usable due to the lower speed limit of the flywheel as described by equation (3-4). To do this, equation (3-21) is used to calculate the flywheel state of charge as a percentage of the usable flywheel energy. The results of the analysis are shown in Figure 3-12 and tabulated results of the time series calculations can be found in Appendix B. The half-life ratings are also given in Table 3-6.

$$ESS_{SOC,t+1} = E_{SOC,t} - \int_{t}^{t+1} P_{loss,max} \cdot \frac{Esoc,t}{E_{max}} dt \qquad \textit{(3-20)}$$

$$ESS_{charge,usable}(\%) = (E_{SOC} - E_{max}(n_u - 1))/E_{usable} \qquad \textit{(3-21)}$$

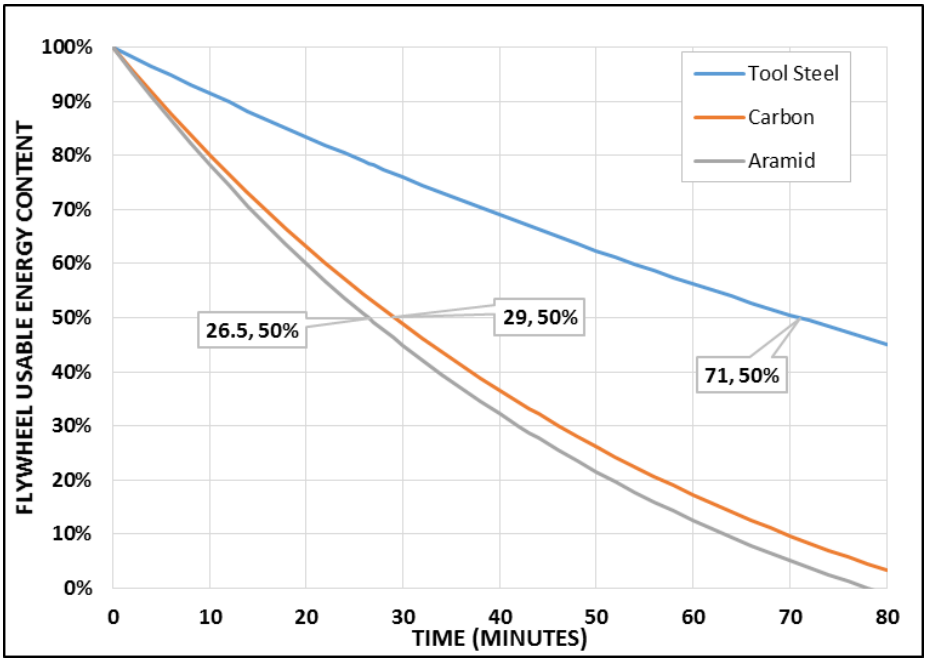

Figure 3-12: Comparison of flywheel self-discharge characteristics

Table 3-6: Power loss calculation results for various flywheels

Parameter	Tool Steel	Carbon – Epoxy	Aramid-Epoxy
$E_{max(stress)}$ (kWh)	1.58	3.69	2.00
E_{usable} (kWh)	1.18	2.77	1.50
Flywheel Mass (kg)	267.1	53.8	47.6
Flywheel Inertia (kg.m^2)	4.821	0.9703	0.8598
Flywheel Speed at E_{max} (rpm)	14 647	49 979	39 127
Drag Power Loss (W)	110	2 831	1 535
Vacuum Pump Power (W)	169	169	169
Vacuum Seal Power Loss (W)	104	356	279
Bearing power Losses (W)	121	83	57
Total Power Loss (W)	624	3 521	2 097
Half-life rating (minutes)	71	29	26.5

Of the three candidate flywheels developed in this section, the carbon composite flywheel considerably outperforms the steel and aramid composite flywheels in terms of energy capacity. The

steel flywheel has a much longer half-life rating when compared to the other two flywheels which means that although it has the lowest energy capacity, a larger portion of its energy will be available for reuse. Although not a critical requirement for this study, the mass of the steel flywheel is considerably higher than that of the composite flywheels. It is also worth noting that the steel flywheel has a much lower maximum speed than the composite flywheels which will impact the transmission overall speed ratio required for this flywheel.

3.4. Transmission

The transmission, responsible for transferring energy between the flywheel and vehicle is characterised in this section. The approach taken in this section is to develop candidate transmissions (topology A and B of section 3.2.2 shown in Figure 3-10) that will meet the requirements of each of the possible system configurations (as discussed in section 3.2.1) as well as each of the candidate flywheels for both train routes analysed in this study.

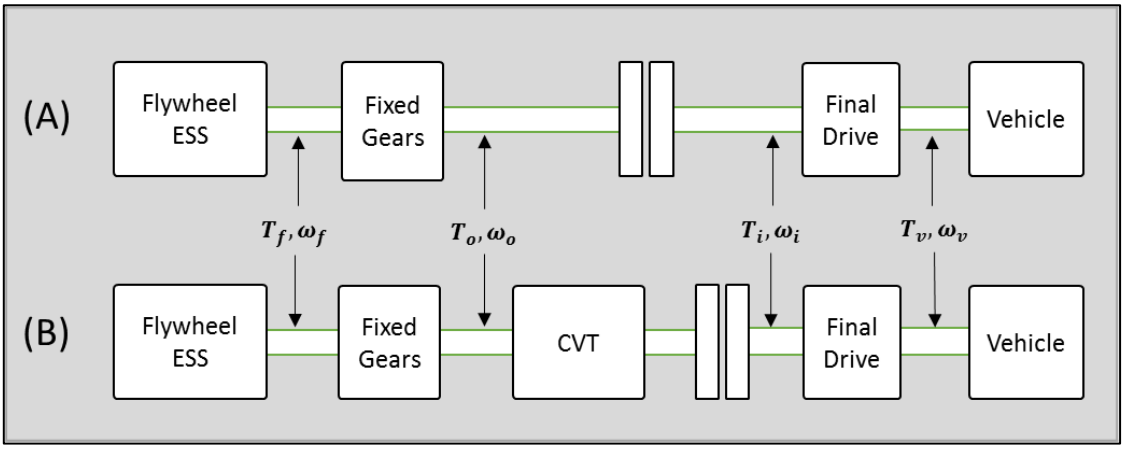

Figure 3-13: Labelled transmission topologies

It was explained previously that the second clutch in topology A is not required for functionality of the transmission but only for better heat dissipation of the high transmission losses. As the thermal analysis of the transmission is beyond the scope of this study, we will omit one of the clutches as can be seen in Figure 3-13. The transmission topologies have also been rearranged in such a way that the components that facilitate power transfer (clutches and CVT) are on the vehicle side of the fixed gear ratios to avoid the need for these components to rotate at the extremely high speeds of the flywheels.

In our analysis of the transmission, we first establish the gear ratios of the CVT, fixed gears and final drives in both topologies which contributes the overall gear ratio of the transmission (R_T) defined by equation (3-22) as the transmission output speed to the flywheel side (ω_f) over the wagon axle speed (ω_v). As topology A has no variable gear ratio component, the transmission only has a single overall gear ratio ($R_{T,A}$) made up of the final drive ratio (R_{FD}) and the ratio of the fixed gears (R_{FG}) as shown by equation (3-23). Topology B has a range of available ratios ($R_{T,B}$) due to the continuously variable transmission component. This ratio spread is limited by the maximum and minimum CVT ratios ($R_{CVT,max}$, $R_{CVT,min}$) as show in equations (3-24) and (3-25). Mechanical CVTs can typically provide a ratio spread ($R_{CVT,spread}$) of 9 as defined by equation (3-27) which is achieved by delivering a minimum gear ratio of 0.33 up to a maximum gear ratio of 3.

$$R_T = \frac{\omega_f}{\omega_v} \quad \textit{(3-22)}$$

$$R_{T,A} = R_{FD}.R_{FG} \quad \textit{(3-23)}$$

$$R_{T,B,MAX} = R_{CVT,max}.R_{FD}.R_{FG} \quad \textit{(3-24)}$$

$$R_{T,B,MIN} = R_{CVT,min}.R_{FD}.R_{FG} \quad \textit{(3-25)}$$

$$R_{CVT,spread} = \frac{R_{CVT,max}}{R_{CVT,min}} \quad \textit{(3-26)}$$

$$R_{REQ} = \frac{\omega_f}{\omega_v} \quad \textit{(3-27)}$$

To determine the gear ratios mentioned above we analyse the required overall gear ratio of the transmission (R_{REQ}) during operation which is defined by equation (3-27) as the flywheel rotational velocity (ω_f) over the rotational velocity of the wagon axle (ω_v). As the analysis of the overall transmission gear ratio considers the operating speed range of the wagon axle and flywheel, and each of the three candidate flywheels have different operating speed ranges, the overall gear ratio requirement varies for each flywheel and is established individually. The operating speed range of the train, and the train wheel axles, could be established from the train data analysed in section 3.1 and used to calculate the wheel axle speed of the train throughout the trip. With this, the required transmission ratios could be calculated for the speed ranges and is shown in Figure 3-14 for the steel flywheel. The shaded area, enclosed by the curves for the required gear ratio for the minimum and maximum flywheel speeds, represents the required transmission ratio.

It is important to consider the nature of typical freight train operations at this stage. Freight trains stop infrequently during operation and the braking and motoring applications of freight trains are largely to maintain the operating speed of the train and occasionally reduce the speed of a train for certain sections the route. For this reason, the RBS will very rarely be used to bring the train to a standstill or pull away from a stationary position or low speed. The freight trains for the routes analysed in this section operate between 20km/h and 80km/h for most of the route. Based on this information and Figure 3-14, the overall transmission ratio must be selected. From the definition of R_{REQ}, we can see that when the RBS delivers braking power, charging the FESS, the overall flywheel to axle ratio (R_T) must increase to allow for an increase in the flywheel speed and potential decrease in the wagon axle speed. The opposite is true for motoring operations as the transmission ratio (R_T) will decrease as the flywheel speed reduces during discharge. If we translate this to Figure 3-14, a charging (braking) application will require an upward shift on the graph from the direction of the blue line (minimum flywheel speed) to the red line (maximum flywheel speed). As the change in train speed, and therefore wagon axle speed, is very low compared to the change in flywheel speed during braking and motoring, a constant wagon axle speed can be assumed for this analysis. Based on this assumption, the shift in operating position on Figure 3-14 will be vertically upward or downward for braking- and motoring applications respectively.

To meet the requirements stated above, the gear ratios for topology B for the tool steel flywheel were selected as shown Figure 3-15. By selecting a fixed gear ratio (combination of final drive and fixed gear

components) of 45, a maximum- ($R_{T,B,MAX}$) and minimum ($R_{T,B,MIN}$) gear ratio of 135 and 15 can be achieved respectively with the incorporation of the CVT. As can be seen in the figure, this overall gear ratio selection allows for vertical movement between the maximum- and minimum flywheel speeds for train speeds of 18 km/h to 80 km/h. The vertical shift on the graph is made possible for this topology by a continuous increase or decrease in the ratio of the CVT. The analysis was repeated for the carbon and aramid flywheels and the resulting figures can be found in Appendix B. The tabulated results are shown in Table 3-7 below.

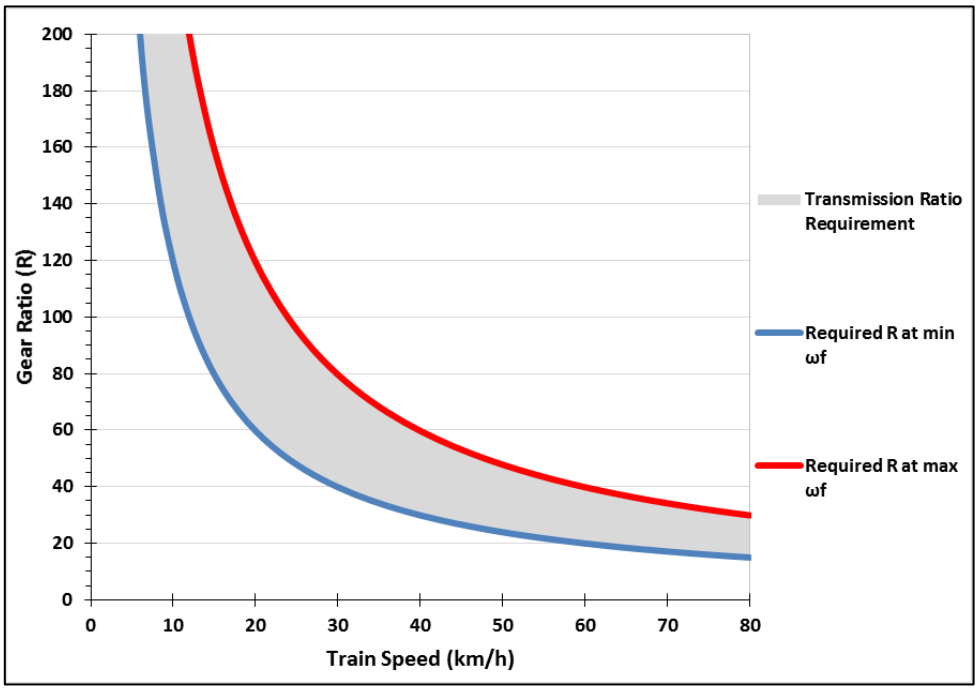

Figure 3-14: Gear ratio analysis for the Tool Steel flywheel

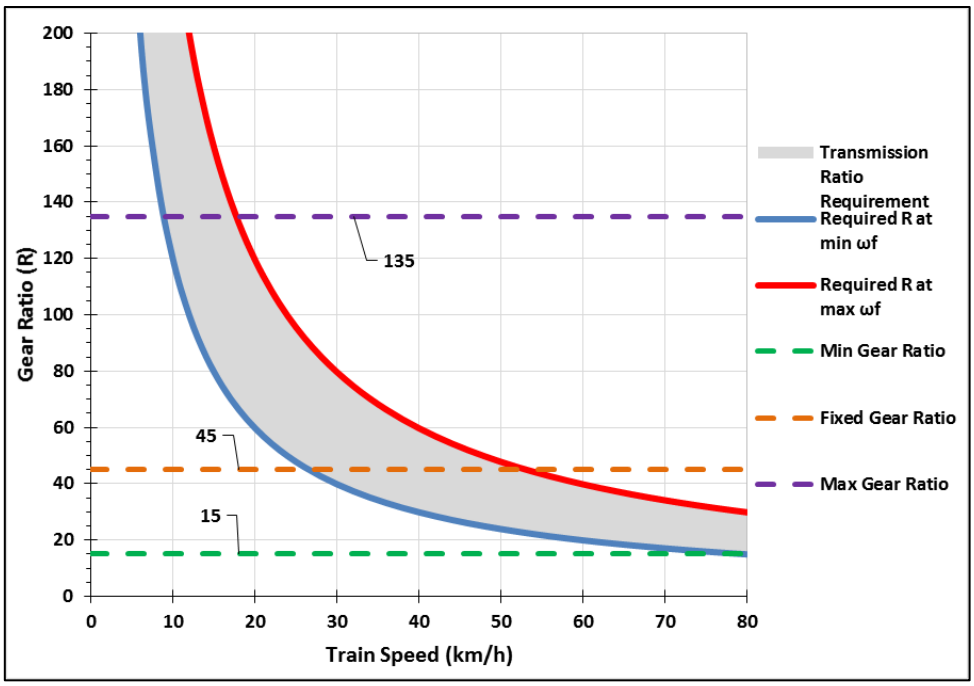

Figure 3-15: Topology B transmission gear ratio analysis for the Tool Steel flywheel

Topology A requires a different approach as it contains no variable ratio component. The only way to affect an increase (or decrease) in the flywheel speed for this topology, is when the input speed to the clutch on the wagon side (ω_i) is higher (or lower) than the input to the clutch on the flywheel side (ω_o). When this is the case, engaging the clutch causes the flywheel speed to increase or decrease depending on whether the clutch input speed (ω_i) is faster or slower than that of the flywheel side input speed. The implication of this approach is that a smaller operating train speed range can be accommodated by the RBS. In Figure 3-16 the analysis of the gear ratio of topology A for the steel flywheel is shown. Keeping the condition stated above in mind, braking applications can only be performed when the transmission ratio (R_T) is larger than the required ratio (R_{REQ}) and the opposite is true for motoring applications. If we translate this to the figure, braking can be performed for the shaded area is below the fixed gear ratio of the transmission and vice versa for motoring applications. An overall gear ratio of 30 was selected to allow for braking applications at the high end of the train speeds range and motoring applications for speeds up to 60km/h. During the concept evaluation, additional gear ratios will be evaluated to find the best suited gearing solution for Topology A. This analysis was repeated for the carbon and aramid flywheels as shown in Appendix B and the results are shown in Table 3-7.

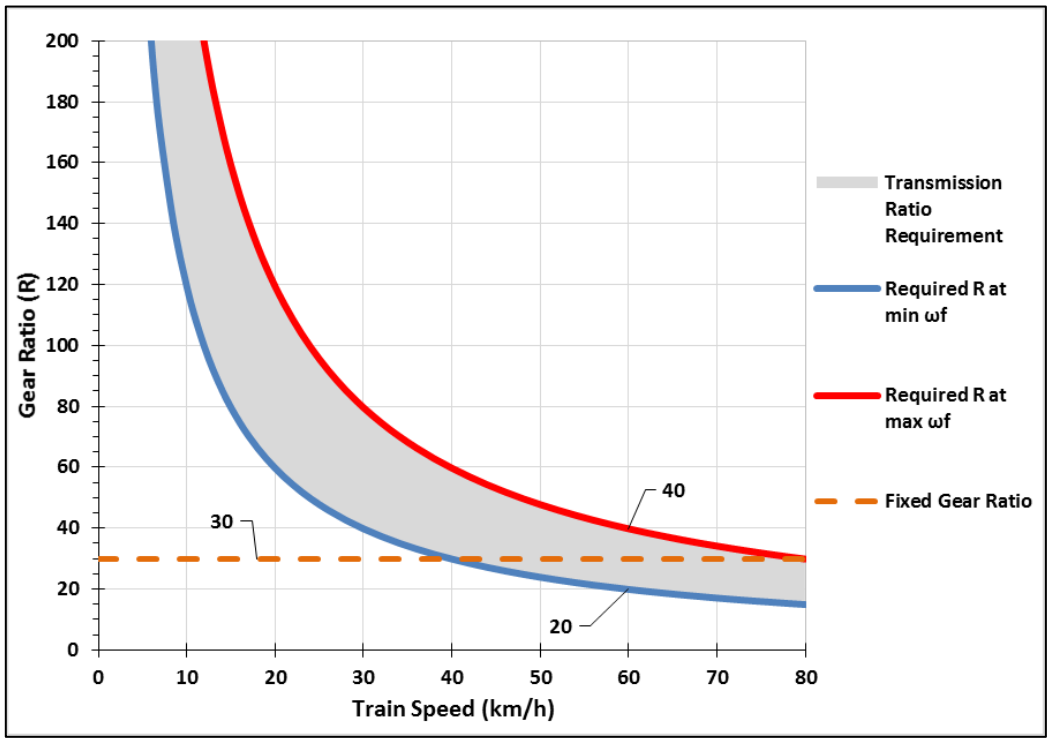

Figure 3-16: Topology A overall transmission gear ratio analysis for the Tool Steel flywheel

With the required overall transmission ratios known, the gear ratios of the final drive and fixed gear components can also be determined. A final drive ratio of 5 is commonly used in the rail industry for locomotive or powered multiple units and therefore this ratio is selected as the final drive ratio in our topologies. With the final drive ratio known, the fixed gear ratio can be calculated and is shown in Table 3-7. Apart from the tool steel topologies, the fixed gear components may require two-stage reduction gears. This however, does not affect the functionality of the system and will be assumed as a single gear set for our application.

Table 3-7: Overall transmission ratios (R_T) for the candidate topologies and flywheels

	Topology B			Topology A		
	Tool Steel	Carbon	Aramid	Tool Steel	Carbon	Aramid
Fixed Gear Ratio ($R_{T,A}$)	45	153	120	30	100	80
Min Ratio ($R_{T,B,MIN}$)	15	51	40	-	-	-
Max Ratio ($R_{T,B,MIN}$)	135	459	360	-	-	-
Final drive gear ratio (R_{FD})	5	5	5	5	5	5
Fixed gear ratio (R_{FG})	9	30.6	24	6	20	16

We can establish the torque rating for the transmission at the flywheel side using equation (3-28). It was concluded in the previous section that based on the achievable flywheel energy storage capacities, at least two RBSs must be installed per rail wagon and therefore, from Figure 3-8, the maximum power for any of the configurations will be 60kW per RBS. Also, the maximum speed for each of the candidate flywheel speeds are given in Table 3-5 and the lower limit of the flywheel speed was set at 50% of the maximum flywheel speed. With this information, the torque at the flywheel side (T_f) can be calculated as shown in Table 3-8. The worst-case torque observed, 78 Nm, is for the steel flywheel at the lower speed limit.

$$P = T.\omega \qquad \textit{(3-28)}$$

Table 3-8: Flywheel torque requirements

Parameter	Tool Steel	Carbon	Aramid
Maximum flywheel speed (rad/s)	1 534	5 234	4 097
Minimum flywheel speed(rad/s)	767	2 617	2 049
Maximum RBS Power (kW)	60	60	60
Minimum Flywheel Torque (Nm) (at ω_f max)	39	11	15
Maximum Flywheel Torque (Nm) (at ω_f min)	78	23	29

The torque at the vehicle side of the transmission (T_v) can also be calculated with equation (3-28) using the system power rating and the vehicle operating speed range obtainable from the train data analysed previously. Further to the power consideration, the torque (T_v) will also be limited by the maximum tractive effort limit. The collective distributed RBS will be limited to not exceed the tractive effort of the locomotive consist, similar to the approach used to establish the maximum power of the regenerative braking units. With the maximum tractive effort of the train obtainable from the train data for each route, and the number of wagons in the train known, the maximum tractive effort for each RBS was calculated as shown in Figure 3-8. Assuming the worst-case in which two systems are installed per wagon, the wheel axle torque (T_v) can be calculated from the tractive effort limit as the wagon wheel diameter is known. The results are shown in Table 3-9 and in Figure 3-17 and the tabulated calculations are shown in Appendix B. For train speeds of up to 23.12 km/h, the maximum torque (T_v) that the RBS will experience is 4041 Nm due to the tractive effort limit and at higher speeds the torque is limited by the power rating of the system.

With the maximum torque at the wheel axle known, as well as the gear ratios of each of the transmission components, the torque and speed range can be calculated for each stage in the transmission using fundamental speed-torque relationships.

Table 3-9: RBS torque limit

	Trip 1	Trip 2
Number of wagons in train	80	50
Maximum tractive effort per wagon (kN)	18.69	11.56
Wagon wheel diameter (m)	0.865	0.865
Maximum torque per wagon (Nm)	8082	5000
Maximum torque: 2 RBS per wagon (Nm)	4041	2500

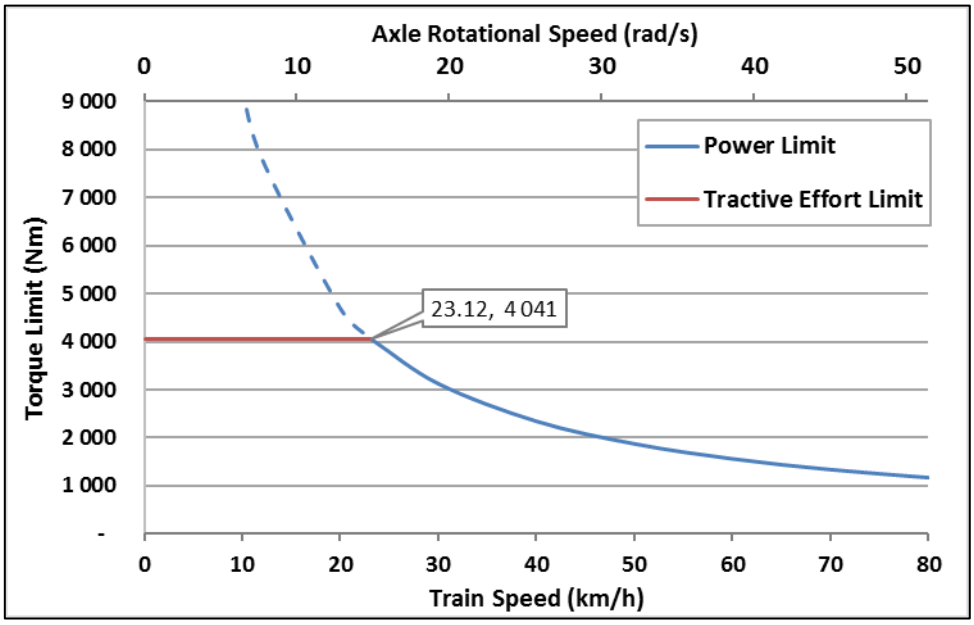

Figure 3-17: Calculation of maximum torque output to wagon wheel axle (T_v)

Lastly, the power losses for each topology can be determined based on the power-loss characteristics of each component. The power-loss models for the generic subcomponents found in the topologies; a clutch ($P_{L,C}$), fixed gears ($P_{L,G}$) and a CVT ($P_{L,CVT}$) are shown in equations (3-29) to (3-31). The CVT efficiency (η_{CVT}) is in practice dependent on the speed of its input and output shafts as well as the transmitted torque, but for this study an average efficiency value will be used. The total power losses for topology A ($P_{L,A}$) and B ($P_{L,B}$) are then characterised as a combination of the power losses of each subcomponent as shown in equations (3-32) and (3-33) respectively.

$$P_{L,C} = T_C.(\omega_i - \omega_o) \quad \textit{(3-29)}$$

$$P_{L,G} = P_G.n_G \quad \textit{(3-30)}$$

$$P_{L,CVT} = P_{CVt}.n_{CVT} \quad \textit{(3-31)}$$

$$P_{L,A} = P_{L,FD} + P_{L,C1} + P_{L,FG} + P_{L,C2} \quad \textit{(3-32)}$$

$$P_{L,B} = P_{L,FD} + P_{L,FG} + P_{L,CVT} + P_{L,C} \quad \textit{(3-33)}$$

3.5. Concept Definition

Now that the possible topologies (section 3.2), flywheels (section 3.3) and transmissions (section 4.4) have been established, a concept matrix can be defined to capture the possible system configurations as is shown in Table 3-10. The first variable to be considered is the number of RBSs that the rail wagons will be equipped with as discussed in section 3.2. In section 3.3 it was concluded that, due to the energy capacity limitations of the flywheel concepts, installing a single RBS on a wagon would not meet the minimum energy storage requirement established in section 3.1. The next variable considered in the concept matrix is the flywheel. The energy capacity requirement per RBS, as shown in Figure 3-9, is compared to the maximum energy storage capacity of each flywheel to determine which flywheels meets the specified range and the qualifying flywheels were subsequently added to the decision matrix. The last variable in the decision matrix is the transmission topologies, of which both (A and B) will be evaluated for each configuration. The gear ratios of the subcomponents of the transmission topologies are selected based on the accompanying flywheel as show in Table 3-7. With this, a total of 10 concepts are identified for evaluation.

Table 3-10: Concept Matrix

Concept	Number of RBS	Flywheel	Transmission Topology	Maximum Energy Storage Capacity (kWh)	Usable Energy Storage Capacity (kWh)
1	2	Carbon	A	7.38	5.54
2			B	7.38	5.54
3	3	Carbon	A	11.07	8.31
4			B	11.07	8.31
5		Aramid	A	6.00	4.50
6			B	6.00	4.50
7	4	Aramid	A	8.00	6.00
8			B	8.00	6.00
9		Steel	A	6.32	4.72
10			B	6.32	4.72

4. System Simulation

In the previous chapter, the distributed regenerative braking system was characterised and developed down to the major component level. The developed concepts incorporate the limitations identified for each of the subsystems in terms of available technology and the specific application thereof. This chapter covers the simulation of the developed concepts to establish the overall performance that can be achieved. The first outcome of the simulations is to verify the functionality of the proposed concepts, ensuring that the RBSs function in the expected manner during train operations. Further to this, the results obtained from the simulations reflect more accurately the achievable performance of the distributed regenerative braking system when compared to the numerical simulations performed in section 3.1.2 which used a generic RBS model and characteristics of the RBS subsystems. Each of the concepts generated in the previous chapter are modelled and simulated to establish their performance. The results obtained are subsequently used to establish the financial benefit and thereby the feasibility of the distributed RBS for freight trains in chapter 5. The last objective of the simulations is to optimize the gear ratio selection of the RBS concepts to achieve the best energy saving performance.

4.1. Simulation Method

In section 2.3, it was found that a system simulation approach has proved to be an efficient method for simulating regenerative braking systems in previous studies. The system simulation tool must allow for the modelling of the mechanical subsystems of the RBS at component level, the interface with the rail vehicle, as well as the control system of the RBS. For this study, the Siemens LMS Imagine. Lab Amesim software package (referred to as Amesim for here) was used to perform these system simulations. Amesim is an integrated multidisciplinary simulation platform which allows for the simulation of multi-domain controlled systems in a single model (Siemens, 2017).

The software provides extensive libraries of predefined physical domain components including mechanical, electrical, hydraulic, pneumatics etc. as well as application specific libraries such as cooling systems, electrical drive systems and powertrains. The software allows for interfacing of components from different libraries and applications when there is a suitable interface and checks whether the interfacing variables are compatible. For this study, components were used from the mechanical-, control and signal- and powertrain libraries. The software did not require any special hardware or dedicated solvers to perform the simulations and all simulations were performed on a Dell M6800 laptop computer (Dell, 2017).

The primary objective of the distributed RBS is to reduce the energy consumption of the train and therefore the simulation process attempts to capture the complexity of the RBS hardware and control it in such a manner that the energy savings are maximised. For this reason, the energy savings achieved is the primary performance measure considered during the simulation process and the optimisation of the RBS will aim to maximise the energy saving. The energy savings provided by a regenerative braking system ($\eta_{RBS,E}$) is a function of three factors; the self-sufficiency of the specific duty cycle (*SS*), the fraction of the braking requirement performed by the RBS ($f_{B,RBS}$) as well as the EROI of the RBS, as shown in equation (4-1). As the self-sufficiency is a function of the train duty cycle and not the RBS performance, it remains unchanged for simulation and only serves as a reference point when evaluating the energy savings achieved as it indicates the maximum potential energy saving. The

control strategy and application of the RBS is therefore implemented in such a way that the combination of the remaining two parameters are maximised.

$$\eta_{RBS,E} = SS \,.\, f_{B,RBS} \,.\, EROI \qquad \textbf{(4-1)}$$

4.2. Simulation Model

4.2.1. Model Overview

As for the simulations performed in section 3.1, the simulation in this chapter is performed at the level of a single rail wagon. This methodology does not consider the in-train longitudinal dynamics and relative motion between freight wagons, but this is not believed to significantly affect the overall energy requirements of the train. The simulation boundary encompasses the RBSs as well as the wagon axle through which power is transferred between the wagon and RBS. The kinematics of the rail wagon is excluded from the simulation. Kinematic models are typically used to establish the power requirement for a specific train route and as this data is already available from in-service measurements, including such a model would simply be an exercise in replicating the in-service data.

A breakdown of the model created to simulate the distributed RBS is shown in Figure 4-1. There are four main subcomponents in the model as seen in the figure. The RBS Hardware component contains all the physical components of the system which includes the flywheel, transmission (either of topology A or B) and the wagon axle. The controller contains the logic which evaluates the current state of the RBS Hardware as well as the Mission Profile and generates control signals accordingly. The Mission Profile component performs the function of importing the in-service train data into the simulation model that serves as input into the Controller component as well as the RBS Hardware as it dictates the speed of the Wagon Axle. Lastly, the Post-processing component is used to extract and process certain critical variables calculated throughout the simulation and generate the performance parameters of the RBS.

4.2.2. RBS Hardware

In this section, the implementation of the RBS Hardware components in the simulation programme is discussed. There are two variations of the RBS Hardware because of the two transmission concepts, topologies A and B and the implementation of these are shown in Figure 4-2 and Figure 4-3 respectively. The green colour of the components is the standard colour for components in the mechanical domain in the simulation software package. The grey objects in the figures represent inputs or outputs from the components. Four of these (labelled 1-4) are outputs from sensors incorporated in the hardware models, these sensors generate signals that are used by the controller to establish the state of the RBS. The input, number 5 for both topologies, is the clutch input signal provided by the controller which fluctuates between 0 and 1, indicating the disengaged and engaged position respectively. The RBS hardware for transmission topology B has an additional input signal, 6, which is the gear ratio of the CVT component. Lastly, both hardware variations have a torque output, labelled 6 and 7 for topology A and B respectively, which is the torque applied to the wagon axle by the RBS.

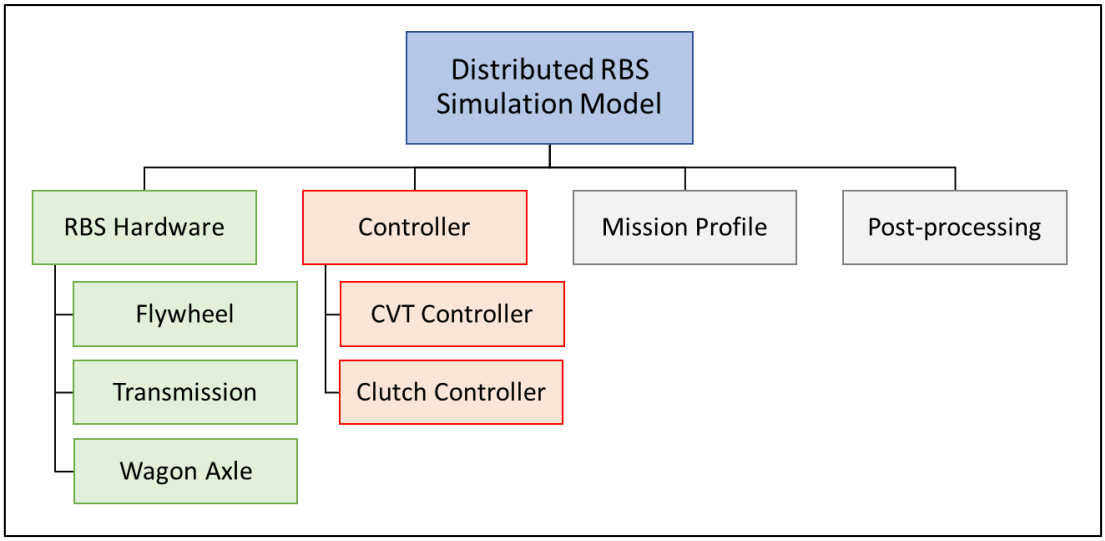

Figure 4-1: Simulation Model Breakdown

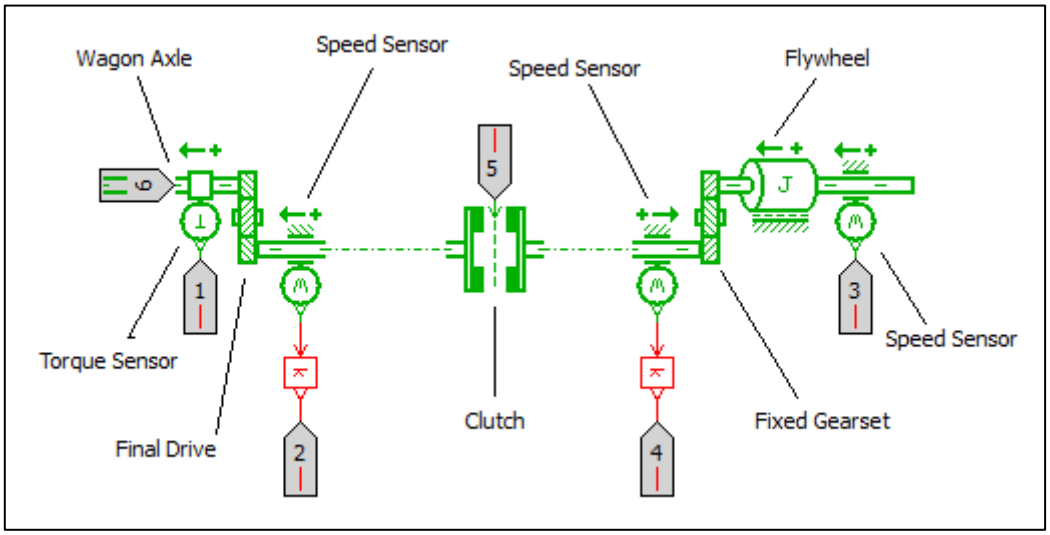

Figure 4-2: RBS Hardware – Topology A

For both topologies, the flywheel energy storage system is modelled using a rotary load with a specified inertia and a viscous friction model which captures the discharge losses of the flywheel. The viscous friction parameter is selected to give the half-life rating characteristic of each flywheel as calculated in section 3.3. The coefficient of viscous friction and resulting self-discharge characteristics for each flywheel are shown in Table 4-1 and Figure 4-4 respectively.

Table 4-1: Coefficient of Viscous Friction for Flywheel Concepts

Flywheel	Coefficient of Viscous Friction (Nm/rpm)
Steel	4.1×10^{-5}
Carbon	2×10^{-5}
Aramid	1.95×10^{-5}

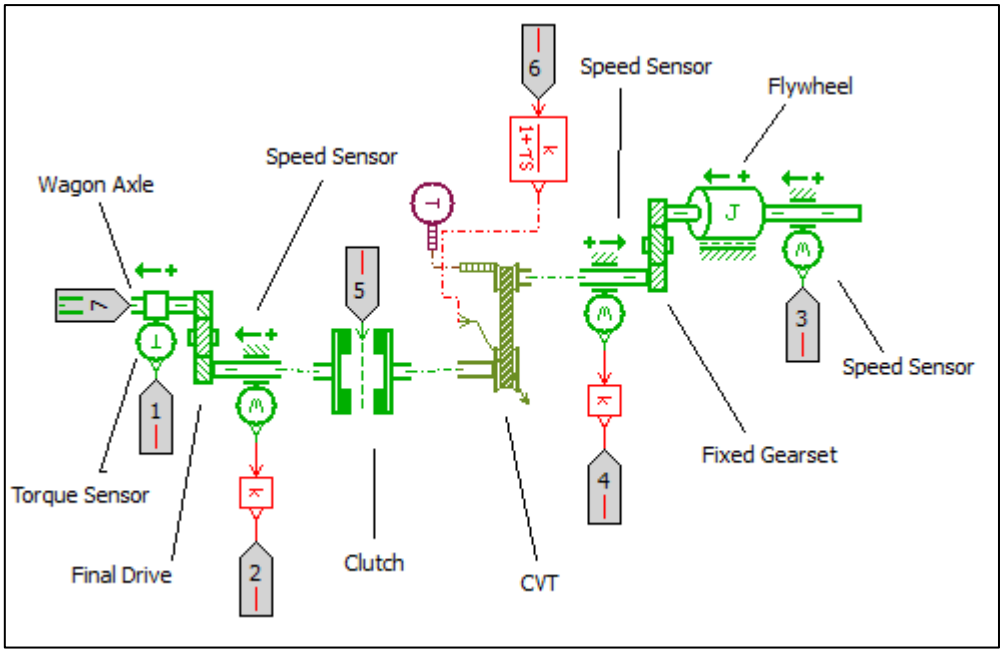

Figure 4-3: RBS Hardware – Topology B

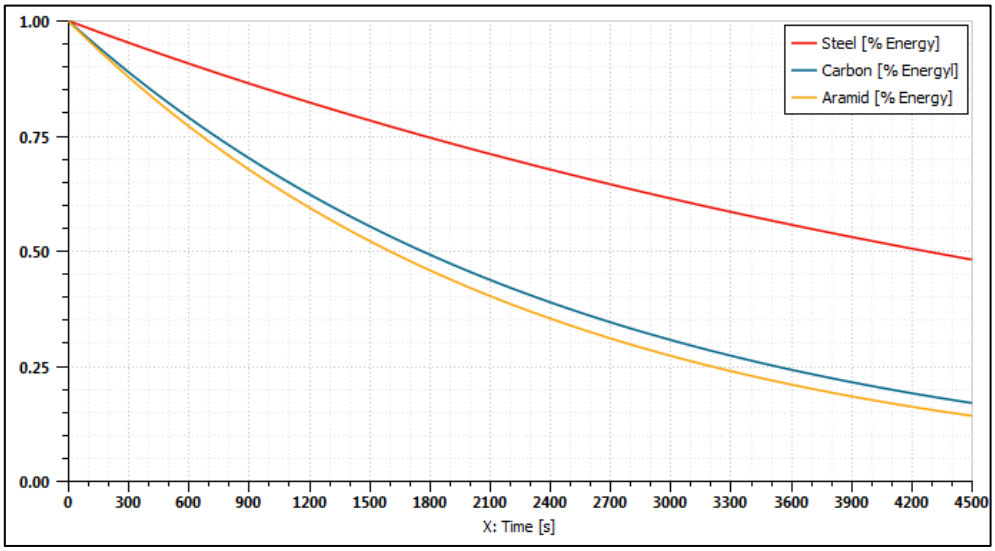

Figure 4-4: Simulated Flywheel Self-Discharge Characteristics

The fixed gears and final drive in each topology are modelled using a fixed gear ratio component with a constant gear efficiency, both of which are defined in the component model. The clutch components of the transmissions are modelled using a Coulomb friction model with a hyperbolic tangent function. The clutch receives a control signal from the controller between zero and one with zero indicating the open position and one the closed position, as discussed above. The clutch torque can also be modulated between zero and the maximum clutch torque when a control signal between 0 and 1 is provided e.g. a control signal of 0.5 will result in a clutch torque of half the maximum clutch torque. The only parameter that must be set for the clutch component is the maximum clutch torque. The maximum clutch torque is derived from the maximum RBS torque on the vehicle side and the final drive gear ratio.

Topology B includes a CVT component which is modelled using a variable gear ratio component in the simulation model. The component receives a control signal indicating the current gear ratio of the CVT. A constant efficiency model is selected for the CVT for which an averaged efficiency value is defined. The CVT component also has a thermal port through which the heat generated due to the CVT losses is dissipated to a thermal sink.

The hardware for each topology can be illustrated as input/output components as shown in Figure 4-5 and Figure 4-6. The illustrations show the signals and parameters, as discussed above, that enter and exit the hardware boundary.

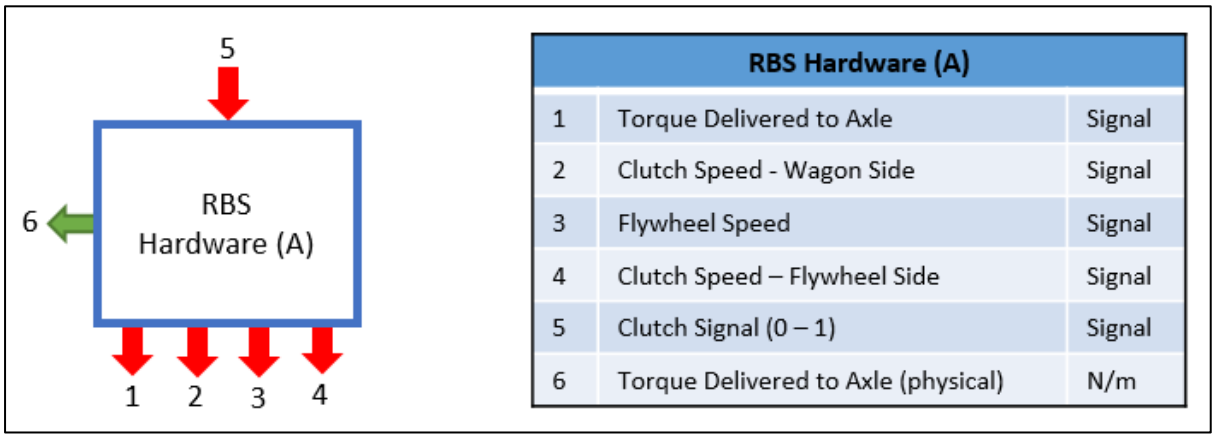

RBS Hardware (A)		
1	Torque Delivered to Axle	Signal
2	Clutch Speed - Wagon Side	Signal
3	Flywheel Speed	Signal
4	Clutch Speed – Flywheel Side	Signal
5	Clutch Signal (0 – 1)	Signal
6	Torque Delivered to Axle (physical)	N/m

Figure 4-5: Topology A Hardware Input/output illustration

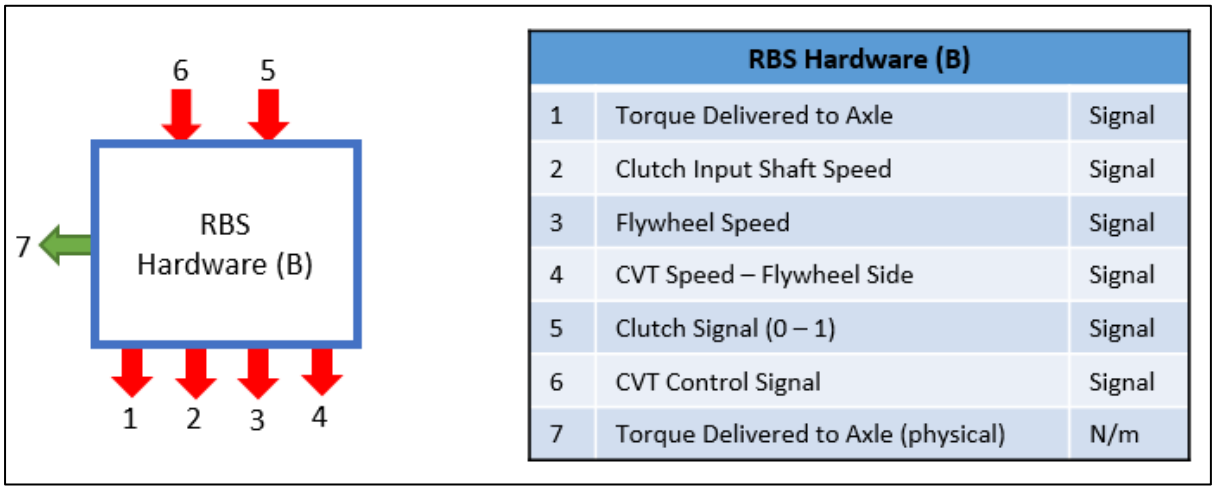

RBS Hardware (B)		
1	Torque Delivered to Axle	Signal
2	Clutch Input Shaft Speed	Signal
3	Flywheel Speed	Signal
4	CVT Speed – Flywheel Side	Signal
5	Clutch Signal (0 – 1)	Signal
6	CVT Control Signal	Signal
7	Torque Delivered to Axle (physical)	N/m

Figure 4-6: Topology B Hardware Input/output illustration

4.2.3. Control System

To simulate the regenerative braking system a control system is required to utilize the system based on the state of the train system and the state of the regenerative braking system. The primary output of the RBS controller is to control the transmission hardware. The controllable hardware in the RBS is the clutch in both topologies A and B as well as the CVT of topology B. This also implies that we will require two versions of the controller for topology A and B respectively. The RBS has three possible operating modes. The first is the motoring mode in which the RBS applies motoring torque to the wagon axle to meet the whole, or part of, the current motoring torque requirement. As for the

motoring mode, the RBS has a braking mode to meet all, or part of, the braking torque requirement. Finally, the RBS has a disengaged mode where it is not applying any torque to the wagon axles.

The parameters that influence the control decisions of the RBS are both dependent on the state of the train and the state of the RBS. There are three requirements that must be met for the RBS to be in the motoring- or braking mode, as illustrated in Figure 4-7. The first requirement is that there must be a torque- or motoring requirement at the current time-step from the train data. The second requirement is that the flywheel must have available capacity to perform either the braking or motoring requirement and lastly the required overall transmission ratio must be within limits to perform either the braking- or motoring operation. If any of the three conditions are not met, the RBS will default to the disengaged mode. Application and selection of the operating mode in the physical system is done by means of the clutch in each topology. For the disengaged mode, the clutch resides in the open position and for the motoring- and braking modes the clutch is in a partially- or fully closed position.

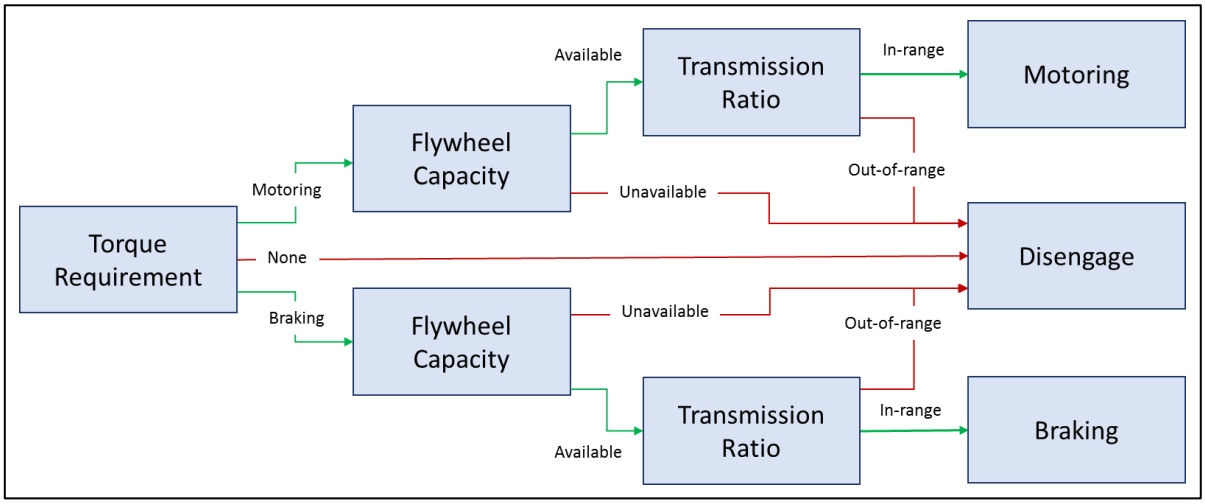

Figure 4-7: Controller Logic Illustration

4.2.3.1. Topology A Control Implementation

An input/output model of the implemented controller for topology A is illustrated in Figure 4-8. The controller receives 5 input signals (signals 3 – 7) and generates two output signals (signals 1 and 2). The implementation of the controller in the simulation software is shown in Figure 4-9.

In Figure 4-9 we see that the clutch signal (1) is generated by a *Clutch Control* component which will be discussed in further detail below. The clutch signal generated by this component passes through a *Rate Limiter* component before exiting the controller to imitate a physical clutch that cannot move from an open to closed (or vice versa) position instantaneously and the rate limiter ensures that such an event takes place over approximately half a second. The other output signal of the controller, the prime mover torque is calculated as the difference between the total torque requirement (signal 7) and the torque being applied by the RBS (signal 3) as defined by equation (3-2) and (3-3) in section 3.1.2. Signals 4 and 5 provide the shaft input speed to the clutch component in the transmission on the flywheel side and the wagon axle side respectively. The flywheel side speed is divided by the train side speed to calculate the current speed ratio across the clutch component. This clutch speed ratio is then provided to the *Clutch Control* component. Some logic is implemented to ensure that the train

signal is never passed as zero as this would cause a division by zero and would result in a simulation failure.

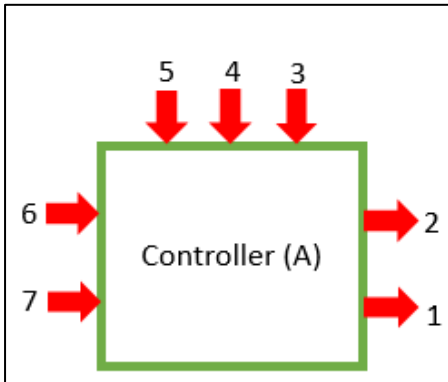

Controller (A)		
1	Clutch Signal (0 – 1) Output	Signal
2	Prime mover torque	Signal
3	Torque Delivered to Axle	Signal
4	Clutch Speed – Flywheel Side	Signal
5	Clutch Speed – Wagon Side	Signal
6	Flywheel Speed	Signal
7	Torque Requirement	Signal

Figure 4-8: Topology A Controller Input/output Illustration

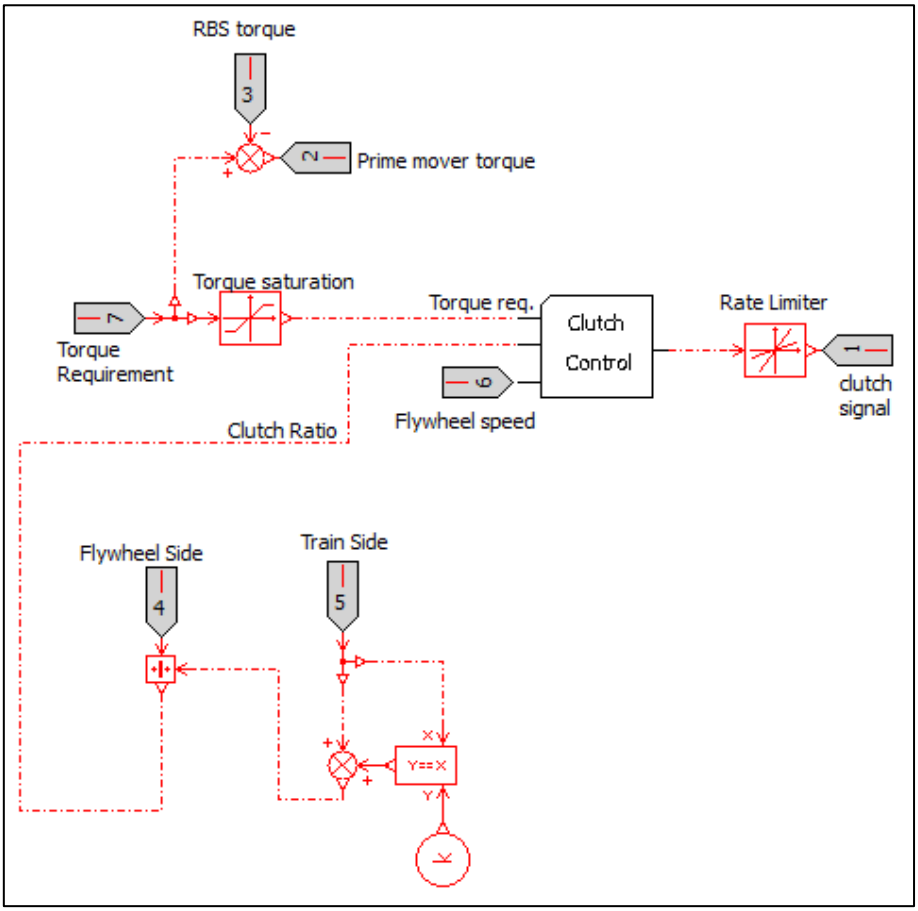

Figure 4-9: Topology A Controller Implementation

The input/output illustration of the *Clutch Control* component is shown in Figure 4-10. The three input signals (torque requirement, clutch speed signal and flywheel speed) are used to test whether the three requirements of Figure 4-7 are met for the clutch to engage the RBS. The output signal of the clutch controller is the control signal between zero and one for the clutch component.

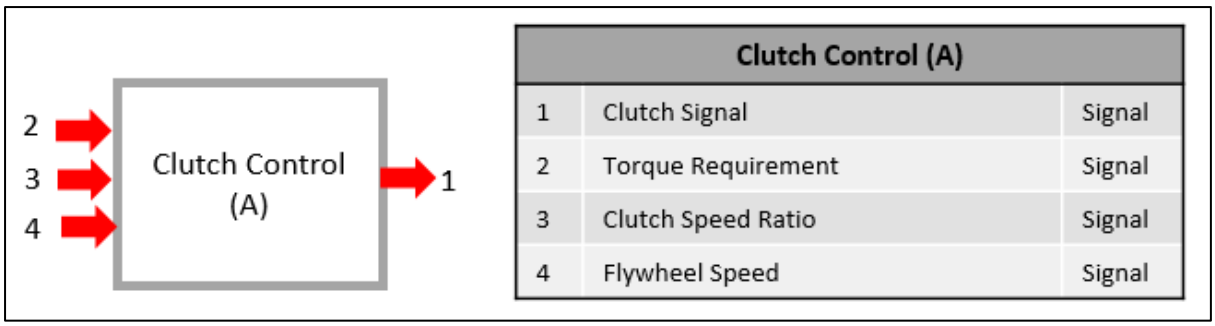

Clutch Control (A)		
1	Clutch Signal	Signal
2	Torque Requirement	Signal
3	Clutch Speed Ratio	Signal
4	Flywheel Speed	Signal

Figure 4-10: Topology A Clutch Control Input/output Illustration

The implementation of the clutch control logic is shown in Figure 4-11. In the implementation, the torque requirement signal (signal 2) is evaluated to establish whether there is currently a motoring or braking requirement. When there is a braking or motoring requirement, the signal transmitters, I and III respectively, transmit a signal value of one and when there is no motoring or braking requirement a signal value of zero is transmitted. The clutch speed ratio is evaluated to determine whether the transmission ratio is in range for motoring or braking. In section 3.4 it was explained that for topology A that relies on power transfer through the slipping clutch, the only way to increase the flywheel speed (i.e. braking) is when the transmission output speed to the flywheel is faster than the current flywheel speed. The opposite is true for reducing the flywheel speed (i.e. motoring). If we narrow this observation down to the clutch where the power transfer is attained, to increase the flywheel speed the clutch input shaft speed on the wagon side must be higher than the clutch input shaft on the flywheel side. In this case, as the clutch engages the clutch torque will cause the flywheel side clutch shaft to increase its speed. Again, the opposite is true for the reduction in flywheel speed. If we define the clutch speed ratio ($R_{Clutch,A}$) as the shaft speed of the flywheel side input shaft (ω_o) over the wagon side input shaft (ω_i) as shown in equation (4-2), it can be said that it is possible to reduce the flywheel speed when the ratio as larger than 1 and increase the flywheel speed when the ratio is less than 1. This logical test is performed in the clutch control component as shown in Figure 4-11. Transmitters A and B transmit a value of one when the transmission ratio allows for motoring and braking respectively and a value of zero when the transmission ratio does not allow for motoring or braking.

$$R_{Clutch,A} = \frac{\omega_0}{\omega_i} \qquad (4\text{-}2)$$

Lastly the flywheel speed is evaluated to establish whether there is capacity to perform braking or motoring. Transmitter X transmits a signal of one while the flywheel speed is lower than the maximum allowed speed which means that there is sufficient capacity to perform braking which will increase the flywheel speed. Transmitter Y transmits a signal of one while the flywheel speed is higher than the minimum flywheel speed which indicates that there is capacity available for motoring which will in turn decrease the flywheel speed. The three signals required for motoring (transmitters I, A, X) are multiplied by each other and outputs a value of one only when all three requirements are met and transmits a signal of one. Once these conditions are met, the signal is multiplied by a factor which indicates how the clutch must be modulated to meet the current torque requirement. This factor is calculated by dividing the current torque requirement by the maximum RBS torque as shown in Figure 4-11. This same process is repeated for the braking applications with Transmitter signals III, C and Y as shown in the figure. The braking and motoring clutch signal is then added to each other as the clutch

will engage for either of these, and is passed through as the output of the clutch control component (signal 1).

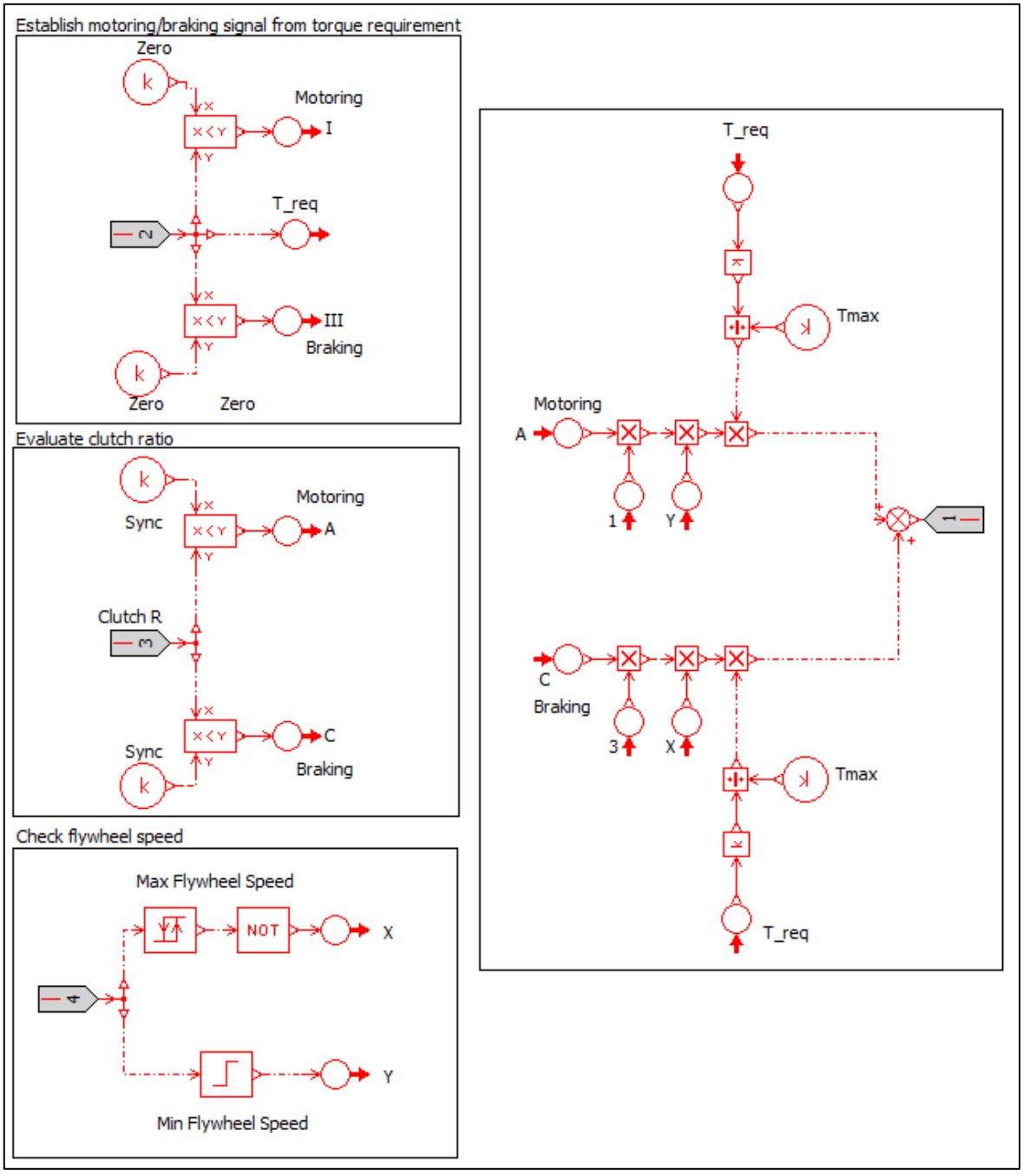

Figure 4-11: Clutch Control Implementation

4.2.3.2. Topology B Control Implementation

The input/output illustration for the topology B controller is shown in Figure 4-12. The only difference in the input/output view of the controller, compared to that of topology A, is that an additional control signal for the CVT component is generated by the controller.

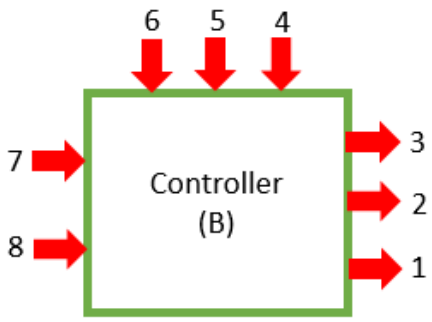

Controller (B)		
1	Clutch Signal (0 – 1) Output	Signal
2	Prime mover torque	Signal
3	CVT Control Signal Output	Signal
4	RBS Torque	Signal
5	CVT Speed – Flywheel Side	Signal
6	CVT Speed – Wagon Side	Signal
7	Flywheel Speed	Signal
8	Torque Requirement	Signal

Figure 4-12: Topology A Controller Input/output Illustration

The implementation of the topology B controller is shown in Figure 4-13. The major difference between the topology A and B controllers is the presence of a PID controller for topology B. The PID controller is used to control the CVT ratio based on the difference between the required torque and the current RBS torque, which serves as the 'error' signal input to the PID controller. It was explained in the previous chapter that the continuous variation of the CVT is the mechanism for power transfer and torque application for this topology and for this reason the CVT ratio control is of critical importance. The signal generated from the PID is passed through two switches before exiting the controller. These switches are activated whenever the required CVT ratio falls outside of the CVT ratio bounds. The CVT ratio is defined as shown in equation (4-3) similar to the clutch ratio defined for topology A. It should be noted that for topology B the ratio is defined as the vehicle side shaft speed over the flywheel side shaft speed (in contrast to our previous analysis) due to the convention of the CVT component in the simulation software in terms of how its shaft speeds at the different ports are defined. With this convention, an increase in the CVT ratio would imply a motoring application. This is particularly important for the definition of the clutch control logic. For topology B, this CVT ratio is provided to the clutch control component as shown in Figure 4-14.

$$R_{CVT,B} = \frac{\omega_i}{\omega_o} \qquad (4\text{-}3)$$

The clutch control implementation for topology B is shown in Figure 4-15. The torque requirement and flywheel speed signals are evaluated as they were for the topology A clutch control. The clutch ratio is evaluated to establish whether it is within the minimum and maximum ratio bounds of the CVT. If the signal is above the maximum CVT ratio, within the CVT ratio bounds or below the minimum ratio, transmitters A, B or C will transmit a signal value of one respectively. When the CVT ratio is within the maximum and minimum bounds, there is a motoring or braking requirement and the flywheel has the available capacity, the clutch in the RBS can be engaged and power transfer is facilitated by the CVT ratio control. This is shown in the implementation by the multiplication of signals B, Y and I for motoring and signals B, X and III for braking. Although power transfer facilitated by the CVT is the primary mechanism for topology B, an additional mechanism for braking is required to ensure the functionality of the RBS. As the flywheel speed will likely be zero at the start of a train trip,

and may coast down to very low speeds during long periods of inactivity, the required overall transmission ratio (R_{REQ}) can approach zero in certain scenarios which would mean that CVT braking will not be possible. To avoid this, a clutch braking functionality is required similar to the mechanism used for power transfer for Topology A. When the CVT ratio is above the maximum CVT bound (i.e. the flywheel speed is to low relative to the vehicle speed) and there is a braking requirement, the clutch will engage to allow for clutched braking. This is shown in the implementation with the multiplication of signals A, X and III as well as the torque factor to modulate the torque output as was done for Topology A. The clutch signals for the braking and motoring scenarios are added together once again and exits the clutch control component.

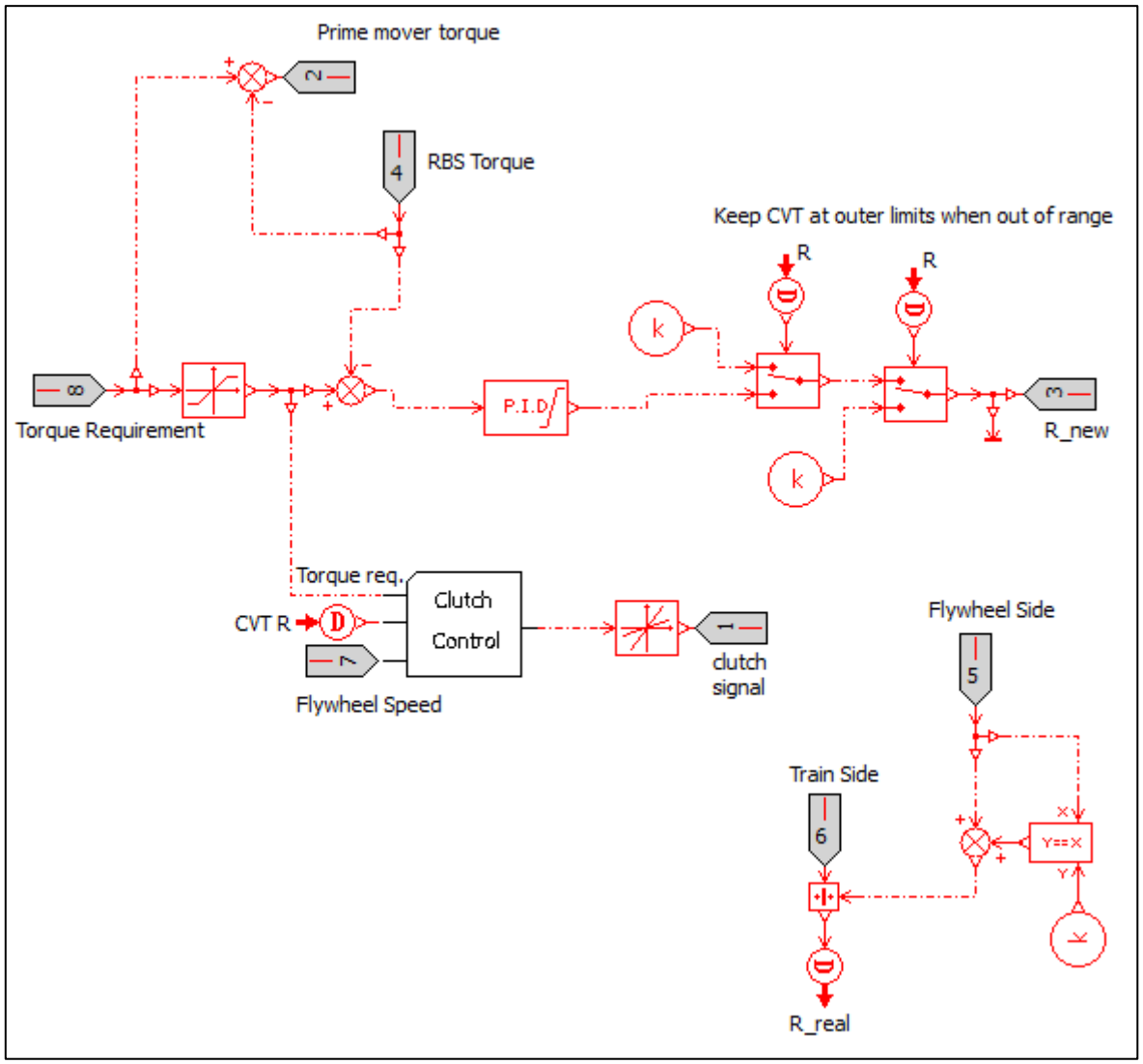

Figure 4-13: Topology B Controller Implementation

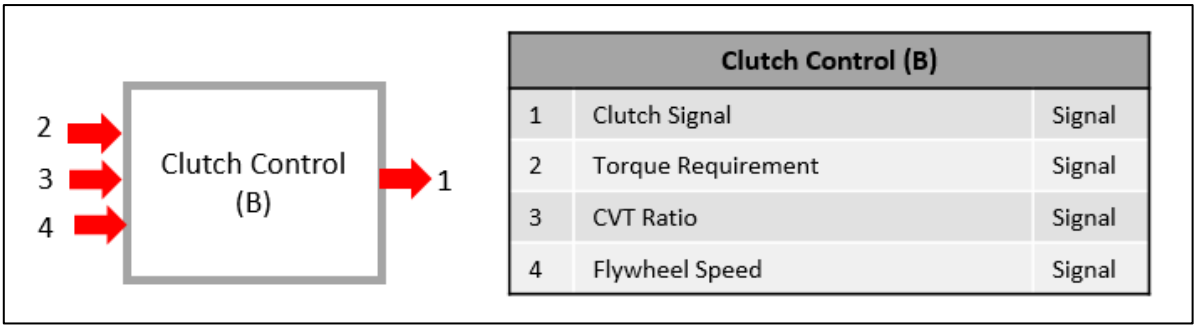

Clutch Control (B)		
1	Clutch Signal	Signal
2	Torque Requirement	Signal
3	CVT Ratio	Signal
4	Flywheel Speed	Signal

Figure 4-14: Topology B Clutch Control Input/output Illustration

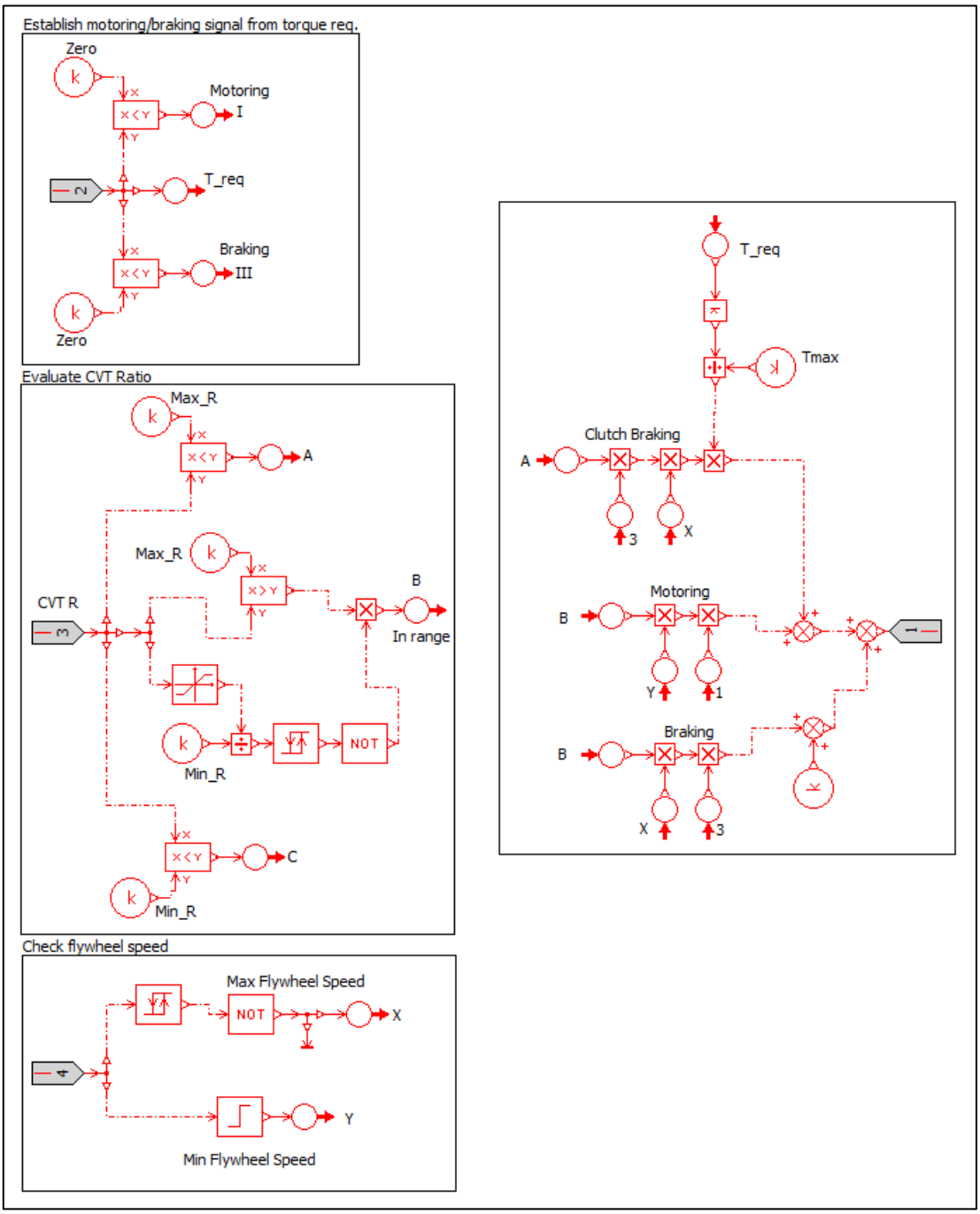

Figure 4-15: Topology B Clutch Control Implementation

4.2.4. Mission Profile

The Mission Profile subcomponent performs the function of importing the measured train data into the simulation model and processing it to deliver the required inputs from the data to the RBS hardware and control system. The two outputs from this component is the torque requirement from the train data as well as the wagon axle speed in radians per second as shown in Figure 4-16. As the simulation is performed at the level of the rail wagon, the power requirement is for a single wagon.

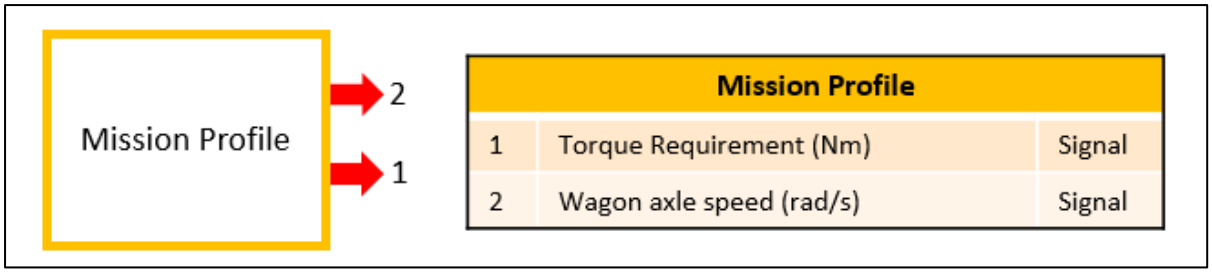

Mission Profile		
1	Torque Requirement (Nm)	Signal
2	Wagon axle speed (rad/s)	Signal

Figure 4-16: Mission Profile Input/output Illustration

The implementation of the mission profile component is shown in Figure 4-17. Two interpolation components are used to import text files that contain the longitudinal train speed and the power requirement per wagon for the train trip respectively. As the train data is provided at a rate of 1Hz, interpolation of this data is required for the simulation which is performed at much smaller time steps. The train speed is divided by the wagon wheel radius (represented by a constant input in the implementation) to calculate the wagon axle speed in radians per second. The axle speed is then passed through a saturation element with a minimum value of 0.1 to avoid that the power requirement is divided by zero which would result in an infinite tractive effort or torque requirement. The power requirement is divided by the wagon axle speed to calculate the torque requirement for the wagon. This torque requirement is then passed through a saturation component to limit the torque to the maximum allowable RBS torque. The wagon axle speed and the torque requirement for the wagon signals are then provided as outputs of the mission profile component.

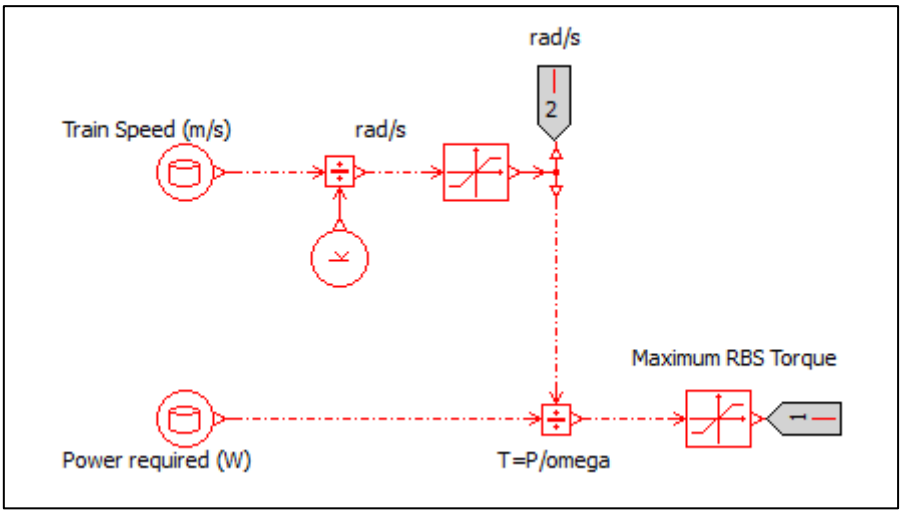

Figure 4-17: Mission Profile Implementation

4.2.5. Post-processing

In section 3.1.2, several key parameters were defined in equations (3-6) to (3-9) which were calculated during the post processing of the simulation in the section. These include the RBS braking fraction, energy saving provided by the RBS and the EROI of the RBS. These parameters must be calculated in the simulation of this chapter to evaluate the overall performance of the RBS. The post processing component requires three inputs to perform these calculations; the wagon axle speed, the torque applied by the RBS and the torque requirement of the wagon as shown in Figure 4-18.

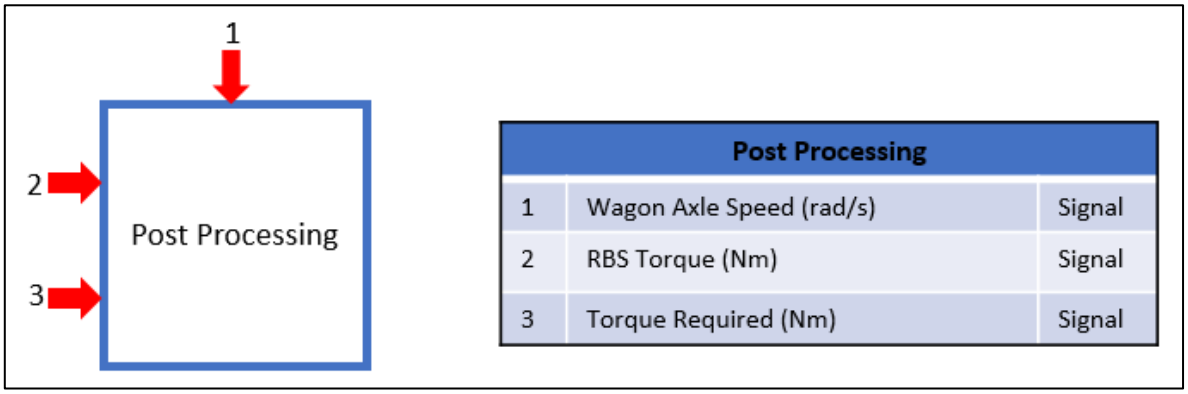

Post Processing		
1	Wagon Axle Speed (rad/s)	Signal
2	RBS Torque (Nm)	Signal
3	Torque Required (Nm)	Signal

Figure 4-18: Post-processing Input/output Illustration

In the post processing implementation, shown in Figure 4-19, saturation components are used to separate both the required torque and RBS torque signals into a motoring torque and braking torque signal. To generate the motoring signal, the torque signal is sent through a saturation component with a minimum output value of zero and for the braking torque signal the saturation element has a maximum output value of zero. The torque signals (motoring and braking) is then multiplied by the wagon axle speed to generate the power signals which in turn are sent through integrator components to perform the integration as shown in equations (3-6) and (3-9). From these signals the performance parameters are calculated as shown in Figure 4-19. The self-sufficiency measure, a characteristic of the train duty cycle calculated in section 3.1.1, is also calculated during the post processing which is used to validate that the measured train data is imported and processing correctly in the simulation model.

4.2.6. Integration

With each of the subcomponents implemented and contained as an input/output model, the components are integrated to form the complete simulation model. The corresponding signals that serve as the inputs and outputs of the respective subcomponents are connected as shown in Figure 4-20. The figure shows the integrated model for topology B which includes the CVT Ratio signals that are not found in the Topology A simulation model.

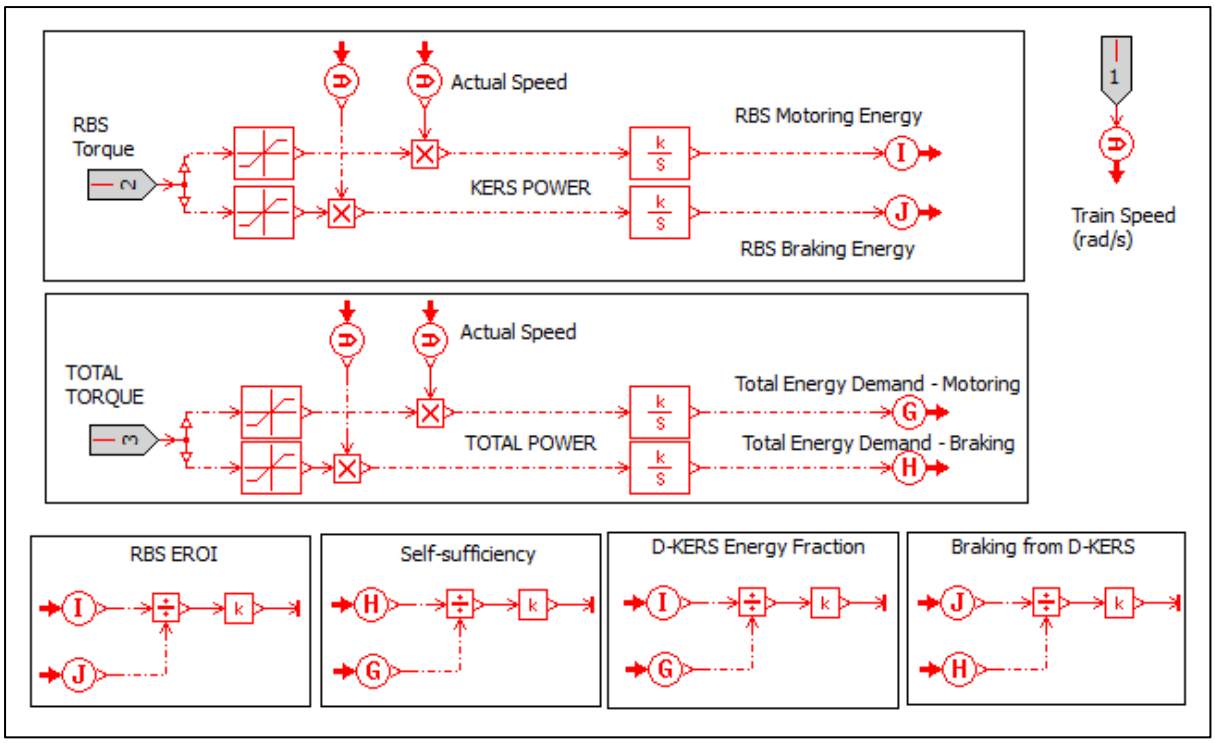

Figure 4-19: Post-processing Implementation

With the conclusion made in section 3.2.1 that at least two regenerative braking systems will be installed on each unpowered wagon, the simulation which is performed at wagon level must accommodate, or allow for, these multiple systems. To incorporate the multiple RBSs in the simulation model, the properties of the multiple systems will be lumped together into a single RBS for the simulation rather than modelling each individual RBS. This is done to avoid unnecessarily increasing the computational expense of the simulations as well as avoiding the need for repeatedly changing the simulation model (or building additional simulation models) for the concepts with varying numbers of RBS. The approach of modelling a single RBS with the lumped properties for the multiple RBS allows for only altering the input parameter set when evaluating the various concepts.

The flywheel parameters of the multiple systems are lumped together as shown in equation (4-4) and (4-5). The flywheel inertia (I_F) and coefficient of viscous friction (μ_F) are multiplied by the number of systems (n_{RBS}) to calculate the lumped parameters. As the maximum flywheel speed is identical for each flywheel, this method ensures that the total energy storage capacity scales with the number of systems installed and ensures that the flywheel half-life discharge rating remains unchanged with the change in the number of systems. In section 3.2.1 it was explained that the total power- and torque-capability for the combination of RBS on a single wagon remain unchanged and equal to the total power- and torque- limit of the locomotive consist, these parameters remain unchanged with a change in the number of RBSs.

$$I_{F,Lumped} = n_{RBS}.I_F \quad \textit{(4-4)}$$

$$\mu_{F,Lumped} = n_{RBS}.\mu_F \quad \textit{(4-5)}$$

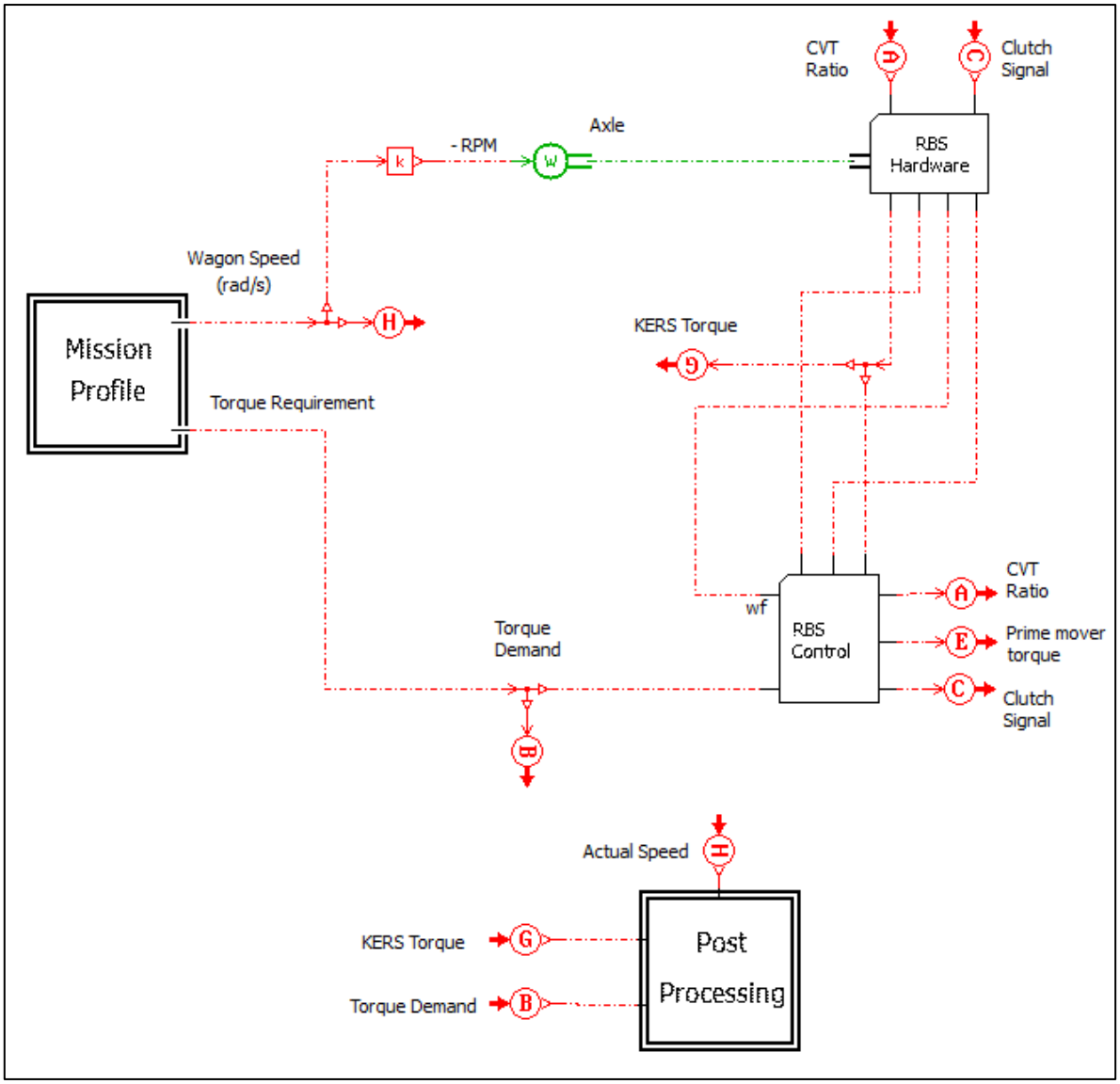

Figure 4-20: Topology B Integrated System Simulation Model

4.3. Simulation Procedure

4.3.1. Model Parameters

Once the construction of the simulation model is completed, the next step is to populate the parameters of each component in the model. Each of the 10 concepts of the RBS that will be simulated, five for topology A and five for topology B, requires a unique set of parameters for the RBS hardware. In Table 4-2 the model parameters related to the flywheel is shown for all 10 concepts. The parameters for the transmission components are grouped based on the topology (A and B) and is shown in Table 4-3 and Table 4-4.

Table 4-2: Flywheel Parameters

Concept	# RBS	Flywheel	Max. Flywheel Speed	Min. Flywheel Speed	Flywheel Inertia[1]	Viscous Friction Coefficient[2]
1	2	Carbon	49 979	24 990	1.941	4.00E-05
2	2	Carbon	49 979	24 990	1.941	4.00E-05
3	3	Carbon	49 979	24 990	2.911	6.00E-05
4	3	Carbon	49 979	24 990	2.911	6.00E-05
5	3	Aramid	39 127	19 564	2.579	5.85E-05
6	3	Aramid	39 127	19 564	2.579	5.85E-05
7	4	Aramid	39 127	19 564	3.439	7.80E-05
8	4	Aramid	39 127	19 564	3.439	7.80E-05
9	4	Steel	14 647	7 324	19.28	1.64E-04
10	4	Steel	14 647	7 324	19.28	1.64E-04

[1]From equation (4-4) and Table 3-6. [2]From equation (4-5) and Table 3-6.

Table 4-3: Topology A Concepts Transmission Parameters

Concept	# RBS	Final Drive Ratio	Reduction Gears Ratio	Reduction Gears Efficiency	Final Drive Efficiency
1	2	5	20	0.97	0.97
3	3	5	20	0.97	0.97
5	3	5	16	0.97	0.97
7	4	5	16	0.97	0.97
9	4	5	6	0.97	0.97

Table 4-4: Topology B Concepts Transmission Parameters

Concept	# RBS	CVT Ratio Min	CVT Ratio Max	Final Drive Ratio	Reduction Gears Ratio	CVT Efficiency	Reduction Gears Efficiency	Final Drive Efficiency
2	2	0.33	3	5	30.6	0.93	0.97	0.97
4	3	0.33	3	5	30.6	0.93	0.97	0.97
6	3	0.33	3	5	24	0.93	0.97	0.97
8	4	0.33	3	5	24	0.93	0.97	0.97
10	4	0.33	3	5	9	0.93	0.97	0.97

In addition to the hardware parameters, the simulation requires parameters that are a specific to the train trip being simulated as shown in Table 4-5.

Table 4-5: Simulation Trip Specific Parameters

Parameter	Trip 1	Trip 2
Maximum RBS Combined Torque (Nm)	8 082	5 000
Maximum Clutch Torque (Nm)	1 616	1 000
Wagon Wheel Contact Diameter (m)	0.433	0.433
Total Time (s)	51 789	55 214

Lastly the parameters for the RBS controller must be specified. As mentioned previously, the parameters required by the controllers are predominantly parameters of the RBS hardware. The Clutch Control component requires parameters such as the maximum clutch torque, maximum flywheel speed and transmission gear ratios. The PID controller responsible for controlling the CVT ratio in topology is the only exception. The selected PID parameters are shown in Table 4-6. The PID parameters were tuned iteratively so that the torque supplied by the RBS follows the required torque as close as possible.

Table 4-6: Topology B PID Controller Parameters

PID Parameter	Value
Anti-windup method	Clamping
Proportional gain	0.01
Integral Gain	0.0001
Derivative Gain	0
Time constant for 1st order lag estimate	0.001
Minimum output value	Min. CVT Ratio
Maximum output value	Max. CVT Ratio
Backtracking gain	0.2

4.3.2. Analysis Procedure

With the model setup complete and input parameters specified the simulations could be performed. To illustrate the simulation results and verify the functionality of the RBS with the topology A transmission, we consider the results obtained for the simulation of concept 1 on trip 1. After this, we review the results for concept 2 for trip 1 for the RBS with topology B transmission. The results obtained for the key performance measures of the RBS are shown in Figure 4-21. The figure shows that the RBS provided 42.5% of the braking requirement, the EROI of the RBS was 16.5% and the energy savings provided was 2.9%. We also see that the self-sufficiency for the simulated route was calculated to be 40.6% which correlates to the self-sufficiency characteristic of the route calculated in chapter 3. From these results, we can verify that equation (4-1) holds for this simulation which provides confidence that the performance measures are calculated correctly by the post-processing component in the simulation.

Next, we look at the torque delivered by the RBS against the torque required by the mission profile for the specific trip. Figure 4-22 shows the torque results for a portion of the trip. It is seen that the RBS functions as desired, providing braking- or motoring torque equal to the required torque as and when it has sufficient capacity and energy available. Figure 4-23 illustrates how the clutch signal is

modulated to deliver the required torque for the same portion of the trip. These results further verify that the RBS functions in the desired manner.

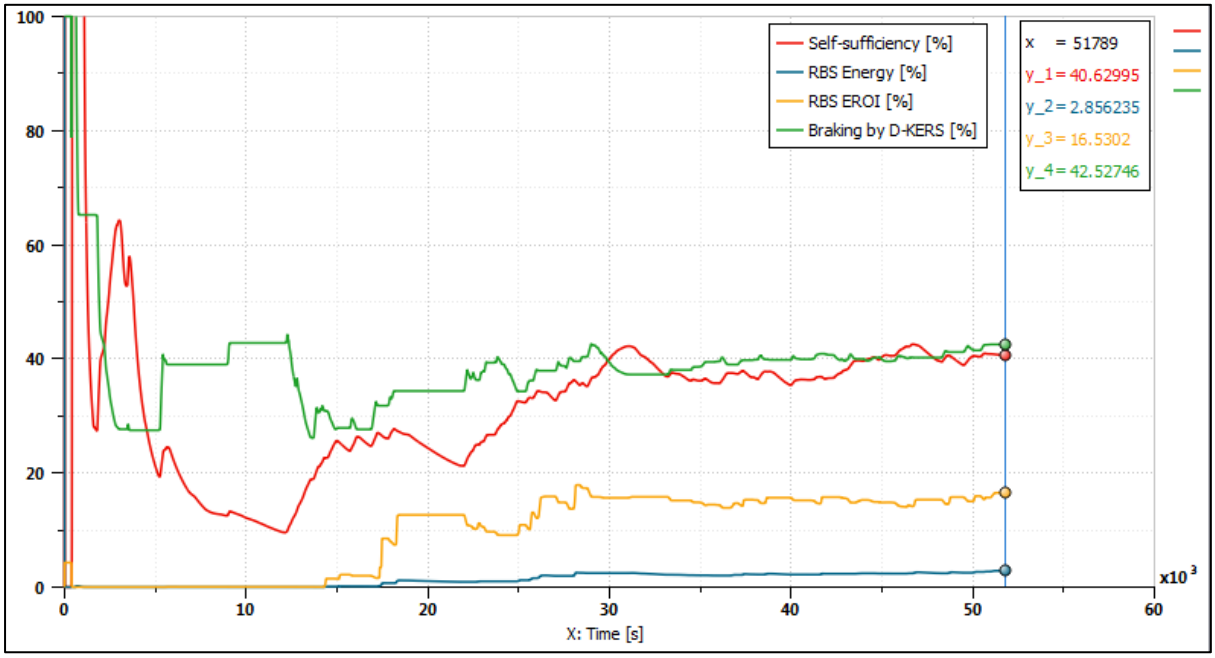

Figure 4-21: Concept 1, Trip 1 – RBS Performance Measures Results

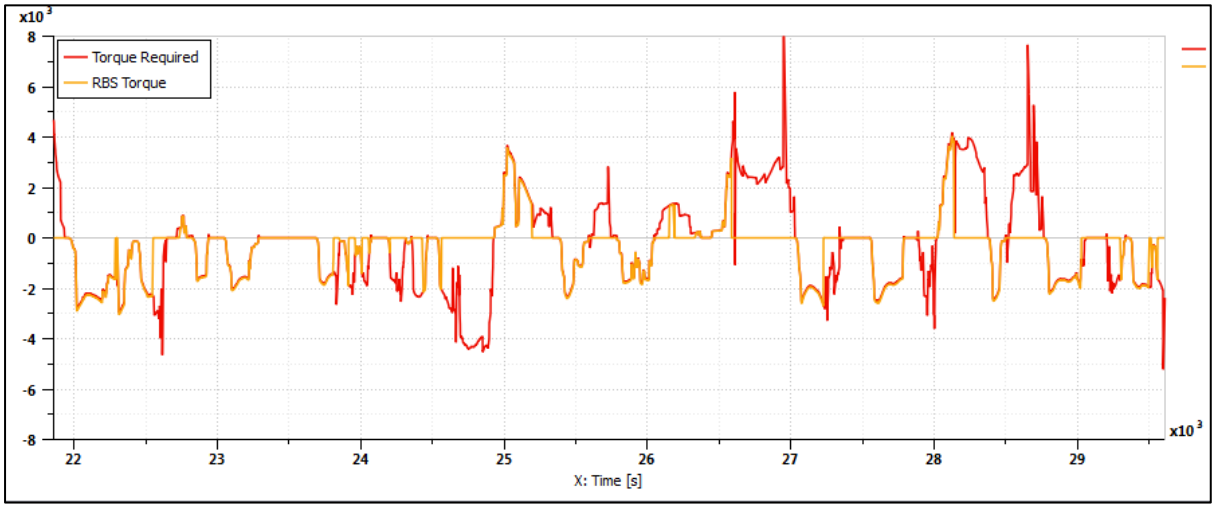

Figure 4-22: Concept 1, Trip 1 – RBS Torque Results

Figure 4-24 shows the flywheel velocity results for the simulated train trip as well as the maximum and minimum flywheel operational velocity. We see that the flywheel never reaches its maximum operational velocity, which indicates that the flywheel capacity is not fully utilized in this case. Figure 4-25 shows the overall transmission ratio (R_T) throughout the trip along with the fixed gear ratio of concept 1. It can be observed that the fixed gear ratio is located towards the lower end of the required gear ratio requirements throughout the trips, which indicates that adjusting (increasing) the fixed gear ratio may improve the performance of the RBS and better utilise the flywheel capacity. It was also discussed in the previous chapter that the selected fixed gear ratios must be optimised using the simulation model due to the limitations of the method used to select the initial gear ratios.

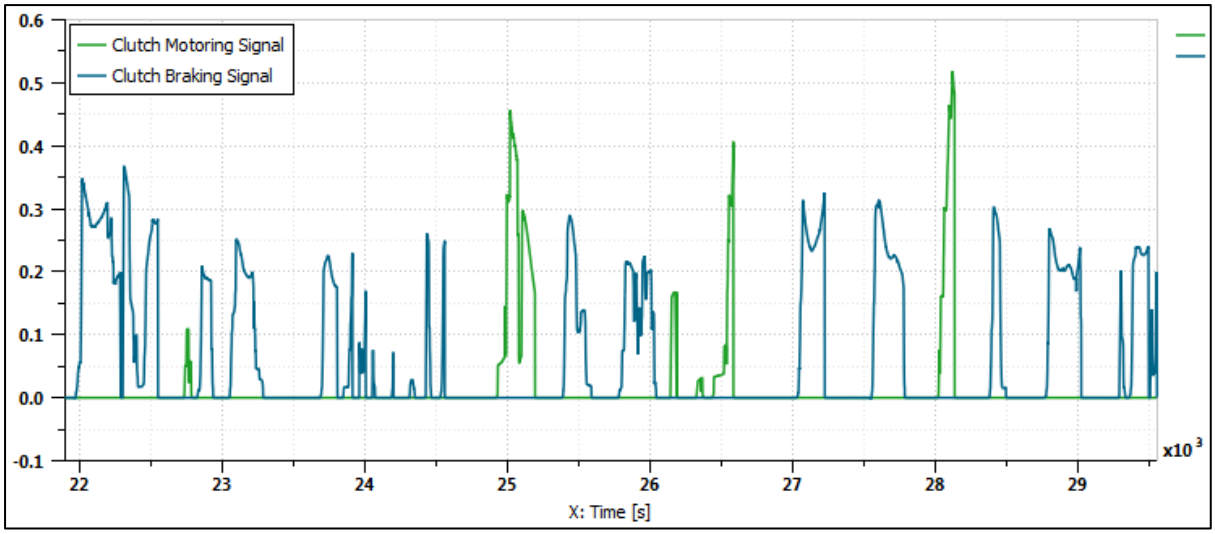

Figure 4-23: Concept 1, Trip 1 – Clutch Signal Results

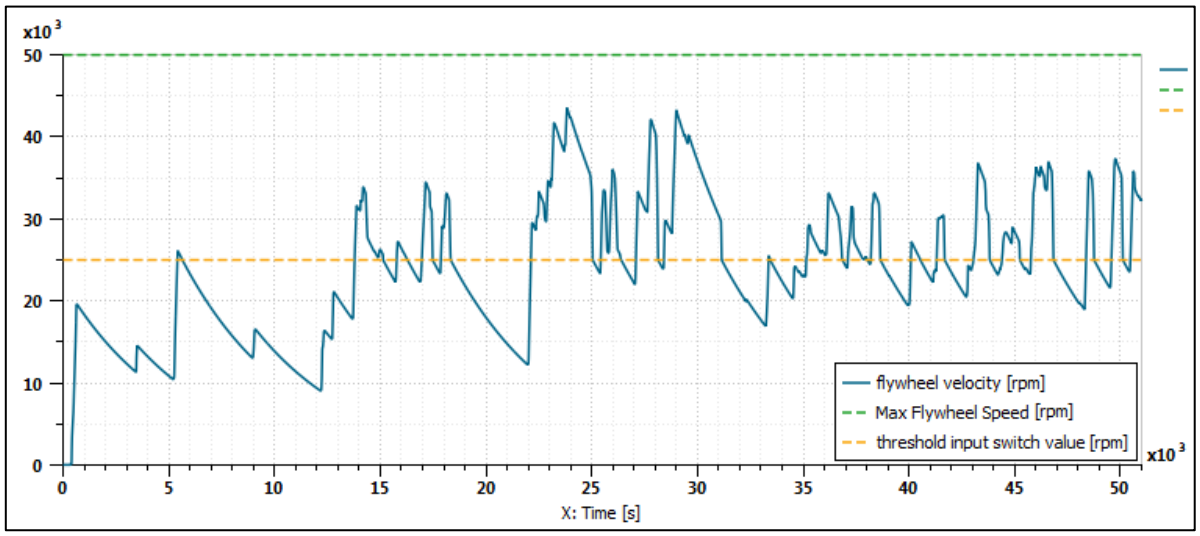

Figure 4-24: Concept 1, Trip 1 – Flywheel Rotational Speed Results

To evaluate and select the best fixed gear ratio for each RBS concept, the concept is simulated for a range of reduction gear ratios for both train trips. The energy savings results are then compared for each iteration and the gear ratio which yields the best results across the two train trips is selected as the final gear ratio. The results for this procedure for concept 1 is shown in Figure 4-26 and it is observed that a reduction gear ratio of 28 (rather than the original gear ratio of 20 as specified in

Table 4-3) delivers the best energy savings results across the two train trips. In Figure 4-27 it can be seen that the modified gear ratio allows for the full capacity of the flywheel to be utilised.

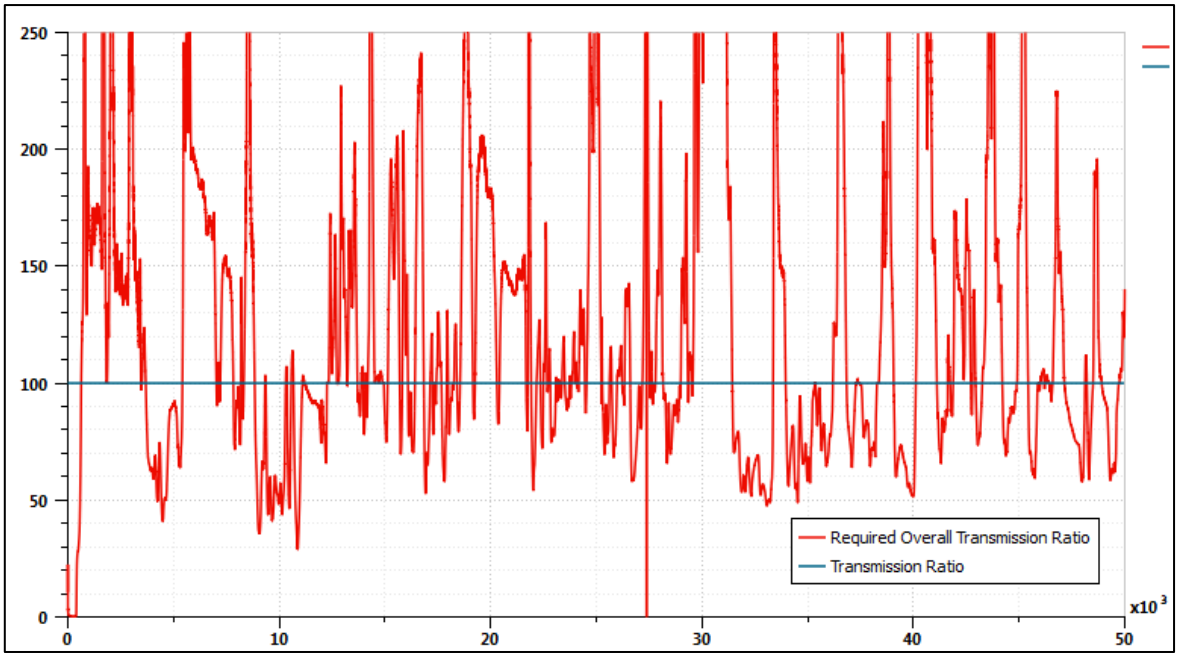

Figure 4-25: Concept 1, Trip 1 – Simulated Overall Transmission Ratio (R_T) Requirement

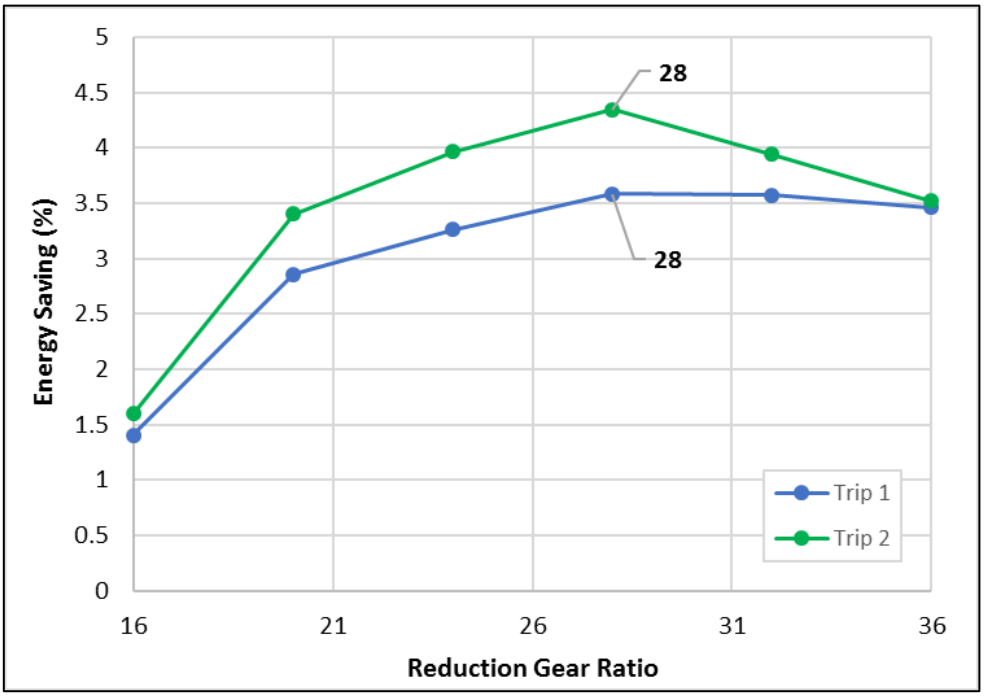

Figure 4-26: Concept 1 – Energy Savings Results for Various Reduction Gear Ratios

This process was repeated for each of the concepts with the topology A transmission and the individual results can be seen in Appendix C. The resulting modified gear ratio for each of the topology A concepts are shown in Table 4-7.

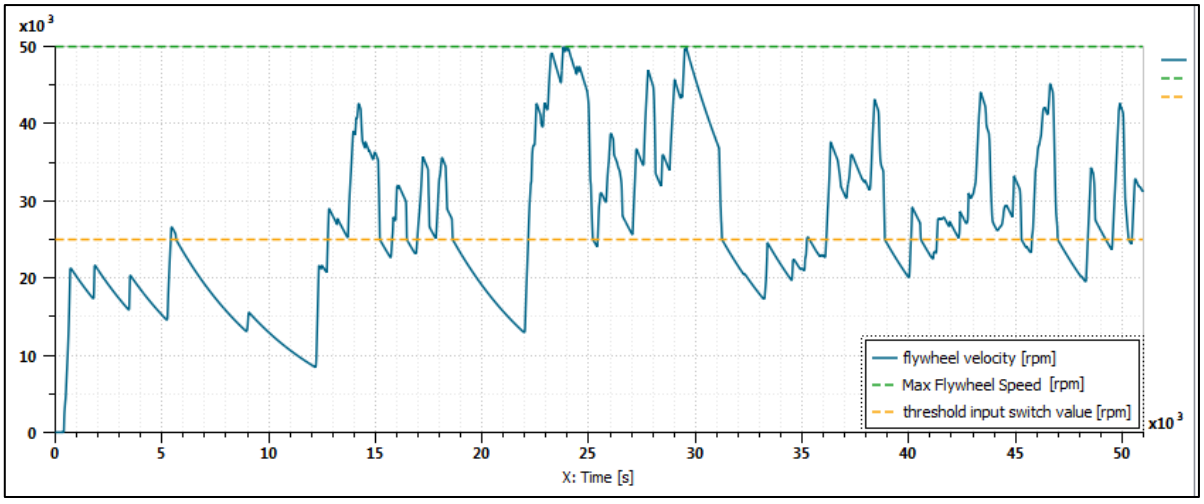

Figure 4-27: Concept 1 (modified), Trip 1 - Flywheel Rotational Speed Results

Table 4-7: Topology A- Optimised Reduction Gear Ratio Results

Concept	Reduction Gear Ratio	
	Original	Modified
1	20	28
3	20	24
5	16	24
7	16	20
9	6	9
11	6	8
13	6	8

The performance measure results for concept 2 on trip 1 are shown in Figure 4-28. Once again, equation (4-1) holds which indicates that the performance measures are processed correctly again and that the RBS is performing its intended function of providing energy savings.

For topology B, rather than modulation of the clutch to achieve the desired torque output, the CVT ratio is varied which in turn varies the overall transmission gear ratio to provide the desired torque. Figure 4-30 shows how the overall transmission ratio (R_T) was varied for a portion of the trip to achieve the required torque along with the required overall transmission ratio ($R_{T,REQ}$) and the minimum and maximum overall transmission ratios ($R_{T,MIN}$ and $R_{T,MAX}$).

Repeating the process performed for concept 1, concept 2 was simulated for a range of reduction gear ratios. The results obtained differed significantly from the previous analysis however, as the range of reduction ratios provided almost identical energy saving results with variations of less than 1.5% observed. This can be attributed to the varying ratio of the CVT component which accommodates a wide range of overall transmission ratios. For this reason, it was not necessary to perform the optimisation procedure used for topology A, and the existing gear ratios remain unchanged for all topology B concepts.

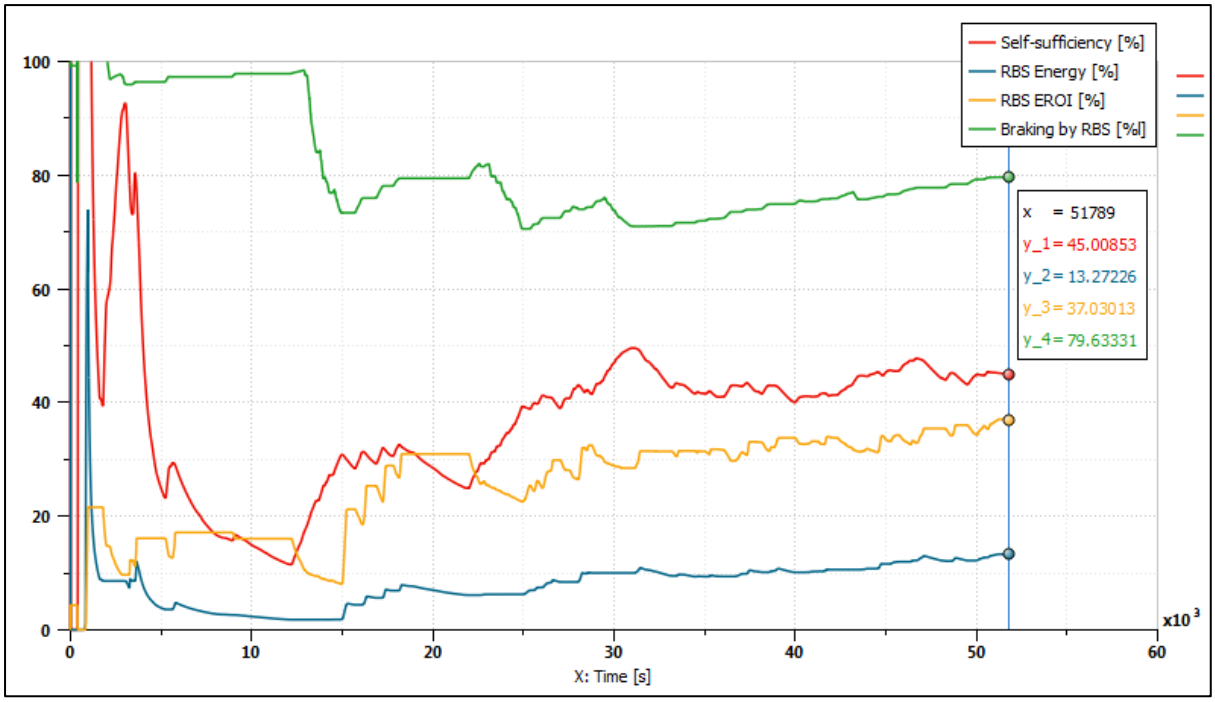

Figure 4-28: Concept 2, Trip 1 – RBS Performance Measure Results

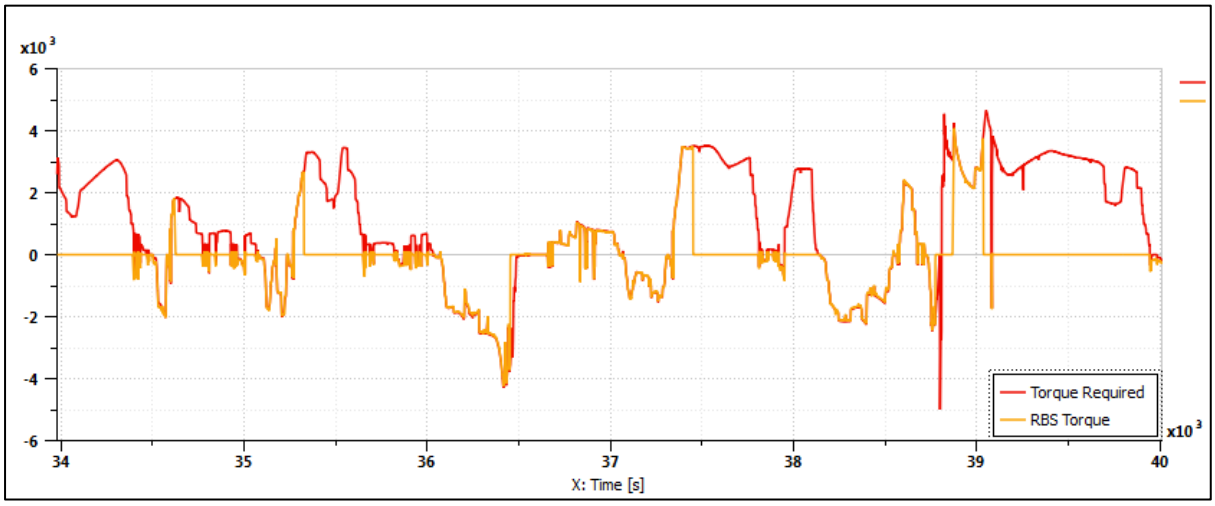

Figure 4-29: RBS Torque Results

4.4. Simulation Results

The analysis procedure described in the previous section was repeated for each of the RBS concepts on both train trips. Due to the initial results obtained which showed that the steel concepts with steel flywheels delivered promising results, it was decided to include four additional concepts to the simulation scope. These concepts are all based on the steel flywheel, due to promising initial results shown by the initial concepts with steel flywheels. The parameters for the additional concepts are specified in Table 4-8, Table 4-9 and Table 4-10.

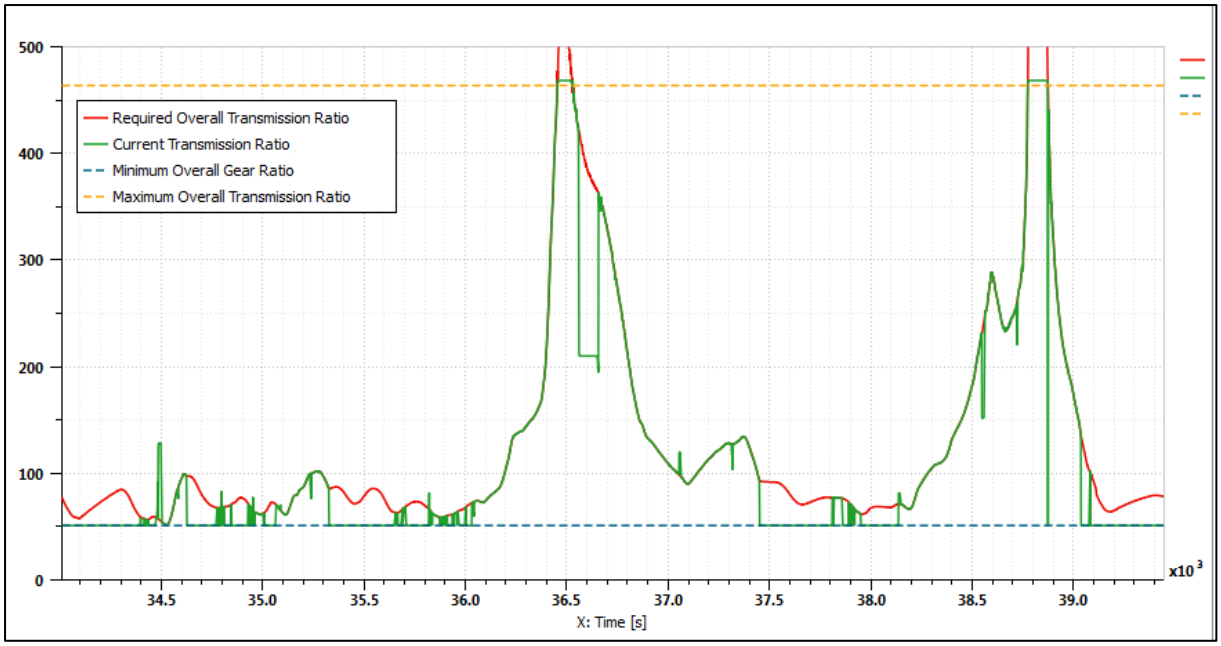

Figure 4-30: Concept 2, Trip 1 – Overall Transmission Ratio Results

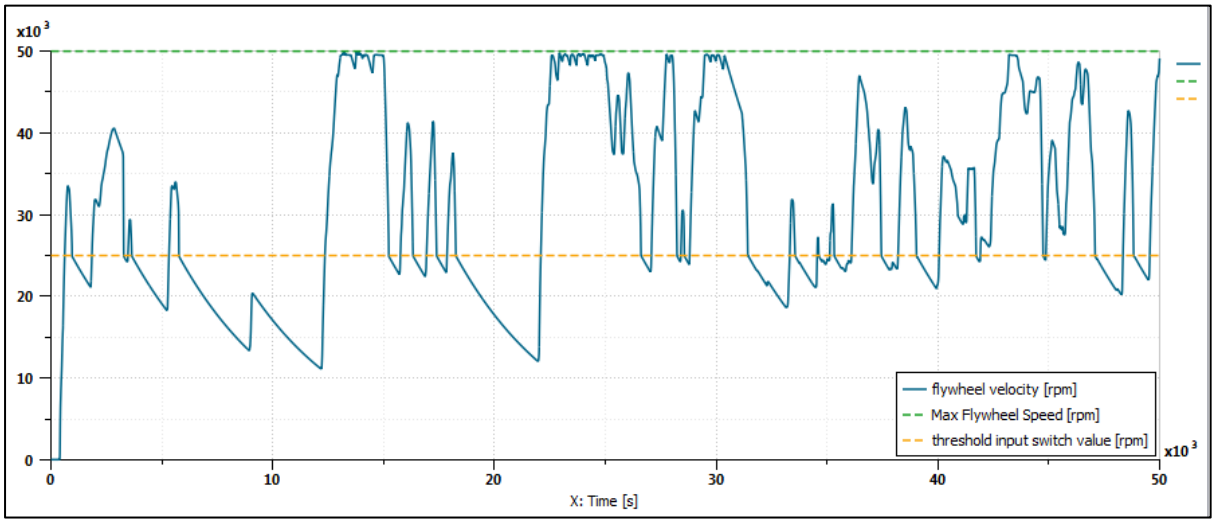

Figure 4-31: Concept 2, Trip 1 - Flywheel Rotational Speed Results

Table 4-8: Additional Concepts Flywheel Parameters

Concept	# RBS	Flywheel	Max. Flywheel Speed	Min. Flywheel Speed	Flywheel Inertia[1]	Viscous Friction Coefficient[2]
11	3	Steel	14 647	7 324	14.46	1.23E-04
12	3	Steel	14 647	7 324	14.46	1.23E-04
13	2	Steel	14 647	7 324	9.64	0.82E-04
14	2	Steel	14 647	7 324	9.64	0.82E-04
[1]From equation (4-4) and Table 3-6. [2]From equation (4-5) and Table 3-6.						

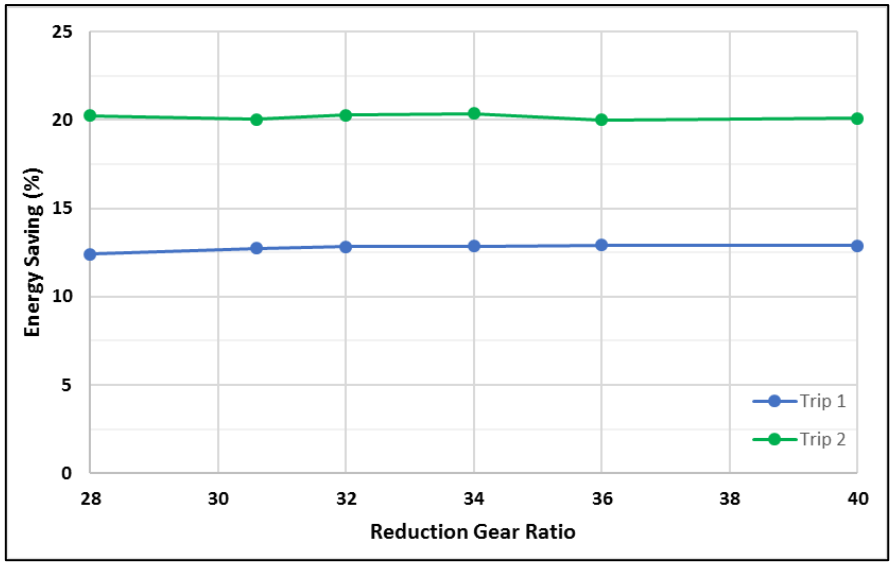

Figure 4-32: Concept 2 – Energy Savings Results for Various Reduction Gear Ratios

Table 4-9: Topology A Additional Concepts Transmission Parameters

Concept	# RBS	Final Drive Ratio	Reduction Gears Ratio	Reduction Gears Efficiency	Final Drive Efficiency
11	3	5	6	0.97	0.97
13	2	5	6	0.97	0.97

Table 4-10: Topology B Addition Concepts Transmission Parameters

Concept	# RBS	CVT Ratio Min	CVT Ratio Max	Final Drive Ratio	Reduction Gears Ratio	CVT Efficiency	Reduction Gears Efficiency	Final Drive Efficiency
12	3	0.33	3	5	9	0.93	0.97	0.97
14	2	0.33	3	5	9	0.93	0.97	0.97

The complete set of tabulated simulation results can be seen in Appendix C. A comparison of the results of the primary RBS performance measure, the energy savings delivered, from the numerical simulation performed in chapter 3 and the results obtained from the simulation in this chapter is shown in Figure 4-33. The energy savings achieved are plotted against the usable energy capacity for each concept, along with the energy savings calculated by the numerical analysis in chapter 3. A 2nd order polynomial trendline was fitted to the simulation results obtained for both the topology A and B concepts. The first observation made is that the energy savings achieved on both train trips are significantly lower than what was calculated numerically. This is especially the case for the concepts with the topology A transmission. We also observe that the trendlines do not indicate an upward trend in energy savings results with an increase in energy storage capacity, as was the case for the numerical analysis.

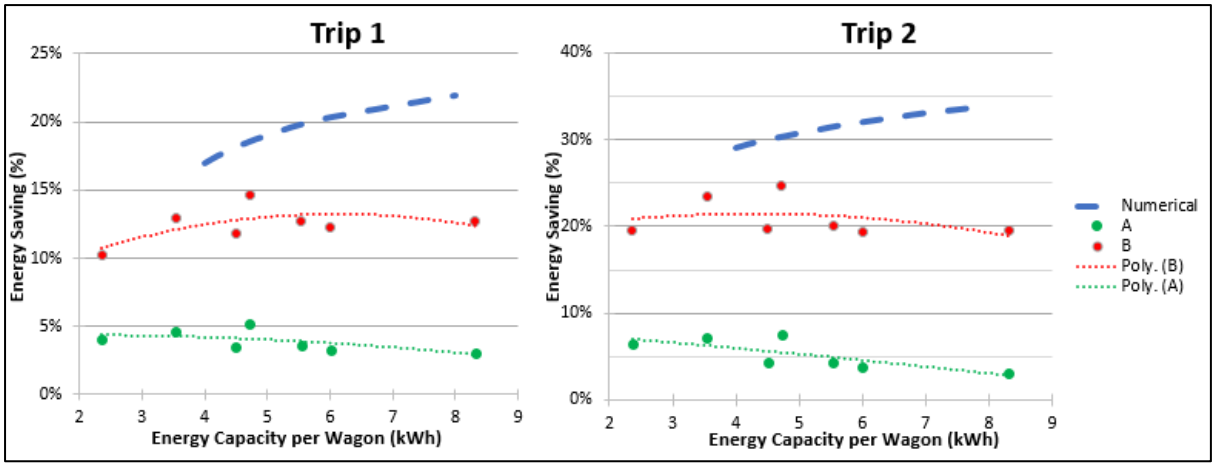

Figure 4-33: Numerical- and Physical System- Simulation Energy Saving Results Comparison

The reason for the underperformance of the RBS when compared to the predicted energy savings from the numerical analysis is uncovered by considering the performance measures of the RBS that ultimately determines the energy savings achieved as shown in equation (4-1). In Figure 4-34, the simulated RBS braking energy fraction ($\eta_{RBS,B}$) is plotted against the usable energy capacity for each concept along with the results from the numerical analysis. For trip 1, we see that the simulated results correlate reasonably well with the numerical analysis results and for topology B the results are higher than what was predicted. For trip 2, the results for the topology B concepts are again higher than the numerical prediction and for topology A the results are slightly lower. We can therefore conclude that the simulated RBS could achieve the predicted braking energy fraction for the majority of the concepts. These results indicate that sufficient energy storage capacity was available to perform braking when required as well as that the transmission could accommodate the speed ranges when braking was required.

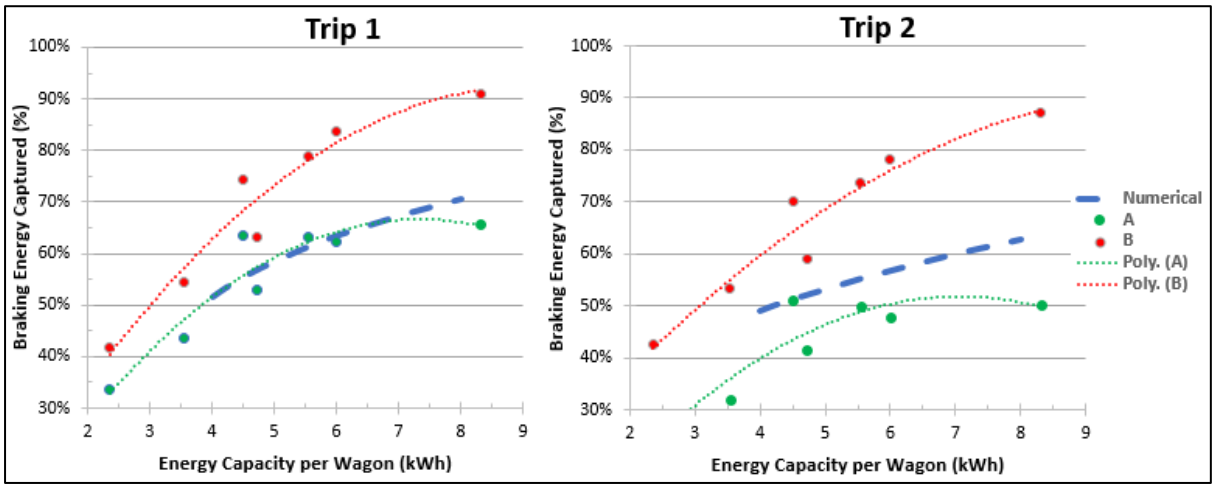

Figure 4-34: Numerical- and Physical System- Simulation Braking Energy Fraction Results Comparison

If we consider the EROI results for the simulated RBS, shown in Figure 4-35, we see a significant underperformance when compared to the numerically predicted results with most concepts achieving an EROI of less than 50%. This is especially the case for the topology A concepts. This indicates that the RBS does not operate with the expected efficiency and a much smaller fraction of the captured braking energy is returned to the freight wagon.

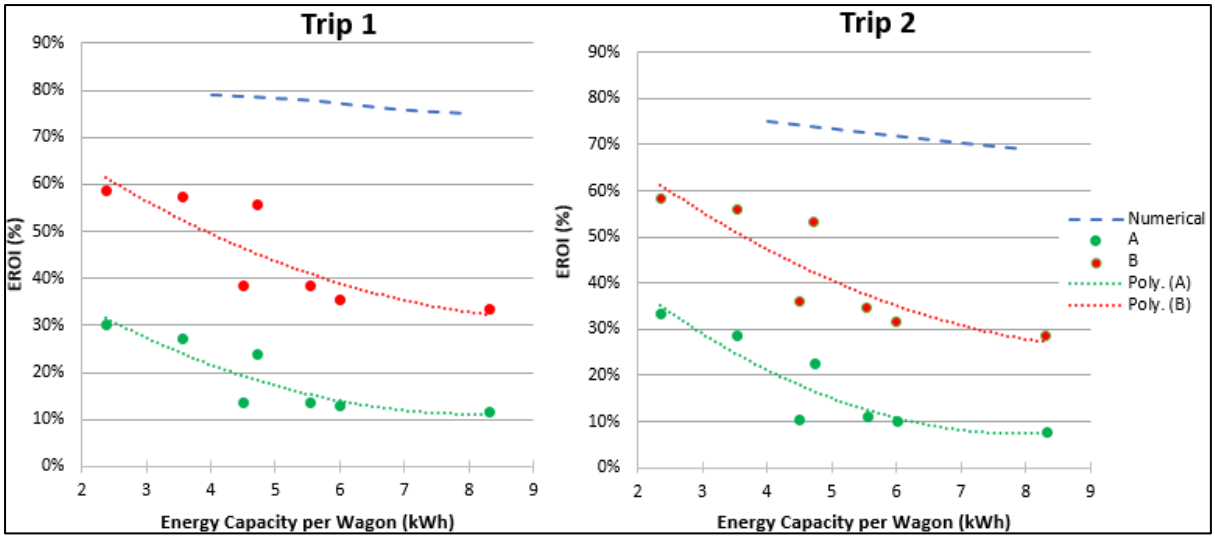

Figure 4-35: Numerical- and Physical System- Simulation EROI Results Comparison

The cause for the lower than expected EROI becomes apparent when the energy losses for the hardware component of the RBS are considered. In Figure 4-36, the energy losses for the hardware components are shown. We see that the flywheel energy losses are a significant contributor of energy losses for all concepts. These high flywheel energy losses are a result of the self-discharge rate of the flywheels. For the numerical analysis, an ESS self-discharge half-life rating of 144 minutes was used based on flywheel characteristics found in the literature. In the analysis performed in section 3.3, we found that flywheels suited to our specific application have much shorter self-discharge times as shown in Figure 3-12. The simulated flywheel energy losses are therefore higher than the numerical analysis prediction which has a negative impact on the EROI. The steel flywheel has the longest half-life rating of the three flywheels simulated and we see that these concepts have significantly less flywheel losses than the other two flywheels. If the EROI for the RBS concepts are plotted against the number of RBSs on the freight wagon for each flywheel type, as shown in Figure 4-37, we see that the steel flywheel concepts have significantly better EROIs compared to their composite and aramid counterparts.

Further to this, we see that the clutch component for the topology A concepts (which facilitates torque modulation for these concepts) is another big contributor to energy losses, exceeding the flywheel energy losses in some cases. If we compare this to the combined CVT and clutch losses for topology B concepts, as these components facilitate torque modulation for these concepts, we see that they lead to much smaller energy losses, roughly a third of the energy losses of the clutch in topology A for corresponding concepts. It is for this reason that the EROI of the topology B concepts is significantly higher than for the corresponding topology A concepts, as shown in Figure 4-37, and therefore these concepts achieve higher energy savings results as was observed in Figure 4-33 and also shown in Figure 4-38.

The underperformance of the topology A transmission, which is less complex and costly than the topology B transmission, is expected and similar results were obtained in the work of Berkel et al. (2014). The magnitude of the underperformance is larger than expected however, with topology A concepts delivering 60-80% less energy savings compared to their topology B counterparts as seen in Figure 4-38. In the work of Berkel et al. the simplified topology achieved roughly 30-40% less energy

savings when compared to the topology which included a CVT component (topology 1 and 2 in the work of Berkel et al.). This significant underperformance significantly affects the financial feasibility of these concepts (chapter 5).

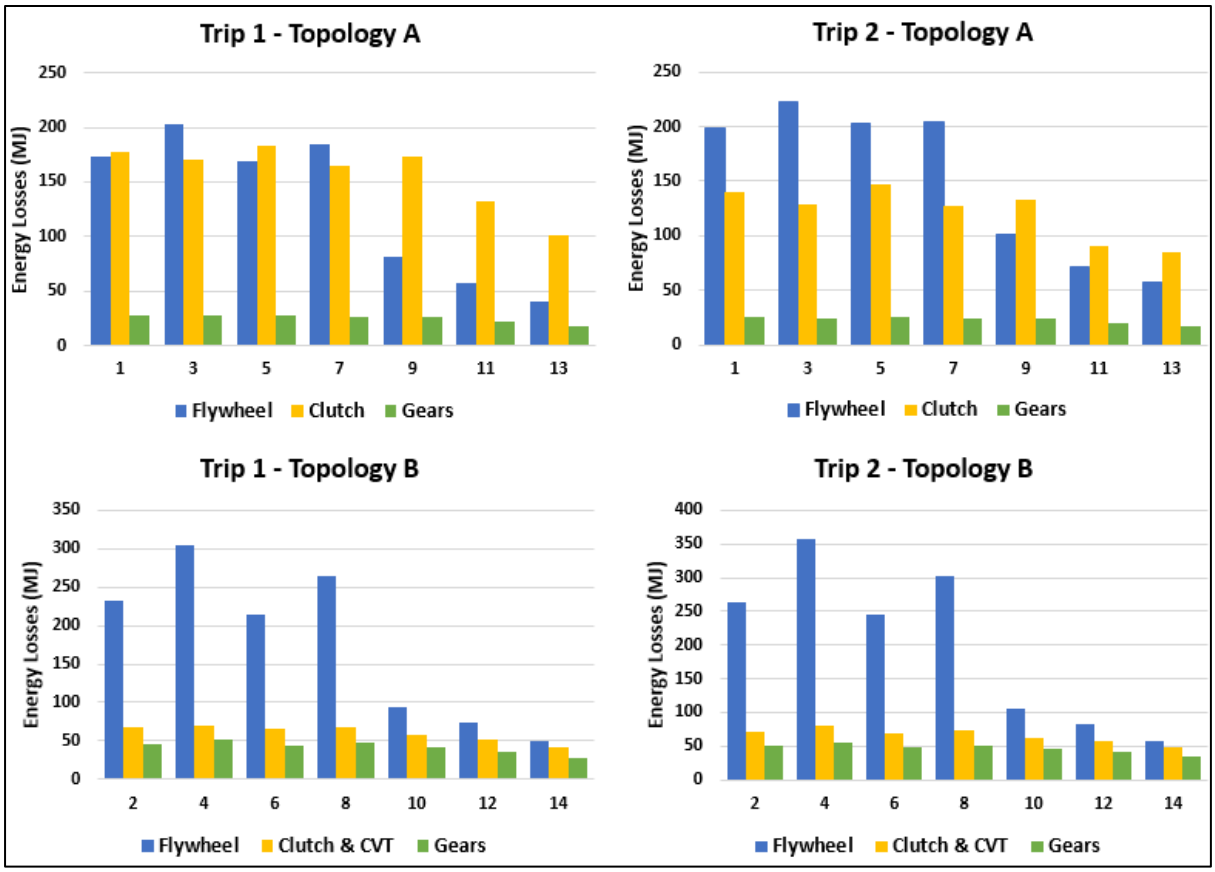

Figure 4-36: Summary of Energy Losses Results

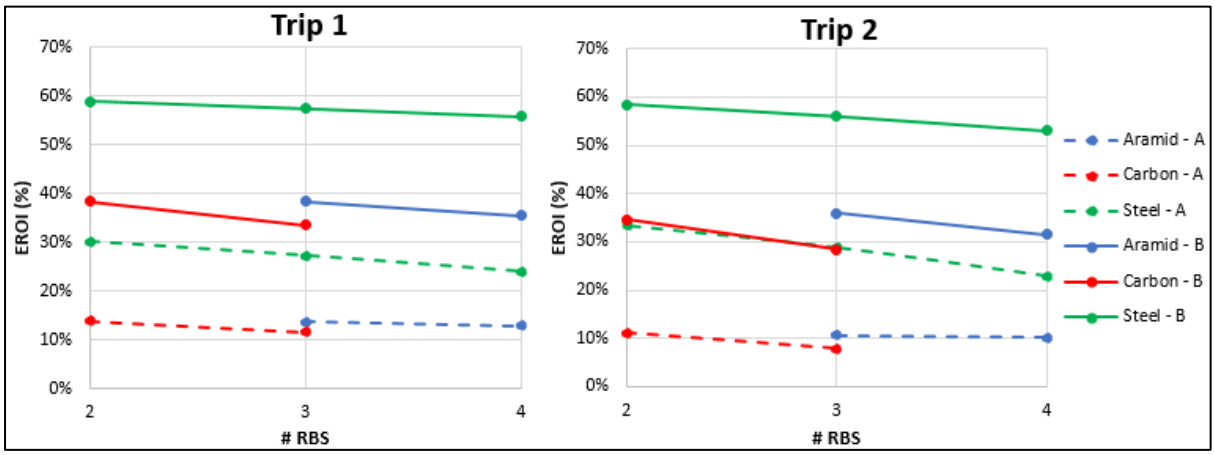

Figure 4-37: Simulated EROI Results

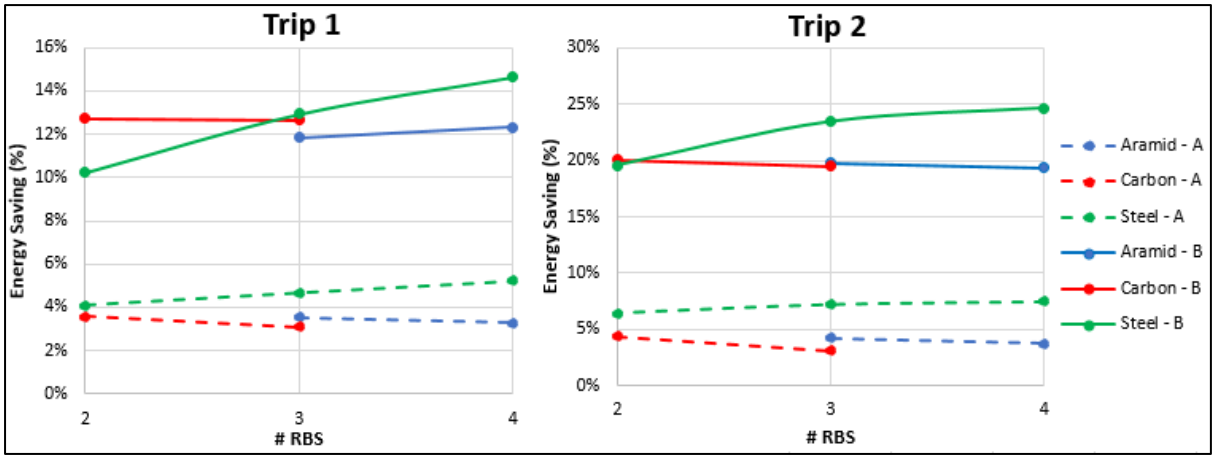

Figure 4-38: Simulated Energy Results

The visualisation of the energy saving results in Figure 4-38 allows us to make certain conclusions about the simulated concepts which permits us to eliminate some the concepts at this stage of the investigation. The first observation we can make is that for the carbon flywheel concepts for both trips and both transmission topologies, increasing the number of RBSs from 2 to 3, decreased the energy savings produced. This counterintuitive observation can be attributed to the fact that as the flywheels have a minimum operational velocity which deems a fraction of the storage capacity unusable, increasing the number of flywheels would increase this unusable capacity. The additional usable energy storage capacity could then not be used in an effective enough manner to overcome the energy lost to the unusable portion of the flywheel capacity. As installing 3 RBSs would be more expensive than installing 2 RBSs, we can with certainty say that this concept would be less financially feasible if it does not deliver an increased amount of energy savings. We therefore eliminate the concepts with 3 carbon flywheels (concepts 3 and 4) from our investigation. The same observation is made for concepts with aramid flywheels and the topology A transmission, and we therefore eliminate the RBS with 4 aramid flywheels and topology A transmission (concept 7).

Further to this, keeping in mind that a steel flywheel concept is expected to cost significantly less than a composite flywheel (carbon and aramid), we can state that for a RBS concept with composite flywheels to be competitive it must deliver more energy savings than for the RBS concept with the same topology and number of flywheels. By this, if we consider the energy savings results for the topology A concepts, we see that neither of the composite flywheels outperforms its steel flywheel counterpart on either of the train trips. We therefore eliminate all concepts with the topology A transmission and composite flywheels (concepts 1 and 5). For topology B, we see that this is the case as well except for the RBS with two carbon flywheels and we therefore eliminate concepts 6 and 8 from our investigation.

The remaining concepts for further investigation can be seen in Table 4-11. The absolute energy savings for each of the remaining concepts are also shown in this table. The absolute energy savings will be used as an input into the financial analyses that will be performed in the following chapter. Although the topology A concepts have proven to deliver much lower energy savings than the topology B counterparts, it remains to be seen whether the lower cost of the topology A concepts will deem these concepts competitive.

Table 4-11: Absolute Energy Saving Results for Remaining Concepts

Concept	*# RBS*	*Flywheel*	*Topology*	*Trip*	*Energy Saving (%)*	*Energy Saving [1] (MJ)*
2	2	Carbon	B	1	12.72	219.8
				2	20.04	217.5
9	4	Steel	A	1	5.22	90.2
				2	7.48	81.2
10	4	Steel	B	1	14.65	253.2
				2	24.63	267.3
11	3	Steel	A	1	4.66	80.6
				2	7.23	78.5
12	3	Steel	B	1	12.94	223.5
				2	23.44	254.4
13	2	Steel	A	1	4.08	70.5
				2	6.44	69.9
14	2	Steel	B	1	10.22	176.7
				2	19.60	212.6

[1] Based on energy consumption per wagon, calculated from total motoring energy for each trip given in Table 3-1 with the number of wagons specified in Table 3-2. Results cross referenced with simulated absolute energy savings for verification.

With the results illustrated in this section, the objectives of this chapter have been successfully reached. The simulation results have verified that the functionality of the various RBS concepts and that they perform their primary objective of affecting energy savings. The simulation models and results were also effectively used to optimise certain parameters of the RBSs. The simulations provided the achievable performance of the RBSs and the results could be compared to that of the numerical analysis performed in chapter 3.

5. Cost-Benefit Analysis

In this section, the financial feasibility of the proposed distributed regenerative braking system is investigated to establish whether the energy savings achieved by the system justifies the capital investment required. This is done by means of a cost-benefit analysis (CBA). The procedure identified from the literature in section 2.6 is used for the CBA.

Step 1 of the CBA, identifying and defining project or system was done in chapter 1 and 2 of this study in which the distributed regenerative braking system is introduced and the goal of the system is defined. Identifying the consequences of the system, step 2 of the CBA, was done in detail in chapters 3 and 4 of this project where the system concept is developed and simulated to establish its performance.

The next step is to select the appropriate type of CBA and accompanying decision criteria. In section 2.6, the different types of CBAs and decision criteria were explained. The financial feasibility is investigated from the perspective of a fleet owner, which may be private- or state-owned company, which would invest in incorporating the distributed regenerative braking system into their fleet for the benefit of reduced energy and operating costs. For this reason, a financial CBA is the most suited analysis for this study. To ensure that a full picture of the financial feasibility is provided, multiple decision criteria are calculated and used to draw conclusions from. The decision criteria that are calculated includes net present value (NPV), internal rate of return (IRR), benefit-cost ratio (BCR) and the payback period.

Step 4, identifying the costs and benefits throughout the life cycle of the system, is detailed in sections 5.1 and 5.2 of this chapter. This includes identifying which cost and benefits of the system are considered economically relevant to the project. Adjustment of the costs and benefits using weight based distributions are not included in this study as it is not always seen as a best practice in CBA as explained in section 2.6 and therefore step 5 is skipped in this chapter. The discounting of the costs and benefits and the calculation of decision criteria, step 6, is performed in section 5.3 and lastly a sensitivity analysis is performed in section 5.4.

5.1. Life Cycle Cost Calculation

The literature reviewed on CBA all agreed that the calculation of the cost (and benefits) throughout the lifecycle of a system is a challenge due to the uncertainty involved with estimating future cost. Careful consideration must also be given to establishing which costs are relevant to the cost benefit analysis. There are three main cost categories that must be considered for the cost benefit analysis: 1) initial capital cost, 2) operation and maintenance costs as well as 3) decommissioning and disposal cost. Furthermore, opportunity cost must also be included as system costs.

The initial capital cost of the system includes the system cost as well as the cost of integrating the system into the freight wagons. As it is envisaged that these systems would be installed to new freight wagons, no cost is associated with downtime of the wagons. The cost of operating a train is not expected to be affected by the introduction of the distributed RBS. As the mass of the system on each wagon is low compared to the total mass of a laden freight wagon (typically less than 1%) it is not expected to significantly increase the energy cost and is also not expected to reduce the maximum payload of the train in general freight train operations. For the heavy haul freight train scenario, an

increase in the wagon tare weight would result in reduced payload as these trains operate on their maximum axle load limit. The regenerative braking system will require maintenance however and this must be accounted for in the life cycle cost. It is assumed that this maintenance can be synchronised with the service intervals of the freight wagons and will therefore not cause any additional downtime. No additional cost is expected for the decommissioning and recycling of the freight wagons due to the presence of the RBS.

5.1.1. Initial Capital Investment

In this section, the initial cost of the RBSs installed on the freight wagons is calculated. This is done by identifying the cost at component level and combining these costs with the cost of auxiliary components and expenses. Although accurate costing of powertrain components as well as flywheel ESS is difficult due to the limited information available from industry, a rough estimation of the cost will provide a good comparative insight into the different flywheels and transmissions used (Berkel, et al., 2014).

The calculation of the flywheel ESS cost is shown in Table 5-1. The cost of the rotor material is taken from Berkel et al. for the steel flywheel and from a composite material supplier for the composite flywheels (AMT Composites, 2018; 2014). In Table 5-2 the calculation of the composite material cost is shown, a processing factor of two is used to calculate the final component cost as seen in the work of Bader (2002). The fibre material typically makes up 60% of a composite component's weight while a less expensive matrix material constitutes the remaining 40% (Bader, 2002). As the fibre material is typically more expensive than the matrix material, calculating the cost for the entire component based on the fibre material cost is a conservative approach from a cost perspective.

The flywheel housing mass is taken as 50% of the steel flywheel mass and used for the composite flywheels as well (Berkel, et al., 2014). The flywheel bearing cost is calculated as 50% of the rotor cost and a fixed cost is included for further flywheel auxiliary components (Rupp, et al., 2016). The total flywheel ESS cost is calculated from the above-mentioned costs, the cost per kWh of energy storage capacity is also calculated and shown in Table 5-1. We see that although the carbon flywheel system is the most expensive, it is by far the cheapest on a per kWh basis. The aramid flywheel is the most expensive flywheel system and the most expensive on a per kWh basis.

The cost of the transmission components was taken from the work of Berkel et al. and are shown in Table 5-3 (2014). Berkel et al. specify both the production- and consumer cost for annual production of 100 000 units of which the latter is used for this study. The specific cost for Topology A includes the cost of two clutches, one set of flywheel reduction gears and a set of fixed gears as per Figure 3-13. The specific cost for the Topology B transmission includes the cost of a CVT, a single clutch, one set of fixed gears and one set of flywheel reduction gears.

Table 5-1: Flywheel Energy Storage System Costing

Flywheel	Steel	Carbon	Aramid
Mass	267.1	53.8	47.6
Energy Capacity (kWh)	1.18	2.77	1.5
Rotor Material Cost (ZAR/kg)[1]	R 206	R 1 333	R 2 382
Rotor Cost	R 55 081	R 71 733	R 113 400
Housing Mass (kg)[2]	133.55	133.55	133.55
Housing Material Cost (ZAR/kg)[3]	R 236	R 236	R 236
Housing Cost	R 31 475	R 31 475	R 31 475
Flywheel Bearings[4]	R 27 541	R 35 867	R 56 700
Auxiliaries[5]	R 11 910	R 11 910	R 11 910
Total Cost	**R 126 007**	**R 150 985**	**R 213 485**
Specific Cost (R/kWh)	R 106 785	R 54 507	R 142 323
Maintenance Cost	R 39 451	R 47 777	R 68 610

[1]Rotor material cost taken from AMT composites pricing and Berkel et al. for steel flywheel **(2014)**. [2]Housing mass 50% of rotor mass for steel flywheel, steel flywheel housing used for composite flywheels **(Berkel, et al., 2014)**. [3]Aluminium housing cost from Berkel et al. **(2014)**. [4]Bearing costs 50% of rotor cost **(Rupp, et al., 2016)**. [5] **(Rupp, et al., 2016)**.

Table 5-2: Composite Flywheels Material Cost

Material	Material Cost (R/kg)	Processing Cost Factor	Total Cost (R/kg)
Carbon	R 667	2	R 1 333
Aramid	R 1 191	2	R 2 382
Sources: **(AMT Composites, 2018; Bader, 2002)**			

Table 5-3: Transmission Components Specific Costs

Component	Cost
CVT (ZAR/kW)	R 420
Clutch (ZAR/kW)	R 36
Fixed Gears (ZAR/kW)	R 8
Flywheel Reduction Gears (ZAR/kW)	R 98
Topology A Specific Cost(ZAR/kW)	R 177
Topology B Specific Cost (ZAR/kW)	R 561
Adaptations (per unit)	R 1 767
Controller & Electronics (per unit)	R 10 000
Source: (Berkel, et al., 2014)	

From the specific cost of the transmissions shown in Table 5-3, the total transmission cost for each freight wagon can be calculated based on the number of RBSs on the wagon. The result of this calculation is shown in Table 5-4. The power rating for each transmission is taken from Figure 3-8.

Table 5-4: Total Transmission Cost per Freight Wagon

# RBS	Power Rating (kW)	Topology	Transmission Components Cost	Auxiliary Component Cost	Total Transmission Cost
2	60.5	A	R 10 729	R 11 768	R 22 497
	60.5	B	R 33 962	R 11 768	R 45 730
3	40.3	A	R 7 147	R 11 768	R 18 915
	40.3	B	R 22 622	R 11 768	R 34 390
4	30.3	A	R 5 373	R 11 768	R 17 141
	30.3	B	R 17 009	R 11 768	R 28 777

With the cost of the transmission and flywheel components known, the total RBS cost per wagon can be calculated for each concept based on the number of RBSs on the wagon, the type of flywheel and the type of topology used. The results of this calculation are shown in Table 5-5. The cost provided in this table is the cost used as the initial capital investment in the CBA.

Table 5-5: Total Regenerative Braking System Cost per Wagon

Concept	# RBS	Flywheel	Topology	Total Flywheel Cost	Total Transmission Cost	Total Cost (per wagon)
2	2	Carbon	B	R 301 970	R 91 460	R 393 430
9	4	Steel	A	R 504 028	R 68 565	R 572 594
10	4	Steel	B	R 504 028	R 115 107	R 619 136
11	3	Steel	A	R 378 021	R 56 744	R 434 766
12	3	Steel	B	R 378 021	R 103 171	R 481 193
13	2	Steel	A	R 252 014	R 44 994	R 297 009
14	2	Steel	B	R 252 014	R 91 460	R 343 474

5.1.2. Maintenance and Operating Cost

The components used for the distributed RBS is largely based on applications from the automotive industry and adapted for the freight wagon application. For automotive applications, maintenance cost is not considered to be significant throughout the life of a vehicle (Berkel, et al., 2014). As the life of a freight wagon (20 years) is approximately twice that of an automotive vehicle, we assume that the regenerative braking system (excluding components designed for infinite life) will require replacing midway through the wagon operating life. The total maintenance cost will therefore be equivalent to the replacement cost of the RBS.

For the flywheel system, the rotor and housing components would be designed for infinitive life and would not need replacing throughout the life of the freight wagon. The resulting maintenance cost for the flywheel system is shown in Table 5-1. The transmission maintenance cost is identical to that of the initial cost of the transmission as the entire transmission would be replaced. The resulting total maintenance cost for each RBS concept is shown in Table 5-6.

Table 5-6: Lifetime Maintenance Cost per Wagon

Concept	# RBS	Flywheel	Topology	Flywheel Maintenance Cost	Transmission Maintenance Cost	Total Cost
2	2	Carbon	B	R 95 553	R 91 460	R 187 013
9	4	Steel	A	R 157 803	R 68 565	R 226 368
10	4	Steel	B	R 157 803	R 115 107	R 272 910
11	3	Steel	A	R 118 352	R 56 744	R 175 096
12	3	Steel	B	R 118 352	R 103 171	R 221 523
13	2	Steel	A	R 78 901	R 44 994	R 123 896
14	2	Steel	B	R 78 901	R 91 460	R 170 361

5.2. System Benefits

The primary benefit brought on by RBSs is energy saving which reduces the operating cost of the vehicle. Another significant benefit is the reduction in greenhouse gases emitted by the vehicle which has costs associated to it in the form of carbon tax and emission trading schemes (Du Plessis, 2011). Other benefits such as reduced maintenance on existing traction systems and braking components, increased range and additional power may also contribute to the worth of a RBS. For this study, the energy savings is considered as the only primary- and economically relevant benefit. The remaining benefits are considered as secondary benefits and, although not included in the CBA, would further support the business case for the distributed RBS.

With the energy savings quantum already established for each of the variations of the RBS, the next step is to convert the energy savings into economic value. In chapter 1, it was explained that the distributed RBS would focus on addressing the diesel-powered freight rail sector. To calculate the cost of traction energy from diesel-powered locomotives, we will utilize the information provided on a typical diesel locomotive in the work of Spiryagin et al. (2015). The diesel locomotive has eight operating positions, referred to as notches in the industry, each with a different power output and accompanying fuel usage and emissions output. The traction power delivered by the traction system to the locomotive wheels is calculated for each notch (1-8) using equation (5-1). The first two terms in the equation, the maximum traction power (P_{max}) and the term containing the notch (N), represent the electrical power delivered to the traction motors of the locomotive. By incorporating the efficiency of the traction motors (η_{TM}) and the efficiency of the final drive gears (η_{FD}), the traction power delivered to the wheels is obtained. The resulting power output for each notch is shown in Table 5-7.

$$P_{TM} = P_{max}\left(\frac{N^2}{64}\right).\eta_{TM}.\eta_{FD} \qquad \textbf{(5-1)}$$

With the power delivered and fuel consumption known for each notch, the energy delivered per litre of diesel fuel can be calculated. If we use the energy content of diesel to calculate the overall efficiency from the fuel tank to the wheels of the locomotive, we see that the locomotive efficiency increase as the locomotive notch increases with a maximum efficiency of 37% in notch 8. At the same time, the cost per unit of energy decreases with each increase in the locomotive notch as the efficiency increases as seen in Table 5-7.

Table 5-7: Locomotive Traction Energy Cost

Notch Selected	On-wheel Traction Power (kW)[1]	Fuel Consumption (L/s)[2]	Fuel Efficiency (kWh/L)	Tractive Effort Efficiency[3]	Traction Energy Cost (ZAR/kWh)[4]
1	46	0.01	0.916	9%	R 13.75
2	182	0.03	1.950	19%	R 6.46
3	410	0.05	2.111	20%	R 5.96
4	729	0.08	2.467	24%	R 5.10
5	1139	0.11	2.952	29%	R 4.27
6	1641	0.15	3.009	29%	R 4.18
7	2233	0.19	3.351	32%	R 3.76
8	2916	0.21	3.830	37%	R 3.29

[1]P_{max} = 3100kW, η_{TM}=96%, η_{FD}=98% (Spiryagin, et al., 2015). [2] (Spiryagin, et al., 2015). [3]Diesel energy content 12.44 kWh/kg, 832g/L. [4]Diesel fuel cost R12.59/L (Republic of South Africa, 2018).

From the results above, it is clear that to accurately determine the amount of fuel savings, and thereby economic benefit, both the amount of energy saved needs the be known as well as the locomotive notch at the time of the energy saving as this affects the fuel efficiency. The fuel savings must therefore be calculated with a time-based simulation, as was done in chapters 3 and 4, at each time step based on the locomotive notch. An alternative to the time-based simulation is to calculate an average energy cost based on a typical duty cycle but this comes with a compromise in accuracy (Spiryagin, et al., 2015).

As notch data is not available for the routes analysed in this study, a time-based simulation incorporating the locomotive notch is not available. It is also not possible to reverse engineer the locomotive notch from the locomotive consist power output as at times when the power requirement is relatively low, one or multiple locomotives can be 'switched off' so that fewer locomotives can operate at higher notches which is more efficient. Therefore, to estimate the fuel savings for this study a typical duty cycle must be used to calculate the average fuel efficiency or the most conservative fuel efficiency (notch 8 efficiency) must be used. For this study, a typical duty cycle will be used as it will provide a more realistic picture of the overall fuel efficiency of a diesel-powered train. The duty cycle generated in the work of Spiryagin et al. is used by taking the total fuel used for each notch and calculating the total energy produced in the notch by using the fuel efficiency calculated in Table 5-7 (2015). From this, the duty cycle for each notch is calculated and the results are shown in Table 5-8.

Next the average energy efficiency is calculated using equation (5-2) from the notch specific fuel efficiency (η_N) and the duty cycle for each notch (DC_N). An averaged fuel efficiency of 3.55 kWh/L is obtained as shown in Table 5-8. The average fuel efficiency is used to calculate the actual fuel savings, and thereby economic value, achieved by the RBS. The energy savings result from Table 4-11 is used to calculate the annual energy savings for each freight wagon if a wagon completes 310 of the simulated trips in a year as shown in Table 5-9. With the total energy savings per annum known, the fuel savings for the year can be calculated using the average fuel efficiency and subsequently the financial savings can be calculated from the specified fuel price. The fuel savings results shown in Table 5-9 is considered to be the primary and only economically relevant benefit of the regenerative braking systems.

Table 5-8: Average Fuel Efficiency Calculation

Notch Selected	Fuel Usage (Litres)	Fuel Efficiency (kWh/L)	Energy Produced (kWh)	Duty Cycle	Average Efficiency Calculation (kWh/L)
1	56	0.92	51	0.1%	0.00
2	139.2	1.95	271	0.8%	0.02
3	441.6	2.11	932	2.7%	0.06
4	566.8	2.47	1398	4.0%	0.10
5	698.1	2.95	2061	5.9%	0.17
6	1260	3.01	3791	10.8%	0.33
7	505	3.35	1692	4.8%	0.16
8	6481	3.83	24 820	70.9%	2.71
				Σ	**3.55**

$$\sum_{N=0}^{8} \eta_N . DC_N \qquad \textit{(5-2)}$$

Table 5-9: Annual Fuel Savings per Freight Wagon

Concept	Trip	Annual Energy Saving (kWh)[1]	Fuel Saving (L)[2]	Fuel Saving (ZAR)[3]
2	1	18 925	5 335	R 67 172
	2	18 725	5 279	R 66 464
9	1	7 766	2 189	R 27 565
	2	6 990	1 971	R 24 809
10	1	21 806	6 147	R 77 397
	2	23 014	6 488	R 81 687
11	1	6 937	1 956	R 24 622
	2	6 758	1 905	R 23 985
12	1	19 250	5 427	R 68 326
	2	21 904	6 175	R 77 747
13	1	6 067	1 710	R 21 535
	2	6 016	1 696	R 21 354
14	1	15 215	4 289	R 54 003
	2	18 308	5 161	R 64 982

[1]85% Utilisation of fleet which results in 310 trips per annum. [2]Fuel efficiency of 3.55kWh/L. [3]Diesel fuel price of R12.59 **(Republic of South Africa, 2018)**.

Although not considered economically relevant at this stage, the reduction in emissions as a result of fuel savings will also be calculated. With South Africa committing to reduce greenhouse gas (GHG) emissions by 34% by 2020 and 42% by 2025 and the imminent introduction of a revised carbon tax bill, carbon taxes and emissions trading may become prevalent across the transport sector in the near future which would make this benefit economically relevant (Du Plessis, 2011; EY, 2017). Diesel fuel

emissions have also been declared carcinogenic by the World Health Organisation and therefore reducing these emissions has corresponding health benefits to society (Spiryagin, et al., 2015).

For the typical locomotive efficiency data provided in the work of Spiryagin et al., the corresponding emissions output data is also provided (2015). The emissions data is provided for nitrogen oxides (NOx), particulate matter (PM), hydrocarbons (HC) and carbon monoxide (CO). The process used for the fuel efficiency calculation is used again to calculate the emissions per unit of energy for each locomotive notch as shown in Table 5-10. To establish the average emissions output per unit of energy, equation (5-2) is used again for the same duty cycle as before and the notch specific fuel efficiency (η_N) replaced by the notch specific emissions output (EO_N), the results are shown in Table 5-10.

Table 5-10: Emission Output

Notch Selected	NOx (g/kWh)	Average NOx Calc.	PM (g/kWh)	Average PM Calc.	HC (g/kWh)	Average HC Calc.	CO (g/kWh)	Average CO Calc.
1	48.98	0.07	0.79	0.00	3.16	0.00	7.11	0.01
2	24.69	0.19	0.59	0.00	1.18	0.01	2.37	0.02
3	24.58	0.65	0.53	0.01	0.70	0.02	1.40	0.04
4	22.51	0.90	0.49	0.02	0.54	0.02	2.07	0.08
5	19.05	1.12	0.44	0.03	0.41	0.02	3.63	0.21
6	18.52	2.01	0.57	0.06	0.39	0.04	9.11	0.99
7	19.35	0.93	0.48	0.02	0.40	0.02	5.08	0.25
8	15.92	11.29	0.73	0.52	0.38	0.27	3.46	2.45
	Σ	**17.16**	**Σ**	**0.67**	**Σ**	**0.41**	**Σ**	**4.04**

The annual energy savings data for each concept of each of the simulated train trips is then used to calculate the total annual emissions output savings for a freight wagon, the results are shown in Table 5-11. The emissions output saving is significant considering that the savings shown are only for a single freight wagon.

5.3. Cost-Benefit Analysis

In this section, the distribution of costs and benefits over the life cycle of the distributed regenerative braking system is defined, discounted and used to calculate the relevant decision criteria. In section 2.6 it was explained that the real lending rate (prime lending rate minus inflation rate) will be used as the discount rate for the CBA. The real prime lending rate is available from the South African Reserve Bank (SARB) (South African Reserve Bank, 2018). As both the prime lending rate and inflation rate fluctuates due to a multitude of factors, the average real prime lending rate over the past 10 years is used as the discount rate for this study. The data was obtained from the SARB website and is shown in Figure 5-1, the discount rate is calculated as 4.1%.

It was also explained in section 2.6 that the costing in a CBA is done in real terms, and therefore the price of a product or service increases or decreases in the analysis only if it increases or decreases relative to inflation. The RBS componentry is considered to be reasonably mature and for this reason we assume that these costs will not deviate from the inflation rate. Therefore, none of the cost will be adjusted with time.

Table 5-11: Annual Emission Reductions

Concept	Trip	Annual Energy Saving (kWh)[1]	Annual Emissions Reduction			
			NOx (kg)	PM (kg)	HC (kg)	CO (kg)
2	1	18 925	324.7	12.68	7.76	76.5
	2	18 725	321.3	12.55	7.68	75.7
9	1	7 766	133.3	5.20	3.18	31.4
	2	6 990	119.9	4.68	2.87	28.2
10	1	21 806	374.2	14.61	8.94	88.1
	2	23 014	394.9	15.42	9.44	93.0
11	1	6 937	119.0	4.65	2.84	28.0
	2	6 758	116.0	4.53	2.77	27.3
12	1	19 250	330.3	12.90	7.89	77.8
	2	21 904	375.9	14.68	8.98	88.5
13	1	6 067	104.1	4.06	2.49	24.5
	2	6 016	103.2	4.03	2.47	24.3
14	1	15 215	261.1	10.19	6.24	61.5
	2	18 308	314.2	12.27	7.51	74.0

[1]85% Utilisation of fleet which results in 310 trips per annum.

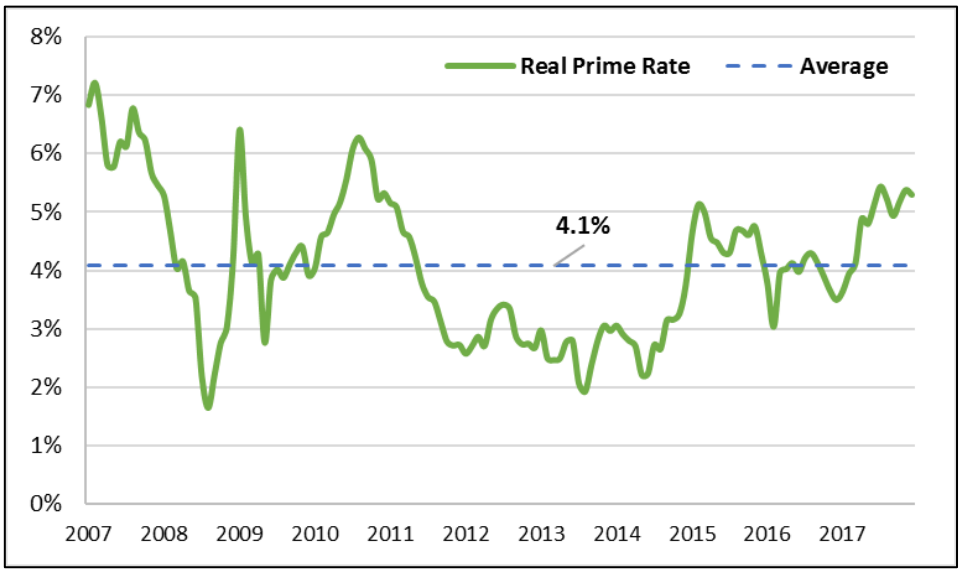

Figure 5-1: Real Prime Lending Rate (South African Reserve Bank, 2018)

The financial benefit of the RBS is directly correlated to the price of diesel fuel and changes in the fuel price will significantly influence the financial case of the system. In the Transnet's Freight and Energy Demand Forecast, the United States (US) Energy Information Administration's (EIA) Annual Energy Outlook report to forecast future energy and fuel prices (Transnet SOC Ltd, 2015). In the 2018 edition of the EIA Annual Energy Outlook, the diesel fuel price forecast is provided up to the year 2050 (U.S. Energy Information Administration, 2018). The forecast presents three cases; a reference case, a high oil price case and a low oil price case. From the data provided the total real fuel price increase is taken over the first 20-year period (2017-2037) to correspond with the 20-year life expectancy of a freight

wagon. From the total increase in fuel price, the annual fuel price escalation (relative to inflation) is calculated using a simple compound interest formula. The results are shown in Table 5-12. For the CBA, the reference fuel price increase is used. The high- and low oil price cases will be considered in the sensitivity analysis that follows in the next section.

Table 5-12: Real Diesel Fuel Price Forecast

Oil Price Case	Total Real Diesel Fuel Price Increase	Annual Real Diesel Price Increase
High	146%	4.6%
Reference	54%	2.2%
Low	-8%	-0.4%
(U.S. Energy Information Administration, 2018)		

With the discount rate as well as the costs and benefits with their associated escalation identified, the CBA can be performed. The distribution of the annual benefits (energy savings) as well as cost (initial capital- and maintenance expenditure) is shown in Table 5-13. The annual fuel savings taken from Table 5-9, escalates in monetary value each year at a rate of 2.2% as the diesel fuel price increases. The nominal cumulative cash flow is calculated using equation (5-3) as shown in Table 5-13, and is used to determine the payback period of the RBS. We see that at six years the initial investment cost has been recovered (i.e. payback achieved) and at the end of the system life an additional net amount of R1 084 561 has been delivered in fuel savings by the RBS. It is important to remember that the nominal cumulative cash flow does not account for the time-value of money.

$$\sum_{t=0}^{n}(\mathrm{B_t} - C_t) \qquad \textit{(5-3)}$$

Next the cash flows are discounted, the costs and benefits are discounted separately as in equation (2-7) and the results are shown Table 5-13. The results are subsequently used to calculate the various decision criteria. The net present value (NPV) is calculated for each year of the project using equation (2-7) and the results are shown in Table 5-13 and visually represented in Figure 5-2. We see that in year 7 the NPV for the project turns positive for the first time and it as at this stage that the project becomes feasible. The NPV increases further throughout the system life and the final NPV, at year 20, for RBS concept 2 on train trip 1 is calculated as R575 839. The Internal Rate of Return (IRR) is calculated using equation (2-8) using the nominal annual cash flow. The IRR is calculated using Excel's built-in IRR function. The results obtained from this function were validated by inputting the IRR obtained into the NPV calculation which should deliver NPV of zero at the end of the system life, which was the case. Lastly, the benefit cost ratio (BCR) is calculated using equation (2-9), dividing the discounted benefits by the discounted costs. This process is repeated for each of the RBS concepts, on each of the train trips, and the results are shown in Table 5-14. The cost and benefit distributions and CBA calculation results, as shown in Table 5-13, can be found in Appendix D for each concept and train route.

Table 5-13: CBA Calculation Results – Concept 2, Trip 1

	Nominal Monetary Values					Discounted (Real) Monetary Values		
Year	Annual Fuel Savings	Initial Capital Expenditure	Maintenance Expenditure	Annual Cashflow	Nominal Cumulative Cash Flow	Discounted Benefits	Discounted Costs	Net Present Value
0	R 0	R -393 430	R -	R -393 430	R -393 430	R 0	R -393 430	R -393 430
1	R 67 172	0	R -	R 67 172	R -326 258	R 64 526	R 0	R -328 904
2	R 68 650	R 0	R -	R 68 650	R -257 608	R 63 349	R 0	R -265 555
3	R 70 160	R 0	R -	R 70 160	R -187 448	R 62 192	R 0	R -203 362
4	R 71 704	R 0	R -	R 71 704	R -115 745	R 61 057	R 0	R -142 305
5	R 73 281	R 0	R -	R 73 281	R -42 464	R 59 943	R 0	R -82 362
6	R 74 893	R 0	R -	R 74 893	R 32 430	R 58 849	R 0	R -23 513
7	R 76 541	R 0	R -	R 76 541	R 108 971	R 57 775	R 0	R 34 262
8	R 78 225	R 0	R -	R 78 225	R 187 195	R 56 720	R 0	R 90 982
9	R 79 946	R 0	R -	R 79 946	R 267 141	R 55 685	R 0	R 146 667
10	R 81 705	R 0	R -	R 81 705	R 348 846	R 54 669	R 0	R 201 336
11	R 83 502	R 0	R -187 013	R -103 511	R 245 334	R 53 671	R -120 203	R 134 804
12	R 85 339	R 0	R -	R 85 339	R 330 674	R 52 691	R 0	R 187 495
13	R 87 217	R 0	R -	R 87 217	R 417 890	R 51 730	R 0	R 239 225
14	R 89 135	R 0	R -	R 89 135	R 507 025	R 50 785	R 0	R 290 010
15	R 91 096	R 0	R -	R 91 096	R 598 122	R 49 859	R 0	R 339 869
16	R 93 100	R 0	R -	R 93 100	R 691 222	R 48 949	R 0	R 388 817
17	R 95 149	R 0	R -	R 95 149	R 786 371	R 48 055	R 0	R 436 872
18	R 97 242	R 0	R -	R 97 242	R 883 612	R 47 178	R 0	R 484 051
19	R 99 381	R 0	R -	R 99 381	R 982 994	R 46 317	R 0	R 530 368
20	R 101 568	R 0	R -	R 101 568	R 1 084 561	R 45 472	R 0	R 575 839
	R 1 665 004	R -393 430	R -187 013			R 1 089 472	R -513 633	

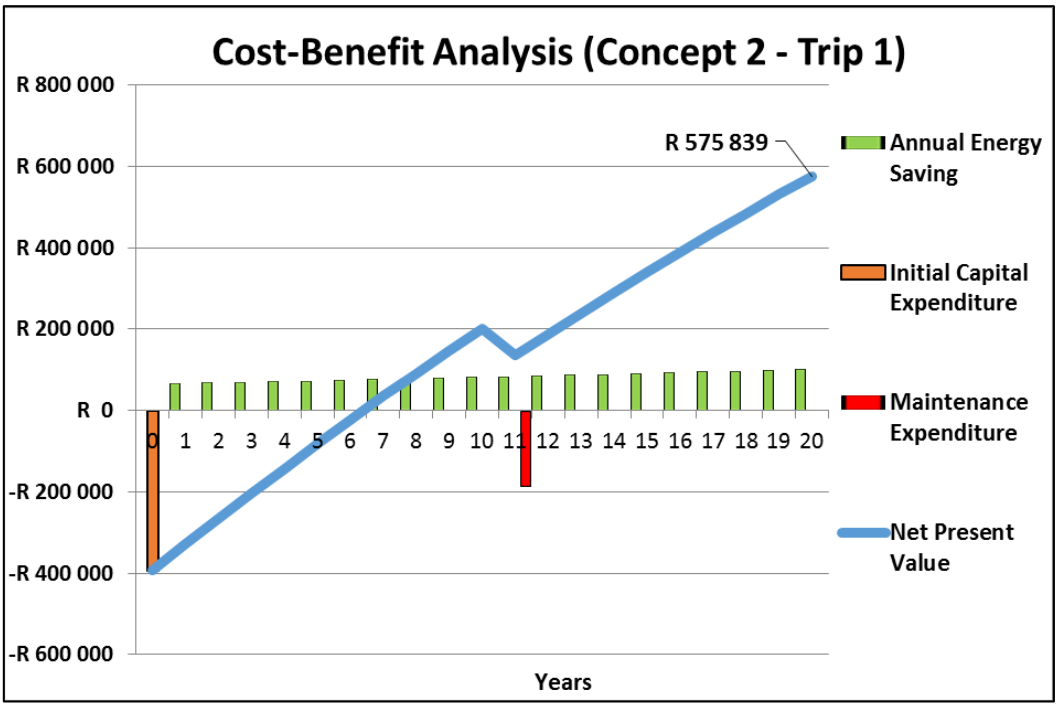

Figure 5-2: CBA Calculation Results – Concept 2, Trip 1

Table 5-14: CBA Overall Results

Concept	Trip	Payback period	NPV	IRR	BCR
2	1	6	R 575 839	16.8%	2.12
2	2	6	R 564 364	16.6%	2.10
9	1	-	R-271 007	-1.9%	0.62
9	2	-	R-315 707	-3.1%	0.56
10	1	8	R 460 761	11.1%	1.58
10	2	8	R 530 347	12.1%	1.67
11	1	20	R-147 963	0.0%	0.73
11	2	-	R-158 289	-0.3%	0.71
12	1	7	R 484 611	13.3%	1.78
12	2	6	R 637 409	15.8%	2.02
13	1	17	R -27 368	3.1%	0.93
13	2	17	R -30 306	3.0%	0.92
14	1	7	R 422 917	15.1%	1.93
14	2	6	R 600 980	19.0%	2.33

The results obtained on the two train routes for each concept is averaged so that the decision criteria can be viewed for the combined performance over the two routes. The results are shown in Table 5-15 along with the defining characteristics of each concept. At this stage, it is possible to make conclusions on the economic feasibility of each of the RBS concepts.

Table 5-15: CBA Averaged Results

Concept	# RBS	Flywheel	Topology	Payback period	NPV	IRR	BCR
2	2	Carbon	B	6	R 570 102	16.7%	2.11
9	4	Steel	A	-	R-293 357	-2.5%	0.59
10	4	Steel	B	8	R 495 554	11.6%	1.62
11	3	Steel	A	20	R-153 126	-0.2%	0.72
12	3	Steel	B	6.5	R 561 010	14.5%	1.90
13	2	Steel	A	17	R -28 837	3.0%	0.92
14	2	Steel	B	6.5	R 511 948	17.0%	2.13

The NPV decision criteria states that for a project to be feasible, the NPV for the project must be greater than zero. We see in the results above that concepts 9, 11, 13 do not meet the criteria while the remaining concepts do meet the criteria. The IRR decision criteria requires an IRR greater than the discount rate, 4.1% for this study, for the project to be feasible. Again, we observe that the criterion is not met by concepts 9, 11 and 13 whilst the remaining concepts meet this criterion. The BCR criteria requires a ratio larger than unity to be achieved for economic feasibility and again concepts 9, 11 and 13 do not meet the criteria. No rigid constraint is set on the payback period, as a guideline we will set a payback period requirement of 50% of the system life, 10 years in this case. We observe that concept 9 never reaches payback, while concepts 11 and 13 reach payback at a very late stage in the system lifecycle. We therefore conclude that based on all four decision criteria, concepts

9, 11 and 13 are not economically feasible. The remaining four concepts (2, 10, 12 and 14) are all deemed economically feasible based on all four of the decision criteria. The differentiating factor between the feasible and non-feasible concepts is clearly the type of topology, with all topology A concepts deemed not feasible and all topology B concepts deemed feasible.

Of the four economically feasible concepts, shown in Table 5-16, the concept that provides the best financial case must be selected as the final RBS concept. To do this, we look at which concepts delivered the best results for each decision criteria. Both concepts 2 and 14 is based on two RBSs per wagon and benefit from the reduced fix cost associated with each RBS that is installed on a wagon (adaptation cost, controller etc.). We see that concept 2 delivered the best results for the payback period and NPV criteria while concepts 14 delivered the best results in both the IRR and BCR criteria as highlighted in Table 5-16. Concept 2 delivers the highest NPV, but this measure does not account for the project size (initial capital cost) and how efficient capital is utilised. The IRR and BCR, which indicates how efficiently capital is used, show that concept 14 delivers the best result and will therefore provide investors with the best return for each South African Rand provided for the project. For this reason, concept 14 is considered to provide the most economic benefit and therefore presents the 'best' solution for the distributed RBS.

Table 5-16: Economically Feasible RBS Concepts

Concept	*# RBS*	*Flywheel*	*Payback period*	*NPV*	*IRR*	*BCR*
2	2	Carbon	6	R 570 102	16.7%	2.11
10	4	Steel	8	R 495 554	11.6%	1.62
12	3	Steel	6.5	R 561 010	14.5%	1.90
14	2	Steel	6.5	R 511 948	17.0%	2.13

5.4. Sensitivity Analysis

With concept 14 identified as the best solution for the distributed RBS, a sensitivity analysis will be performed to investigate the effect on the feasibility of the project if certain parameters were to alter from the predicted values used in the RBS. This analysis will address the uncertainty involved with certain parameters and provide further confidence in the results of the CBA. In section 2.6 it was explained that a gross sensitivity analysis will be performed for this study, in which a single variable is altered at a time whilst recording the effect on the CBA results. A combined worst- and best-case scenario will also be investigated.

There are numerous parameters that can be evaluated in the sensitivity analysis but we will only consider three parameters for this study, namely the system cost, system performance (energy savings delivered) and the diesel fuel price escalation. The discount rate is a common parameter to include in a sensitivity analysis, but as the IRR far exceeds the discount rate for this project a reasonable change in the discount rate will not affect the outcome of the CBA.

The sensitivity analysis is performed for concept 14 on train route 1 as this is the train route on which the system delivered less favourable CBA results and the sensitivity analysis will therefore deliver conservative results. The NPV results for the sensitivity analysis of the energy savings delivered by the distributed RBS is shown in Figure 5-3. The CBA was performed again while both increasing and decreasing the energy savings delivered by the RBS by 20%. The results in the figure illustrate the

effect on the economic feasibility of the system if the energy savings delivered by the system were to be lower or higher than expected. We observe that for a reduction in energy savings by 20%, the NPV for the overall project decreases from R422 917 to R247 739. The IRR also decreases from 15.1% to 11% as show in Table 5-17. The economic return on the project is reduced significantly if the energy savings delivered are reduced, we do however observe that the project remains economically feasible with a NPV comfortably above zero and an IRR more than double the minimum required rate (discount rate). In contrast, if the energy savings delivered were to be higher than expected by 20% due to higher utilization of the system for example, the NPV (R598 095 from R422 917) and IRR (18.9% from 15.1%) increase significantly and the financial case for the project becomes even stronger.

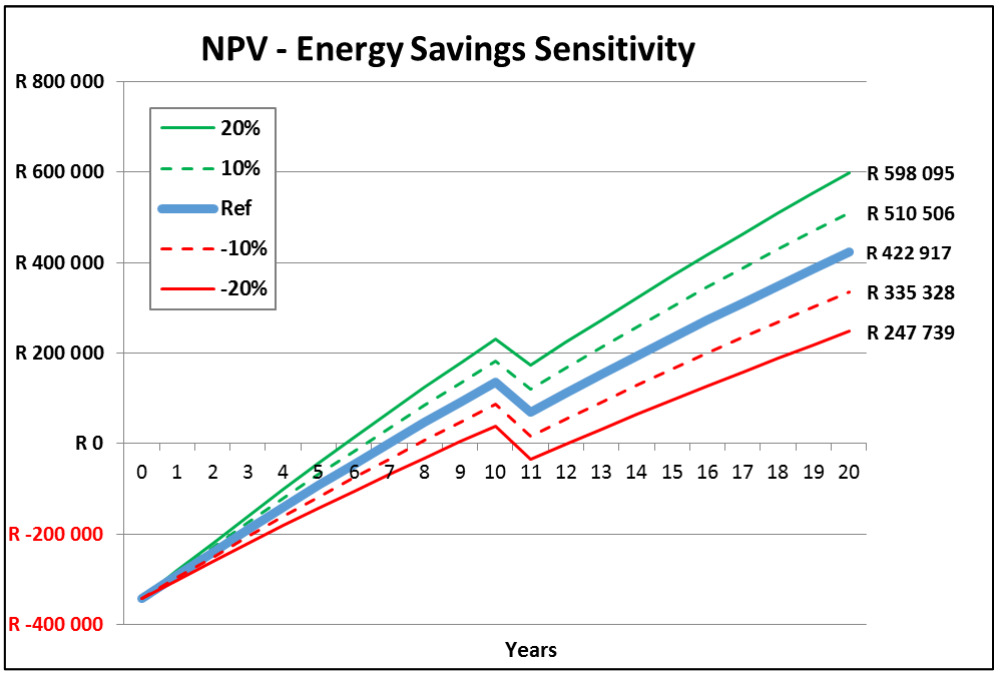

Figure 5-3: Energy Savings Sensitivity Analysis Results – Concept 14, Trip 1

If we consider the sensitive analysis for the cost of the RBS, a similar observation is made from the CBA results (NPV and IRR). The NPV decreases from R422 917 to R332 322 whilst the IRR decreases from 15.1% to 11.7% in the case where the RBS cost is 20% more than expected. The CBA results also improve significantly in the case where the RBS cost is less than expected. In both cases the distributed RBS remains economically feasible. The variation in the escalation of diesel fuel price identified in the EIA Annual Energy Outlook was investigated in the sensitivity analysis with the results shown in Figure 5-5. Similar results are obtained for this analysis in terms of NPV and IRR.

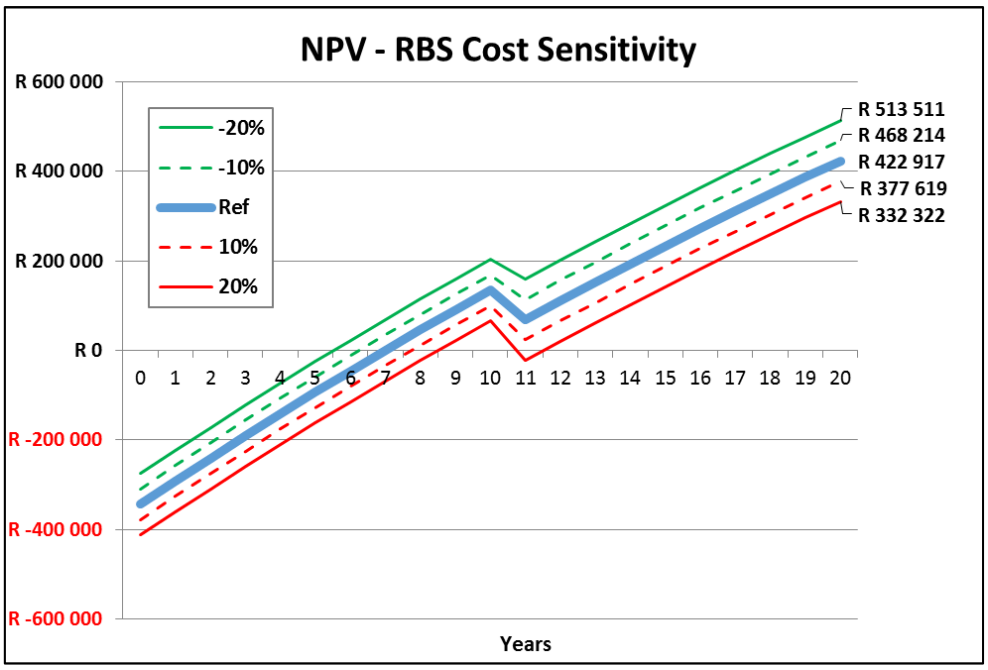

Figure 5-4: RBS Cost Sensitivity Analysis Results – Concept 14, Trip 1

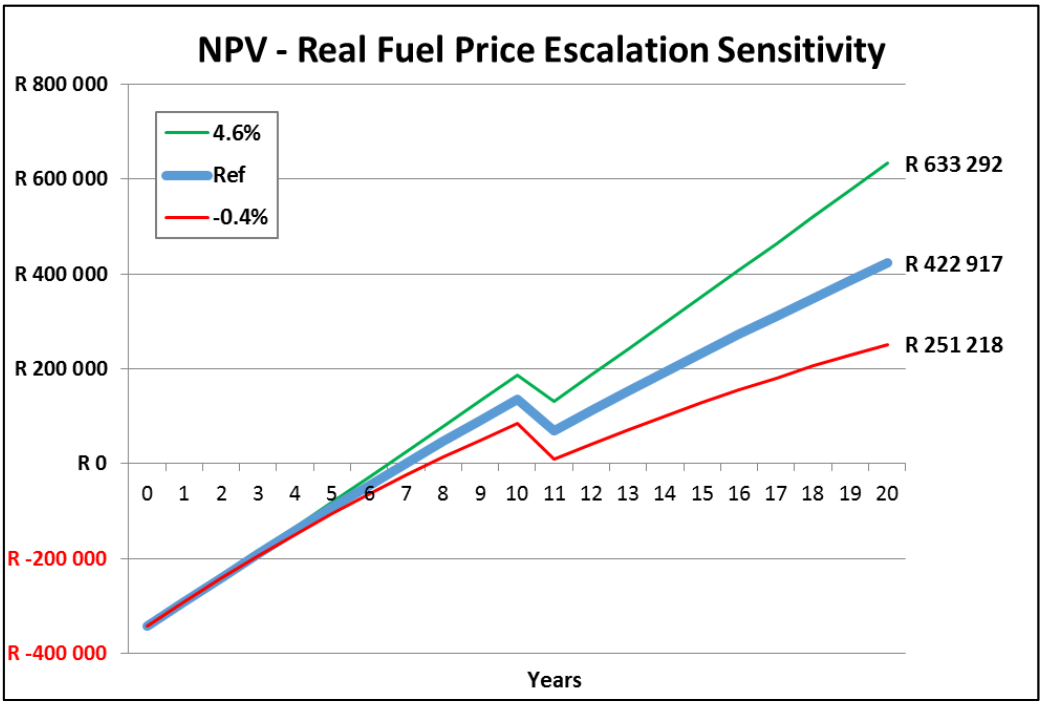

Figure 5-5: Fuel Price Escalation Sensitivity Analysis Results – Concept 14, Trip 1

The sensitivity analyses performed have all indicated that if the energy savings delivered by the RBS, the cost of the RBS and the cost of diesel fuel varies from their predicted values in the CBA the project would still comfortably remain economically feasible for the negative scenarios. There is also significant improvement in the economic case of the project in the instances where the parameters are altered to the positive scenarios. As a last test of the robustness of the financial case for this project, a combined best case and worst-case scenario is defined and investigated. The combined worst-case scenario is defined as a 20% decrease in the energy savings delivered, 20% increase in the

RBS cost and an annual escalation in real diesel price of -0.4%. The best-case scenario is a 20% in energy savings delivered, 20% decrease in RBS cost and an annual escalation of 4.6 in real diesel fuel price. The results of this analysis are shown in Figure 5-6 and Table 5-17. It is seen that for the worst-case scenario the project remains economically feasible by a small margin with the NPV remaining positive and the IRR remaining higher than the discount rate. For the best-case scenario, we observe a more than two-fold increase in the NPV for the project as well as a significant increase in the IRR.

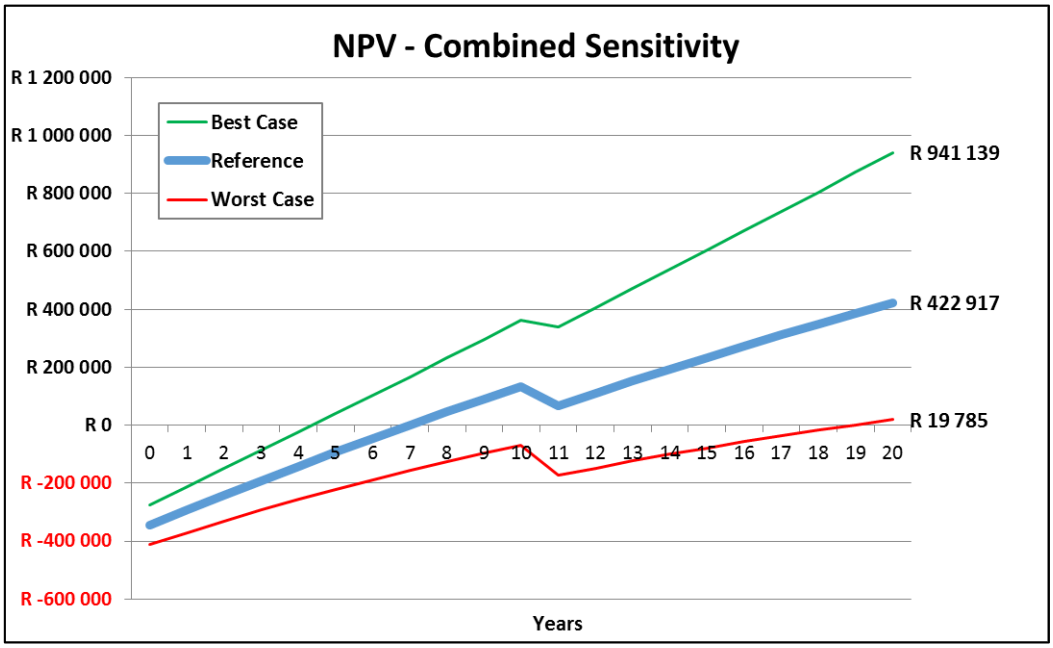

Figure 5-6: Combined (Worst- and Best Case) Sensitivity Analysis Results – Concept 14, Trip 1

Table 5-17: Sensitivity Analysis IRR Results - Concept 14, Trip 1

Energy Savings	IRR	System Cost	IRR	Diesel fuel inflation	IRR	Combined	IRR
-20%	11.0%	-20%	19.8%	-	-	-	-
-10%	13.1%	-10%	17.3%	-0.4%	12.1%	Best	26.9%
Reference	15.1%	Reference	15.1%	Reference	15.1%	Reference	15.1%
10%	17.0%	10%	13.3%	4.6%	17.8%	Worst	4.7%
20%	18.9%	20%	11.7%	-	-	-	-

The CBA performed in this chapter indicates that the distributed regenerative braking system is economically feasible for a number of the proposed concepts. The four decision criteria used (payback period, NPV, IRR and BCR) provided non-conflicting results in identifying the feasible concepts. These results were also used to obtain the concept that promised the best financial case. Once the 'best concept' for the proposed system was identified, the sensitivity analysis verified the robustness of this concepts financial case. For all the sensitivity analyses performed, the project remained economically feasible and beneficial. These results further support the business case of the proposed concept.

6. Conclusions, Discussion and Recommendations

6.1. Conclusions

The core aim of this study is to determine whether a novel regenerative braking system (RBS) proposed in a patent by Transnet SOC is both technically and economically feasible. In chapter one, based on a review and analysis of RBSs in the rail industry it was found that the proposed system would overcome certain technical constraints that has limited the application of regenerative braking in the freight rail industry. The research objectives and a research methodology was subsequently defined to meet the core aim of the study.

The literature review provided in chapter 2 provides insight into the state of the art of flywheel based RBS and the existing applications of these systems in both the automotive and rail industry. The literature review showed that although these systems have been commercialised in the automotive sector and have also been the subject of extensive research in the rail industry, no record was found of a FESS beyond the prototype stage in the rail industry. Methodologies used for analysing and simulating flywheel based RBSs and train systems in the literature are also identified and discussed in the review.

A workable system concept was generated in chapter 3 by establishing the requirements of the proposed RBS through numerical simulations and further developing the proposed system based on the technological characteristics and constraints identified for flywheel based RBSs. The process started with a top-down approach by firstly analysing the train system as a whole with the results feeding into the following system level until the lowest system level was reached. A bottom-up approach was subsequently used as the results of the analysis of the lowest system level fed back up to inform the design decisions at higher levels. This process delivered 10 candidate concepts for the proposed system that promised to meet the system requirements.

The study then moves on to simulate the synthesised system concepts using physical system simulation software with the goal of determining the energy savings delivered by each concept, the primary performance measure of the RBS. The simulation model developed successfully captured the complexity of the flywheel energy storage system (FESS), mechanical transmission, control system and the mission profile of the train system on a single freight wagon. The simulation procedure and analysis of results is described in detail and provides insight into the functionality of the RBS and the two transmission topologies. A procedure used for optimising the gear ratios of the transmission components is also provided along with the results obtained. Four additional system concepts were introduced in this section based on initial findings from the simulation results to bring the total number of candidate concepts to 14. The following observations were made regarding the performance of the RBS in the proposed application:

1. Candidate concepts with the topology B transmission, which includes a continuously variable transmission, delivered significantly better results than all concepts utilising topology A which only relies on frictional elements for the transfer of power.
2. It was observed that the energy savings delivered does not necessarily increase with an increase in energy storage capacity as predicted by the numerical analysis, as a larger un-usable energy capacity and self-discharge characteristics negatively impact energy savings.

3. The energy savings results from the physical system simulation were much lower than predicted by the numerical analysis in the previous chapter which was based on characteristics obtained in literature. Altough the braking energy captured by the RBSs coincided well with the numerical analysis, the return efficiency of the systems were found to be significantly lower than expected.

Upon investigation of the energy savings results obtained for each of the candidate concepts, 7 of the candidate concepts could be eliminated from the study before proceeding to the cost-benefit analysis (CBA).

A CBA follows the simulation chapter. The CBA results not only succeeded in determining the economic feasibility of each candidate concept, but was also used to select the 'best' concept which provides the highest return on investment. The system costing (initial capital- and maintenance cost) as well as an analysis of the system benefits are included in the CBA. The energy savings delivered was found to be the only economically relevant benefit of the RBS. Although not considered economically relevant at this stage, it was also shown that there is a significant benefit in the form of reduced emissions output as a result of the energy savings delivered by the RBS. The decision criteria chosen for the CBA provided unanimous results as to which concepts were economically feasible. The results indicated that all the concepts with topology A transmissions are not economically feasible and all topology B concepts are economically feasible by a comfortable margin. Of the candidate concepts deemed economically feasible, concept 14 was found to present the best investment opportunity as it delivers the most efficient use of capital invested. A sensitivity analysis was also performed which showed that for each of the cases investigated, the proposed distributed RBS remains economically feasible. The results also showed that the financial case significantly improves for the positive cases in the sensitivity analysis.

From the findings presented in this study as summarised above, we can conclude that the research methodology for the study was executed successfully and that each of the research objectives were met at set out in chapter 1. We can also conclude that the results from this study indicates that the proposed distributed regenerative braking for freight trains is both technically and economically feasible, answering the problem statement for this study successfully. The findings with regards to the technological state-of-the-art of flywheel energy storage systems (FESS) and the outcomes of the concept generation activities, showed that the technical means exist to implement the proposed distributed RBS. Furthermore, based on the findings of the system simulation we can conclude that such a system would deliver satisfactory performance and attractive energy savings results. The economic findings indicated that the cost of implementing and maintaining such a system on freight wagons is low enough that the system is economically feasible.

6.2. Discussion

It was mentioned above that the research methodology defined in chapter 1 was executed successfully and as a result the set of research objectives, and the overall goal of the study, was achieved. The methodology developed in this study for establishing the technical and economic feasibility of a RBS can be considered novel and a contribution to the field by this study. A holistic approach is taken to the problem statement in which both the RBS technology and railway landscape is approached from a broad perspective and a high system level. The information obtained from the

higher-level analyses feeds into the analysis of the lower system levels and vice versa. Both the technical and economic perspectives of an RBS are considered thoroughly to give a complete picture of the proposed technology.

By successfully reaching the objectives of the study, conclusions are made on the feasibility of regenerative braking on diesel-powered freight trains with on-board energy storage in a distributed manner for the first time. In chapter 1 it was explained that there are technical challenges and limitations from implementing RBSs with on-board energy storage for diesel-powered freight trains and that the proposed distributed RBS could overcome some of these challenges and limitations. By demonstrating the technical and economic feasibility of the proposed system, a promising new solution for diesel-powered freight trains is presented. Further to this, the findings of both the numerical analyses in chapter 3 and the system simulation of chapter 4 confirmed the potential of regenerative braking systems on freight trains and the value of pursing these systems, regardless of the specific means of implementation. This finding is in line with those of other studies for the rail industry.

6.3. Recommendations

As the distributed RBS was shown to be technically- and economically feasible from the perspective of a rail operator or owner, it is recommended that the technology be considered as solution to regenerative braking by industry role players and further evaluated by means of a proof-of-concept prototype. The distributed RBS is shown to not only economically feasible, but provides a promising business opportunity with competitive return on investment as well as providing a means of significantly reducing harmful and GHG emissions. This is further supported by the findings that regenerative braking in the railway industry, regardless of the means, shows promise to significantly reduce energy consumption and GHG emissions and that it should be pursued by railway operators.

The proposed system offers a pro-active means for governments to meet pledges for reduction in emissions, rather than policies such emissions tax. The proposed RBS would be worth pursuing from a government level as a means of reducing national carbon emissions while providing a good financial return on investment at the same time. A social cost-benefit analysis (CBA) would the appropriate analysis in this case as government is concerned not only with financial return but also the impact on the broader economy and society. The analysis could include effects of pursuing this project such as contribution to gross domestic product, monetary value of reduced emission, job creation and contribution to society all of which would further improve the business case of the proposed system.

A recommendation for further work is therefore the execution a social CBA from a governmental perspective. This study could consider two scenarios, first the case where the freight rail network is owned and operated by a private entity and secondly the case where the freight rail network is owned and operated by government (or state-owned entity) as is the case in the South African context.

Further to this, it is recommended that the technical feasibility of the proposed RBS be further evaluated for alternative energy storage technologies and power converter technologies. Although flywheels were found to present favourable characteristics for the specific application, an in-depth analysis of other commercialised energy storage technologies are required to conclusively establish the best energy storage technology, performance and cost wise, for the application. Electrical energy storage technologies such as batteries and supercapacitors, and the accompanying electrical motors

that serve as the power converters, are benefiting from economies of scale with the increased uptake of these technologies in the road transport sector and may prove to deliver highly cost-effective solutions.

With regards to the methodology of analysing the technical feasibility and performance of candidate solutions, the approach of simulating only a single freight wagon should be validated by simulating a complete train set. The results must be analysed to investigate whether the in-train dynamics and relevant motion between freight wagons affect the requirements or performance of the RBS on each vehicle. An analysis of the dynamic and loading affects brought on by installing RBS in wagon bogies must be performed to insure there are no adverse effects or safety risks imposed by doing so. Another opportunity for further work would be to formulate the design process of chapter 3 as an optimisation problem based on the parameterised models of the subsystems and components to provide a method for finding the optimal system concept.

7. List of References

Akli, C. R., Roboam, X., Sareni, B. & Jeunesse, A., 2007. Energy management and sizing of a hybrid locomotive. *IEEE European Conference on Power Electronics and Applications,* pp. 1-10.

AMT Composites, 2018. *AMT Composite Pricelist.* [Online] Available at: http://www.amtcomposites.co.za/ [Accessed 15 February 2018].

Ashely, S., 1996. Designing safer flywheels. *Mechanical Engineering,* Issue November 1996, pp. 88-91.

Bader, M. G., 2002. Selection of composite materials and manufacturing routes for cost- effective performance. *Elsevier Composite Part A: Applied Science and Manufacturing,* Volume 33, pp. 913-934.

Barrero, R., Tackoen, X. & van Mierlo, J., 2010. Stationary or onboard energy storage systems for energy. *Proceedings of the Institution of Mechanical Engineers, Part F: Journal of Rail and Rapid Transit,* 224(3), pp. 207-225.

Bayrak, A., 2015. *Topology considerations in hybrid vehicle powertrain architecture design.* [Online] Available at: https://deepblue.lib.umich.edu/ [Accessed 19 July 2018].

Berkel, K. V. et al., 2014. Topology and flywheel size optimization for mechanical hybrid powertrains. *IEEE Transactions on Vehicular Technology,* 63(9), pp. 4192-4205.

Beukes, J., 2013. *An economic analysis of concentrator photovoltaic technology use in South Africa : a case study,* Port Elizabeth: Faculty of Business and Economic Sciences at the Nelson Mandela Metropolitan University.

British Standard, 2009. *Railway applications - Wheelsets and bogies - Non-powered axles - Design method.* [Online] Available at: https://shop.bsigroup.com/ [Accessed 2019 July 2018].

British Standards Institution, 2005. *Wrought steels for mechanical and allied engineering purposes (PD970:2005).* [Online] Available at: https://shop.bsigroup.com/ [Accessed 19 July 2018].

Cengel, Y. A. & Cimbala, J. M., 2010. *Fluid Mechanics Fundamentals and Applications.* 2nd ed. New York: McGraw Hill.

Chymera, M., Renfrew, A. C. & Barnes, M., 2008. *Analyzing the potential of energy storage on electrified transit systems.* Seoul, Korea, Proceedings of the 8th World Congress of Railway Research.

Cook, L. M., Curran, W. T., McConnel, R. & Smith, A. K., 1979. *Flywheel energy storage switcher,* Washington D.C.: U.S. Department of Transportation, Federal Railroad Administration, Office of Research and Development.

DEAT, 2004. *Cost Benefit Analysis, Integrated Environmental Management, Information Series 8,* Pretoria: Department of Environmental Affairs and Tourism.

Dell, 2017. *Precision M6800.* [Online] Available at: http://www.dell.com/en-us/work/shop/dell-laptops-and-notebooks/precision-m6800/spd/precision-m6800-workstation
[Accessed 7 December 2017].

Druten, R. M. v., 2001. *Transmission design of the Zero Inertia Powertrain,* Eindhoven: CIP-Data Library Technische Universiteit Eindhoven.

Du Plessis, P., 2011. *The potential of solar process heat for South African industry,* Cape Town: University of Cape Town.

European Commission, 2015. *Paris Agreement.* [Online] Available at: https://ec.europa.eu/clima/policies/international/negotiations/paris_en [Accessed 21 March 2018].

EY, 2017. *EY Global Tax Alert.* [Online] Available at: http://www.ey.com/gl/en/services/tax/international-tax/alert--south-africa-publishes-second-draft-carbon-tax-bill-for-public-comment
[Accessed 14 March 2018].

Foiadelli, F., Roscia, M. & Zaninelli, D., 2006. *Optimization of storage devices for regenerative braking energy in subway systems.* Montreal, Canada, IEEE Power Engineering Society General Meeting, pp. 1-6.

Fujii, T., Teraya, N. & Osawa, M., 2014. *JR EAST Technical Review No.4-Summer 2004.* [Online] Available at: http://www.jreast.co.jp/e/development/tech/pdf_4/Tech-no.4-62-70.pdf [Accessed 29 March 2016].

Genta, G., 1985. *Kinetic Energy Storage: Theory and Practice of Advanced Flywheel Systems ,* Oxford: Butterworth & Co..

Gibson, R. F., 2012. *Principles of Composite Material Mechanics.* 3rd ed. Boca Raton: CRC Press.

GKN Land Systems, 2015. *GKN Hybrid Power.* [Online] Available at: http://www.gkn.com/landsystems/brands/hybrid-power/Pages/default.aspx [Accessed 25 May 2016].

GKN Land Systems, 2016. *GKN Hybrid Power.* [Online] Available at: http://www.gkn.com/landsystems/brands/hybrid-power/Pages/default.aspx [Accessed 13 September 2016].

González-Gil, A., Palacin, R. & Batty, P., 2013. Sustainable urban rail systems: Strategies and technologies for optimal management of regenerative braking energy. *Energy Conversion and Management,* 75(0), pp. 374-388.

González-Gil, A., Palacin, R. & Batty, P., 2013. Sustainable urban rail systems: Strategies and technologies for optimal management of regenerative braking energy. *Energy Conversion and Management,* 75(0), pp. 374-388.

Gräbe, P., 2008. Rail Transport. In: *Locomotive Systems, Performance and Maintenance.* Pretoria: University of Pretoria.

Hayes, R. J., Kajs, J. P., Thompson, R. C. & Beno, J. H., 1998. Design and testing of a flywheel battery for a transit bus. *Society of Automotive Engineer,* Issue 1999-01-1159.

Herbst, J. D. et al., 1998. Design, fabrication , and testing of 10 MJ composite flywheel energy storage rotors. *SAE Technical Paper Series,* 3(724).

Herbst, J. D., Thelen, R. F. & Walls, W. A., n.d. *Status of advanced locomotive propulsion system (ALPS) project, The University of Texas at Austin - Center for Electromechanics.* [Online] Available at: http://www.utexas.edu/research/cem/publications/doc/PN%20249%20Herbst.pdf [Accessed 16 May 2016].

Hillmansen, S. & Roberts, C., 2007. Energy storage devices in hybrid railway vehicles: a kinematic analysis. *Proceedings of the Institution of Mechanical Engineers, Part F: Journal of Rail and Rapid Transit,* Volume 221, pp. 135-143.

International Union of Railways, 2013. *Railway Handbook 2013: Energy Consumption and C02 Emissions.* [Online] Available at: http://www.uic.org/IMG/pdf/2013_uic-iea_railway_handbook_web_low.pdf [Accessed 12 February 2016].

Jaafar, A. et al., 2009. Sizing and energy management of a hybrid locomotive based on flywheel and accumulators. *IEEE Transactions on Vehicular Technology,* 58(8), pp. 3947-3958.

Jaafar, A., Sareni, B. & Roboam, X., 2013. A systemic approach integrating driving cycles for the design of hybrid locomotives. *IEEE Transactions on Vehicular Technology,* 62(8), pp. 3541-3550.

Janse van Rensburg, P. J. & Groenwold, A. A., 2011. Energy storage in composite flywheel rotors. *University of Stellenbosch: Department of Mechanical and Mechatronic Engineering.*

Kok, D., 1999. *Design optimisation of a flywheel hybrid vehicle,* Eindhoven: CIP Data Library Technische Universiteit Eindhoven.

Krack, M., Secanell, M. & Mertiny, P., 2011. Rotor design for high-speed flywheel energy storage systems. *Energy Storage in the Emerging Era of Smart Grids,* September.pp. 41-68.

Mathworks, 2016. *Simscape.* [Online] Available at: http://www.mathworks.com/products/simscape/ [Accessed 31 July 2016].

Modelica, 2016. [Online] Available at: https://www.modelica.org/ [Accessed 26 July 2016].

Murphy, B. T., Beno, J. H. & Bresie, D. A., 1997. *Bearing loads in a vehicular flywheel battery.* Detroit, SAE International Congress and Exposition.

National Treasury, Republic of South Africa, 2010. *Reducing greenhouse gas emissions: the carbon tax option.* [Online]

Available at: www.treasury.gov.za/
[Accessed 17 March 2018].

Navigant Research, 2011. *Hybrid electric locomotives will utilize 514 megawatt hours of battery capacity by 2020.* [Online]
Available at: http://www.navigantresearch.com/newsroom/hybrid-electric-locomotives-will-utilize-514-megawatt-hours-of-battery-capacity-by-2020
[Accessed 31 March 2016].

NSK, 2017. *NSK Motion & Control.* [Online]
Available at: http://www.nsk.com/
[Accessed 26 August 2017].

Oak Ridge National Laboratory, 2015. *Transportation Energy Data Book.* [Online]
Available at: http://cta.ornl.gov/
[Accessed 11 February 2016].

Okou, R., 2010. High speed flywheel and test rig design for rural energy storage. *University of Cape Town.*

Painter, T. D. & Barkan, C. P., 2006. *Prospects for dynamic brake energy recovery on North American freight locomotives.* Atlanta, Joint Rail Conference.

Pichot, M. et al., 1997. The flywheel battery containment problem. *SAE International Congress and Exposition.*

Rail Industry Resource Center, 2002. *Rail Power Green Goat.* [Online]
Available at: http://railindustry.com/coverage/2002/2002g02a.html
[Accessed 4 April 2016].

Railway Gazette, 2007. *GE unveils hybrid locomotive.* [Online]
Available at: http://www.railwaygazette.com/news/single-view/view/ge-unveils-hybrid-locomotive.html
[Accessed 4 April 2016].

Read, M. G., Smith, R. A. & Pullen, K. R., 2015. Optimisation of flywheel energy storage systems with geared transmission for hybrid vehicles. *Mechanismand Machine Theory,* Volume 87, pp. 191-209.

Republic of South Africa, 2018. *Department of Energy.* [Online]
Available at: http://www.energy.gov.za/
[Accessed 15 February 2018].

Ricardo PLC, 2015. *Significant fuel savings and rapid payback shown for rail flywheel hybrid technology.* [Online]
Available at: http://www.ricardo.com/en-GB/News--Media/Press-releases/News-releases1/2015/Significant-fuel-savings-and-rapid-payback-shown-for-rail-flywheel-hybrid-technology/
[Accessed 31 March 2016].

Rodrigue, J.-P., Slack, B. & Comtois, C., 2013. *The geography of transport systems.* [Online] Available at: https://people.hofstra.edu/geotrans/eng/ch3en/conc3en/ch3c1en.html [Accessed 11 February 2016].

Rupp, A., Baier, H., Mertiny, P. & Secanell, M., 2016. Analysis of a fl ywheel energy storage system for light rail transit. *Energy,* Volume 107, pp. 625-638.

Siemens, 2016. *LMS Imagine.Lab Amesim.* [Online] Available at: https://www.plm.automation.siemens.com/en_us/products/lms/imagine-lab/amesim/ [Accessed 26 July 2016].

Siemens, 2017. *LMS Imagine.Lab Amesim.* [Online] Available at: https://www.plm.automation.siemens.com/en/products/lms/imagine-lab/amesim/ [Accessed 7 December 2017].

SKF, 2017. *SKF.* [Online] Available at: http://www.skf.com/africa/en/index.html [Accessed 26 August 2017].

Smith, W. F., 1990. *Principles of Materials Science and Engineering.* 2nd ed. New York: McGraw-Hill Education.

South African Government, 2015. *About SA: Energy.* [Online] Available at: http://www.gov.za/about-sa/energy [Accessed 9 January 2016].

South African Reserve Bank, 2018. *South African Reserve Bank Historical Rates.* [Online] Available at: https://www.resbank.co.za/ [Accessed 15 March 2018].

Spiryagin, M. et al., 2015. Application of flywheel energy storage for heavy haul locomotives. *Applied Energy,* Volume 157, pp. 607-618.

Steiner, M., Klohr, M. & Pagiela, S., 2007. Energy storage system with ultracaps on board of railway vehicles. *IEEE Conference: Power Electronics and Applications.*

Sun, Y., Cole, C. & Spiryagin, M., 2013. Conceptual designs of hybrid locomotives for application as heavy haul trains on typical track lines. *Proceedings of the Institution of Mechanical Engineers, Part F: Journal of Rail and Rapid Transit,* 227(5), pp. 439-452.

Sun, Y. et al., 2013. Longitudinal heavy haul train simulations and energy analysis for typical Australian track routes. *Proceedings of the Institution of Mechanical Engineers, Part F: Journal of Rail and Rapid Transit,* 228(4), pp. 355-366.

Tesla Motors, 2016. *Tesla Model S Specifications.* [Online] Available at: https://www.teslamotors.com/support/model-s-specifications [Accessed 28 March 2016].

Thoolen, F. J., 1993. *Development of an advanced high speed flywheel energy storage system,* Eindhoven: CIP-Data Koninkluke Bibliotheek, Den Haag.

Torotrak Group, 2016. *Torotrak Group: Flybrid.* [Online] Available at: http://www.torotrak.com/products-partners/products/flybrid/ [Accessed 23 March 2016].

Transnet SOC Ltd, 2015. *Long Term Planning Framework: Freight and Energy Demand Forecast.* [Online] Available at: http://www.transnet.net/ [Accessed 12 February 2016].

Transnet State Owned Company, 2015. *Annual Integrated Report,* Johannesburg: Transnet SOC.

Transnet, S. L., 2016. *Regenerative Railway Braking System.* Patent Cooperation Treaty, Patent No. PCT/IB2016/051876.

U.S Department of Energy, 2003. *Federal Technology Alert: Flywheel Energy Storage.* [Online] Available at: www.eere.energy.gov/femp

U.S. Energy Information Administration, 2018. *Annual Energy Outlook.* [Online] Available at: https://www.eia.gov/outlooks/aeo/ [Accessed 15 March 2018].

Ultimate Transmissions, 2011. *Ultimate Transmissions.* [Online] Available at: http://www.ultimatetransmissions.com/ut.php?ABOUT_US [Accessed 7 August 2016].

Ultra Low Emission Vehicle - Transport using Advanced Propulsion, 2005. *ULEV-TAP Public Report.* [Online] Available at: http://www.ulev-tap.org/ [Accessed 15 May 2016].

United Nations Climate Change, 2016. *The Paris Agreement.* [Online] Available at: http://unfccc.int/2860.php [Accessed 25 March 2018].

US Energy Information Administration, 2015. *Frequently Asked Questions.* [Online] Available at: http://www.eia.gov/tools/faqs/faq.cfm?id=447&t=1 [Accessed 11 11 2015].

van der Meulen, D. & Moller, F., 2014. Sustainable heavy haul traction energy: A review of systemic issues. *Journal of Rail and Rapid Transit,* 228(6), pp. 687-694.

Vazquez, S. et al., 2010. Energy storage systems for transport and grid applications. *IEEE Transactions on Industrial Electronics,* 57(12), pp. 3881-3895.

Vroemen, B. G., 2001. *Component Control for The Zero Inertia Powertrain,* Eindhoven: CIP-Data Library Technische Universiteit Eindhoven.

Williams Grand Prix Engineering Limited, 2014. *Successfully Incubating Technology - Flywheel Energy Storage.* [Online]

Available at: http://www.williamsf1.com/advanced-engineering/case-studies/incubating-technology [Accessed 25 May 2016].

Wu, Q., Luo, S. & Cole, C., 2014. Longitudinal dynamics and energy analysis for heavy haul trains. *Journal of Modern Transportation,* 22(April), pp. 127-136.

Appendix A Chapter 1 Calculation Results

Table A-1: EROI Calculation Results as Illustrated in Figure 1-1.

Time (min)	Lithium-Ion	Lithium-Polymer	Super-capacitor	Flywheel
0	86.25%	82.50%	92.50%	94.25%
15	86.25%	82.50%	92.21%	91.30%
30	86.25%	82.50%	91.92%	88.45%
45	86.24%	82.50%	91.64%	85.69%
60	86.24%	82.49%	91.35%	83.01%
75	86.24%	82.49%	91.06%	80.42%
90	86.24%	82.49%	90.78%	77.90%
105	86.24%	82.49%	90.50%	75.47%
120	86.24%	82.49%	90.21%	73.11%
135	86.23%	82.49%	89.93%	70.83%
150	86.23%	82.49%	89.65%	68.61%
165	86.23%	82.49%	89.37%	66.47%
180	86.23%	82.48%	89.09%	64.39%
195	86.23%	82.48%	88.81%	62.38%
210	86.22%	82.48%	88.53%	60.43%
225	86.22%	82.48%	88.26%	58.54%
240	86.22%	82.48%	87.98%	56.71%

Table A-2: Lifecycle Cost Calculation Results as Illustrated in Figure 1-2.

	Capita Cost per kWh (Lower Bound)	Capita Cost per kWh (Upper Bound)	Durability (cycles)	Cost per kWh cycle (Lower Bound)	Cost per kWh cycle (Upper Bound)
Lithium-Ion	R 7,500	R 37,500	68 971	R 0.11	R 0.54
Super-capacitors	R 4,500	R 30,000	525 000	R 0.01	R 0.06
Flywheels	R 15,000	R 75,000	1 000 000	R 0.02	R 0.08
Lithium Poly	R 13,500	R 19,500	9 234	R 1.46	R 2.11

Table A-3: ESS Sizing Results

	Requirement	Mass	Volume	Energy Capacity Oversize
Lithium-Ion	Energy	664.53	0.33	**12.63**
	Power	8333.33	4.17	
Lithium-Polymer	Energy	664.53	0.66	**6.89**
	Power	4545.45	4.55	

Appendix B Chapter 3 Calculations

Section 3.1 Calculations

Table B-4

Trip 1		
ESS Capacity (kWh)	**ESS Capacity (per wagon)**	**Percentage Braking Energy Captured**
64	0.8	20.785
128	1.6	37.242
192	2.4	50.492
256	3.2	61.792
320	4	70.845
384	4.8	77.632
448	5.6	82.005
512	6.4	85.553
576	7.2	87.826
640	8	89.438
704	8.8	91.049
768	9.6	92.661
832	10.4	93.984
896	11.2	95.192
960	12	96.401
1024	12.8	97.541
1088	13.6	98.346
1152	14.4	99.152
1216	15.2	99.716

Table B-5

Trip 2		
ESS Capacity (kWh)	**ESS Capacity (per wagon)**	**Percentage Braking Energy Captured**
79	1.58	36.608
158	3.16	55.675
237	4.74	67.075
316	6.32	73.205
395	7.9	77.502
474	9.48	80.842
553	11.06	84.182
632	12.64	87.456
711	14.22	90.128
790	15.8	92.508
869	17.38	94.512

Section 3.1.2 Calculations

Table B-6

Trip 1									
ESS Capacity per Wagon (kWh)	Total Motoring Energy (kJ)	Total Braking Energy (kJ)	Braking Energy Captured (kJ)	Percentage Braking Energy Captured	Motoring Energy Delivered by RBS (kJ)	Energy Recovered /Energy Capacity	Energy Saved (%)	Energy Saved/ Self-Sufficiency (%)	EROI (%)
4	1727836	717659	370682	51.7%	292875	20.3	17.0%	40.8%	79.0%
4.2	1727836	717659	382645	53.3%	301952	20.0	17.5%	42.1%	78.9%
4.4	1727836	717659	392847	54.7%	309181	19.5	17.9%	43.1%	78.7%
4.6	1727836	717659	402845	56.1%	316694	19.1	18.3%	44.1%	78.6%
4.8	1727836	717659	411619	57.4%	322901	18.7	18.7%	45.0%	78.4%
5	1727836	717659	419424	58.4%	328074	18.2	19.0%	45.7%	78.2%
5.2	1727836	717659	427153	59.5%	333675	17.8	19.3%	46.5%	78.1%
5.4	1727836	717659	434910	60.6%	338880	17.4	19.6%	47.2%	77.9%
5.6	1727836	717659	441802	61.6%	343312	17.0	19.9%	47.8%	77.7%
5.8	1727836	717659	448700	62.5%	347466	16.6	20.1%	48.4%	77.4%
6	1727836	717659	455097	63.4%	350871	16.2	20.3%	48.9%	77.1%
6.2	1727836	717659	460752	64.2%	353745	15.8	20.5%	49.3%	76.8%
6.4	1727836	717659	466149	65.0%	356828	15.5	20.7%	49.7%	76.5%
6.6	1727836	717659	471520	65.7%	359439	15.1	20.8%	50.1%	76.2%
6.8	1727836	717659	476885	66.5%	362103	14.8	21.0%	50.5%	75.9%
7	1727836	717659	482295	67.2%	365064	14.5	21.1%	50.9%	75.7%
7.2	1727836	717659	487254	67.9%	367857	14.2	21.3%	51.3%	75.5%
7.4	1727836	717659	491804	68.5%	370296	13.9	21.4%	51.6%	75.3%
7.6	1727836	717659	496376	69.2%	373376	13.6	21.6%	52.0%	75.2%
7.8	1727836	717659	500949	69.8%	375926	13.4	21.8%	52.4%	75.0%
8	1727836	717659	505470	70.4%	378575	13.1	21.9%	52.8%	74.9%

Table B-7

Trip 2									
Energy Capacity per Wagon (kWh)	Total Motoring Energy (kJ)	Total Braking Energy (kJ)	Braking Energy Captured (kJ)	Percentage Braking Energy Captured	Motoring Energy Delivered by RBS (kJ)	Energy Recovered / Energy Capacity	Energy Saved (%)	Energy Saved/Self-Sufficiency (%)	EROI (%)
4	1084563	851679	418752	49.2%	314506	21.8	29.0%	36.9%	75.1%
4.2	1084563	851679	426978	50.1%	319243	21.1	29.4%	37.5%	74.8%
4.4	1084563	851679	434094	51.0%	323149	20.4	29.8%	37.9%	74.4%
4.6	1084563	851679	441007	51.8%	326768	19.7	30.1%	38.4%	74.1%
4.8	1084563	851679	447312	52.5%	329850	19.1	30.4%	38.7%	73.7%
5	1084563	851679	453648	53.3%	333373	18.5	30.7%	39.1%	73.5%
5.2	1084563	851679	460044	54.0%	336146	18.0	31.0%	39.5%	73.1%
5.4	1084563	851679	466472	54.8%	339419	17.5	31.3%	39.9%	72.8%
5.6	1084563	851679	472790	55.5%	342619	17.0	31.6%	40.2%	72.5%

5.8	1084563	851679	478463	56.2%	345011	16.5	31.8%	40.5%	72.1%
6	1084563	851679	483943	56.8%	347557	16.1	32.0%	40.8%	71.8%
6.2	1084563	851679	489502	57.5%	349918	15.7	32.3%	41.1%	71.5%
6.4	1084563	851679	494944	58.1%	352353	15.3	32.5%	41.4%	71.2%
6.6	1084563	851679	500487	58.8%	354580	14.9	32.7%	41.6%	70.8%
6.8	1084563	851679	505974	59.4%	357120	14.6	32.9%	41.9%	70.6%
7	1084563	851679	511429	60.0%	359234	14.3	33.1%	42.2%	70.2%
7.2	1084563	851679	516161	60.6%	361119	13.9	33.3%	42.4%	70.0%
7.4	1084563	851679	520831	61.2%	362767	13.6	33.4%	42.6%	69.7%
7.6	1084563	851679	525487	61.7%	364553	13.3	33.6%	42.8%	69.4%
7.8	1084563	851679	530152	62.2%	366352	13.0	33.8%	43.0%	69.1%
8	1084563	851679	534842	62.8%	368045	12.8	33.9%	43.2%	68.8%

Section 3.2.2

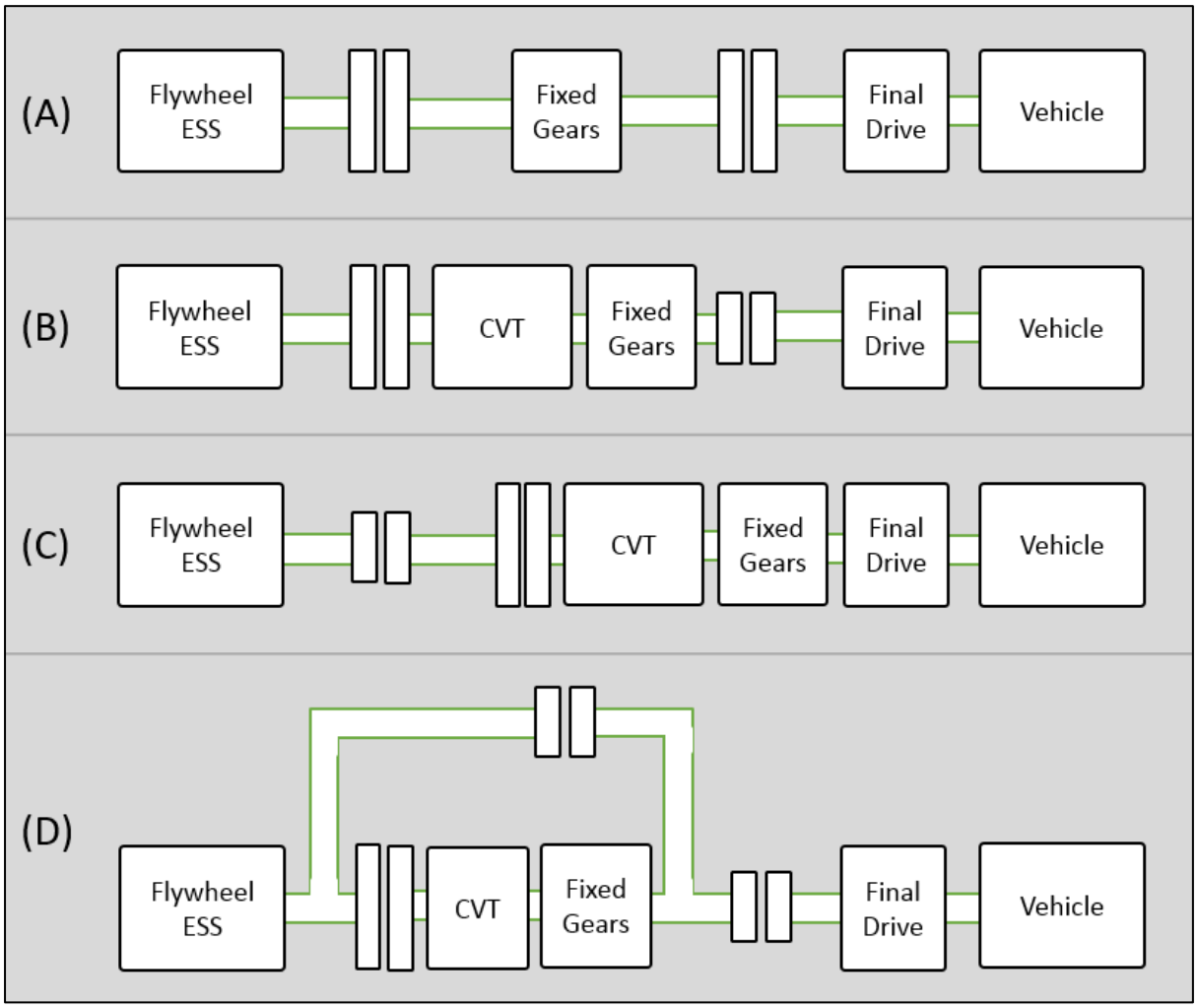

Figure B-1: Topology Concepts

Section 3.3 Calculations

Wendt (1933) investigated instability phenomena in the circumference gap of rotating cylinders as well, and he divided the region with vortices in a laminar and a turbulent region:

$Re_c < Re_{c,\,crit}$	:	laminar couette flow
$Re_{c,\,crit} < Re_c < 400$	:	laminar flow with Taylor vortices
$400 < Re_c < 10^4$	:	turbulent flow with Taylor vortices
$Re_c > 10^4$	:	full turbulent flow

For this purpose, Wendt introduced the critical Reynolds number $Re_{c,crit}$:

$$Re_{c,crit} = \left[\frac{\omega \cdot R \cdot t}{\nu}\right]_{crit} \approx 41.2 \cdot \sqrt{\frac{1 + \frac{1}{2}\cdot\frac{t}{R}}{\frac{t}{R}}}\,, \qquad (3.10)$$

Figure B-2: Flywheel Drag Calculations (Kok, 1999)

Regime k	Circumference torque coefficient	Application range [1]
I	$C_{circ} = 3.6 \cdot \left(\frac{t}{R}\right)^{-0.25} \cdot \frac{\left(1+\frac{t}{R}\right)^2}{2+\frac{t}{R}} \cdot Re_c^{-1}$	$Re_c < Re_{c,crit}$
II	$C_{circ} = 10^{const1 \cdot \log(Re_c) + const2}$	$Re_{c,crit} < Re_c < 400$
III	$C_{circ} = 0.920 \cdot \left(\frac{t}{R} \cdot \left(1+\frac{t}{R}\right)\right)^{0.25} \cdot \mathrm{Re}_c^{-0.5}$	$max\left(Re_{c,crit}, 400\right) < Re_c < 10^4$
IV	$C_{circ} = 0.146 \cdot \left(\frac{t}{R} \cdot \left(1+\frac{t}{R}\right)\right)^{0.25} \cdot Re_c^{-0.3}$	$Re_c > 10^4$

Figure B-3: Flywheel Drag Calculations (Kok, 1999)

m	Side plane friction coefficient	Application range*	$Re_{s,\,m\rightarrow m+1}$
I	$C_{side} = 2\pi \cdot \left(\frac{s}{R}\right)^{-1} \cdot Re_s^{-1}$	$0 < Re_s < Re_{s,I\rightarrow II}$	$Re_{s,I\rightarrow II} = 2.9 \cdot \left(\frac{s}{R}\right)^{-\frac{11}{5}}$
II	$C_{side} = 3.7 \cdot \left(\frac{s}{R}\right)^{\frac{1}{10}} \cdot Re_s^{-\frac{1}{2}}$	$Re_{s,I\rightarrow II} < Re_s < Re_{s,II\rightarrow III}$	$Re_{s,II\rightarrow III} = 4.6\cdot 10^6 \cdot \left(\frac{s}{R}\right)^{+\frac{16}{15}}$
III	$C_{side} = 8.0\cdot 10^{-2} \cdot \left(\frac{s}{R}\right)^{-\frac{1}{6}} \cdot Re_s^{-\frac{1}{4}}$	$Re_{s,II\rightarrow III} < Re_s < Re_{s,III\rightarrow IV}$	$Re_{s,III\rightarrow IV} = 7.8\cdot 10^{-3} \cdot \left(\frac{s}{R}\right)^{-\frac{16}{3}}$
IV	$C_{side} = 1.0\cdot 10^{-2} \cdot \left(\frac{s}{R}\right)^{\frac{1}{10}} \cdot Re_s^{-\frac{1}{5}}$	$Re_s > Re_{s,III\rightarrow IV}$	

**: Regimes II and III are only valid for s/R ratios as illustrated in Figure 3.9.*

Figure B-4: Flywheel Drag Calculations (Kok, 1999)

Table B-8: Flywheel Self-Discharge Calculation to determine half-life rating in minutes

	Tool Steel		Carbon		Aramid	
Time (minutes	Absolute Energy Content (MJ)	Useful energy content(%)	Absolute Energy Content (MJ)	Useful energy content(%)	Absolute Energy Content (MJ)	Useful energy content(%)
0	5.688	100%	13.284	100%	7.2	100%
2	5.61312	98%	12.86148	96%	6.94836	95%
4	5.539226	97%	12.4524	92%	6.705515	91%
6	5.466304	95%	12.05633	88%	6.471157	87%
8	5.394343	93%	11.67286	84%	6.24499	82%
10	5.323329	91%	11.30158	80%	6.026728	78%
12	5.253249	90%	10.94212	76%	5.816094	74%
14	5.184093	88%	10.59408	73%	5.612821	71%
16	5.115846	87%	10.25712	70%	5.416653	67%
18	5.048499	85%	9.930877	66%	5.227341	63%
20	4.982037	83%	9.615008	63%	5.044645	60%
22	4.916451	82%	9.309187	60%	4.868335	57%
24	4.851728	80%	9.013092	57%	4.698187	54%
26	4.787857	79%	8.726416	54%	4.533985	51%
26.5	4.7721	79%	8.657026	54%	4.494369	50%
27	4.756394	78%	8.588188	53%	4.4551	49%
28	4.725086	77%	8.451608	51%	4.377247	48%
29	4.693984	77%	8.317199	50%	4.300755	46%
30	4.663087	76%	8.184927	49%	4.225599	45%
32	4.6017	75%	7.924592	46%	4.077914	42%
34	4.54112	73%	7.672537	44%	3.935391	40%
66	3.673812	53%	4.576771	13%	2.228742	8%
68	3.625448	52%	4.431199	11%	2.150847	6%
70	3.577721	51%	4.290257	10%	2.075675	5%
71	3.554171	50%	4.222027	9%	2.039403	4%
72	3.530777	49%	4.154883	8%	2.003764	4%
74	3.484296	48%	4.02273	7%	1.933733	2%

Section 3.4 Calculations

Table B-9: Transmission Torque Rating Calculation

	Trip 1: PHB-RCHB	Trip 2: JHB - DBN
Maximum motoring tractive effort (kN)	1418	578
Maximum braking tractive effort (kN)	761	418
Number of wagons in train	80	50
Maximum tractive effort per wagon (kN)	17.73	11.56
Wagon wheel diameter (m)	0.865	0.865
Maximum torque per wagon (Nm)	7666	5000
Maximum torque per RBS (Nm)	3833	2500

Table B-10: Transmission Torque Limit vs. Speed Calculation

Speed (km/h)	Speed (m/s)	Axle Speed (rad/s)	Torque Limit from Power (Nm)	Torque Limit from Tractive Effort (Nm)
0.1	0.0	0.1	934 200	4041
5	1.4	3.2	18 684	4041
10	2.8	6.4	9 342	4041
12	3.3	7.7	7 785	4041
20	5.6	12.8	4 671	4041
23.12	6.4	14.8	4 041	4041
30	8.3	19.3	3 114	4041
40	11.1	25.7	2 336	4041
50	13.9	32.1	1 868	4041
60	16.7	38.5	1 557	4041
70	19.4	45.0	1 335	4041
80	22.2	51.4	1 168	4041

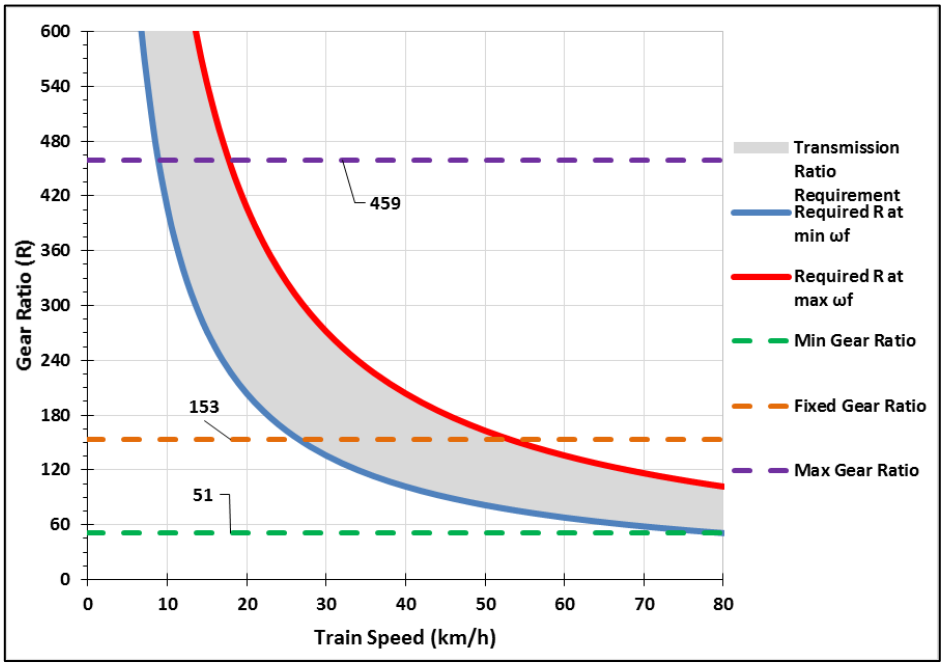

Figure B-5: Topology B transmission gear ratio analysis for the carbon flywheel

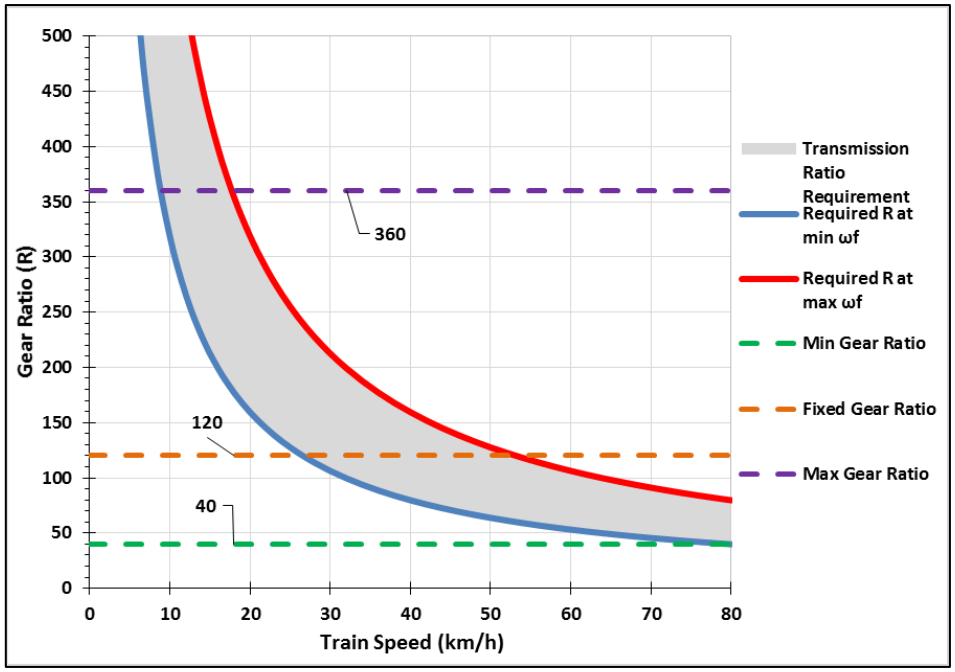

Figure B-6: Topology B transmission gear ratio analysis for the aramid flywheel

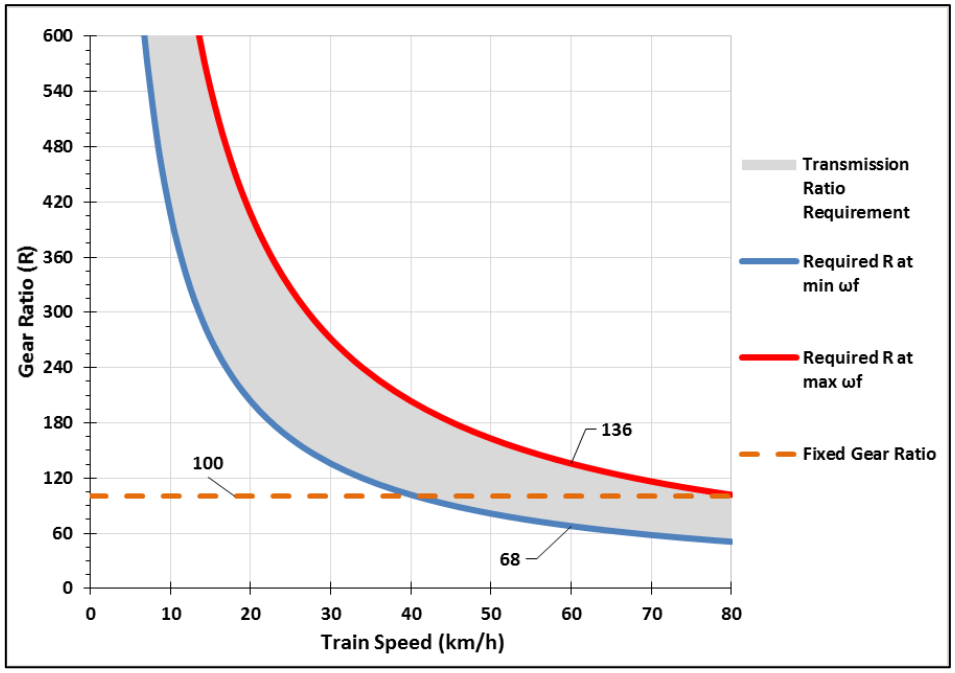

Figure B-7: Topology A overall gear ratio analysis for the carbon flywheel

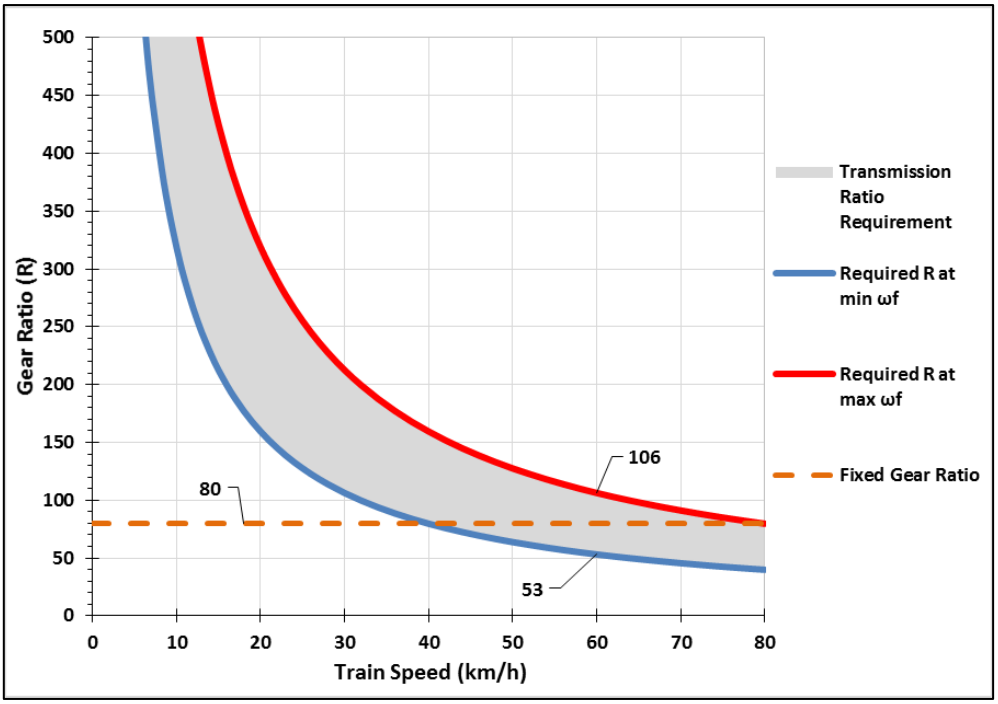

Figure B-8: Topology A overall gear ratio analysis for the aramid flywheel

Appendix C Chapter 4 Simulation Results

Section 4.4: Simulation Results

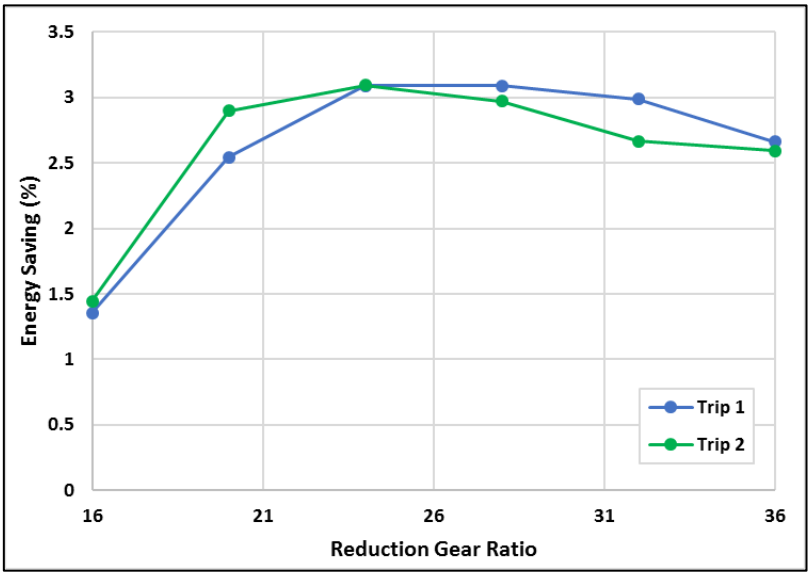

Figure C-9: Concept 3 – Energy Savings Results for Various Reduction Gear Ratios

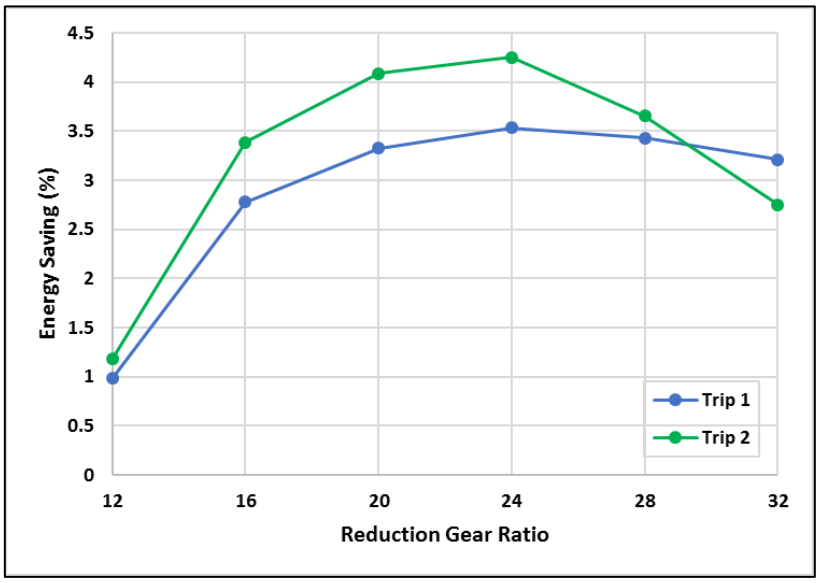

Figure C-10: Concept 5– Energy Savings Results for Various Reduction Gear Ratios

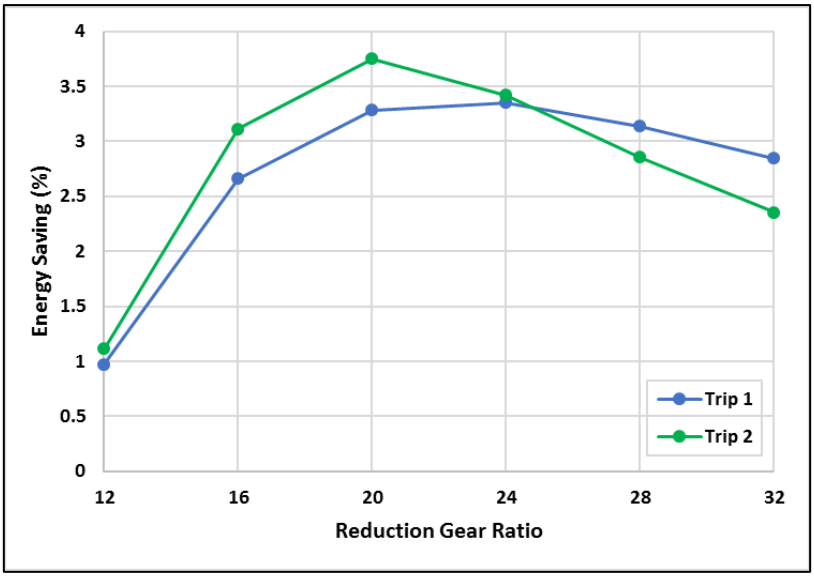

Figure C-11: Concept 7– Energy Savings Results for Various Reduction Gear Ratios

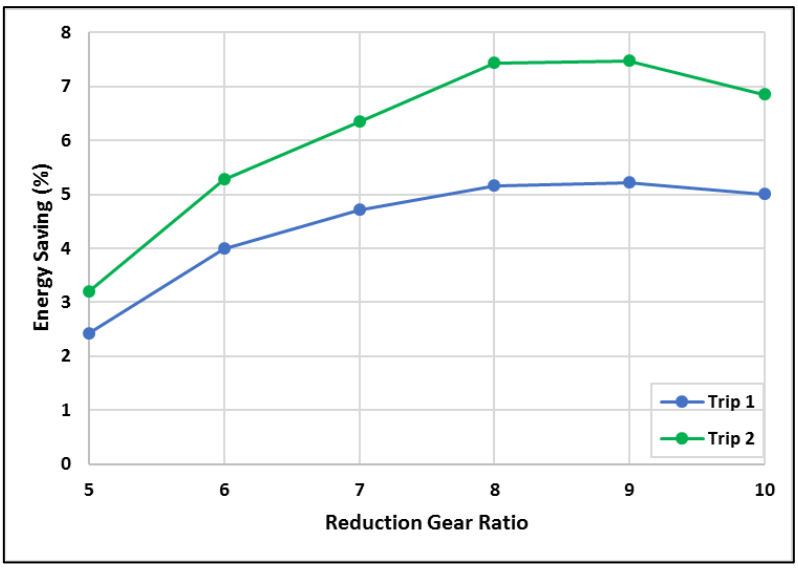

Figure C-12: Concept 9– Energy Savings Results for Various Reduction Gear Ratios

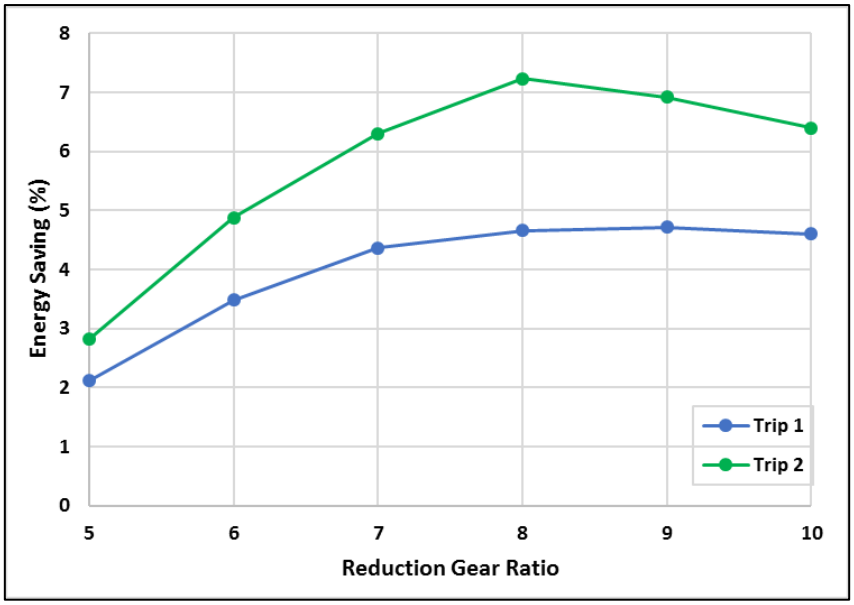

Figure C-13: Concept 11– Energy Savings Results for Various Reduction Gear Ratios

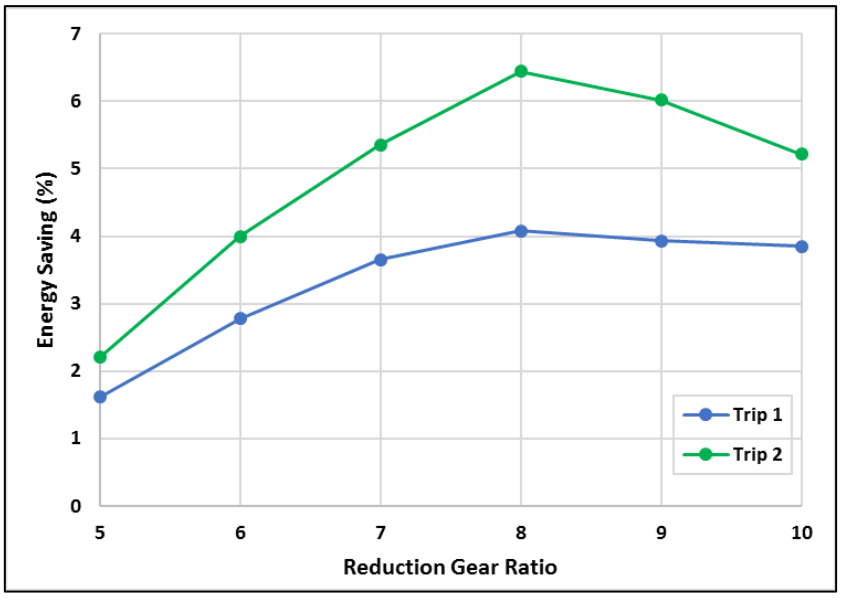

Figure C-14: Concept 13– Energy Savings Results for Various Reduction Gear Ratios

Table C-11: Simulation Results – Performance Measures

Concept	*Trip*	*# RBS*	*Flywheel*	*Topology*	*Energy Saving (%)*	*EROI (%)*	*Braking (%)*
1	1	2	Carbon	A	3.57	13.87	63.33
1	2	2	Carbon	A	4.38	11.16	49.89
2	1	2	Carbon	B	12.72	38.42	79.00
2	2	2	Carbon	B	20.04	34.60	73.61
3	1	3	Carbon	A	3.09	11.66	65.56
3	2	3	Carbon	A	3.09	7.91	50.14
4	1	3	Carbon	B	12.66	33.53	91.06
4	2	3	Carbon	B	19.51	28.48	87.17
5	1	3	Aramid	A	3.54	13.74	63.56
5	2	3	Aramid	A	4.25	10.64	51.22
6	1	3	Aramid	B	11.85	38.43	74.36
6	2	3	Aramid	B	19.76	35.92	70.07
7	1	4	Aramid	A	3.28	12.95	62.37
7	2	4	Aramid	A	3.75	10.10	47.99
8	1	4	Aramid	B	12.32	35.50	83.66
8	2	4	Aramid	B	19.33	31.52	78.10
9	1	4	Steel	A	5.22	23.97	52.92
9	2	4	Steel	A	7.48	22.84	41.50
10	1	4	Steel	B	14.65	55.78	63.33
10	2	4	Steel	B	24.63	53.09	58.95
11	1	3	Steel	A	4.66	27.31	43.48
11	2	3	Steel	A	7.23	28.85	31.92
12	1	3	Steel	B	12.94	57.37	54.36
12	2	3	Steel	B	23.44	56.01	53.33
13	1	2	Steel	A	4.08	30.23	33.66
13	2	2	Steel	A	6.44	33.39	24.61
14	1	2	Steel	B	10.22	58.87	41.87
14	2	2	Steel	B	19.60	58.44	42.67

Table C-12: Simulation Results – Energy Losses

Concept	*Trip*	*Topology*	*Flywheel (MJ)*	*Reduction Gears (MJ)*	*CVT (MJ)*	*Clutch (MJ)*	*Final Drive (MJ)*	*Total (MJ)*
1	1	A	174	12	0	177	15	379
3	1	A	204	13	0	170	16	402
5	1	A	170	12	0	184	15	381
7	1	A	185	12	0	164	15	376
9	1	A	82	13	0	173	14	281
11	1	A	58	11	0	133	12	213
13	1	A	41	9	0	101	9	160
1	2	A	198	11	0	139	14	363
3	2	A	223	10	0	129	14	376
5	2	A	203	11	0	148	14	376
7	2	A	205	10	0	127	13	356
9	2	A	101	11	0	133	13	258
11	2	A	72	10	0	91	10	183
13	2	A	57	8	0	85	9	160
2	1	B	232	23	55	12	24	346
4	1	B	305	25	61	9	26	426
6	1	B	214	21	51	15	22	324
8	1	B	264	23	56	12	25	381
10	1	B	95	21	50	8	21	195
12	1	B	74	18	44	8	19	162
14	1	B	50	14	34	8	14	121
2	2	B	264	24	59	12	26	385
4	2	B	358	27	66	13	29	493
6	2	B	245	23	56	13	25	362
8	2	B	303	25	61	13	26	428
10	2	B	106	23	54	7	23	213
12	2	B	83	21	50	7	21	183
14	2	B	58	17	41	7	17	140

Appendix D Chapter 5 Cost-Benefit Analysis Results

Table D-13: CBA Calculation Results Concept 2, Trip 2

	Nominal Monetary Values					Discounted (Real) Monetary Values		
Year	Annual Fuel Savings	Initial Capital Expenditure	Maintenance Expenditure	Annual Cashflow	Nominal Cumulative Cash Flow	Discounte Benefits	Discounted Costs	Net Present Value
0	R 0	R -393 430	R -	R -393 430	R -393 430	R 0	R -393 430	R -393 430
1	R 66 464	0	R -	R 66 464	R -326 965	R 63 847	R 0	R -329 583
2	R 67 927	R 0	R -	R 67 927	R -259 039	R 62 681	R 0	R -266 902
3	R 69 421	R 0	R -	R 69 421	R -189 618	R 61 537	R 0	R -205 364
4	R 70 948	R 0	R -	R 70 948	R -118 669	R 60 414	R 0	R -144 950
5	R 72 509	R 0	R -	R 72 509	R -46 160	R 59 312	R 0	R -85 639
6	R 74 104	R 0	R -	R 74 104	R 27 944	R 58 229	R 0	R -27 410
7	R 75 735	R 0	R -	R 75 735	R 103 679	R 57 166	R 0	R 29 757
8	R 77 401	R 0	R -	R 77 401	R 181 080	R 56 123	R 0	R 85 880
9	R 79 104	R 0	R -	R 79 104	R 260 183	R 55 099	R 0	R 140 978
10	R 80 844	R 0	R -	R 80 844	R 341 027	R 54 093	R 0	R 195 071
11	R 82 623	R 0	R -187 013	R -104 391	R 236 637	R 53 106	R -120 203	R 127 974
12	R 84 440	R 0	R -	R 84 440	R 321 077	R 52 136	R 0	R 180 110
13	R 86 298	R 0	R -	R 86 298	R 407 375	R 51 185	R 0	R 231 295
14	R 88 196	R 0	R -	R 88 196	R 495 571	R 50 251	R 0	R 281 546
15	R 90 137	R 0	R -	R 90 137	R 585 708	R 49 333	R 0	R 330 879
16	R 92 120	R 0	R -	R 92 120	R 677 828	R 48 433	R 0	R 379 312
17	R 94 146	R 0	R -	R 94 146	R 771 974	R 47 549	R 0	R 426 861
18	R 96 218	R 0	R -	R 96 218	R 868 192	R 46 681	R 0	R 473 542
19	R 98 334	R 0	R -	R 98 334	R 966 526	R 45 829	R 0	R 519 371
20	R 100 498	R 0	R -	R 100 498	R 1 067 024	R 44 993	R 0	R 564 364
	R 1 647 467	R -393 430	R -187 013			R 1 077 996	R -513 633	

Table D-14: CBA Calculation Results Concept 9, Trip 1

	Nominal Monetary Values					Discounted (Real) Monetary Values			
Year	Annual Fuel Savings	Initial Capital Expenditure	Maintenance Expenditure	Annual Cashflow	Nominal Cumulative Cash Flow	Discounted Benefits	Discounted Costs	Net Discounted Flow	Net Present Value
0	R 0	R -572 594	R -	R -572 594	R -572 594	R 0	R -572 594	R -572 594	R -572 594
1	R 27 565	0	R -	R 27 565	R -545 028	R 26 480	R 0	R 26 480	R -546 114
2	R 28 172	R 0	R -	R 28 172	R -516 857	R 25 996	R 0	R 25 996	R -520 118
3	R 28 791	R 0	R -	R 28 791	R -488 065	R 25 522	R 0	R 25 522	R -494 596
4	R 29 425	R 0	R -	R 29 425	R -458 640	R 25 056	R 0	R 25 056	R -469 540
5	R 30 072	R 0	R -	R 30 072	R -428 568	R 24 599	R 0	R 24 599	R -444 941
6	R 30 734	R 0	R -	R 30 734	R -397 834	R 24 150	R 0	R 24 150	R -420 791
7	R 31 410	R 0	R -	R 31 410	R -366 424	R 23 709	R 0	R 23 709	R -397 082
8	R 32 101	R 0	R -	R 32 101	R -334 323	R 23 276	R 0	R 23 276	R -373 806
9	R 32 807	R 0	R -	R 32 807	R -301 516	R 22 851	R 0	R 22 851	R -350 955
10	R 33 529	R 0	R -	R 33 529	R -267 987	R 22 434	R 0	R 22 434	R -328 521
11	R 34 267	R 0	R -226 368	R -192 101	R -460 088	R 22 025	R -145 498	R -123 473	R -451 994
12	R 35 020	R 0	R -	R 35 020	R -425 068	R 21 623	R 0	R 21 623	R -430 371
13	R 35 791	R 0	R -	R 35 791	R -389 277	R 21 228	R 0	R 21 228	R -409 143
14	R 36 578	R 0	R -	R 36 578	R -352 699	R 20 841	R 0	R 20 841	R -388 302
15	R 37 383	R 0	R -	R 37 383	R -315 316	R 20 460	R 0	R 20 460	R -367 841
16	R 38 205	R 0	R -	R 38 205	R -277 110	R 20 087	R 0	R 20 087	R -347 754
17	R 39 046	R 0	R -	R 39 046	R -238 064	R 19 720	R 0	R 19 720	R -328 034
18	R 39 905	R 0	R -	R 39 905	R -198 159	R 19 360	R 0	R 19 360	R -308 674
19	R 40 783	R 0	R -	R 40 783	R -157 376	R 19 007	R 0	R 19 007	R -289 667
20	R 41 680	R 0	R -	R 41 680	R -115 696	R 18 660	R 0	R 18 660	R -271 007
	R 683 265	R -572 594	R -226 368			R 447 085	R -718 091		

Table D-15: CBA Calculation Results Concept 9, Trip 2

	Nominal Monetary Values					Discounted (Real) Monetary Values			
Year	Annual Fuel Savings	Initial Capital Expenditure	Maintenance Expenditure	Annual Cashflow	Nominal Cumulative Cash Flow	Discounte Benefits	Discounted Costs	Net Discounte d Flow	Net Present Value
0	R 0	R -572 594	R -	R -572 594	R -572 594	R 0	R -572 594	R -572 594	R -572 594
1	R 24 809	0	R -	R 24 809	R -547 784	R 23 832	R 0	R 23 832	R -548 761
2	R 25 355	R 0	R -	R 25 355	R -522 429	R 23 397	R 0	R 23 397	R -525 364
3	R 25 913	R 0	R -	R 25 913	R -496 516	R 22 970	R 0	R 22 970	R -502 394
4	R 26 483	R 0	R -	R 26 483	R -470 034	R 22 551	R 0	R 22 551	R -479 843
5	R 27 066	R 0	R -	R 27 066	R -442 968	R 22 139	R 0	R 22 139	R -457 704
6	R 27 661	R 0	R -	R 27 661	R -415 307	R 21 735	R 0	R 21 735	R -435 969
7	R 28 270	R 0	R -	R 28 270	R -387 037	R 21 338	R 0	R 21 338	R -414 630
8	R 28 891	R 0	R -	R 28 891	R -358 146	R 20 949	R 0	R 20 949	R -393 681
9	R 29 527	R 0	R -	R 29 527	R -328 619	R 20 567	R 0	R 20 567	R -373 115
10	R 30 177	R 0	R -	R 30 177	R -298 442	R 20 191	R 0	R 20 191	R -352 923
11	R 30 841	R 0	R -226 368	R -195 527	R -493 970	R 19 823	R -145 498	R -125 675	R -478 599
12	R 31 519	R 0	R -	R 31 519	R -462 451	R 19 461	R 0	R 19 461	R -459 138
13	R 32 212	R 0	R -	R 32 212	R -430 238	R 19 106	R 0	R 19 106	R -440 032
14	R 32 921	R 0	R -	R 32 921	R -397 317	R 18 757	R 0	R 18 757	R -421 275
15	R 33 645	R 0	R -	R 33 645	R -363 672	R 18 415	R 0	R 18 415	R -402 860
16	R 34 386	R 0	R -	R 34 386	R -329 286	R 18 079	R 0	R 18 079	R -384 782
17	R 35 142	R 0	R -	R 35 142	R -294 144	R 17 749	R 0	R 17 749	R -367 033
18	R 35 915	R 0	R -	R 35 915	R -258 229	R 17 425	R 0	R 17 425	R -349 608
19	R 36 705	R 0	R -	R 36 705	R -221 523	R 17 107	R 0	R 17 107	R -332 502
20	R 37 513	R 0	R -	R 37 513	R -184 010	R 16 794	R 0	R 16 794	R -315 707
	R 614 951	R -572 594	R -226 368			R 402 384	R -718 091		

Table D-16: CBA Calculation Results Concept 10, Trip 1

	Nominal Monetary Values					Discounted (Real) Monetary Values			
Year	Annual Fuel Savings	Initial Capital Expenditure	Maintenance Expenditure	Annual Cashflow	Nominal Cumulative Cash Flow	Discounted Benefits	Discounted Costs	Net Discounted Flow	Net Present Value
0	R 0	R -619 136	R -	R -619 136	R -619 136	R 0	R -619 136	R -619 136	R -619 136
1	R 77 397	0	R -	R 77 397	R -541 739	R 74 348	R 0	R 74 348	R -544 787
2	R 79 100	R 0	R -	R 79 100	R -462 639	R 72 992	R 0	R 72 992	R -471 796
3	R 80 840	R 0	R -	R 80 840	R -381 800	R 71 659	R 0	R 71 659	R -400 136
4	R 82 618	R 0	R -	R 82 618	R -299 182	R 70 351	R 0	R 70 351	R -329 785
5	R 84 436	R 0	R -	R 84 436	R -214 746	R 69 067	R 0	R 69 067	R -260 718
6	R 86 293	R 0	R -	R 86 293	R -128 452	R 67 807	R 0	R 67 807	R -192 911
7	R 88 192	R 0	R -	R 88 192	R -40 261	R 66 569	R 0	R 66 569	R -126 342
8	R 90 132	R 0	R -	R 90 132	R 49 871	R 65 354	R 0	R 65 354	R -60 988
9	R 92 115	R 0	R -	R 92 115	R 141 986	R 64 161	R 0	R 64 161	R 3 174
10	R 94 141	R 0	R -	R 94 141	R 236 128	R 62 990	R 0	R 62 990	R 66 164
11	R 96 213	R 0	R -272 910	R -176 697	R 59 431	R 61 841	R -175 413	R -113 572	R -47 408
12	R 98 329	R 0	R -	R 98 329	R 157 760	R 60 712	R 0	R 60 712	R 13 304
13	R 100 493	R 0	R -	R 100 493	R 258 252	R 59 604	R 0	R 59 604	R 72 908
14	R 102 703	R 0	R -	R 102 703	R 360 956	R 58 516	R 0	R 58 516	R 131 424
15	R 104 963	R 0	R -	R 104 963	R 465 918	R 57 448	R 0	R 57 448	R 188 872
16	R 107 272	R 0	R -	R 107 272	R 573 190	R 56 399	R 0	R 56 399	R 245 271
17	R 109 632	R 0	R -	R 109 632	R 682 822	R 55 370	R 0	R 55 370	R 300 641
18	R 112 044	R 0	R -	R 112 044	R 794 866	R 54 359	R 0	R 54 359	R 355 001
19	R 114 509	R 0	R -	R 114 509	R 909 375	R 53 367	R 0	R 53 367	R 408 368
20	R 117 028	R 0	R -	R 117 028	R 1 026 403	R 52 393	R 0	R 52 393	R 460 761
	R 1 918 449	R -619 136	R -272 910			R 1 255 310	R -794 549		

Table D-17: CBA Calculation Results Concept 10, Trip 2

	Nominal Monetary Values					Discounted (Real) Monetary Values			
Year	Annual Fuel Savings	Initial Capital Expenditure	Maintenance Expenditure	Annual Cashflow	Nominal Cumulative Cash Flow	Discounte Benefits	Discounted Costs	Net Discounted Flow	Net Present Value
0	R 0	R -619 136	R -	R -619 136	R -619 136	R 0	R -619 136	R -619 136	R -619 136
1	R 81 687	0	R -	R 81 687	R -537 449	R 78 470	R 0	R 78 470	R -540 666
2	R 83 484	R 0	R -	R 83 484	R -453 964	R 77 038	R 0	R 77 038	R -463 628
3	R 85 321	R 0	R -	R 85 321	R -368 643	R 75 632	R 0	R 75 632	R -387 997
4	R 87 198	R 0	R -	R 87 198	R -281 445	R 74 251	R 0	R 74 251	R -313 745
5	R 89 116	R 0	R -	R 89 116	R -192 329	R 72 896	R 0	R 72 896	R -240 849
6	R 91 077	R 0	R -	R 91 077	R -101 252	R 71 566	R 0	R 71 566	R -169 284
7	R 93 081	R 0	R -	R 93 081	R -8 172	R 70 259	R 0	R 70 259	R -99 025
8	R 95 128	R 0	R -	R 95 128	R 86 957	R 68 977	R 0	R 68 977	R -30 048
9	R 97 221	R 0	R -	R 97 221	R 184 178	R 67 718	R 0	R 67 718	R 37 670
10	R 99 360	R 0	R -	R 99 360	R 283 538	R 66 482	R 0	R 66 482	R 104 152
11	R 101 546	R 0	R -272 910	R -171 364	R 112 174	R 65 269	R -175 413	R -110 144	R -5 992
12	R 103 780	R 0	R -	R 103 780	R 215 954	R 64 077	R 0	R 64 077	R 58 086
13	R 106 063	R 0	R -	R 106 063	R 322 017	R 62 908	R 0	R 62 908	R 120 993
14	R 108 397	R 0	R -	R 108 397	R 430 413	R 61 760	R 0	R 61 760	R 182 753
15	R 110 781	R 0	R -	R 110 781	R 541 195	R 60 632	R 0	R 60 632	R 243 386
16	R 113 218	R 0	R -	R 113 218	R 654 413	R 59 526	R 0	R 59 526	R 302 911
17	R 115 709	R 0	R -	R 115 709	R 770 122	R 58 439	R 0	R 58 439	R 361 351
18	R 118 255	R 0	R -	R 118 255	R 888 377	R 57 373	R 0	R 57 373	R 418 724
19	R 120 856	R 0	R -	R 120 856	R 1 009 234	R 56 326	R 0	R 56 326	R 475 049
20	R 123 515	R 0	R -	R 123 515	R 1 132 749	R 55 298	R 0	R 55 298	R 530 347
	R 2 024 794	R -619 136	R -272 910			R 1 324 895	R -794 549		

Table D-18: CBA Calculation Results Concept 11, Trip 1

	Nominal Monetary Values					Discounted (Real) Monetary Values			
Year	Annual Fuel Savings	Initial Capital Expenditure	Maintenance Expenditure	Annual Cashflow	Nominal Cumulative Cash Flow	Discounted Benefits	Discounted Costs	Net Discounted Flow	Net Present Value
0	R 0	R -434 766	R -	R -434 766	R -434 766	R 0	R -434 766	R -434 766	R -434 766
1	R 24 622	0	R -	R 24 622	R -410 144	R 23 652	R 0	R 23 652	R -411 114
2	R 25 164	R 0	R -	R 25 164	R -384 980	R 23 220	R 0	R 23 220	R -387 893
3	R 25 717	R 0	R -	R 25 717	R -359 263	R 22 797	R 0	R 22 797	R -365 096
4	R 26 283	R 0	R -	R 26 283	R -332 980	R 22 381	R 0	R 22 381	R -342 716
5	R 26 861	R 0	R -	R 26 861	R -306 119	R 21 972	R 0	R 21 972	R -320 744
6	R 27 452	R 0	R -	R 27 452	R -278 667	R 21 571	R 0	R 21 571	R -299 173
7	R 28 056	R 0	R -	R 28 056	R -250 611	R 21 177	R 0	R 21 177	R -277 995
8	R 28 673	R 0	R -	R 28 673	R -221 938	R 20 791	R 0	R 20 791	R -257 205
9	R 29 304	R 0	R -	R 29 304	R -192 634	R 20 411	R 0	R 20 411	R -236 793
10	R 29 949	R 0	R -	R 29 949	R -162 685	R 20 039	R 0	R 20 039	R -216 755
11	R 30 608	R 0	R -175 096	R -144 489	R -307 174	R 19 673	R -112 543	R -92 870	R -309 625
12	R 31 281	R 0	R -	R 31 281	R -275 893	R 19 314	R 0	R 19 314	R -290 311
13	R 31 969	R 0	R -	R 31 969	R -243 923	R 18 961	R 0	R 18 961	R -271 349
14	R 32 673	R 0	R -	R 32 673	R -211 251	R 18 615	R 0	R 18 615	R -252 734
15	R 33 391	R 0	R -	R 33 391	R -177 860	R 18 276	R 0	R 18 276	R -234 458
16	R 34 126	R 0	R -	R 34 126	R -143 734	R 17 942	R 0	R 17 942	R -216 516
17	R 34 877	R 0	R -	R 34 877	R -108 857	R 17 615	R 0	R 17 615	R -198 901
18	R 35 644	R 0	R -	R 35 644	R -73 213	R 17 293	R 0	R 17 293	R -181 608
19	R 36 428	R 0	R -	R 36 428	R -36 785	R 16 977	R 0	R 16 977	R -164 631
20	R 37 230	R 0	R -	R 37 230	R 445	R 16 668	R 0	R 16 668	R -147 963
	R 610 307	R -434 766	R -175 096			R 399 346	R -547 309		

Table D-19: CBA Calculation Results Concept 11, Trip 2

	Nominal Monetary Values					Discounted (Real) Monetary Values			
Year	Annual Fuel Savings	Initial Capital Expenditure	Maintenance Expenditure	Annual Cashflow	Nominal Cumulative Cash Flow	Discounte Benefits	Discounted Costs	Net Discounted Flow	Net Present Value
0	R 0	R -434 766	R -	R -434 766	R -434 766	R 0	R -434 766	R -434 766	R -434 766
1	R 23 985	0	R -	R 23 985	R -410 780	R 23 041	R 0	R 23 041	R -411 725
2	R 24 513	R 0	R -	R 24 513	R -386 267	R 22 620	R 0	R 22 620	R -389 105
3	R 25 052	R 0	R -	R 25 052	R -361 215	R 22 207	R 0	R 22 207	R -366 898
4	R 25 603	R 0	R -	R 25 603	R -335 612	R 21 802	R 0	R 21 802	R -345 096
5	R 26 167	R 0	R -	R 26 167	R -309 445	R 21 404	R 0	R 21 404	R -323 692
6	R 26 742	R 0	R -	R 26 742	R -282 703	R 21 013	R 0	R 21 013	R -302 679
7	R 27 331	R 0	R -	R 27 331	R -255 372	R 20 630	R 0	R 20 630	R -282 049
8	R 27 932	R 0	R -	R 27 932	R -227 441	R 20 253	R 0	R 20 253	R -261 796
9	R 28 546	R 0	R -	R 28 546	R -198 894	R 19 884	R 0	R 19 884	R -241 912
10	R 29 174	R 0	R -	R 29 174	R -169 720	R 19 521	R 0	R 19 521	R -222 391
11	R 29 816	R 0	R -175 096	R -145 280	R -315 000	R 19 164	R -112 543	R -93 379	R -315 770
12	R 30 472	R 0	R -	R 30 472	R -284 528	R 18 815	R 0	R 18 815	R -296 956
13	R 31 143	R 0	R -	R 31 143	R -253 385	R 18 471	R 0	R 18 471	R -278 484
14	R 31 828	R 0	R -	R 31 828	R -221 557	R 18 134	R 0	R 18 134	R -260 350
15	R 32 528	R 0	R -	R 32 528	R -189 029	R 17 803	R 0	R 17 803	R -242 547
16	R 33 244	R 0	R -	R 33 244	R -155 786	R 17 478	R 0	R 17 478	R -225 069
17	R 33 975	R 0	R -	R 33 975	R -121 811	R 17 159	R 0	R 17 159	R -207 910
18	R 34 722	R 0	R -	R 34 722	R -87 089	R 16 846	R 0	R 16 846	R -191 064
19	R 35 486	R 0	R -	R 35 486	R -51 602	R 16 539	R 0	R 16 539	R -174 525
20	R 36 267	R 0	R -	R 36 267	R -15 335	R 16 237	R 0	R 16 237	R -158 289
	R 594 527	R -434 766	R -175 096			R 389 020	R -547 309		

Table D-20: CBA Calculation Results Concept 12, Trip 1

	Nominal Monetary Values					Discounted (Real) Monetary Values			
Year	Annual Fuel Savings	Initial Capital Expenditure	Maintenance Expenditure	Annual Cashflow	Nominal Cumulative Cash Flow	Discounted Benefits	Discounted Costs	Net Discounted Flow	Net Present Value
0	R 0	R -481 193	R -	R -481 193	R -481 193	R 0	R -481 193	R -481 193	R -481 193
1	R 68 326	0	R -	R 68 326	R -412 867	R 65 635	R 0	R 65 635	R -415 558
2	R 69 829	R 0	R -	R 69 829	R -343 038	R 64 437	R 0	R 64 437	R -351 121
3	R 71 365	R 0	R -	R 71 365	R -271 672	R 63 261	R 0	R 63 261	R -287 860
4	R 72 935	R 0	R -	R 72 935	R -198 737	R 62 106	R 0	R 62 106	R -225 754
5	R 74 540	R 0	R -	R 74 540	R -124 197	R 60 973	R 0	R 60 973	R -164 781
6	R 76 180	R 0	R -	R 76 180	R -48 017	R 59 860	R 0	R 59 860	R -104 921
7	R 77 856	R 0	R -	R 77 856	R 29 839	R 58 767	R 0	R 58 767	R -46 154
8	R 79 569	R 0	R -	R 79 569	R 109 407	R 57 695	R 0	R 57 695	R 11 541
9	R 81 319	R 0	R -	R 81 319	R 190 726	R 56 642	R 0	R 56 642	R 68 183
10	R 83 108	R 0	R -	R 83 108	R 273 835	R 55 608	R 0	R 55 608	R 123 790
11	R 84 937	R 0	R -221 523	R -136 587	R 137 248	R 54 593	R -142 384	R -87 791	R 35 999
12	R 86 805	R 0	R -	R 86 805	R 224 053	R 53 597	R 0	R 53 597	R 89 596
13	R 88 715	R 0	R -	R 88 715	R 312 768	R 52 618	R 0	R 52 618	R 142 214
14	R 90 667	R 0	R -	R 90 667	R 403 434	R 51 658	R 0	R 51 658	R 193 872
15	R 92 661	R 0	R -	R 92 661	R 496 096	R 50 715	R 0	R 50 715	R 244 587
16	R 94 700	R 0	R -	R 94 700	R 590 795	R 49 789	R 0	R 49 789	R 294 377
17	R 96 783	R 0	R -	R 96 783	R 687 579	R 48 881	R 0	R 48 881	R 343 257
18	R 98 912	R 0	R -	R 98 912	R 786 491	R 47 989	R 0	R 47 989	R 391 246
19	R 101 088	R 0	R -	R 101 088	R 887 579	R 47 113	R 0	R 47 113	R 438 359
20	R 103 312	R 0	R -	R 103 312	R 990 892	R 46 253	R 0	R 46 253	R 484 611
	R 1 693 608	R -481 193	R -221 523			R 1 108 188	R -623 577		

Table D-21: CBA Calculation Results Concept 12, Trip 2

	Nominal Monetary Values					Discounted (Real) Monetary Values			
Year	Annual Fuel Savings	Initial Capital Expenditure	Maintenance Expenditure	Annual Cashflow	Nominal Cumulative Cash Flow	Discounte Benefits	Discounted Costs	Net Discounted Flow	Net Present Value
0	R 0	R -481 193	R -	R -481 193	R -481 193	R 0	R -481 193	R -481 193	R -481 193
1	R 77 747	0	R -	R 77 747	R -403 446	R 74 685	R 0	R 74 685	R -406 508
2	R 79 457	R 0	R -	R 79 457	R -323 989	R 73 322	R 0	R 73 322	R -333 186
3	R 81 205	R 0	R -	R 81 205	R -242 783	R 71 983	R 0	R 71 983	R -261 203
4	R 82 992	R 0	R -	R 82 992	R -159 792	R 70 669	R 0	R 70 669	R -190 534
5	R 84 818	R 0	R -	R 84 818	R -74 974	R 69 380	R 0	R 69 380	R -121 154
6	R 86 684	R 0	R -	R 86 684	R 11 709	R 68 113	R 0	R 68 113	R -53 041
7	R 88 591	R 0	R -	R 88 591	R 100 300	R 66 870	R 0	R 66 870	R 13 830
8	R 90 540	R 0	R -	R 90 540	R 190 840	R 65 650	R 0	R 65 650	R 79 479
9	R 92 531	R 0	R -	R 92 531	R 283 371	R 64 451	R 0	R 64 451	R 143 931
10	R 94 567	R 0	R -	R 94 567	R 377 938	R 63 275	R 0	R 63 275	R 207 206
11	R 96 648	R 0	R -221 523	R -124 876	R 253 063	R 62 120	R -142 384	R -80 264	R 126 942
12	R 98 774	R 0	R -	R 98 774	R 351 836	R 60 986	R 0	R 60 986	R 187 929
13	R 100 947	R 0	R -	R 100 947	R 452 783	R 59 873	R 0	R 59 873	R 247 802
14	R 103 168	R 0	R -	R 103 168	R 555 951	R 58 781	R 0	R 58 781	R 306 582
15	R 105 437	R 0	R -	R 105 437	R 661 388	R 57 708	R 0	R 57 708	R 364 290
16	R 107 757	R 0	R -	R 107 757	R 769 146	R 56 654	R 0	R 56 654	R 420 945
17	R 110 128	R 0	R -	R 110 128	R 879 273	R 55 620	R 0	R 55 620	R 476 565
18	R 112 551	R 0	R -	R 112 551	R 991 824	R 54 605	R 0	R 54 605	R 531 170
19	R 115 027	R 0	R -	R 115 027	R 1 106 850	R 53 609	R 0	R 53 609	R 584 779
20	R 117 557	R 0	R -	R 117 557	R 1 224 408	R 52 630	R 0	R 52 630	R 637 409
	R 1 927 123	R -481 193	R -221 523			R 1 260 986	R -623 577		

Table D-22: CBA Calculation Results Concept 13, Trip 1

	Nominal Monetary Values					Discounted (Real) Monetary Values			
Year	Annual Fuel Savings	Initial Capital Expenditure	Maintenance Expenditure	Annual Cashflow	Nominal Cumulative Cash Flow	Discounted Benefits	Discounted Costs	Net Discounted Flow	Net Present Value
0	R 0	R -297 009	R -	R -297 009	R -297 009	R 0	R -297 009	R -297 009	R -297 009
1	R 21 535	0	R -	R 21 535	R -275 474	R 20 687	R 0	R 20 687	R -276 322
2	R 22 008	R 0	R -	R 22 008	R -253 466	R 20 309	R 0	R 20 309	R -256 013
3	R 22 493	R 0	R -	R 22 493	R -230 973	R 19 938	R 0	R 19 938	R -236 075
4	R 22 987	R 0	R -	R 22 987	R -207 985	R 19 574	R 0	R 19 574	R -216 500
5	R 23 493	R 0	R -	R 23 493	R -184 492	R 19 217	R 0	R 19 217	R -197 283
6	R 24 010	R 0	R -	R 24 010	R -160 482	R 18 866	R 0	R 18 866	R -178 417
7	R 24 538	R 0	R -	R 24 538	R -135 944	R 18 522	R 0	R 18 522	R -159 895
8	R 25 078	R 0	R -	R 25 078	R -110 866	R 18 184	R 0	R 18 184	R -141 711
9	R 25 630	R 0	R -	R 25 630	R -85 236	R 17 852	R 0	R 17 852	R -123 859
10	R 26 194	R 0	R -	R 26 194	R -59 042	R 17 526	R 0	R 17 526	R -106 332
11	R 26 770	R 0	R -123 896	R -97 126	R -156 168	R 17 206	R -79 634	R -62 428	R -168 760
12	R 27 359	R 0	R -	R 27 359	R -128 809	R 16 892	R 0	R 16 892	R -151 868
13	R 27 961	R 0	R -	R 27 961	R -100 848	R 16 584	R 0	R 16 584	R -135 284
14	R 28 576	R 0	R -	R 28 576	R -72 272	R 16 281	R 0	R 16 281	R -119 002
15	R 29 205	R 0	R -	R 29 205	R -43 068	R 15 984	R 0	R 15 984	R -103 018
16	R 29 847	R 0	R -	R 29 847	R -13 221	R 15 692	R 0	R 15 692	R -87 326
17	R 30 504	R 0	R -	R 30 504	R 17 283	R 15 406	R 0	R 15 406	R -71 920
18	R 31 175	R 0	R -	R 31 175	R 48 458	R 15 125	R 0	R 15 125	R -56 795
19	R 31 861	R 0	R -	R 31 861	R 80 319	R 14 849	R 0	R 14 849	R -41 946
20	R 32 562	R 0	R -	R 32 562	R 112 880	R 14 578	R 0	R 14 578	R -27 368
	R 533 785	R -297 009	R -123 896			R 349 274	R -376 643		

Table D-23: CBA Calculation Results Concept 13, Trip 2

	Nominal Monetary Values					Discounted (Real) Monetary Values			
Year	Annual Fuel Savings	Initial Capital Expenditure	Maintenance Expenditure	Annual Cashflow	Nominal Cumulative Cash Flow	Discounte Benefits	Discounted Costs	Net Discounted Flow	Net Present Value
0	R 0	R -297 009	R -	R -297 009	R -297 009	R 0	R -297 009	R -297 009	R -297 009
1	R 21 354	0	R -	R 21 354	R -275 655	R 20 513	R 0	R 20 513	R -276 496
2	R 21 823	R 0	R -	R 21 823	R -253 832	R 20 138	R 0	R 20 138	R -256 358
3	R 22 303	R 0	R -	R 22 303	R -231 528	R 19 771	R 0	R 19 771	R -236 587
4	R 22 794	R 0	R -	R 22 794	R -208 734	R 19 410	R 0	R 19 410	R -217 177
5	R 23 296	R 0	R -	R 23 296	R -185 438	R 19 056	R 0	R 19 056	R -198 122
6	R 23 808	R 0	R -	R 23 808	R -161 630	R 18 708	R 0	R 18 708	R -179 414
7	R 24 332	R 0	R -	R 24 332	R -137 298	R 18 366	R 0	R 18 366	R -161 048
8	R 24 867	R 0	R -	R 24 867	R -112 431	R 18 031	R 0	R 18 031	R -143 017
9	R 25 414	R 0	R -	R 25 414	R -87 017	R 17 702	R 0	R 17 702	R -125 315
10	R 25 973	R 0	R -	R 25 973	R -61 043	R 17 379	R 0	R 17 379	R -107 936
11	R 26 545	R 0	R -123 896	R -97 351	R -158 394	R 17 062	R -79 634	R -62 572	R -170 508
12	R 27 129	R 0	R -	R 27 129	R -131 265	R 16 750	R 0	R 16 750	R -153 758
13	R 27 726	R 0	R -	R 27 726	R -103 540	R 16 445	R 0	R 16 445	R -137 313
14	R 28 336	R 0	R -	R 28 336	R -75 204	R 16 144	R 0	R 16 144	R -121 169
15	R 28 959	R 0	R -	R 28 959	R -46 245	R 15 850	R 0	R 15 850	R -105 319
16	R 29 596	R 0	R -	R 29 596	R -16 649	R 15 560	R 0	R 15 560	R -89 759
17	R 30 247	R 0	R -	R 30 247	R 13 598	R 15 276	R 0	R 15 276	R -74 482
18	R 30 913	R 0	R -	R 30 913	R 44 511	R 14 998	R 0	R 14 998	R -59 485
19	R 31 593	R 0	R -	R 31 593	R 76 104	R 14 724	R 0	R 14 724	R -44 761
20	R 32 288	R 0	R -	R 32 288	R 108 391	R 14 455	R 0	R 14 455	R -30 306
	R 529 296	R -297 009	R -123 896			R 346 337	R -376 643		

Table D-24: CBA Calculation Results Concept 14, Trip 1

	Nominal Monetary Values					Discounted (Real) Monetary Values			
Year	Annual Fuel Savings	Initial Capital Expenditure	Maintenance Expenditure	Annual Cashflow	Nominal Cumulative Cash Flow	Discounted Benefits	Discounted Costs	Net Discounted Flow	Net Present Value
0	R 0	R -343 474	R -	R -343 474	R -343 474	R 0	R -343 474	R -343 474	R -343 474
1	R 54 003	0	R -	R 54 003	R -289 471	R 51 877	R 0	R 51 877	R -291 597
2	R 55 192	R 0	R -	R 55 192	R -234 279	R 50 930	R 0	R 50 930	R -240 668
3	R 56 406	R 0	R -	R 56 406	R -177 873	R 50 000	R 0	R 50 000	R -190 668
4	R 57 647	R 0	R -	R 57 647	R -120 226	R 49 088	R 0	R 49 088	R -141 580
5	R 58 915	R 0	R -	R 58 915	R -61 312	R 48 192	R 0	R 48 192	R -93 388
6	R 60 211	R 0	R -	R 60 211	R -1 100	R 47 312	R 0	R 47 312	R -46 076
7	R 61 536	R 0	R -	R 61 536	R 60 435	R 46 449	R 0	R 46 449	R 372
8	R 62 889	R 0	R -	R 62 889	R 123 325	R 45 601	R 0	R 45 601	R 45 973
9	R 64 273	R 0	R -	R 64 273	R 187 598	R 44 768	R 0	R 44 768	R 90 741
10	R 65 687	R 0	R -	R 65 687	R 253 285	R 43 951	R 0	R 43 951	R 134 693
11	R 67 132	R 0	R -170 361	R -103 229	R 150 056	R 43 149	R -109 500	R -66 350	R 68 342
12	R 68 609	R 0	R -	R 68 609	R 218 665	R 42 362	R 0	R 42 362	R 110 704
13	R 70 118	R 0	R -	R 70 118	R 288 783	R 41 588	R 0	R 41 588	R 152 293
14	R 71 661	R 0	R -	R 71 661	R 360 445	R 40 829	R 0	R 40 829	R 193 122
15	R 73 238	R 0	R -	R 73 238	R 433 682	R 40 084	R 0	R 40 084	R 233 206
16	R 74 849	R 0	R -	R 74 849	R 508 531	R 39 353	R 0	R 39 353	R 272 559
17	R 76 496	R 0	R -	R 76 496	R 585 027	R 38 634	R 0	R 38 634	R 311 193
18	R 78 178	R 0	R -	R 78 178	R 663 205	R 37 929	R 0	R 37 929	R 349 122
19	R 79 898	R 0	R -	R 79 898	R 743 103	R 37 237	R 0	R 37 237	R 386 359
20	R 81 656	R 0	R -	R 81 656	R 824 760	R 36 557	R 0	R 36 557	R 422 917
	R 1 338 595	R -343 474	R -170 361			R 875 890	R -452 974		

Table D-25: CBA Calculation Results Concept 14, Trip 2

	Nominal Monetary Values					Discounted (Real) Monetary Values			
Year	Annual Fuel Savings	Initial Capital Expenditure	Maintenance Expenditure	Annual Cashflow	Nominal Cumulative Cash Flow	Discounte Benefits	Discounted Costs	Net Discounted Flow	Net Present Value
0	R 0	R -343 474	R -	R -343 474	R -343 474	R 0	R -343 474	R -343 474	R -343 474
1	R 64 982	0	R -	R 64 982	R -278 492	R 62 423	R 0	R 62 423	R -281 051
2	R 66 412	R 0	R -	R 66 412	R -212 080	R 61 283	R 0	R 61 283	R -219 768
3	R 67 873	R 0	R -	R 67 873	R -144 208	R 60 165	R 0	R 60 165	R -159 603
4	R 69 366	R 0	R -	R 69 366	R -74 842	R 59 067	R 0	R 59 067	R -100 536
5	R 70 892	R 0	R -	R 70 892	R -3 950	R 57 989	R 0	R 57 989	R -42 548
6	R 72 452	R 0	R -	R 72 452	R 68 502	R 56 930	R 0	R 56 930	R 14 383
7	R 74 046	R 0	R -	R 74 046	R 142 547	R 55 891	R 0	R 55 891	R 70 274
8	R 75 675	R 0	R -	R 75 675	R 218 222	R 54 871	R 0	R 54 871	R 125 145
9	R 77 339	R 0	R -	R 77 339	R 295 561	R 53 870	R 0	R 53 870	R 179 015
10	R 79 041	R 0	R -	R 79 041	R 374 602	R 52 886	R 0	R 52 886	R 231 901
11	R 80 780	R 0	R -170 361	R -89 581	R 285 021	R 51 921	R -109 500	R -57 578	R 174 323
12	R 82 557	R 0	R -	R 82 557	R 367 578	R 50 974	R 0	R 50 974	R 225 296
13	R 84 373	R 0	R -	R 84 373	R 451 951	R 50 043	R 0	R 50 043	R 275 339
14	R 86 229	R 0	R -	R 86 229	R 538 180	R 49 130	R 0	R 49 130	R 324 469
15	R 88 126	R 0	R -	R 88 126	R 626 307	R 48 233	R 0	R 48 233	R 372 702
16	R 90 065	R 0	R -	R 90 065	R 716 372	R 47 353	R 0	R 47 353	R 420 055
17	R 92 047	R 0	R -	R 92 047	R 808 418	R 46 488	R 0	R 46 488	R 466 544
18	R 94 072	R 0	R -	R 94 072	R 902 490	R 45 640	R 0	R 45 640	R 512 184
19	R 96 141	R 0	R -	R 96 141	R 998 631	R 44 807	R 0	R 44 807	R 556 991
20	R 98 256	R 0	R -	R 98 256	R 1 096 888	R 43 989	R 0	R 43 989	R 600 980
	R 1 610 723	R -343 474	R -170 361			R 1 053 953	R -452 974		